COLOR TELEVISION PICTURE TUBES

SUPPLEMENT 1

Advances in Image Pickup and Display

A. M. Morrell

RCA ELECTRONIC COMPONENTS DIVISION
LANCASTER, PENNSYLVANIA

H. B. Law
E. G. Ramberg
E. W. Herold

RCA LABORATORIES
PRINCETON, NEW JERSEY

ACADEMIC PRESS New York and London 1974

A Subsidiary of Harcourt Brace Jovanovich, Publishers

ACADEMIC PRESS, INC.
111 Fifth Avenue, New York, New York 10003

United Kingdom Edition published by
ACADEMIC PRESS, INC. (LONDON) LTD.
24/28 Oval Road, London NW1

LIBRARY OF CONGRESS CATALOG CARD NUMBER: 73-18958

ISBN 0-12-022151-9

PRINTED IN THE UNITED STATES OF AMERICA

Color Television Picture Tubes

Advances in

IMAGE PICKUP AND DISPLAY

edited by

B. Kazan

IBM WATSON RESEARCH CENTER
YORKTOWN HEIGHTS, NEW YORK

Supplement 1

Color Television Picture Tubes

Contents

Foreword

This supplement to *Advances in Image Pickup and Display* is concerned entirely with color television picture tubes. Color television picture tubes are already in such widespread use that no serious effort is needed to convince the reader of the importance of such devices to the field of imaging. Aside from the development of the black-and-white picture tube and the invention of electron-beam camera tubes such as the iconoscope, no other single device has contributed to the growth of television and so fully augmented its potential as the shadow-mask color tube.

A few words are, perhaps, in order explaining the reason for devoting an entire volume to color television picture tubes. As one can expect, in view of the extended history of research, development, and commercial production of present shadow-mask tubes, many publications exist covering individual phases of the subject. However, no comprehensive or cohesive treatment exists in the literature covering the entire subject. Included in this supplement are not only a broad discussion of the basic principles and operation of such tubes but also an extensive analysis of the electron-optical factors determining tube brightness as well as a detailed analysis of the interrelated factors involved in the design of the mask and screen and their influence on color purity. In addition, the book contains an unusual amount of important and, to a large extent, heretofore unpublished information on the details of construction and fabrication of shadow-mask tubes.

The reader should be reminded that a number of other types of color tubes have also been extensively studied over the years as possible contenders for use in commercial television. Here again, many publications exist but no comprehensive treatment exists covering this effort. A significant portion of this book has thus been devoted to reviewing and analyzing these other schemes, making clear their significant advantages and disadvantages compared to the shadow-mask tube. Finally, it should be noted that, although color tubes have been in commercial production for many years, continuous improvements have taken place and significant new developments have been occurring up to the present time. In keeping with the general intent of the series, it is thus felt that the book, aside from its other functions, will serve to bring the reader up to date on recent advances in the field.

All of the authors of this supplement have been so intimately connected with the development of color television picture tubes that they need no special introduction. As indicated in their preface, so many other individuals have played important and essential roles in the development of the color tube that acknowledgement of each one separately is hardly possible in a short introductory statement. One particular name, however, stands out above all others and must be mentioned—that of David Sarnoff—who was the guiding light of RCA from its inception and Chairman of the Board through the years during which color television was developed to a state of commercial reality. His unusual faith in the value of research in general and his unyielding conviction that color television tubes could be made a commercial reality in the face of seemingly insurmountable technical difficulties undoubtedly accelerated the development of this field by many years.

B. KAZAN

Preface

This volume is the first comprehensive review of the vast amount of scientific and technological information on color picture tubes that has accumulated over the past 25 years. Color television as we know it today was made possible only by the mass production of a picture tube that appeared to be a technical impossibility in 1949. It required the development of technology for manufacturing cathode-ray structures having specifications for precision, uniformity, and reliability that had not been achieved or even attempted with such large structures in forty prior years of electron tube production. In particular, the shadow-mask color tube ranks, along with the semiconductor device and its many offspring, as one of the most remarkable achievements of electronics in this century. The authors have been involved with color television picture tubes since their inception, but the work we describe is that of thousands of researchers, most of whom are unpublished and unsung contributors to this most exciting engineering adventure. We have included references to much published work, but the names are only a few of the many engineers engaged in this work. In addition, we must credit the managers, the production personnel, and the executives and financial entrepreneurs whose expertise, dedication to success, and willingness to take risk, made the shadow-mask tube a reality.

In our volume, we cover all types of color picture tubes, but greatest space has been allotted to the shadow-mask type because it is so predominant. We hope that those who wish a better understanding of either its basic principles or technology will find our text of value. Beyond this, our descriptions of nonshadow-mask tubes should help those readers who want to evaluate the future potential of these methods, as well as those who wish to approach the problem of picture reproduction afresh.

Parts of our book are purely descriptive, if only a word-picture is needed, but other parts are mathematical and analytical for persons who are deeply committed to a quantitative and detailed approach to tube design and performance.

In concluding this preface, we express our sincere appreciation to Dr. Benjamin Kazan, editor of this series, for his encouragement and his review

of our manuscript. Others who were exceptionally helpful to us were our many colleagues at the RCA Corporation, particularly those at the David Sarnoff Research Center and the Engineering Department in Lancaster, Pennsylvania.

Princeton, New Jersey

A. M. MORRELL
H. B. LAW
E. G. RAMBERG
E. W. HEROLD

CHAPTER 1

Introduction

Some of the earliest thoughts of television included the concept of pictures in full color. Inventions were made by the score and were almost universally confined to paper designs (*1*). The few demonstrations of the 1920's used scanning-disc techniques and showed only that the concepts of color, in terms of tristimulus phenomena, were applicable to electrical control. By 1940, however, black-and-white electronic television with camera tubes and a cathode-ray-tube reproducer was well advanced.

That year, an impressive demonstration was made (*2*) of color television using a synchronized rotating color wheel in front of a black-and-white picture tube. The picture was then modulated sequentially in accordance with the three color-component luminances. Unfortunately, mechanical limitations of size and rotational speed are sufficiently severe so that this type of field-sequential color picture reproduction has disappeared. (Rotating color filters, however, remain useful in small sizes, for use with TV cameras, such as those used in early television from the moon.)

The major challenge that faced inventors and promoters of color television was to find a picture reproduction method that compared in simplicity to that of the black-and-white cathode-ray tube.* Optical superposition of pictures from three tubes was tried and is still in use in projection systems. For direct viewing on a single picture tube, however, the first successful demonstration was made in early 1950 using an internal structure that is commonly known as the shadow mask (*3*, *4*). This type of tube employs three electron beams which pass through a common deflec-

* For a bibliography and description of important early work not otherwise referred to herein, see Herold (*1*).

tion yoke (*5*), with one beam for each primary phosphor color, i.e., red, green, and blue. The beams are "shadowed" by a perforated metal mask so that each beam can strike but one color of phosphor. The shadow-mask tube was intensively developed in the 1950–1957 period and many basic improvements were made. Of these, the most important were the use of a curved mask (*6*) (initially, it was flat), the use of photodeposited phosphor dots (*7*), better phosphors, and refinements of technology in manufacture that led to better uniformity and lower cost. However, two different single-beam tubes were also developed. In the one, then known as the Lawrence tube (*8*), vertical phosphor stripes were used to form a line screen that was spaced from a wire grill on which a high-frequency potential was impressed to deflect the beam from one phosphor color element to another. The other single-beam type also used vertical phosphor stripes and a single beam, but required no mask or grill (*9*). Instead, the phosphor screen supplied an index signal to switch the beam control to whichever color signal corresponded to the phosphor being struck. This early period also led to proposed variations of the three-beam shadow-mask tube, some using wire grills and line screens instead of perforated masks (*10–12*). Although the principles of other types of color tubes still survive in the laboratory, the three-beam shadow-mask method outdistanced its competitors and achieved commercial success (*13*, *14*).

From 1955 to 1967, about 15 million shadow-mask color picture tubes were made, and manufacture of a highly satisfactory product became routine. Round metal envelopes were replaced by glass ones (*15*); these were then changed to a rectangular shape, picture size was increased, and deflection angles (total swing across diagonal axis) were changed from 70° to 90° thereby improving picture sharpness and decreasing tube length (*16–18*). By 1973, color television was well established in most industrially sophisticated countries of the world, and of the order of 20 million color picture tubes were being made each year, worldwide. Improvements and innovations were added to the basic shadow-mask principle. Among the more important were a trend to even larger deflection angles of 110°, and use of a black matrix that surrounded each phosphor element so as to reduce reflected light and increase contrast (*19*, *20*). Coupled with new, highly efficient, color phosphors, some using rare-earth elements (*21*, *22*), these improvements permitted major increases in picture brightness. For the electron beam, there were modifications in the gun for both the most common triangular arrangement and also for the in-line arrangement of beams (*23*, *24*). Although the most common aperture shape in the shadow mask remained circular, several commercial types were introduced that used vertically elongated apertures (*24*, *25*). The phosphor

screens in these types resembled the vertical line screen of the early single-beam tubes mentioned above, although the principles were those of the shadow mask.

In this discussion, we shall first review the fundamental principles that underlie any color picture tube and classify the several methods that make such a tube possible. Because of its predominance, greatest attention will thereafter be given to the shadow-mask method and its principles of design and manufacture. Some of the other methods. particularly those that do not appear to have been entirely abandoned, will also be described, but in less detail. The emphasis, throughout, will be on tubes for full color display, i.e., tubes providing the three primary colors and a luminance range (gray scale) sufficient for good contrast and satisfactory picture rendition. It is evident that there are applications that are considerably less demanding; for example, two-color systems or systems for alpha-numerics or line drawings in which color is used but no "gray scale" requirement is imposed. Such displays can be made with the cathode-ray tube methods herein covered, but permit employment of many other methods not included in the present volume.

CHAPTER 2

Requirements of a Color Picture Reproducer

The variables in a reproduced picture may be briefly listed as size and shape, sharpness and resolution, brightness (luminance), contrast, and color hue and saturation. Some of these are related in that one can be traded off for another in the design of a reproducer. Also of importance are such matters as white balance and uniformity, the "gamma" or degree of nonlinearity of light output vs. electrical input, and spatial coincidence when separate color images are superimposed. Each of these factors will be discussed in turn.

The size of a reproduced color picture is one of the most flexible of the requirements. Direct-view picture tubes, as of 1973, range in size from 266 mm (9V) diagonal to as much as 667 mm (25 V). Projected pictures can be much larger. Because of the well-known psychological principle of "size constancy" with distance (*26*), large pictures are more pleasing than small ones, even when the latter are viewed at shorter distances and subtend the same angle at the eye. Since present television systems transmit a rectangular picture with a 4:3 aspect ratio, the reproduced picture should conform to this aspect ratio to avoid picture distortion or loss of information. It is common practice to overscan or use a raster that exceeds the phosphor screen size which, especially for circuits employing tubes, may be needed to provide for possible raster shrinkage with use of the receiver. Overscanning, of course, causes a loss of picture information and brightness, but makes objects appear slightly larger.

Sharpness and resolution of a color picture reproducer are best discussed in terms of the modulation transfer function (MTF), i.e., the sine-wave luminance response curve plotted against spatial frequency (*27*, *28*).

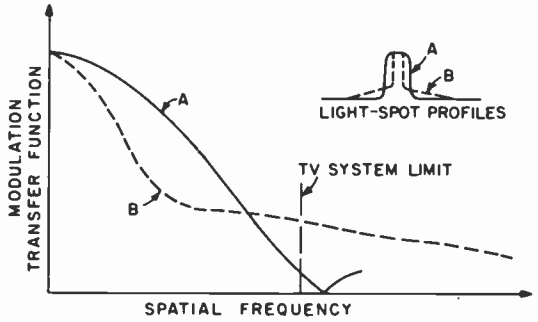

Fig. 2.1. Response curves for two hypothetical picture tubes. Tube A will have a much sharper picture even though it will not show scanning lines as well and will have only half the resolution of Tube B.

Sharpness is the subjective effect on the viewer of step-function changes in scene luminance, and resolution is the ability to distinguish detail. In terms of the MTF, limiting resolution is determined by the highest spatial frequency that is discernible, and sharpness is determined by the shape of the MTF response at frequencies below the resolution limit. In television, there is a resolution limit imposed by the system itself. In addition, the eye has its own MTF and resolution limit that depends on the viewing distance and the pupil diameter. A picture reproducer need not have resolution beyond the limit of the television system and the eye. Below this limit, however, the reproducer should have a luminance MTF as close as possible to 100%. For most existing color TV systems, the upper limit for the resolution of the system is between 350 and 600 TV line numbers (equivalent to 175 to 300 line pairs per picture height). The smaller numbers are in the horizontal direction and the larger are the extreme imposed by the scanning lines, neglecting the "Kell" factor reduction in vertical resolution (*29*) by 0.7. With bright pictures and close viewing distance, the luminance MTF of the eye is not limiting and can be disregarded. Because the eye is relatively insensitive to color in small detail, the MTF for color is of even less importance. However, known reproducers tend to have equal MTF responses for the three primary colors, i.e., they exceed the perceptual requirements substantially.

To illustrate the significance of the above, Fig. 2.1 shows modulation transfer functions for two hypothetical color TV picture tubes. Tube A has a nearly ideal flat-topped light-spot profile, while Tube B has a much smaller central spot but wide flaring skirts similar to a halo. The light-spot profile and the MTF response curves are Fourier transforms of each other. Although reproducer B has much higher limiting resolution than A, and

A has poorer responses at the scanning line frequency, A will nevertheless have a much sharper picture and would be preferred over B for the TV system limit shown in Fig. 2.1, and possibly for any other system as well (*30*).

A projected still color picture continues to give greater satisfaction as highlight brightness is increased up to some few thousands of candela per square meter.* In television systems employing 50 fields/sec, flicker begins to be annoying as brightness is increased above approximately 200 cd/m² when using the exponentially decaying phosphors commonly used in direct-view picture tubes. Somewhat brighter pictures would be tolerable if the "on" time for a picture element were more nearly square-topped. With 60-field/sec systems using phosphors, flicker becomes annoying with peripheral vision at something over 350 cd/m² but can be tolerated with on-center viewing up to considerably more than that (*31*). Such high luminance values are readily obtained on direct-view tubes but are much more difficult to achieve in projection systems. The eye is so adaptive, however, that pictures of only a few candela per square meter are pleasing if viewed in sufficient darkness. On the other hand, in home television the ambient illumination is often appreciable and high brightness is decidedly advantageous. Under such conditions, brightness and contrast are closely related, because the ambient light is often reflected and diffused from the face of the picture tube and raises the black level.

Contrast is one of the most perceptible factors in a reproduced picture, particularly when the picture is in color. If the ratio of the highest luminance to the lowest is reduced because of ambient light, color saturation also is reduced and the picture appears "washed out" in both color and in contrast (*22*). To improve contrast under ambient light, brightness has often been sacrificed, as with direct-view picture tubes in which a neutral-density absorbing glass is used to reduce the effect of the ambient illumination. Such glass is effective because the ambient light is diffused by the white phosphor and passes through the faceplate twice, while light emitted from the phosphor passes through only once. In more recent designs of shadow-mask tubes, a black matrix surrounds the phosphor dots (*20*), thereby reducing the need for absorption in the glass and permitting greater brightness. In darkness, the contrast ratio of direct-view picture tubes is limited by electron and optical scattering to the order of 50:1, but this contrast ratio can give an excellent picture. Projected pictures usually have a lower contrast ratio than this. Many home direct-view picture tubes are viewed with about 250 lux ambient illumination and have a contrast ratio of under 10:1; yet this condition is accepted.

* 1 footlambert (fL) = 3.43 cd/m² = 3.43 nits.

Human perception of absolute color hue and saturation is extremely diverse, both because of individual variations and because the eye is primarily conscious of color differences and not of absolute color. On the other hand, a color television system must be designed to permit a relatively high degree of color fidelity. Fortunately, only three primary colors are sufficient; if there is a match between the primaries at the camera end and those used for the picture reproduction, accurate colors will result and perceived color differences will be equally correct. Using the International Commission of Illumination chromaticity diagram shown in Fig. 2.2 (known as the CIE diagram), the entire range of colors observed by the normal eye is found within the horseshoe-shaped figure (*32*). Any color may be represented by the x, y coordinates in this diagram, with the hue angularly displaced around the central "white" region and the saturation increasing from the center out to the curved border. Combinations of two colors lie on the line joining their two coordinate points. The three primary points specified for most color television systems throughout the world are indicated on the diagram by open circles and, except for a region in the green-cyan range, cover enough of the area to produce very satisfactory color accuracy. The "white" point for the system is also indicated and corresponds closely to the radiated color of a blackbody at 6500°K, an approximation to daylight.

For the reproducer to do maximum justice to the system, its primary colors should correspond with the system primaries. Phosphors available for color picture tubes permit this, but not always under highest efficiency, i.e., maximum brightness. For this reason, compromises are usually made, particularly for the red and the green phosphors. The adaptability of the viewer and the propensity of most viewers to trade off some color fidelity for brightness have led to acceptance of picture-tube colors displaced from the specified system, as indicated in Fig. 2.2 by the crosses and the dashed triangle joining them. The greatest loss of saturated color is in the cyan-to-green region, but a brighter picture is obtained with excellent color fidelity in the red-to-yellow-green region. Fortunately, it has been shown that few objects and scenes require the missing region of color (*22*). In the United States, because there has been a consumer preference for a very bluish "white" for monochrome television, color receivers are normally adjusted for a white point close to the 9300°K blackbody point, another expedient deviation from the system. It is likely that, as color becomes predominant in television and improvements are made in phosphors, the white point and the three primary colors will eventually match those for which the system was designed.

With all systems of color television, the reproducer with its associated circuits must be controllable independently for each color primary. The

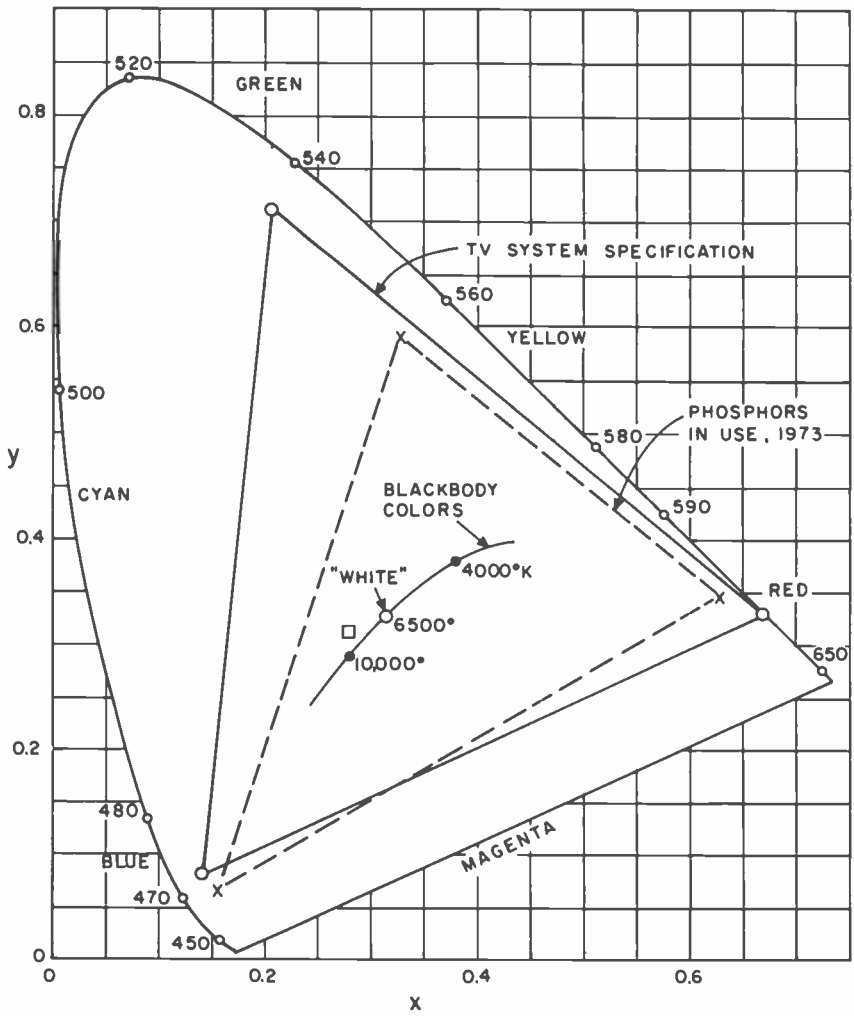

Fig. 2.2. The CIE color diagram. The specified color system primaries and white point are shown by the open circles. Typical United States color picture tube phosphors are shown by crosses and the frequently used white by the square.

color produced with any one or any fixed arbitrary combination of the three primaries must be uniform over the entire picture area. The white balance, i.e., the combination of the three primaries to produce white, must be either controllable or fixed at a point in the CIE diagram suitable for the system. In addition to these requirements, the white balance and

the color uniformity must be invariant with the light output, from dark to bright. For example, in a picture tube that uses three electron beams, one for each color, this requirement imposes close similarity in the control characteristic for each of the beams. It is much more easily achieved if the phosphors have spectral characteristics and efficiencies such that the white balance is obtained with equal current from each beam.

All commonly used color television systems, in order to improve signal-to-noise ratio (and for other reasons as well), transmit an electrical signal that is not linearly proportional to the desired light output at the reproducer. Instead, the signal has an amplitude compression that corresponds to a fractional power law, where the exponent is approximately 0.46, otherwise known as a "gamma" of 0.46. In a color television system, true color fidelity requires restoration of proportionality so that the reproduced luminance is proportional to the original luminance. For this reason, the transmitted signal, with its gamma value of 0.46, must be expanded by a 2.2 power law (the reciprocal of 0.46) to produce the brightness variations in the reproduced picture. Fortunately, this expansion is easily done by the electron gun used for most color television picture tubes. Experimentally, it is found that practical gun designs have a nonlinear light output vs. control signal characteristic that approximates a power law with an exponent somewhere between 2 and 3. Because the contrast range in practical systems is limited to about 50:1, this is transmitted in compressed form by a voltage range of $50^{0.46}$:1 (or about 6:1). Thus, the signal range over which the picture tube gun must approximate the desired 2.2 power law is not large. Furthermore, the signal amplitude is adjustable (this is done by the contrast control and video drive circuits in TV receivers), and so is the background level (adjustable by the brightness control). When these degrees of freedom are included, it is found that picture-tube guns can be made to approximate the desired gamma value of 2.2 within the signal limits of importance. Practical guns used in picture tubes, therefore, are capable of faithful color rendition, even though they may not have constant-power-law characteristics. In any picture reproducer having a radically different relation between light output and signal than that of the cathode-ray tube, electrical gamma compensation must be introduced.

The last requirement of a color picture reproducer is pertinent only when the viewed picture is a superposition of three separately generated pictures as, for example, in the common shadow-mask tube, or in three superposed projected pictures. This final requirement is coincidence. The separate images should be in coincidence, preferably up to the limit of resolution, and they must stay in coincidence at any brightness level

and over the entire picture area. Fortunately, minor deviations from coincidence are not noticeable at larger viewing distances. The effect is also less critical than one might suppose because so much of the luminance information is contained in the green signal, and the color acuity of the eye is less for small detail in the other colors. In practice, coincidence has not been a problem when color television pictures are reproduced by well-designed and well-adjusted shadow-mask tubes or separately projected color images.

CHAPTER 3

Classification of Methods for Color Picture Reproducers

An earlier paper (*1*) reviewed many color picture tube proposals in the patent literature prior to 1951. The ideas are extensive and most of them are no longer considered feasible. In this chapter, we shall confine ourselves to a general classification of methods that are still of interest, putting them in perspective. Detailed description follows in Chapters 5–9 and the reader is also referred to these chapters for literature references.

The most obvious way of producing a color television picture is to superpose optically three separate pictures, one for each primary color. This method is still used in large-screen projection systems, and it was once even used for experimental home receivers. However, a large and unattractive bulk is needed for mirrors or for other optics. Much more interesting are methods in which the superposition of the three pictures is direct, as on the face of a picture tube. One way to accomplish this is to segment color phosphors into small triplet groups or triads, with one phosphor element of each triad for each primary color. When such a screen is viewed at a distance, the red, green, and blue pictures appear superposed even though they are actually produced by closely spaced fine lines or dots. A second class of device uses a nonsegmented or continuous phosphor screen that has several color layers. The same spot on the screen can produce any primary color (or a combination of colors) by varying the electron beam velocity, hence its penetration into the layers.

3.1 Segmented Phosphor Screens

Returning to the first class of device with its segmented phosphor screen, it is necessary to have independent control of each color. If scanning

of the electron beam were sufficiently accurate, one could assume that the beam position would be exactly determined at any given time. In that case, one could rely on the scanning linearity to register the electron beam with the proper color. The incoming color signals could then be programmed so that the beam intensity is exactly correct for a given primary at exactly the time the beam is striking that color phosphor. Attempts were made to do this, both with horizontal stripes of alternate red, green, and blue (R, G, B) phosphor and with similar vertical stripes, but it was much too difficult to get the required accuracy. For this reason, all the surviving methods that employ a segmented screen make use of some auxiliary structure at or near the phosphor screen and in accurate register with the color triplets, whether they be stripes, dots, or any other shape. As we shall see, this structure eliminates any need for extremely accurate scanning.

3.1.1 The Shadow-Mask Tube

The auxiliary structure at the screen that has been most successful is that of the shadow-mask tube. In this type of color picture tube, three closely spaced electron guns produce beams that pass through holes or slits in a metal mask where the mask is spaced apart from but close to the phosphor screen. Mask and phosphor screen are at the same voltage, so the electrons travel in essentially straight lines. At the point where the electrons from one of the guns impinge on the screen, one of the color phosphors is deposited in a spot or line that approximates the size of the mask opening. All other parts of the phosphor screen are in the "shadow" of the phosphor mask, as far as this one gun is concerned. The guns are separated in such a manner that the three color phosphor segments do not overlap. Each gun controls the light from only one phosphor, so the tube can be thought of as three cathode-ray tubes, physically interlaced in the same envelope and with the same deflecting system. The tube is useful for any incoming television signal that can be separated into red, green, and blue components, one for each gun, and so has wide flexibility.

The principle of the shadow-maks tube is illustrated in Fig. 3.1 in two different forms. In one case, round openings in the mask are used and the phosphor dots are also round. This structure is the original form of the shadow mask and as of 1973 is still predominant. Another form uses a mask having elongated slits and a faceplate on which vertical lines of alternately red, green, and blue emitting phosphors are deposited. Although only center lines are shown in Fig. 3.1, in each case there are three electron beams that originate from three independent electron guns (one for each color). These guns are closely spaced, and the electron beams make

an angle of only 1° with each other as they pass through the shadow mask. A single system deflects all three beams, and the three beams converge to approximately the same point on the screen. With the circular hole and its round phosphor dot, the most common gun configuration is a triangle or delta arrangement. The slit shadow mask uses in-line guns. Since the electron-beam spot usually covers more than one opening in the shadow mask, the phosphor dots or the phosphor line widths are smaller than the electron beam spot. As a result, screen structure is not generally noticed in normal picture viewing.

In both the hole and the slit arrangements, it is necessary that each electron beam strike only one color at all deflection angles. The tolerance built in to assure this condition requires either that the phosphor dot or line be slightly larger than the mask opening (known as positive tolerance), or that each individual phosphor area be smaller than its corresponding mask opening (known as negative tolerance). In either case, a slight shift

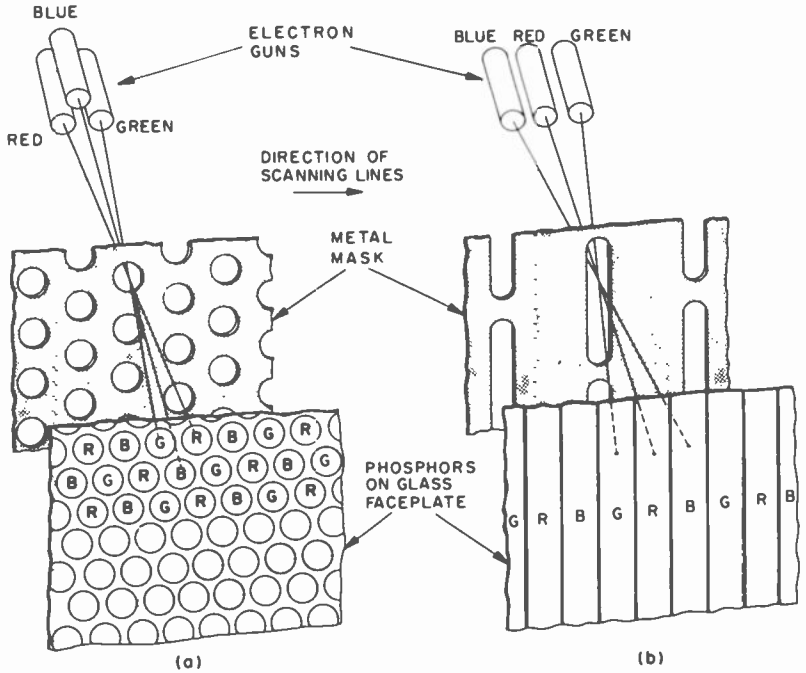

Fig. 3.1. Schematic of two shadow-mask systems: (a) with round holes and delta guns and (b) with slit openings and in-line guns. In actual tubes, mask and faceplate are curved.

in beam landing does not change the brightness or the color purity. To improve contrast, all screen areas not covered by phosphor may be coated with black inert material (called a matrix); alternatively, the faceplate glass may be tinted with a neutral gray. The brightest pictures are obtained with nearly transparent glass using a black matrix. Other factors that contribute to brightness are a high voltage on the phosphor screen and a large deflection angle. The large angle allows a reduction in gun-to-screen distance which minimizes spot size at high currents.

The complexities of process technology and the details of shadow-mask tube design defy simple description and the reader is referred to Chapter 5 in which these matters are discussed in detail. Suffice it to say here that, because the electron shadows and the shadows of a light beam are almost identical, the phosphor areas can be located by photodeposition, and this has been the clue to successful mass production.

3.1.2 The Focus-Mask Tube

It is evident from Fig. 3.1 that much of the electron beam is intercepted by the shadow mask and never reaches the phosphor screen to produce light. If the phosphor-dot screen shown in Fig. 3.1 is operated at a higher voltage than that of the shadow mask, the electrons will no longer travel in straight lines beyond the mask and will be focused into a spot smaller than the shadow-mask opening. Each opening acts as a focusing lens. Because of this focusing action, the round apertures in the mask of Fig. 3.1 can be enlarged and yet the electrons will not exceed their intended phosphor area. The larger apertures greatly reduce the beam current intercepted by the shadow mask and increase picture brightness correspondingly. In some forms, the focus mask consists of a grill of vertical wires (with corresponding vertical phosphor stripes) rather than a mask with round apertures (*10*, *11*). This variation is sometimes known as the focus-grill tube.

Unfortunately, the simple focus-mask principle has disadvantages and has not had wide use as of 1973. Because the mask apertures are much larger than the phosphor elements, simple photodeposition techniques for forming the phosphor screen are no longer applicable, and mass production with uniform performance is much more difficult. Another disadvantage is the undesired excitation of phosphor areas by secondary electrons scattered from the mask (or generated at the phosphor screen and reflected back to other areas). These undesirable effects are caused by the phosphor screen being operated at a much higher voltage than the mask. In a simple focus-mask tube the scattered electrons reduce the contrast and dilute the colors; but with more complex structures that use

an additional grill of wires (*12*), these effects can be overcome. The entire subject is treated in detail in Chapter 6.

One version of the focus-mask tube (*10*) uses only a single electron beam with a coplanar dual vertical grill of wires and vertical red, green, and blue phosphor stripes aligned with the wires. In this version, every other wire is connected electrically to form a two-electrode deflecting system. These deflecting electrodes are driven with a high-frequency alternating voltage; the single electron beam is then deflected in synchronism with a corresponding color control signal on the gun. This type of color picture tube shares the disadvantages of other focus-mask tubes and, in addition, requires a relatively high-power radio-frequency deflecting source that must be carefully shielded in order not to produce radio-frequency interference. The design principles for such tubes are also covered in Chapter 6.

3.1.3 Beam-Index Tubes

As we have seen, each of the above segmented phosphor screens requires a nearby structure, the shadow mask or focus mask, in exact register with the phosphor segments. If the register structure is coplanar and integral with the phosphor screen, a much simpler tube results. Such a structure

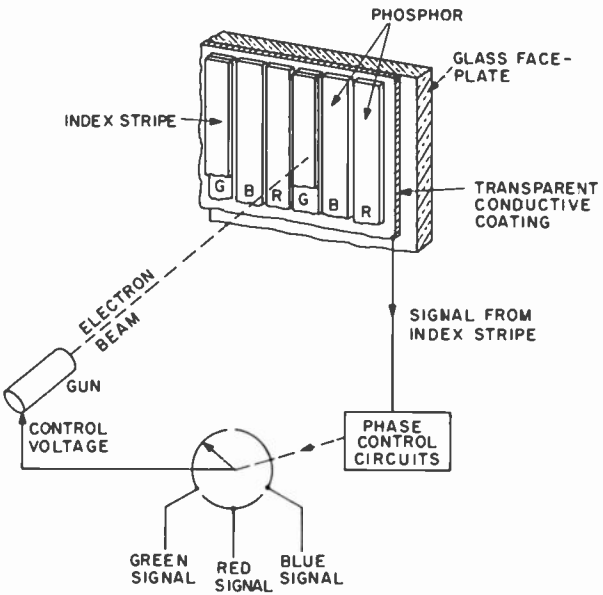

Fig. 3.2. Beam-index tube principle. Deflection system is not shown.

is used in the beam-index tube, which uses fine vertical stripes of phosphor resembling those shown for the slit shadow mask in Fig. 3.1b. As shown in Fig. 3.2, the faceplate is covered with alternate vertical red, green, and blue phosphor stripes separated by a guard band of black inert material. In register with these stripes is an index stripe, which may be on every green stripe as shown, or spaced in some other manner bearing a rational numerical relationship to the phosphor periodicity.

In the beam-index tube there is no image coincidence problem because only one electron beam is necessary, and the electron gun and deflection system are superficially not much more complex than in a black-and-white picture tube. The purpose of the index stripe is to produce a signal that can be used to phase an electronic switch, shown in Fig. 3.2 as if it were a rotating mechanical switch. At exactly the time that the electron beam is striking any one color phosphor, the switch connects the electron gun to the appropriate color signal. Thus, in distinction to the three-gun shadow mask, in the beam-index tube the colors are produced in time sequence, red, green, blue, one after the other.

In spite of its apparent simplicity, other difficulties handicap such a picture tube system. Whereas in the shadow-mask tube the phosphor segments can be much smaller than the electron beam spot, in the beam-index system the spot must be sufficiently small so that the beam will not strike more than one color at a time. Thus, the stripes must be either coarser and more visible or the electron beam current must be limited to avoid spot-spreading and loss of color purity. Because the index signal is generated by the electron beam (for example, producing secondary electron emission or radiation from an ultraviolet phosphor), the beam current cannot be reduced to zero or phase information for the electronic switch will be lost, thus limiting the picture contrast. Although no electron beam current is lost to an intercepting shadow mask, the three colors must share the same beam, and picture brightness may therefore not be superior to that of shadow-mask tubes. Above all, whereas the three-gun tubes have built-in color separation, the beam-index system is entirely dependent on somewhat complex external circuitry for correct color switching. Beam-index systems have been demonstrated in the laboratory, but, as of 1973, they have not become a commercial product.

3.2 Uniform Phosphor Screens (Penetration Tubes)

It is possible to produce more than one color from a transversely uniform (unsegmented) phosphor screen if the screen consists of three thin layers of different color phosphors as shown in Fig. 3.3. An electron beam will

penetrate into such layers more or less deeply, depending on its velocity. By control of beam current the luminance is varied, and by changing the beam velocity the color can be varied. Such velocity-sensitive screens can be made either by three uniform layers, one on top of the other as shown in Fig. 3.3, or by a single layer in which each small phosphor particle contains three layers. In either case, the light generated by one layer should not be absorbed by other layers. More saturated color primaries are often produced by inserting barrier layers between the phosphors. This method of making color picture tubes has been used experimentally with both a single electron beam and with three closely spaced adjacent separate beams of different velocities. The single-beam tube requires time sharing of the three colors and high-speed switching of very high voltages. The three-beam type involves difficulties in deflection and coincidence of images. Commercial manufacture of either type has been limited to displays other than for television.

3.3 Other Methods

Experimental direct-view tubes of many other kinds have been tried, and it is worth mentioning the endeavors to change the form-factor of the conventional picture tube. For this, a quasi-flat structure has received much attention, with an electron beam entering approximately parallel, instead of perpendicular, to the phosphor screen. The deflection systems are then required to bend the beam sharply so as to strike the appropriate phosphor segments. Severe practical difficulties have prevented commercial exploitation as of 1973.

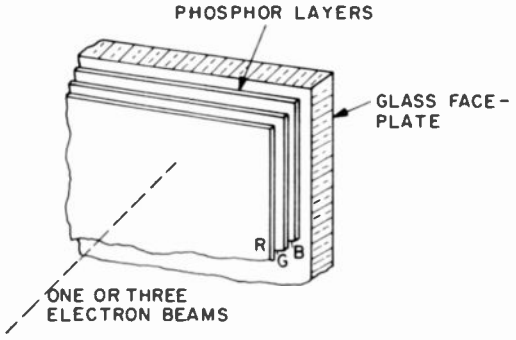

Fig. 3.3. Schematic of penetration tube. When three beams are used, each has a different velocity. With one beam, it is switched in time sequence to three different velocities.

For large-screen color television displays (for example, greater than 1 m), projection systems are the only ones that have achieved success. The first one to be used consisted of three small picture tubes, each of a different primary color. The three pictures were simultaneously projected in superposition on the screen. With large-aperture optics, such as Schmidt systems, adequate brightness can be achieved for modest-size screens viewed in the dark. Another approach has been to use a single three-color picture tube in an optical projection system, but this is even more limited in the attainable brightness.

For the largest screens and brightest pictures, various light valve systems have been proposed, notably the Eidophor. This system consists of an oil film on which small surface deformations are produced by the electrostatic forces resulting from electric charges deposited by a scanning electron beam. The diffraction by the film of light from an external source, together with a schlieren optical system, produces the projected picture. Three complete light valves, one for each primary color, may be used for producing color pictures by optically superposing the color pictures. Although such a system can produce high quality pictures, it is very costly. A more sophisticated light-valve arrangement for color television projection has also achieved commercial use. In this method, a single high-resolution electron beam is used to scan the oil film, and the scanning beam produces at each picture element three diffraction gratings of different spacing and direction. One of these, for controlling the green primary light, consists of the adjacent lines of the scanning raster itself whose sharpness is locally modulated. The other two consist of lines perpendicular to the scanning lines produced by high-frequency modulation of the electron beam. These gratings cause the three color components of a white light source to be diffracted at different angles at the surface of the oil film. Using the schlieren system, the intensity of each component is controlled by the beam modulation that produces the grating effect.

CHAPTER 4

Limiting Factors on Screen Brightness in Picture Tubes

The preceding chapter described a variety of ways in which color television pictures may be reproduced. Most of them use cathode-ray-tube technology based on deflection of an electron beam that strikes a phosphor screen. These share some general limitations. There are other limitations that depend on the type of tube.

To produce a sharp and bright picture, an electron beam should carry large current and form a small spot at the phosphor screen, resulting in high current density. The current must also be controllable down to a negligible value by a signal voltage. An electron gun producing such a spot generates a small source of electrons that is imaged by an electron lens into the spot on the screen. Since a deflection system of minimum power is desirable, the active deflection volume should be small, requiring a gun of small diameter. If the tube is to be short, the gun cannot be long, and the deflection angle must be large. Some of these requirements are mutually contradictory. This chapter describes the limits to which an optimal compromise is subject. There are some simple fundamentals that lie behind these limits.

(1) The spot at the screen has a current density that depends on that of the cathode, so that maximum cathode current density is desirable.

(2) The spot at the screen becomes smaller and the current density greater when the image distance of the main lens is decreased, corresponding to a larger deflection angle for fixed picture size. A large deflection angle, however, requires large deflection power.

(3) The spot at the screen becomes smaller and the current density greater when the object distance of the main lens is increased or the gun is

made longer. A longer gun increases the tube length and the required electron lens diameter.

(4) The spot at the screen can be made smaller if the lens aberrations are reduced. This requires a large lens diameter and correspondingly large deflection power.

(5) High light outputs and small spot diameters are achieved with high screen voltages; these require large deflection power.

Compromises are obviously needed in any practical design. Additional limitations, calling for further compromises, occur (a) when three beams are used in a single envelope, as with the shadow-mask tube, and (b) when a single gun must reproduce the three primary colors in time sequence, as with the line-screen index tube. The basic limitations on screen brightness for all these cases are the subject of Chapter 4.

4.1 Beam Current Limits in Cathode-Ray Tubes

Functionally, the electron gun in a cathode-ray tube may be regarded as composed of a beam-forming system, which concentrates the electron emission from the cathode so as to form a narrow beam constriction or crossover, and a "final lens," which images the crossover onto the screen, forming the scanning spot (Fig. 4.1). The crossover radius is given by the product of the focal length of the beam-forming region and the ratio of the average initial velocity of the electrons (determined by the effective cathode temperature) to the electron velocity at the crossover. To a first approximation, it is independent of the diameter of the emitting area of the cathode and of the convergence angle at the crossover, which is proportional to this diameter. Similarly, the magnification of the crossover by the final lens is given simply by the product of the ratio of the image and object distances of the final lens and the ratio of the electron velocities at the crossover and at the screen and is thus, also, independent of the convergence angle at the crossover and the cathode area contributing to the beam. It might be concluded that the contributing cathode area and the covergence angle at the crossover could be increased indefinitely without increasing the spot size on the screen. However, the spot diameter is not simply the product of the crossover diameter by the final-lens magnification, but is augmented, as a result of the aberration of the final lens, by an amount proportional to the third power of the convergence angle at the crossover.

As a result, referring once again to Fig. 4.1, there is an optimum convergence angle α_1 for any prescribed spot diameter d_s [Eq. (4.19)]* and the maxi-

* Reference is made to equations appearing at a later point in the text to give the reader insight into the quantitative relationships without demanding familiarity with their derivation.

mum beam current within the spot is proportional to the 8/3 power of the spot diameter [Eq. (4.21)].

The maximum spot current for prescribed spot diameter also depends on the aberration constant of the final lens. This aberration constant Cf_2 is primarily a function of the clear or unobstructed diameter D of the electrodes (or pole pieces) of the final lens and of its focal length f_2 and depends relatively little on the lens type. Thus, substitution of the relationship between the aberration constant and the clear diameter and focal length for a favorable and commonly used lens type (the equidiameter-cylinder accelerating lens) leads to a generally valid expression for the upper limit to the beam current set by thermal spread and lens aberrations, in terms of cathode emission j_0, cathode temperature T, screen voltage V, and geometrical parameters [Eqs. (4.22) and (4.24)].

Thermal spread and aberration are not the only factors which limit the current that can be concentrated in a spot of given dimensions. Another factor is the mutual repulsion of the beam electrons, or the space-charge forces, in the drift region between the gun and the screen. The current limit established by space charge becomes significant at relatively high beam current values and is proportional to the 3/2 power of the screen voltage, the square of the convergence angle in the drift region, and to a universal function of the ratio of spot diameter to beam diameter at the entrance to the drift region [Eq. (4.27)].

The results of the mathematical analysis which follows are given not merely in the form of equations but are also represented graphically for a tube with 500 scanning lines in the picture with a picture diagonal of 635 mm (25 in.), 90° deflection, a screen voltage of 25 kV, a cathode temperature of 1160°K (characteristic of an oxide cathode), and a cathode emission of 1 A/cm². Figure 4.3 shows the upper limit to the beam current established by thermal spread and final-lens aberration, Fig. 4.8 shows the limit determined by space charge in the drift region, while Figs. 4.4–4.7 show the diameter of the emitting region of the cathode, the beam diameter at the final lens, the voltage ratio of the final lens, and the magnification of the final lens, respectively. Throughout, the quantity in question is plotted as a function of the clear diameter of the final lens, with the focal length of the beam-forming region as parameter. The focal length of the beam-forming region is determined by the dimensioning and spacing of the electrodes in the beam-forming region and by their potentials.

Figures 4.3 and 4.8 indicate the advantage of a large clear diameter of the final lens for achieving high beam current. It must be remembered, however, that the analysis of this chapter is limited to the undeflected beam. With deflection (particularly, deflection through large angles), both the power needed for deflection and the aberrations contributed by the de-

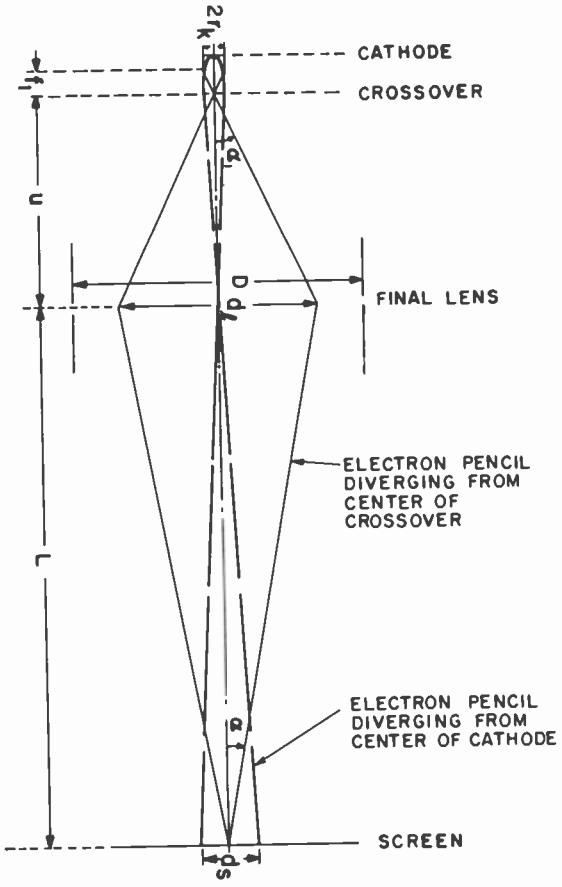

Fig. 4.1. Schematic diagram of electron-optical system forming the spot on the screen.

verge to (or appear to diverge from) a "crossover," which, in turn, is imaged electron optically on the screen to form the spot. The crossover is the point at which the "principal rays," or the electrons leaving points of the cathode with zero initial velocity, intersect the axis of the system. We can assign to the electric fields forming the crossover, or to the "first lens" of the electron gun, a focal length f_1, defined by

$$f_1 = r_k/\sin \alpha_1 \tag{4.6}$$

Here α_1 is the angle of inclination at the crossover of a principal ray leaving a cathode point a distance r_k from the axis. The crossover is at object dis-

tance u from the object-side principal plane of the "second lens" or "final lens" of the gun, and the screen lies at image distance L from the image-side principal plane of the same lens. If the potential at the crossover is V_1, the magnification of the spot with respect to the crossover is given by

$$M = L/u(V_1/V)^{1/2} = \sin \alpha_1/\sin \alpha(V_1/V)^{1/2} \tag{4.7}$$

Here α and V are the angle of convergence and potential, respectively, at the spot.

The preceding description is always valid, irrespective of the complexity of the imaging system of the gun, provided that axial symmetry is maintained. It is true that the parameters f_1, u, L, and M are constants only for small values of α and the corresponding quantities α_1 and r_k. For larger angles of inclination it is necessary to take account of the "spherical aberration" or aperture defect of the electron-optical system. Analytically it is then still convenient to treat the crossover as aberration-free and to include the aberration of the first lens in the aberration of the final lens system.

D. B. Langmuir (*33*) has shown that for an aberration-free system with a cathode with uniform emission current density j_0 on an emitting area of radius r_k, the current distribution at the crossover is given by

$$j_1(r_1) = j_0 \sin^2 \alpha_1 \frac{eV_1}{kT} \exp\left(-\frac{eV_1}{kT}\frac{r_1^2}{f_1^2}\right) \tag{4.8}$$

Here e is the magnitude of the electron charge.

Similarly, the current in the spot is given by

$$j(r) = j_0 \sin^2 \alpha \frac{eV}{kT} \exp\left(-\frac{eV}{kT}\frac{u^2}{L^2 f_1^2} r^2\right) \tag{4.9}$$

It will be noted that the emitting area of the cathode does not affect the current distribution in either case, but only the magnitude of the current, through the factors $\sin^2 \alpha_1$ and $\sin^2 \alpha$, respectively. Every point of the cathode contributes an identical gaussian distribution with a (1/e) radius $f_1(kT/eV_1)^{1/2}$ or $f_1(L/u)(kT/eV)^{1/2}$, respectively.

The quantity $\sin \alpha$ is related to the emitting radius r_k of the cathode by Eqs. (4.6) and (4.7) only if there are no current-limiting apertures in the system. However, Eq. (4.9), with α signifying the actual convergence half-angle of the electron pencils at the screen, is still completely valid if the limiting aperture is in the plane of a cathode image. The coefficient $j_0 \sin^2 \alpha(eV/kT)$ represents the current density at the center of the spot formed by the aberration-free system even if the last-mentioned condition is not satisfied.

Equations (4.8) and (4.9) assume uniform current density in the emitting area of the cathode. This condition is never satisfied. Even if the emission at the center of the cathode is saturated, space-charge limitation effects an emission reduction before the periphery of the emitting region is reached. In analogy with a simple plane diode we can assume that, under conditions of space-charge limitation, the emission current density is proportional to the 3/2 power of the field at the cathode surface in the absence of space charge.

The radius r_k of the emitting region and the field at the surface of the cathode can be simply derived from the familiar expression for the potential distribution in an axially symmetric system

$$V(z, r) = V(z, 0) - \tfrac{1}{4}V''(z, 0) \cdot r^2 + \cdots \tag{4.10}$$

Here z is the distance from the cathode along the axis, r is the distance from the axis, and primes indicate differentiations with respect to z. Accordingly, the field at the cathode surface is given by

$$V'(0, r) = V'(0, 0) - \tfrac{1}{4}V'''(0, 0) \cdot r^2 + \cdots \tag{4.11}$$

$$\cong V'(0, 0)\{1 - r^2/r_k^2\} \tag{4.12}$$

with

$$r_k = 2[V'(0, 0)/V'''(0, 0)]^{1/2} \tag{4.13}$$

Since, as Ploke (*34*) has shown in greater detail, $V'(0, 0)$, the field at the center of the cathode in the absence of space charge, is proportional to the drive voltage, the product of the current density (which, with space-charge limitation, is proportional to $V'(0, 0)^{3/2}$) and emitting area, or the total cathode current, becomes proportional to the 2.5 power of the drive voltage. In terms of the current density at the center of the cathode, the total cathode current is given, in accord with Eq. (4.12), by

$$I_k = \int_0^{r_k} j_0(1 - r^2/r_k^2)^{3/2} 2\pi r \, dr = 0.4 j_0 \pi r_k^2 \tag{4.14}$$

In the absence of current-limiting apertures, Eq. (4.14) represents also the total current in the electron beam. In this case, space-charge limitation reduces the expressions in Eqs. (4.8) and (4.9) by a factor 0.4.

The cathode area which can be utilized for beam formation is in practice limited by the spherical aberration of the final-lens system. If the spot is focused to the narrowest constriction of the imaging pencils, the spot image is extended radially by an amount

$$\Delta r_s = \tfrac{1}{4}C f_2 \alpha_1^3 [(M + 1)^4/M^3] \tag{4.15}$$

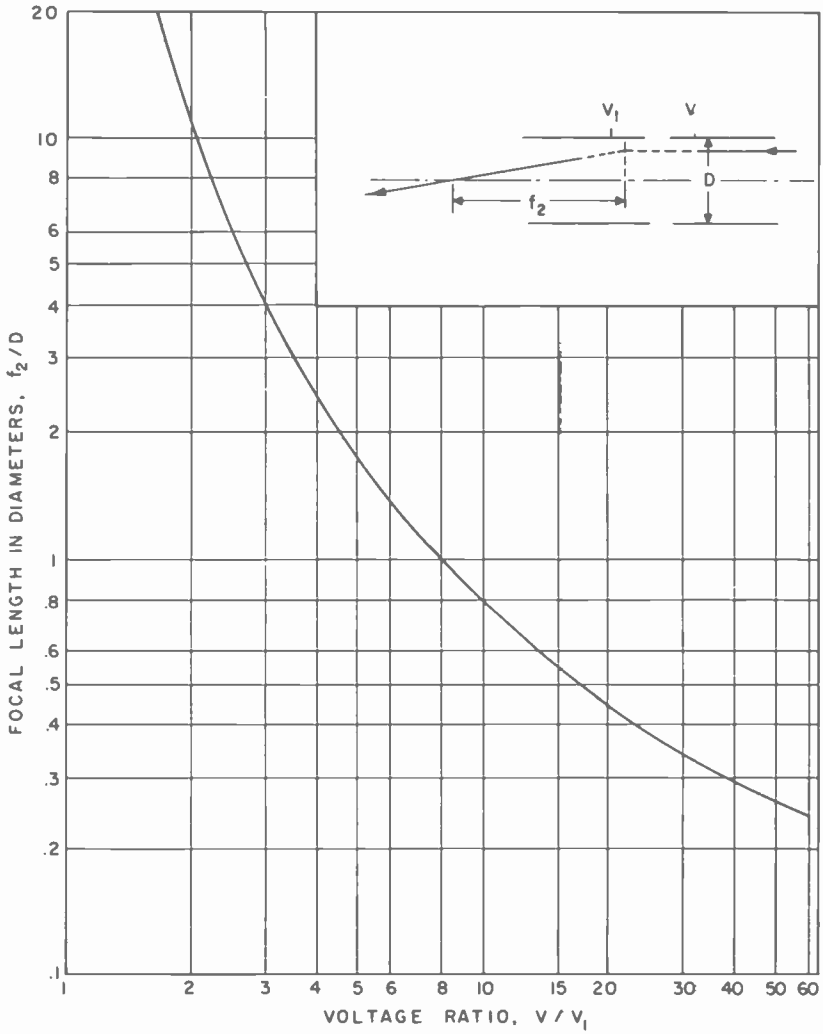

Fig. 4.2. Low-voltage-side focal length of equidiameter cylinder accelerating lens as function of voltage ratio (D is the internal diameter of cylinders).

Here Cf_2 is the spherical aberration constant of the final lens. It has been found (*35*) that the dimensionless coefficient C is given by a functional variation of the form

$$C = \text{const}(f_2/D)^n, \qquad f_2/D \gg 1 \tag{4.16}$$

with practically the same value for the constant factor and the exponent n for a wide range of electrostatic and magnetic lenses. D represents the clear diameter of the electrodes or pole pieces forming the lens. More specifically, data given by von Ardenne (*36*) for the commonly used equi-diameter-cylinder accelerating lenses yield

$$C = 6.8(f_2/D)^{1.78} \tag{4.17}$$

The superposition of spherical aberration on the gaussian aberration-free spot distribution is quite complex. We shall, as a convenient approximation, assume that the geometric spot width and the spot width owing to spherical aberration add quadratically. We select the convergence angle α_1 so as to maximize the total current to the effective spot area,

$$I_s = 0.4\pi j_0 \frac{r_{s0}^2}{M^2} \frac{eV_1}{kT} \alpha_1^2 \tag{4.18}$$

Here $r_{s0} = f_1(L/u)(kT/eV)^{1/2}$ is the aberration-free spot radius. With Eq. (4.15) we find for the value of α_1 which maximizes the spot current,

$$\alpha_1 = \frac{M}{M+1}\left[\frac{d_s}{(M+1)Cf_2}\right]^{1/3} \tag{4.19}$$

The effective spot area is then

$$\tfrac{1}{4}\pi d_s^2 = \tfrac{4}{3}\pi r_{s0}^2 \tag{4.20}$$

The optimum beam current is given by Eq. (4.18), substituting α_1 from Eq. (4.19). We find

$$I_{s,\,opt} = \frac{0.3}{4}\pi j_0 \frac{d_s^{8/3}}{[(M+1)Cf_2]^{2/3}} \frac{eV}{kT} \frac{f_2^2}{L^2} \tag{4.21}$$

With Eq. (4.17) we obtain

$$I_{s,\,opt} = 0.066 \frac{D^{1.186} f_2^{0.814}}{L^{2.667}} d_s^{2.667} \left(\frac{V}{V_1}\right)^{0.333} \left(\frac{11{,}600V}{T}\right) j_0 \tag{4.22}$$

The spot current is thus proportional to the 8/3 power of the spot diameter d_s, to the ultor voltage V, to the emission current density j_0 and approximately to the final lens aperture diameter D. Putting the spot diameter equal to the center-to-center scanning line separation,*

$$d_s = (1.2L \tan \theta_m)/N \tag{4.23}$$

* Setting the image distance L equal to the separation of deflection center and screen, we neglect the separation of lens principal plane and deflection center. This leads to an overestimate of the achievable beam current.

where θ_m is the half-angle of deflection and N is the line number (e.g., $N = 500$), we find

$$I_{s,\,opt} = 6.8 \times 10^{-9}(\tan\theta_m)^{2.667} D^{1.186} f_2^{0.814} (V/V_1)^{0.333} (11{,}600V/T) j_0 \quad (4.24)$$

The refractive power of the equidiameter-cylinder accelerating lens is given, according to Morikawa (*37*), by the expression

$$D/f_2 = 0.659 e^{x/2} x^2 (0.99998 - 0.1457x^2 + 0.01219x^4 - 0.00076x^6 \cdots) \quad (4.25)$$

with

$$x = \tfrac{1}{2} \ln(V/V_1) \quad (4.26)$$

This functional relationship is plotted in Fig. 4.2.

Figures 4.3–4.7 aim to give an idea of the numerical parameters of an electron gun in which the emission area of the cathode is matched to the geometric spot size so as to achieve maximum current in the spot. The tube is assumed to be a 90° deflection tube with a 635-mm screen diagonal, with

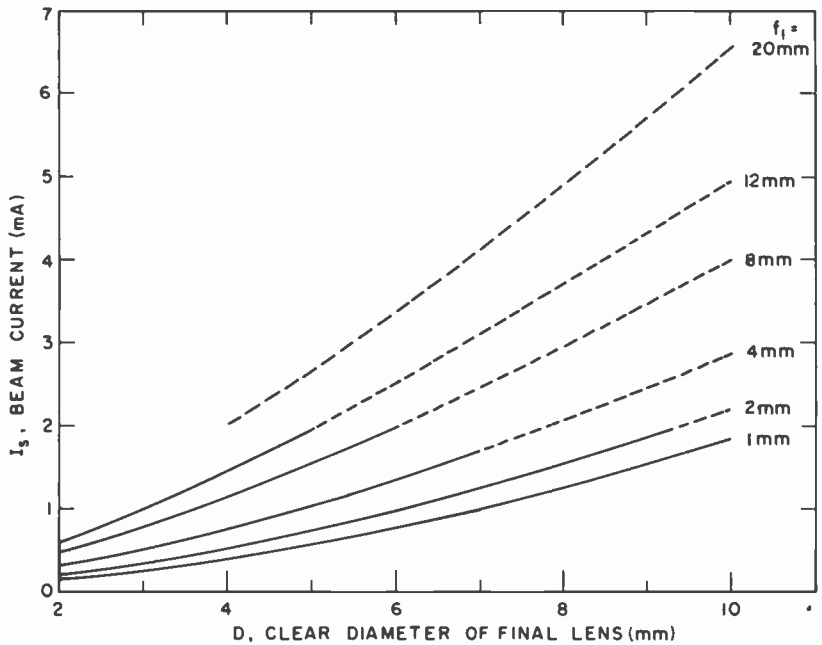

Fig. 4.3. Upper limit to spot current determined by initial velocity distribution of beam electrons. $j_o = 1$ A/cm²; $V = 25$kV; $N = 500$; $\theta_m = 45°$, picture diameter, 635 mm; hence $L = 317.5$ mm and $d_s = 0.762$ mm.

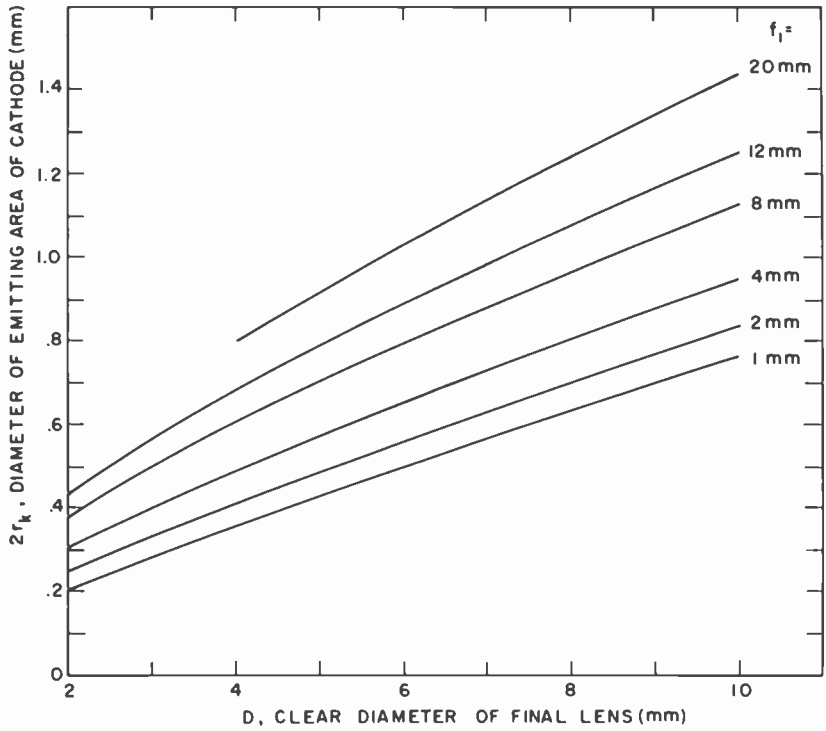

Fig. 4.4. Diameter of emitting area leading to curves in Fig. 4.3.

500 scanning lines, yielding [from Eq. (4.23)], $d_s = 0.762$ mm. A maximum cathode current density $j_0 = 1$ A/cm², an ultor voltage $V = 25$ kV, and an effective cathode temperature of 1160°K are assumed. The quantities plotted are the total beam current I_s, the diameter of the current-emitting area of the cathode, $2r_k$, the beam diameter at the principal planes of the final lens, the final-lens voltage ratio V/V_1, and the final-lens magnification M. The independent variable is the clear diameter D of the final lens (assumed to be a simple acceleration lens) and the parameter is the focal length f_1 of the beam-forming system.

The beam currents in Fig. 4.3 represent upper limits to the space-charge-limited current which can be approached if the gun design is optimized for any one indicated choice of the clear diameter of the final lens and focal length of the image-forming system. The remaining figures show the values which the other gun parameters take on for this choice.

The computations leading to Fig. 4.3 take account of space charge only insofar as it affects the variation in emitted current over the area of the

cathode. They do not, in particular, take account of the limitation of current which can be delivered in a spot of prescribed size imposed by space-charge spreading of the beam in the drift region between gun and screen. As shown, for example, by Schwartz (*38*), the space-charge limit to the spot current for a monocentric converging beam is given by

$$(I_s)_{\text{space-charge limit}} = V^{3/2}(d_1/2L)^2 F(d_s/d_1) \tag{4.27}$$

Here d_1 is the beam diameter at entrance into the drift space of length L, as shown for example in Fig. 4.5, and $F(d_s/d_1)$ is a universal function of the ratio of the spot diameter d_s to the initial beam diameter. A plot of this function is given by Schwartz.

A space-charge limit to the current as given by Eq. (4.27) has been plotted in Fig. 4.8 for the 635-mm 90° tube with $N = 500$ and the beam diameters given in Fig. 4.5. Comparison with Fig. 4.3 shows that space

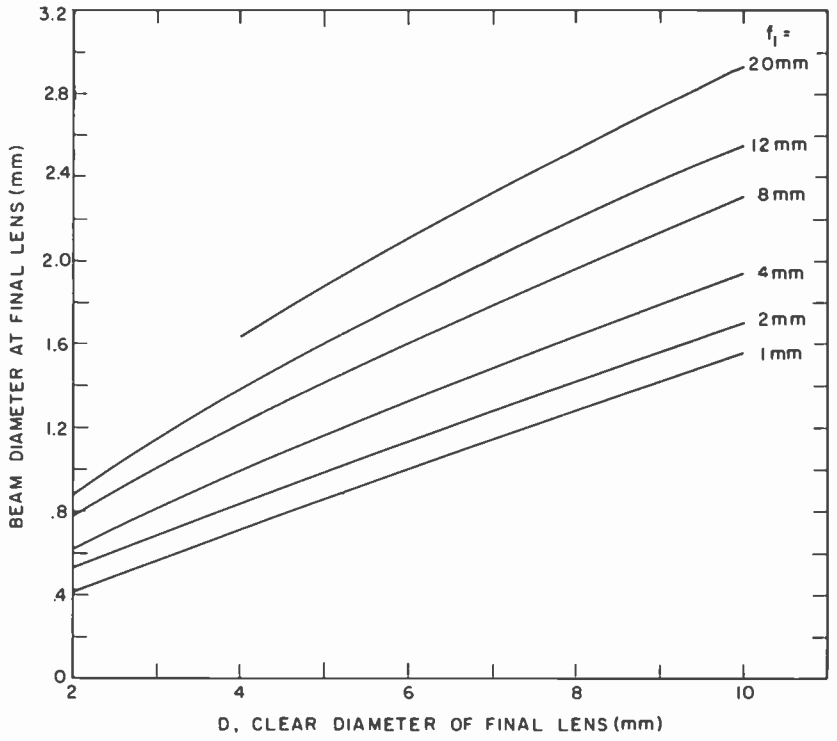

Fig. 4.5. Diameter of beam at principal planes of final lens for conditions leading to curves in Fig. 4.3.

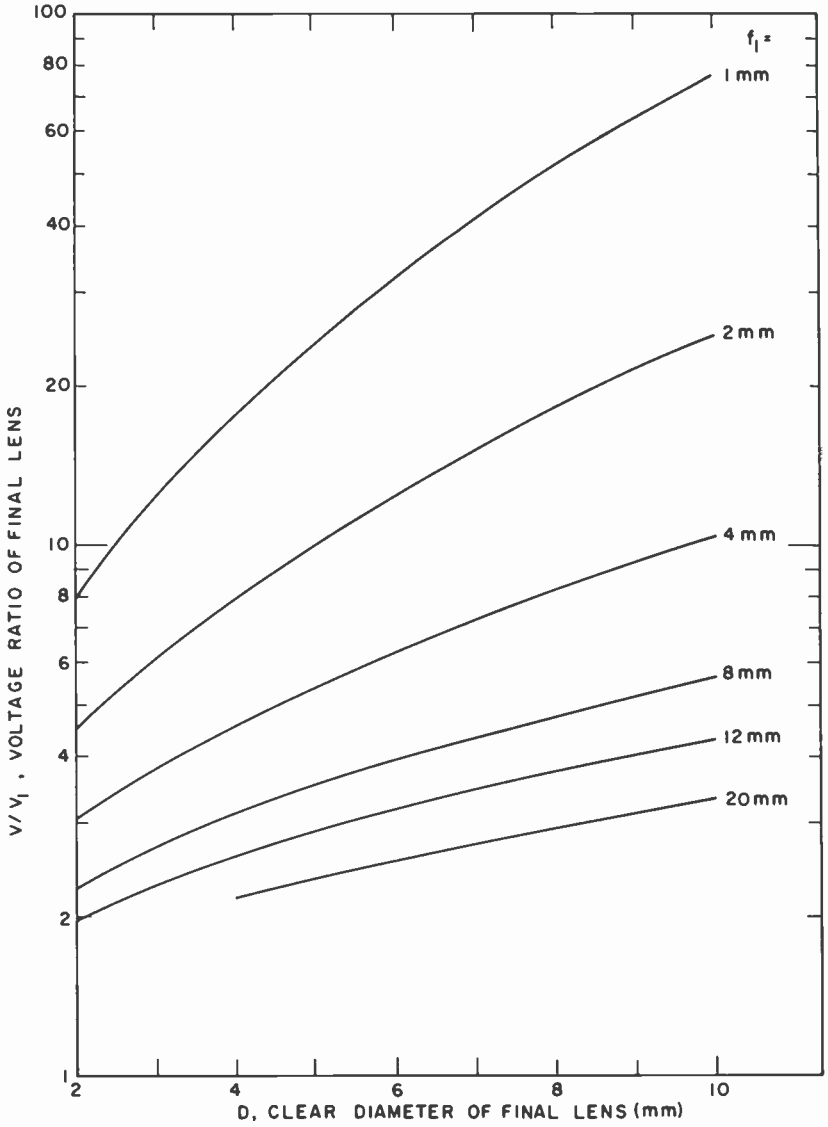

Fig. 4.6. Voltage ratio for equidiameter accelerating final lens for guns corresponding to Fig. 4.3.

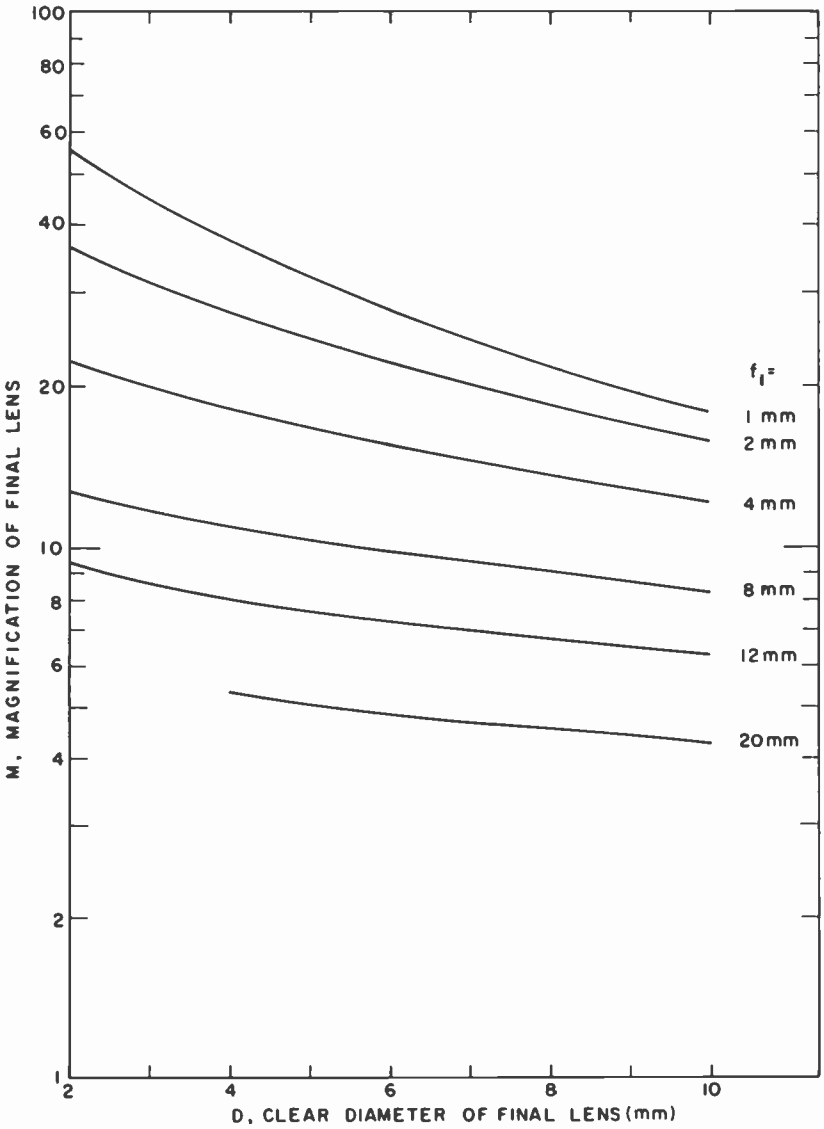

Fig. 4.7. Magnification of final lens corresponding to Fig. 4.6.

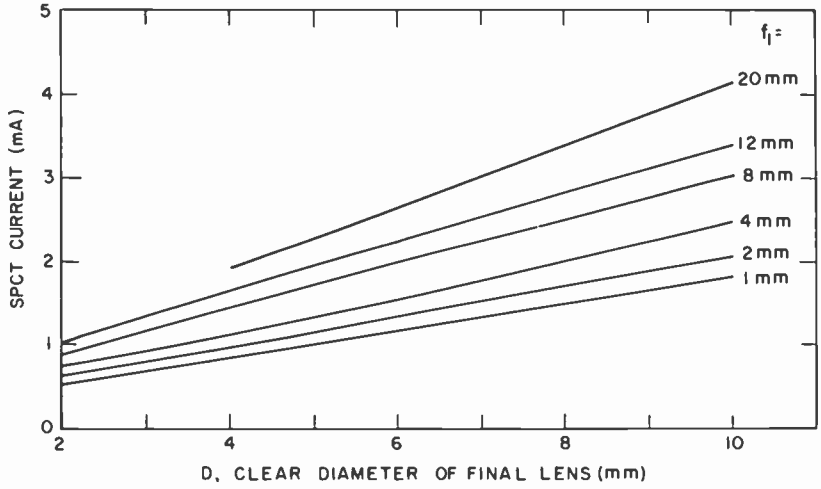

Fig. 4.8. Upper limit to spot current determined by space-charge spreading in drift region (for beam diameters at final lens given by Fig. 4.5).

charge imposes, for large values of the beam-forming system focal length f_1 and the clear diameter of the final lens D, a lower limit on the spot current than is imposed by the initial velocity distribution. This would no longer be true if the maximum emission density of the cathode were reduced to 0.5 A/cm². This would reduce the ordinates in Fig. 4.3 by a factor 2, but would have no effect on Fig. 4.8. The closeness of the space-charge limit to the thermal limit indicates, in any case, that proper consideration of space charge would lead to stronger final lenses at high currents and to upper limits to the spot current which are lower than those shown in Fig. 4.3.

4.2 Three-Beam Tubes

The screen-brightness considerations presented so far apply quite generally, and in particular also to black-and-white viewing tubes. In color viewing tubes employing three beams, there are two additional factors which reduce the attainable screen brightness. One of these, which will not be considered further at this point, is the replacement of the single white phosphor in the black-and-white viewing tubes by three red, green, and blue primary-color phosphors which do not possess as high an average conversion efficiency as the white phosphor. The other factor is the need to introduce some kind of mask to stop beam electrons which would otherwise

be incident on the "wrong" phosphors. The screen brightness is then reduced by a factor equal to the electron transmission of the mask. As will be seen in Chapter 6, electric fields at the mask may be used to reduce the diameters of the electron pencils transmitted by the mask apertures, permitting greatly increased mask transmission. In the simplest "focus-mask" tube designs the requirement of lower anode voltage and unfavorable contrast properties offset the gain in mask transmission.

The usual shadow mask (Fig. 4.9) has a hexagonal array of round apertures of diameter B and center-to-center separation a. The three-component electron guns form a triangular "delta" arrangement, so that the beam-cross-section centers in the deflection plane have a common separation s from the tube axis. We shall call the beam diameters in the deflection plane d_1, since they differ but slightly from the beam diameters at the principal plane of the final lens. The beam cross sections in the deflection plane, located a distance p from the mask, project onto the screen, a distance q from the mask, a set of electron spots. This set, ideally, coincides with an array of round phosphor dots having diameters D_s and covers the screen surface.

The condition that the dots corresponding to a single aperture form a contiguous triad may be written

$$D_s/\sqrt{3} = s(q/p) \tag{4.28}$$

and the further condition that the dot triads fit together or "nest" so as to

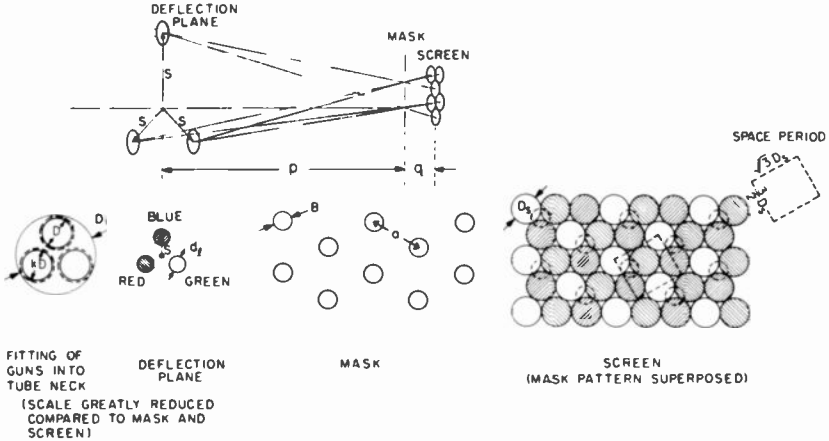

Fig. 4.9. Shadow-mask tube with hexagonal dot array; beam cross sections in deflection plane, mask pattern, and screen pattern.

uniformly cover the screen becomes

$$[(p + q)/p]a = \sqrt{3}D_s \tag{4.29}$$

Finally, the condition that the electron spots equal the phosphor dots in size determines the maximum value of the aperture diameter B consistent with the attainment of color purity,

$$[(p + q)/p]B + (q/p)\, d_1 = D_s \tag{4.30}$$

The maximum value T_m of the mask transmission,

$$T = (\pi/2\sqrt{3})B^2/a^2 \tag{4.31}$$

is obtained by substituting the value of B from Eq. (4.30) in Eq. (4.31),

$$T_m = (\pi/6\sqrt{3})(1 - d_1/s\sqrt{3})^2 \tag{4.32}$$

Let the inner diameter of the gun neck be D_i, the external diameter of the individual component gun be kD ($k > 1$), and the internal clear diameter of the final lens of the gun be D. Then, if the gun dimensions are made as large as possible (to minimize the spherical aberration), we have

$$D_i = kD(1 + 2/\sqrt{3}) = 2.154kD, \qquad kD = s\sqrt{3} \tag{4.33}$$

Hence, we can write in place of Eq. (4.32),

$$T_m = 0.302(1 - d_1/kD)^2 \tag{4.34}$$

Since the current reaching the screen* is proportional to d_1^2T, the optimum choice of d_1 in the absence of spherical aberration would be $kD/2$, leading to a mask transmission T_m of only 0.075. In practice, as shown in Fig. 4.5, spherical aberration limits d_1 to smaller values, ranging from $0.15D$ to $0.4D$. For example, for $d_1/kD = 0.3$, we would obtain $T_m = 0.15$. Shadow-mask tubes with screens fully covered by phosphor dots have generally employed masks with transmissions of this order. The requirement of providing printing tolerances and of accounting for imperfect registration between electron spots and dots tends to reduce the permissible mask transmission.

In the negative-tolerance matrix-screen shadow-mask tubes described in Chapter 5, Section 5.5, the phosphor dots are reduced in size and surrounded by a black matrix, diminishing the reflectivity of the viewing screen for ambient light. Since, here, the electron spots projected on the screen are larger than the phosphor dots, the dot size, along with the mask transmission, limits the efficiency with which the beam current delivered by any one gun is utilized for the excitation of the phosphor of the correspond-

* For uniform current density in the beam!

ing color. This efficiency can be made larger, however, than the mask transmission in shadow-mask tubes with nonmatrix screens. A typical value for the current utilization efficiency of negative-matrix tubes distributed in 1973 is 0.23. In such tubes, with a measured phosphor conversion efficiency of 40 lm/ W (when the three beam currents are adjusted to produce a black-and-white image) and a faceplate transmission of 0.85, the efficiency with which the beam power is utilized for useful light production becomes 8 lm/W.

By comparison, typical values of phosphor screen conversion efficiencies of black-and-white tubes of the same period are found to be 46 lm/W. With 78% faceplate transmission, the efficiency with which the beam power is utilized for the production of useful light becomes here 36 lm/W.

Compare now shadow-mask tubes and black-and-white tubes with identical cathode emission density, neck and bulb dimensions, and screen voltage. The maximum clear diameter of the final lens of the black-and-white tube gun can now be made 2.2 times as large as the clear diameter of one of the three-component, color-tube guns. Correspondingly, according to Eq. (4.24), the maximum current for the single gun of the black-and-white tube would be 2.5 times as large as that for one of the three-component guns of the color tube. If equal currents in the three-color-tube guns produce white, we would expect for the ratio of the maximum screen brightness of the color tube to that of the black-and-white tube,

$$\frac{\text{max. screen brightness for color tube}}{\text{max. screen brightness for black-white tube}} = \frac{8 \cdot 3}{36 \cdot 2.5} = 0.27$$

Since the beam power, and hence the screen brightness, is proportional to the square of the screen voltage, a negative-matrix shadow-mask tube operated at 27.5 kV should be capable of the same screen brightness as a black-and-white tube of similar dimensions operated at 14.3 kV.

With an in-line gun, slit mask and continuous-line phosphor screen (Fig. 4.10), we must write

$$D_s = s(q/p), \qquad [(p + q)/p]a = 3D_s \tag{4.35}$$

$$[(p + q)/p]B + (q/p)d_1 = D_s$$

Here D_s, s, a, B, and d_1 all denote dimensions in a direction transverse to the slits and phosphor lines.

With

$$T = (1 - c)B/a \tag{4.36}$$

we find

$$T = \tfrac{1}{3}(1 - c)(1 - d_1/s) \tag{4.37}$$

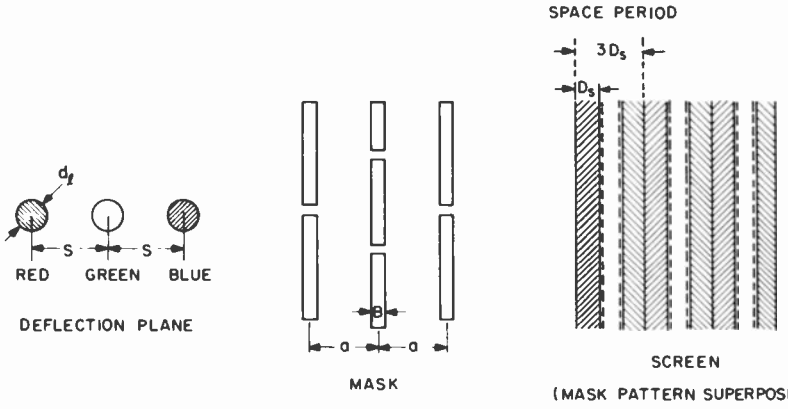

Fig. 4.10. Shadow-mask tube with slit mask and in-line gun: beam cross sections in deflection plane, mask pattern, and screen pattern.

Here c is the ratio of the bridge length to the slit length in the mask, which is a small quantity for masks having a bridge as shown in Fig. 4.10 and zero for masks with a continuous slit as in the Trinitron (*24*, *39*). The aberrations of a large, single final lens, traversed at its center by the three beams, should permit a larger value of D, and hence of d_1, than in triple guns with separate focusing systems. The relation between D_i and s, corresponding to Eq. (4.33) for the delta system, is $D_i = 3s$.

4.3 Single-Gun Tubes

In all single-gun systems there is a loss in brightness resulting from the fact that the beam can be on any one of the three phosphors for at most one-third of the scanning time. Even a duty cycle of one-third will give high color purity only with the employment, for example, of rectangular waves to switch the beam from one phosphor to the next. The high subcarrier frequency makes the generation of such switching waves commonly impractical. Thus, either sinusoidal switching or switching waves formed by a few harmonics are employed. Color purity then demands a duty cycle substantially less than one-third. A fraction of this intensity loss (as compared with three-beam systems) may be made up by the use of guns with final lenses of larger clear diameter than is possible with three guns.

As compared with a black-and-white viewing tube of the same dimensions and anode voltage, the screen brightness (at equal screen voltage) is reduced by the indicated duty cycle, the ratio of the average phosphor

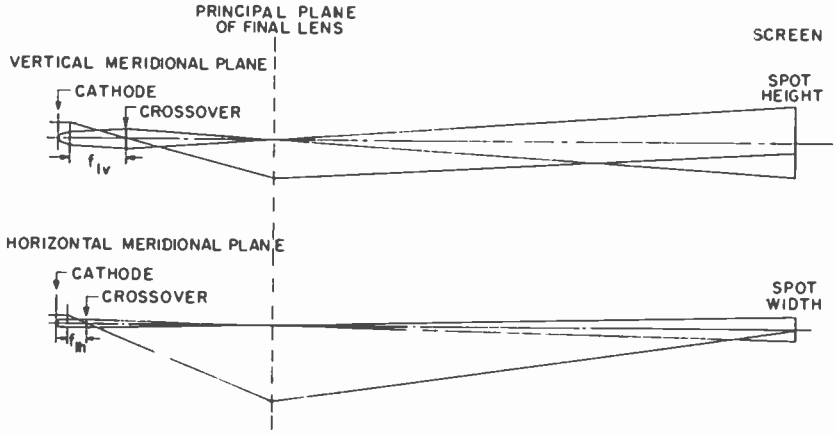

Fig. 4.11. Generation of elliptical spot with elliptical grid aperture (schematic).

conversion efficiency to the conversion efficiency of the white phosphor, and the transmission of the color selection mask, if used. As already noted, the advantage of a high-transmission focus mask is offset, in simple tube designs, by reduced screen contrast and the need for a lower anode voltage.

In single-gun tubes without color selection mask (beam-index tubes) and vertical-phosphor-line screen, the horizontal dimensions of the electron spot must be small enough to fit into a single phosphor line. Since the width of a color group of three phosphor lines limits the horizontal resolution of the screen, it is reasonable to match color group width and maximum permissible vertical spot diameter. The horizontal spot diameter then becomes one-third the vertical spot diameter.

Perhaps the simplest way of achieving the desired vertically elongated spot is the use of an elliptical grid aperture with the long axis in the vertical direction (Fig. 4.11). The focal length in the vertical plane f_{lv} will then be larger than the focal length in the horizontal plane, f_{lh}; if $u \gg f_{lv}, f_{lh}$, the ratio of the vertical and horizontal dimensions of the (aberration-free) spot will then be $f_{lv} : f_{lh}$.* At the same time, the divergence angle in the vertical direction will be so much smaller than that in the horizontal direction that the spot size will not be increased by spherical aberration in the vertical direction.

If the reasoning following Eq. (4.18) is now applied to the generalized

* Hasker (40) considers the design of a gun in which the vertical dimension of the emitting region is much greater than the horizontal dimension and the vertical crossover coincides approximately with the final focusing lens.

current expression

$$I_s = 0.4\pi j_0 \frac{r_{sov} r_{soh}}{M^2} \frac{eV_1}{kT} \alpha_{1v} \alpha_{1h} \tag{4.38}$$

we find for the optimum current in a spot with dimensions $(D_s/3) \times D_s$ in terms of that for a round spot with diameter D_s,

$$(I_{s,\,opt})_{ell} = \frac{1}{3^{8/3}} \frac{r_{kv}}{r_{kh}} (I_{s,\,opt})_{round}$$

$$= 0.053 \frac{r_{kv}}{r_{kh}} (I_{s,\,opt})_{round} \tag{4.39}$$

Here r_{kv}/r_{kh} denotes the ratio of the vertical and horizontal dimensions of the emitting area on the cathode. Since, for the required ratio $f_{1v}/f_{1h} = 4$, this can scarcely be greater than 2, we must expect the reduction in the horizontal dimensions of the spot by a factor of 3 to lead to a spot current reduction by a factor of the order of 10. A more complex electron-optical arrangement for achieving the elongated spot could lead to a lower current loss. However, at best the current reduction factor could be raised to $3^{-4/3} = 0.23$.

With a round spot an appreciable gain in spot current (without loss in color purity) can be achieved by making the phosphor stripes narrower than one-third the color group width, separating them by black guard bands as shown in Fig. 4.12. Assuming the spot to be of uniform intensity and the phosphor line width to be equal to w, the spot may have a diameter d_s' given by

$$d_s' = \tfrac{2}{3} d_s - w \tag{4.40}$$

where d_s is the width of a color group. The ratio of the effective screen current to that for a spot with diameter D_s and a uniformly coated screen is then

$$r = (d_s'/d_s)^{8/3}(4A/\pi d_s'^2) \tag{4.41}$$

or

$$r = (2/\pi)[2/3(1 + y)]^{8/3}[\arcsin y + y(1 - y^2)^{1/2}] \tag{4.42}$$

with

$$y = w/d_s' = (2d_s/3w - 1)^{-1} \tag{4.43}$$

Here A is the spot area intercepted by a phosphor line on which it is centered. For a fully covered screen ($w = d_s/3$), $r = 0.053$; r reaches its maximum value 0.070 for 2/3 phosphor coverage ($w = 2d_s/9$). For guard bands equal in width to the phosphor stripes ($w = d_s/6$), $r = 0.066$, which is only slightly less and will lead to smaller contrast loss arising from the diffuse reflection by the phosphor screen of ambient light.

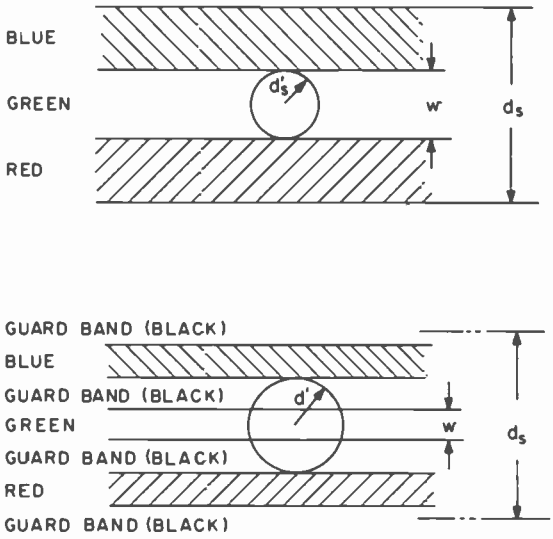

Fig. 4.12. Increase in spot diameter permitted by the use of guard bands.

Indeed, if all the contrast loss is ascribed to diffusely reflected ambient light and the reflection factor of the black guard band materials is set equal to zero, an even smaller phosphor coverage is found to be advantageous. Let us assume that a faceplate filter with transmission T_0 is required to give adequate contrast in the absence of guard bands. To yield the same contrast with guard bands the faceplate transmission can be increased to T, given by

$$T/T_0 = 3^{5/3} r(d_s/w) \tag{4.44}$$

The screen brightness reduction (compared to a tube with full screen coverage, a filter of transmission T_0, and a spot of diameter d_s) is given by

$$\begin{aligned} r\,(T/T_0) &= (2^{19/3}/\pi^2 3^{8/3})[y(1+y)^{13/3}]^{-1}[\arcsin y + y(1-y^2)^{1/2}]^2 \\ &= [0.437/y(1+y)^{13/3}][\arcsin y + y(1-y^2)^{1/2}]^2 \end{aligned} \tag{4.45}$$

This quantity has a maximum equal to 0.164 at $y = 0.28$, $3w/d_s = 0.437$, with $T/T_0 = 2.64$. At $y = 0.333$, $3w/d_s = 0.5$ we have $rT/T_0 = 0.162$ with $T/T_0 = 2.46$. Thus, the effective intensity loss factor, imposed by the requirement of achieving color purity, becomes approximately 1/6. This is about the same as the beam-absorption factor of a shadow mask in a tube with full screen coverage. The residual intensity disadvantage of the one-gun beam-index tube, as compared with the shadow-mask tube, is its limited duty factor.

CHAPTER 5

Shadow-Mask Tube

5.1 Principles of Operation

The shadow-mask color picture tube, already touched upon in Section 3.1.1, is discussed in greater detail in this chapter. Figure 5.1 illustrates a typical 25V, 90° tube having a diagonal of 25 in. (25V) and 90° deflection (total sweep across the diagonal).* This tube employs a gun arrangement that generates three independent electron beams. These beams are closely spaced within a common neck, use a common magnetic deflection yoke for scan, and strike a shadow mask having a multiplicity of apertures. The typical shadow mask contains approximately 350,000 apertures in a hexagonal array with center-to-center spacing of about 0.6 mm. Corresponding to each aperture is a triad of red, green, and blue emitting phosphor dots, 0.35 mm in diameter, which are approximately tangent to each other. The

* As a result of a Federal Trade Commission ruling in 1966 on the advertising of TV receivers, the Electronic Industry Association adopted a revised system of nomenclature for commercial color tubes in the United States. A first number followed by "V" indicates the viewable screen diagonal rounded to the nearest inch. Previous to 1966 the first number, without the letter V, referred to the bulb diagonal instead of the screen diagonal. The second and third letters, upon application by a tube maker to the Electronic Industry Association for a tube-type number, are assigned to reflect characteristics such as deflection angle, screen type, mounting hardware. The suffix P22 refers to a three-color phosphor screen. An example of a color-tube-type designation, for a color tube having a diagonal screen dimension of approximately 25 in., is 25VABP22.

In Europe, a similar tube could be designated as A67–120X. In this system, the letter A indicates a picture tube, 67 refers to the bulb diagonal to the nearest centimeter, and the X indicates a color tube. The 120 arbitrarily reflects characteristics such as the deflection angle, screen type, and mounting hardware.

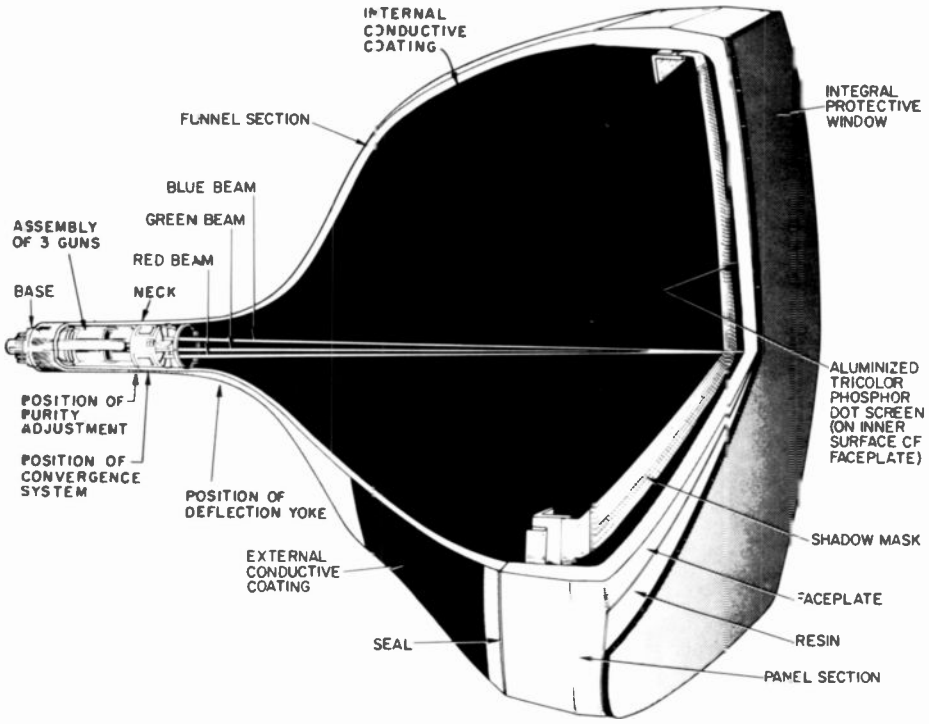

Fig. 5.1. Typical 25V, 90° shadow-mask color tube.

electron guns in a typical tube are arranged in a triangular configuration within a 36-mm outside diameter neck. The three close-spaced electron beams, when undeflected, are aimed at the center of the screen at an angle of 1° from the center line of the tube system. As a result of the spacing of the electron guns from each other, and the 13- or 14-mm separation of the shadow mask and faceplate, the beam from the red gun can strike only the red phosphor elements and is shadowed from the phosphor elements of the other two colors by the aperture mask. A similar situation exists for beams from the green and blue guns. Pure primary-color fields can be obtained by this arrangement and, of course, any combination of primary colors.

In addition to deflection by the common magnetic yoke to produce a scanned raster, a small change in angle of each individual beam is accomplished when needed to obtain convergence of the beams at the screen by activation of internal pole pieces at the anode end of the electron gun (see Section 5.3.6). These internal pole pieces are excited by currents through magnetic components around the neck of the tube. The currents in the

components have wave shapes that enable the three beams, when scanned, to maintain coincidence at all positions on the screen. The incremental deflection induced by these currents, called dynamic convergence, is of the order of 1° for each of the beams.

5.2 Early Shadow-Mask Tubes

5.2.1 Phosphor Screens

The pressures to start color broadcasting in the late 1940's greatly accentuated work on a direct-view color tube. Although several possible approaches existed (*1*), the shadow-mask tube was singled out for concentrated effort. However, a very practical consideration presented itself—how could such a structure be built with the phosphor elements correctly positioned, especially with tubes made in mass production?

At that time the state of the art of depositing phosphor screens for black-and-white tubes involved settling the phosphor powder on the faceplate from a water suspension. Screens consisting of phosphor lines for experimentation with color had been made by covering the surface with a grill of wires or ribbons before settling and then lifting the grill. No method was available for producing such a screen when the mask was located at a distance from the surface as would be required in the shadow-mask color tube.

A solution to the phosphor-element location problem was found in the "lighthouse" principle (*41*). This principle takes advantage of the fact that in field-free space electrons travel in straight paths as does light. Thus, proper location of phosphor elements can be found as the terminal points of light paths at the screen plane when light rays are properly substituted for electron paths. That is, light emitted from a source placed at the center of deflection of one of the electron beams will pass through the mask apertures and strike the screen plane where corresponding phosphor elements should be placed.

In first attempts to employ this principle, a flat metal shadow mask and flat screen were used. The mask was produced by an etching process (*42*) and had a fine enough array to avoid structure visibility problems in the picture. The positions of the phosphor elements were then recorded through this mask on a photographic plate placed at the screen plane and this was used to make a thin metal settling mask by etching apertures in the metal where the phosphor should be placed (*41*). The settling mask was positioned three times against the faceplace surface to settle a nested array of red, green, and blue phosphor elements. However, it soon proved more practical to make a "silk screen" from the photographic plate and to print the phosphor elements instead of settling them (*43*).

In these early experimental tubes, no attempt had yet been made to produce interchangeable flat masks and phosphor screens, so a photographic plate was exposed for each tube and a silk screen made and used to print the phosphor screen. Good tubes could be produced this way, but having to expose a photographic plate and make a silk screen for each tube was a very expensive process to contemplate for mass production of color tubes.

To avoid the need for a photographic plate and silk screen for each tube, effort was directed toward achieving interchangeable flat shadow masks and phosphor screens (*44*). Some progress was made, but there were other practical difficulties. For example, the flat mask, although mounted under tension on a frame, was subject to "oil-canning" when heated by electron bombardment, causing loss of color purity. Also, the internal flat glass phosphor plate could not be safely heated and cooled as quickly as desired for rapid tube processing.

These and other consequences of using flat structures led to placing the screen on the inside surface of the curved faceplate for use in conjunction with a curved mask (*6*). Interchangeable mask and screen structures now became much more difficult to achieve but, on the other hand, the need for interchangeable structures became less acute because of the adoption of a photodeposition process for printing the phosphor (*7*). In this new system, the lighthouse principle is still employed to locate the correct phosphor position; but the need for photographic plates and silk screens is avoided even though noninterchangeable masks are used. The procedure consisted of assigning a given mask to a given glass faceplate panel to make a unique assembly. The screen is then made by first applying one of the color phosphors, mixed with a photosensitive binder, to the screen substrate surface and exposing the mixture through the mask with a UV light source placed at the appropriate deflection center. The binder hardens upon exposure to UV light and retains the phosphor while the unexposed binder and phosphor can be washed away. The process is repeatable and, by deposition of the other two colors, three interlaced arrays of phosphor elements are obtained that are precisely placed. Similar procedures are still used in the production of shadow-mask color tubes.

5.2.2 Bulbs

Early experimental bulbs were round in shape for maximum strength and ease of construction. They were spun out of 430-alloy metal in two parts—a cone section permitting a 45° deflection angle and a topcap or panel section (*45*). Both contained flanges for welding the two parts together. The panel also contained a flange at its other end to which a spherical faceplate glass was hot sealed prior to joining the funnel and topcap. Also prior to this joining, a flat mask-phosphor screen assembly was fabricated as a separate

entity and mounted on brackets at the large end of the metal cone. In a later type, the funnel and topcap were made of glass with the metal flanges hot sealed to the glass (*44*). The flanges were welded for final closure as before, after insertion of the flat mask-phosphor screen assembly. In both the metal and glass-flanged bulbs, the internal mask-screen assembly required very slow warm-up and cooling in processing to prevent breakage of the phosphor screen plate.

As mentioned in Section 5.2.1, the next major innovation was the placing of phosphor directly on the inside curved surface of the panel and the use of a mask with corresponding curvature as the only internally supported structure (*6*). Next a 21-in. round, two-piece metal envelope with 70° deflection (*13*) was developed, also with phosphor on the faceplate. Finally, a two-piece, all-glass bulb was developed which was sealed with glass frit (*15*). Then, even as now (1973), the parts comprised a funnel section and a faceplate panel section with the internal conductive coatings and the phosphor screen applied while the tube is open.

The frit for closing the two-piece color bulb is a low-temperature "solder glass" which works as follows. The solder glass in powder form in an organic binder is applied to the seal edge. The funnel and panel are aligned in a jig and held in contact by gravity. As the temperature is raised the binder burns out and the solder glass becomes vitreous. The fluid glass wets the seal surfaces and fills the gap between them. The temperature is further raised to about 445°C and held for one hour. During this time the solder glass irreversibly devitrifies to a ceramic-like material to make a strong, gas-tight seal.

The two-piece feature of a color bulb is not an additional cost factor because the funnel and panel of even a black-and-white picture tube are made separately. A subsequent hot seal by the bulb maker fuses the two together by melting the glass. In the shadow-mask tube, however, such hot sealing is not permissible because of heat damage to the shadow mask and phosphor screen, which must be in place before sealing.

Two-piece rectangular bulbs with rounded corners and slightly rounded sides were successfully designed (*16*) which enabled more of the transmitted picture to be fully displayed than with round bulbs. In successive designs the corners became sharper and the sides straighter until the picture is now severely rectangular. The tube length decreased as the deflection angle was increased from an initial 45° to 70° and then to 90°. By 1973, 110° deflection was very common.

5.2.3 Electron Gun

Early experimental shadow-mask color tubes were of two types which differed primarily in the way the three electron beams were handled. In

one type a cluster of three guns in the neck of the tube was used. This is the arrangement subsequently developed commercially for the shadow-mask tube (*4*). In the second type, a single gun producing a single beam was employed. Here external magnetic components were used to sequentially position the beam in the neck of the tube so as to simulate the beams in the triple-gun system (*46*). The arrangement performed satisfactorily except insofar as the brightness was severely limited by having current available from only one gun instead of three.

The three closely spaced beams must be coincident or converged at the screen and remain so as the beams are deflected over the screen. Misalignment of the gun structures makes it necessary to provide adjustment for obtaining accurate coincidence of the spots in the center (static convergence) and it is also necessary to provide means to maintain this coincidence during scan (dynamic convergence).

In an early three-gun tube with the guns parallel to one another, an electrostatic lens common to all three beams was used at the anode end of the gun cluster to perform both static and dynamic convergence. Small external permanent magnets were used for fine adjustments of coincidence at the center. An improved system eliminated the electrostatic convergence lens by employing magnetic means for bending the beams to obtain coincidence. In this system magnetic pole pieces in a convergence cage on the gun are actuated by external magnets to give individually controlled radial motions to the beams synchronized with scan. In addition, the blue gun is provided with lateral motion of its beam to give the degree of freedom of motion necessary to insure convergence. The amount and type of motion needed is dependent on deflection-yoke design. The yoke design is also concerned with obtaining maximum screen tolerance as well as achieving acceptable pincushion distortion. However, for larger scan angles, circuit pincushion correction became necessary and emphasis was placed primarily on designing yokes for improved convergence and screen tolerance characteristics.

Each shadow mask color gun must be capable of very high current, relative to a black-and-white tube gun, to produce adequate brightness because much of the beam current is absorbed by the mask and produces no light. High gun currents are needed to help overcome this loss, which requires careful gun design to obtain satisfactory resolution. The situation has been aggravated by a reduction in tube neck diameter from the early 50.8-mm neck size down to 29 mm to avoid increasing deflection power in successive designs as the deflection angle has increased. The advent of in-line gun tubes has further restricted the diameter of the gun lenses that can be used because of the less compact gun structure that must fit into the small neck.

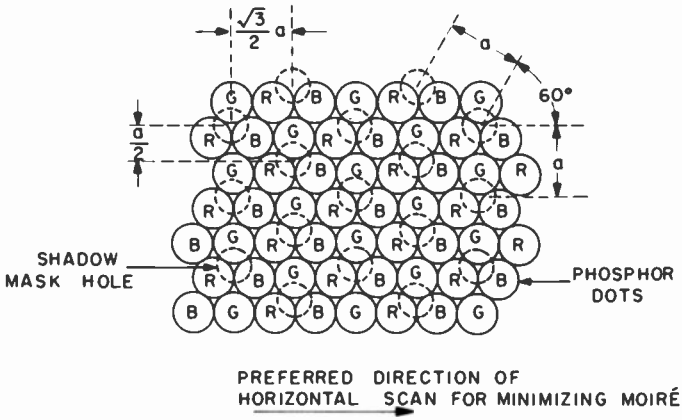

Fig. 5.2. Mask-aperture and phosphor-dot arrays in shadow-mask tube. The dotted circles represent the mask apertures (with diameter B).

5.3 Shadow-Mask Tube Technological Developments

5.3.1 Screen and Mask Geometry

Figure 5.2 shows the basic geometric plan view of a hexagonal array of round apertures in a flat shadow mask, together with the phosphor-dot screen. The apertures have a diameter B and are equally spaced a distance a apart. Figure 5.3 represents a cross section through a line of apertures in a flat mask spaced a distance q from a flat screen. A point source of radiation, offset by an amount s from the color tube axis, is placed a distance p from the mask and L from the screen.

Radiation emitted from the source forms a dot pattern on the screen plate with an element spacing D and a magnification of the mask aperture $\lambda = L/p$. Two other sources, located 120° about the tube axis and also at a distance s from the axis, will form similar patterns that will nest perfectly with the first pattern, provided appropriate dimensions are chosen.

In practice the source has a finite size, m, as indicated in Fig. 5.4. The radiation is UV light when printing the phosphor screen and electrons in the finished tube. If the projected pattern is to form tangent elements of diameter R for maximum screen utilization, then it is easy to show that the following relations hold:

$$q = aL/3s, \qquad R = \sqrt{3}as/(3s - a), \qquad B = (a/3)(\sqrt{3} - m/s) \quad (5.1)$$

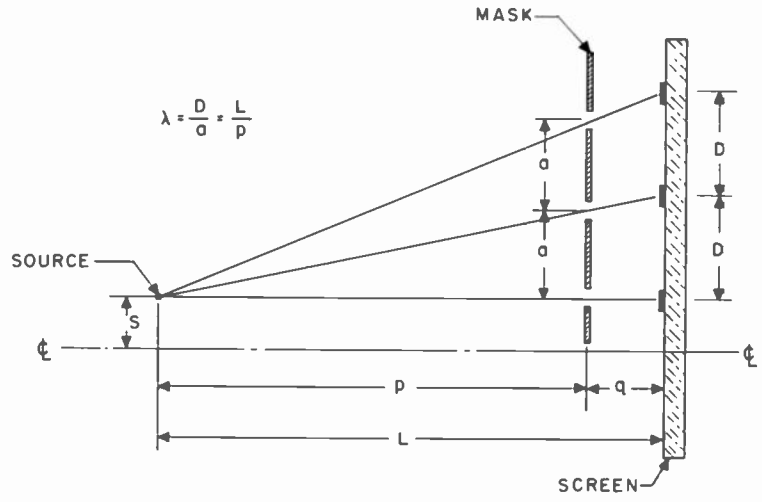

Fig. 5.3. Planar mask-screen geometry.

and the mask transmission is

$$T = (\pi/2\sqrt{3})(B/a)^2 \tag{5.2}$$

The geometry of the color tube is somewhat more complicated because the faceplate is spherically curved or may even have a compound curvature in the larger sizes. The mask is also curved to obtain the best possible nest-

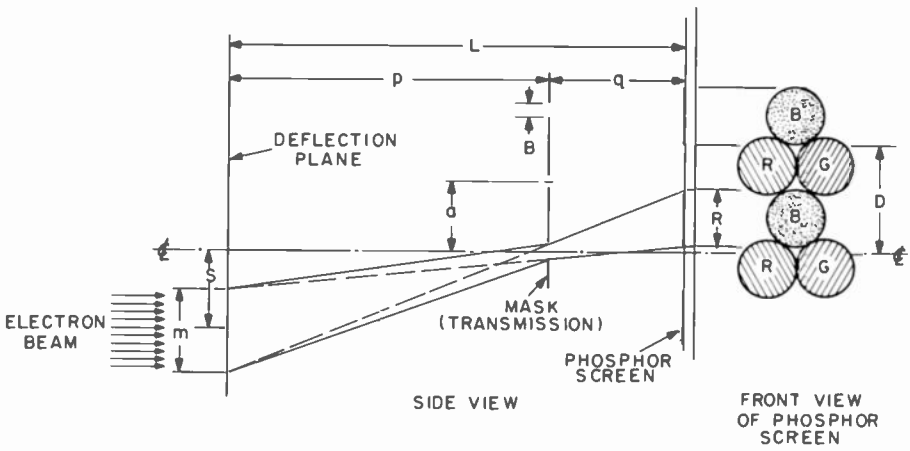

Fig. 5.4. Determination of phosphor-dot size and phosphor-dot nesting.

ing of the phosphor dot patterns on the screen. However, curving of the mask and screen introduces geometric distortions in the beam-landing triads or obliquity errors that do not exist with flat structures. There are other nongeometric errors in the landing patterns that are caused by deflection and convergence of the beams as well as by ambient magnetic fields. These factors will be discussed in Section 5.3.2. However, the effect of geometric relationships between the scanning pattern and the aperture pattern of the mask on the reproduced picture will be considered at this point.

Moiré Considerations

An important consideration in the selection of spacing of apertures in the shadow mask is the influence this spacing has on the interaction of the apertures with the pattern generated by the raster scan lines to produce moiré. If the distance between horizontal rows of apertures in the shadow mask and the spacing between the horizontal scan lines happens to coincide, or is an exact multiple, there may be little effect, but any minor deviation from this coincidence of spacing can easily cause a modulation in the intensity of the beam passing through the mask. Thus, a change in raster height or nonlinear vertical scan may produce a moiré pattern. In any event, it is necessary to carefully select the spacing of the mask apertures so that moiré is held to a minimum.

Consideration must be given to a number of practical factors, first of which is the number of scan lines that will be used for the picture tube under consideration. In the United States 525 scan lines is standard. In much of Europe 625 is the accepted standard, but in some countries 819 scan lines are the standard. In any of these cases the active lines, or the total lines minus the number of lines used for blanking, must be considered in the calculations. A second factor is the amount of overscan that will be used in the particular receiver (causing top and bottom raster lines to be deflected off the screen) since this will obviously affect the spacing of the visible scan lines. A third is the variation that can be expected in the vertical height due to normal variations in line voltages and other factors affecting the circuitry of the vertical deflection system. Pincushion distortion will also affect the spacing of the scan lines to some degree.

Table I gives a set of scan-line spacings and corresponding mask-aperture spacings to give minimum moiré for several sizes of typical picture tubes when used with 525 and 625 scanning-line systems. The mathematical basis for choosing aperture-mask spacings will be given below. In addition, a general criterion is to use an aperture spacing in the mask small enough to

TABLE I

MASK-APERTURE SPACINGS FOR MOIRÉ MINIMA IN SEVERAL COMMERCIAL PICTURE TUBES

U.S. commercial type designation	Raster[a] height (mm)	Screen height (mm)	Aperture spacing, a (mm)	Scan-line spacing, h (mm)	Approx. ratio h/a
		525 Scan-Line System[b]			
25V	423.4	395.8	0.627	0.877	11/8
21V	360.4	336.7	0.650	0.746	9/8
19V	324.5	303.3	0.587	0.672	9/8
		625 Scan-Line System[b]			
25V	411.6	395.8	0.627	0.716	9/8
21V	350.2	336.7	0.676	0.609	7/8
19V	315.4	303.3	0.617	0.549	7/8

[a] Calculated on the basis of 7% overscan for the 525 scan-line system and 4% overscan for the 625 line system.

[b] The 525 scan-line system, with retrace blanking, has 483 active lines; the 625 system has 575 active lines.

minimize visibility of the screen structure, but large enough to avoid excessive practical problems in producing the apertures in the shadow mask and printing the phosphor elements with controlled size.

Mathematical Considerations of Screen Moiré

We will assume that the picture is viewed from a sufficient distance that the dot-triad separation lies well beyond the limit of resolution and that the same applies for the center-to-center spacing of the scanning lines, h. As already mentioned, the interaction of the scanning line pattern with the mask-aperture pattern can give rise to intensity fluctuations, or moiré, in the image field, with a period large enough to be readily visible (*47*, *48*). The variation in intensity of the scanning lines transmitted through the shadow mask, which is responsible for the observed moiré, is minimized when the direction of scan is perpendicular to a set of rows of adjoining apertures (Fig. 5.2). The mask transmission for a scanning line then becomes a maximum when the scanning line is centered on a row of apertures and becomes a minimum when it lies halfway between two aperture rows, a distance $a/4$ away. If the scanning-line separation (in the mask plane)

differs only little from $a/2$, the space period of the horizontal moiré bars becomes very large. The number N_m of moiré bars in the picture is given by

$$N_m = N - 2V/a = N - [\tfrac{1}{2}(3\sqrt{3})n_a]^{1/2}$$
$$= N - 1.612\sqrt{n_a} = (V/h)(1 - 2h/a) \tag{5.3}$$

Here a rectangular field with aspect ratio 4 : 3 and vertical height V (in the mask plane!) has been assumed; N is the number of scanning lines and n_a the number of apertures in the field.

Assume that the current distribution in the scanning line is gaussian:

$$f(y) = (1.665/d_s\sqrt{\pi}) \exp[-(1.665y/d_s)^2] \tag{5.4}$$

Here d_s is the "line width," defined as the transverse distance between the two points at which the current density has dropped to half its maximum value. For unit current falling on unit area of the mask, the current density on the mask is given by

$$I_0(y) = (1.665h/d_s\sqrt{\pi}) \sum_{m=-\infty}^{\infty} \exp\{-[1.665(y + mh)/d_s]^2\}$$

$$= 1 + 2\sum_{n=1}^{\infty} \exp\{-[n\pi d_s/(1.665h)]^2\} \cos(2\pi ny/h) \tag{5.5}$$

If we fix the coordinate origin at the center of a mask aperture in the center of the field, and the scanning-line center is a distance c from the mask-aperture center, we can write for the current density distribution

$$I_0(y; c) = 1 + \sum_{n=1}^{\infty} c_n \cos[2\pi n(y - c)/h]$$

$$c_n = 2 \exp\{-[n\pi d_s/(1.665h)]^2\} \tag{5.6}$$

The modulation of the light distribution is, of course, large only if the scanning lines are narrow. Thus, for

$d_s = h$, $c_1 = 0.057$, $c_2 = 0.0000013$, $\cdots$

$d_s = 0.5h$, $c_1 = 0.821$, $c_2 = 0.057$, $c_3 = 0.00066$, $\cdots$

$d_s = 0.4h$, $c_1 = 1.132$, $c_2 = 0.205$, $c_3 = 0.01187$, $\cdots$

We can also express the transmission $T(x, y)$ of the mask as a Fourier series. If an angle α is formed between the scanning-line direction defined as

the x direction and a normal to a row of close-spaced mask apertures (Fig. 5.5), the transmission of a mask with apertures of diameter B is given by

$$T(x, y) = T + \sum_{n_1=0}^{\infty} \sum_{m_1=-\infty}^{\infty} c_{m_1,n_1} \cos\left[\frac{2\pi}{a}\left(\frac{m_1}{\sqrt{3}}(x\cos\alpha + y\sin\alpha) + n_1(y\cos\alpha - x\sin\alpha)\right)\right] \quad (5.7)$$

with

$$T = \frac{\pi B^2}{2a^2\sqrt{3}}$$

$$c_{m_1,n_1} = [1 + (-1)^{m_1+n_1}] \frac{B}{a(m_1^2 + 3n_1^2)^{1/2}} J_1\left(\frac{\pi B(m_1^2 + 3n_1^2)^{1/2}}{a\sqrt{3}}\right) \quad (5.8)$$

Here J_1 is the first-order Bessel function. The product $T(x, y)I_0(y; c)$, as given by Eqs. (5.6) and (5.7), gives the intensity distribution directly in front of the mask. If the scale is simply enlarged by the magnification factor

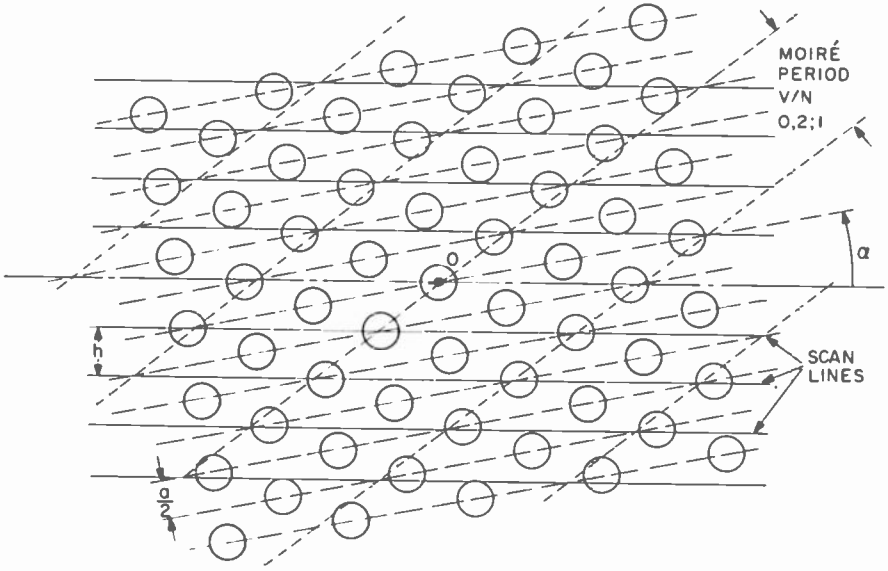

Fig. 5.5. Formation of moiré for arbitrary angle between mask pattern and scanning lines.

L/p, the low-spatial-frequency beat components in this product also describe the moiré observed at the screen, since the macroscopic intensity variations are not affected by the spreading of the individual electron pencil transmitted by a mask aperture between mask and screen. We can write for the difference-frequency term between the mask transmission term (m_1, n_1) and the current density term n,

$$m_{m_1,n_1;n} \cos\left\{\frac{2\pi N_{n_1,m_1;n}}{V}(x \cos \alpha_{m_1,n_1;n} + y \sin \alpha_{m_1,n_1;n}) + \frac{2\pi nc}{h}\right\} \quad (5.9)$$

Here the line number $N_{m_1,n_1;n}$ of moiré bars, referred to the vertical height V of the picture, the angular inclination $\alpha_{m_1,n_1;n}$ to the horizontal in which the moiré intensity variation progresses, and the modulation amplitude $m_{m_1,n_1;n}$ of the moiré are given by:

$$N_{m_1,n_1;n} = \frac{V}{h}\left[\frac{h^2}{a^2}\left(\frac{m_1^2}{3} + n_1^2\right) - \frac{2nh}{a}\left(\frac{m_1}{\sqrt{3}} \sin \alpha + n_1 \cos \alpha\right) + n^2\right]^{1/2} \quad (5.10)$$

$$\tan \alpha_{m_1,n_1;n} = \frac{n_1 \cos \alpha + (m_1/\sqrt{3}) \sin \alpha - (na/h)}{(m_1/\sqrt{3}) \cos \alpha - n_1 \sin \alpha} \quad (5.11)$$

$$m_{m_1,n_1;n} = \exp\left[-\left(\frac{n\pi d_s}{1.665h}\right)^2\right] \times \frac{4a\sqrt{3}}{\pi B(m_1^2 + 3n_1^2)^{1/2}} J_1\left(\frac{\pi B(m_1^2 + 3n_1^2)^{1/2}}{a\sqrt{3}}\right) \quad (5.12)$$

The ratio h/a, wherever it occurs, is here the ratio of line spacing to aperture-center spacing in the mask plane. In terms of the mask transmission T, given in Eq. (5.8), the moiré modulation amplitudes can be rewritten:

$$m_{m_1,n_1;n} = 4 \exp\left[-\left(\frac{n\pi d_s}{1.665h}\right)^2\right] \frac{J_1(s)}{s}$$

$$s = \left(\frac{2\pi T(m_1^2 + 3n_1^2)}{\sqrt{3}}\right)^{1/2} \quad (5.13)$$

Figures 5.6–5.9 show the space frequencies of the moiré components in line numbers $N_{m_1,n_1;n}$ or ratios of the picture height to the space period as well

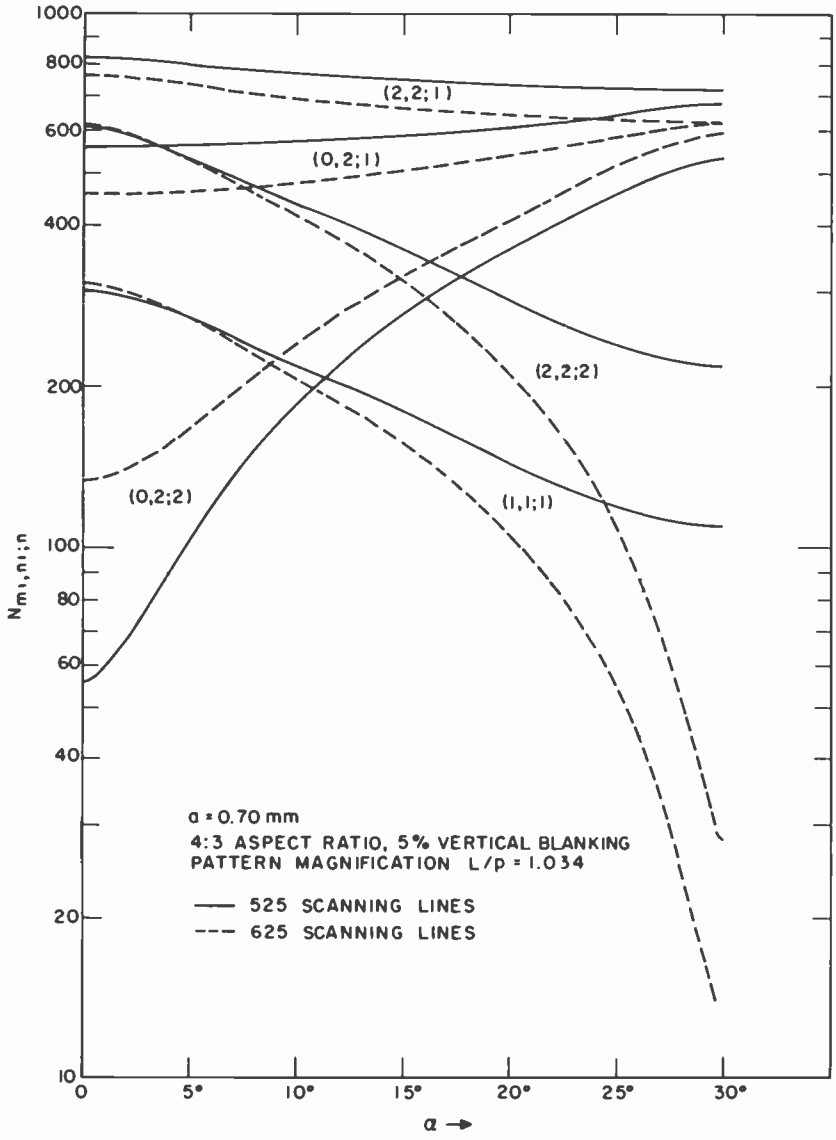

Fig. 5.6. Moiré frequencies in line numbers for 635-mm picture.

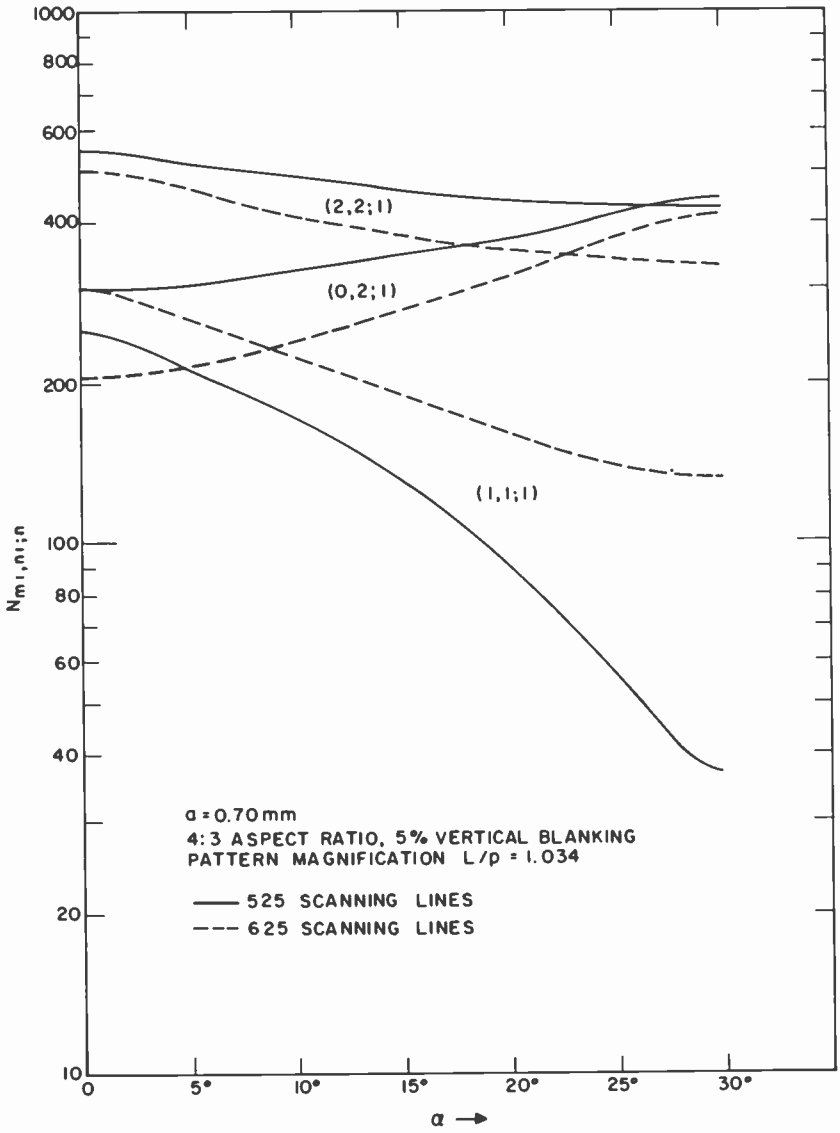

Fig. 5.7. Moiré frequencies in line numbers for 483-mm picture.

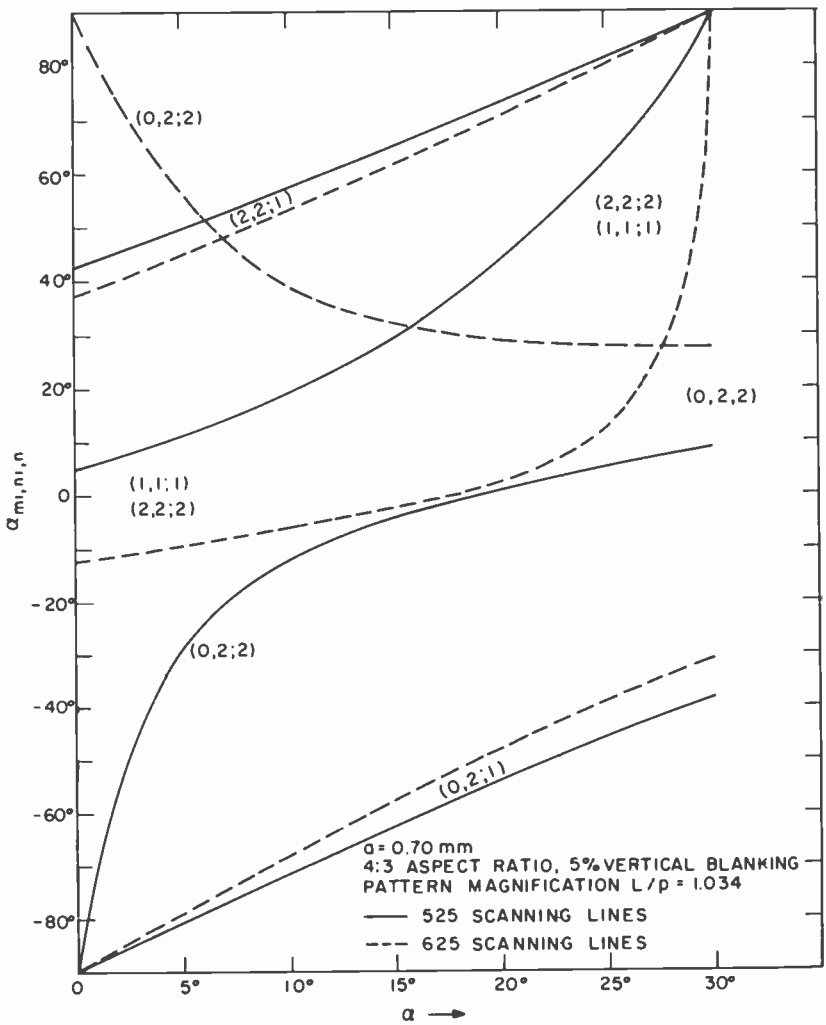

Fig. 5.8. Direction of moiré intensity variation for 635-mm picture.

as the direction $\alpha_{m_1,n_1;n}$ of the corresponding intensity variation for a fixed mask-aperture spacing $a = 0.70$ mm, two different picture sizes (635-mm and 483-mm diagonal) and two different scanning line numbers (525 and 625 for the full frame period).*

* In practice, the value of a would vary in proportion to the picture diagonal.

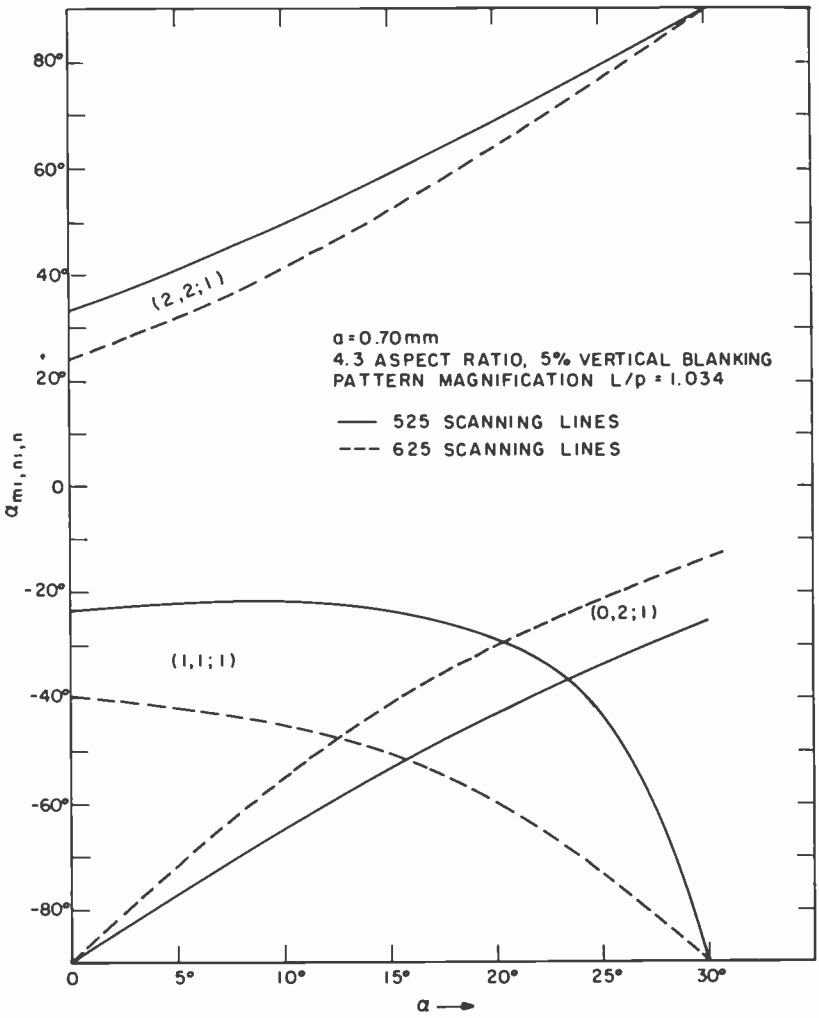

Fig. 5.9. Direction of moiré intensity variation for 483-mm picture.

In Figs. 5.6 and 5.7 only those terms leading to values of $N_{m_1,n_1;n}$ very much smaller than the scanning-line number contribute noticeable moiré. For the most favorable direction of scan ($\alpha = 0$) these are the terms (0, 2; 2) and (1, 1; 1) for the 635-mm picture and the terms (0, 2; 1) and (1, 1; 1) for the 483-mm picture; for the least favorable direction of scan ($\alpha = 30°$), the terms (2, 2; 2) and (1, 1; 1) contribute and we note that the moiré

periods are very much larger and hence more prominent than for $\alpha = 0$. We also note that the magnitude of the moiré periods differs materially for a 525 and a 625 line scan, indicating that the exact choice of the mask-aperture separation a, as a function of the scanning-line number, can be significant for the observation of moiré effects.

If there are two moiré components of comparable intensity and period and different directions, a dot moiré is observed. This condition is met by the (0,2; 1) and (1, 1; 1) components in the 483-mm picture for $\alpha = 0$. However, very crude moiré is invariably a bar moiré. Furthermore, for both $\alpha = 0°$ and $\alpha = 30°$ the crude moiré bars are parallel to the horizontal scanning direction.

Figure 5.10 shows that the modulation amplitude decreases with increasing mask transmission and is largest for the (1, 1; 1) term. Terms with $n = 2$ or greater are generally insignificant, even when the half-value width d_s is only half the center-to-center spacing h of the scanning lines. For a substantially flat field ($d_s = h$), the moiré amplitudes are always very small.

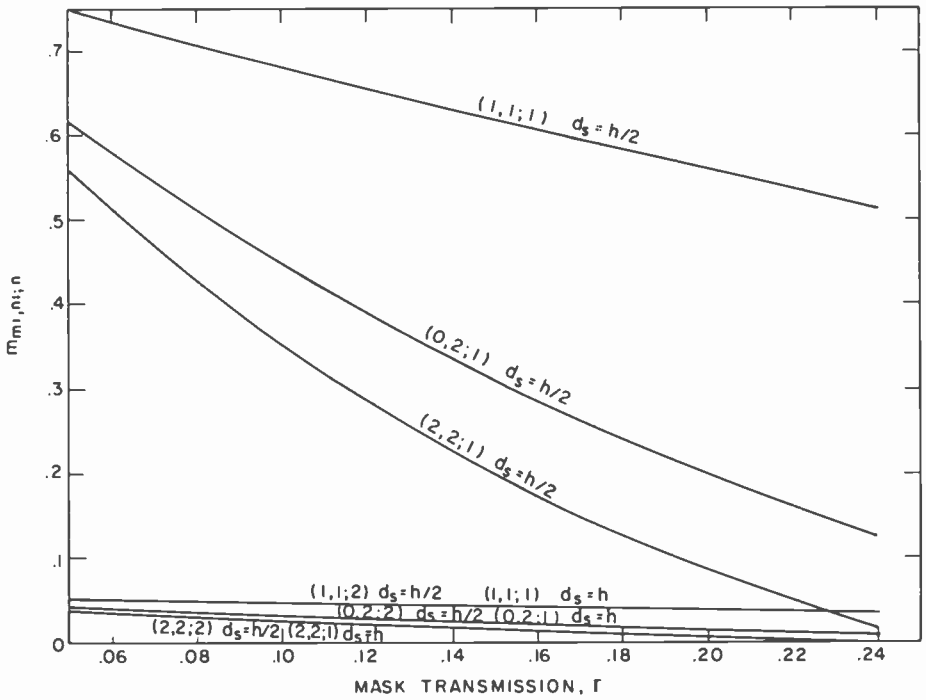

Fig. 5.10. Modulation amplitudes of moiré as function of mask transmission T.

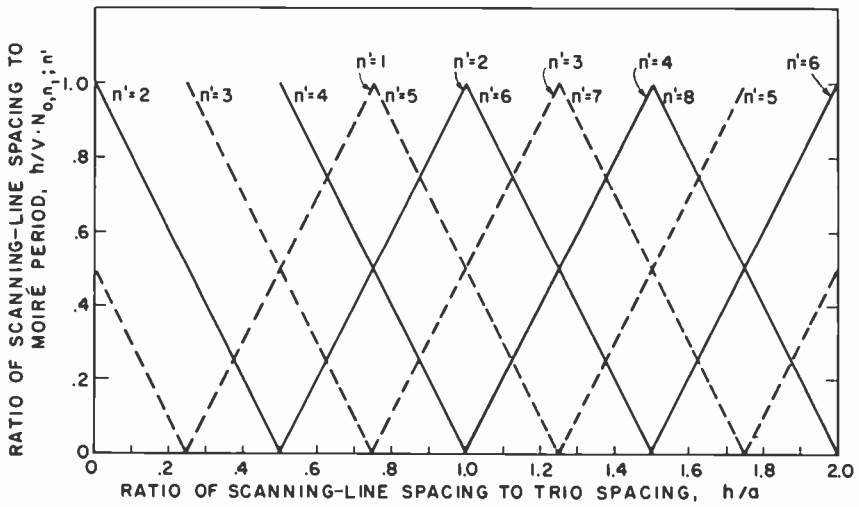

Fig. 5.11. Moiré line number $N_{0,n_1;n'}$ as function of ratio h/a of scanning-line spacing to triad-line spacing ($\alpha = 0$, $n_1 = 2$).

In the preceding treatment we have computed the moiré as though phosphor dots of only one color were excited. With perfect registration, the simultaneous excitation of all three dot systems results in the formation of three identical moiré patterns with a maximum spatial separation equal to $a/2$. This is equivalent to a single moiré pattern in which the several components are attenuated by factors no smaller than

$$\cos\left(\frac{\pi}{2}\frac{N_{m_1,n_1;n}}{N}\frac{a}{h}\right)$$

Since, for perceptible moiré $N_{m_1,n_1;n} \ll N$, this factor is always very nearly equal to 1, so that the modulation amplitudes given by Fig. 5.10 are applicable irrespective of the color of the picture. With imperfect registration, the amplitude attenuation of the moiré may be greater; however, even then Fig. 5.10 provides a good estimate, since the luminance variation is determined primarily by the green component.

Recapitulating, moiré effects are most prominent when the scanning lines are sharply focused, i.e., at relatively low levels of picture brightness. To minimize observable moiré for the preferred direction of scan, values of the mask-aperture separation a that are close to twice the scanning-line spacing h, should be avoided absolutely; crude moiré of relatively low intensity is also observed for a approximately equal to h. All this applies for a scan

direction normal to rows of apertures and perfect interlace, which has been assumed throughout the preceding analysis. With imperfect interlace, i.e., if the scanning lines of even fields do not fall midway between the scanning lines of odd fields, the period of the scanning pattern becomes $2h$. Correspondingly, for the preferred direction of scan ($\alpha = 0$), the line numbers for horizontal moiré become

$$N_{0,n_1;n'} = \frac{V}{h}\left[n_1\frac{h}{a} - \frac{n'}{2}\right], \qquad n' = 1, 2, 3, \ldots, \quad n_1 = 2, 4, 6, \ldots \tag{5.14}$$

These moiré line numbers, in relative measure, are plotted in Fig. 5.11 for $n_1 = 2$, as function of the ratio h/a. The solid lines correspond to even n' and apply, thus, for perfect interlace; the broken lines (odd n'!) are added if there is a deviation from perfect interlace.

Figure 5.11 shows that the maximum moiré period is minimized (or the minimum moiré line number maximized) if h/a is an odd multiple of 1/8, such as 0.875 or 1.125; the maximum moiré period then becomes four times the line spacing. It is true that, with this choice of h/a, the moiré period approaches an infinitely large value for $n_1 = 4$. However, even for complete loss of interlace, the moiré amplitude, given in this case by Eq. (5.12) with h replaced by $2h$, becomes very small for $n_1 = 4$; for $h/a = 1.125$ and a mask transmission $T = 1/6$, we find, for the very narrow line width $d_s = h/2$,

$$m_{0,4;9} = \exp\left[-\left(\frac{9\pi}{4 \times 1.665}\right)^2\right](2\sqrt{3}\pi T)^{-1/2}J_1[4(2\sqrt{3}\pi T)^{1/2}]$$

$$= -3.8 \times 10^{-9}$$

Thus, consideration of $n_1 = 2$ is quite sufficient.

If the tube is to be employed for a wide range of different TV line standards and, hence, a wide range of values of h/a, it may become impracticable to rely on moiré suppression through appropriate choices of this ratio. Even then, upper limits to the moiré period, independent of h/a, can be established by the appropriate choice of α, the angle between the scanning lines and the aperture row normals (*49*). Replacing, in Eq. (5.10), n by $n'/2$ so as to free it from the limitation of perfect interlace, we find that the moiré line number, regarded as function of h/a, is minimized for

$$\frac{h}{a} = \frac{n'}{2[(m_1^2/3) + n_1^2]}\left(\frac{m_1}{\sqrt{3}}\sin\alpha + n_1\cos\alpha\right) \tag{5.15}$$

For this value of h/a we find

$$(N_{m_1,n_1;n'})_{\min} = \frac{n'V}{2h[(m_1^2/3) + n_1^2]^{1/2}}\left(\frac{m_1}{\sqrt{3}}\cos\alpha - n_1\sin\alpha\right) \tag{5.16}$$

We thus find for the significant moiré components (for $h/a \cong 1$, $\alpha = 10°$):

(m_1, n_1)	h/a	$(N_{m_1,n_1;n'})_{\min}$	$(N_{m_1,n_1;n'})_{\min}$
(1, 1)	$\frac{3}{8}n'\left(\cos\alpha + \frac{\sin\alpha}{\sqrt{3}}\right)$,	$\frac{n'V}{4h}(\cos\alpha - \sqrt{3}\sin\alpha)$,	$0.342\frac{V}{h}$, $0.513\frac{V}{h}$
(0, 2)	$\frac{n'}{4}\cos\alpha$,	$\frac{n'V}{2h}\sin\alpha$,	$0.347\frac{V}{h}$
(2, 2)	$\frac{3}{16}n'\left(\cos\alpha + \frac{\sin\alpha}{\sqrt{3}}\right)$,	$\frac{n'V}{4h}(\cos\alpha - \sqrt{3}\sin\alpha)$,	$0.855\frac{V}{h}$

It is seen that for $\alpha = 10°$ the moiré periods do not exceed three times the scanning-line separation.

In practice, scanning distortion leads to some variation in both α and h/a. This, and the screen curvature, will lead to some variation in the period and orientation of the moiré in the image field. The magnitude of these variations can be inferred from Eqs. (5.10) and (5.11).

Shadow-mask tubes with vertical line screens and masks containing vertical-slit apertures separated by horizontal webs, as shown in Fig. 3.1(b), have moiré properties similar to those of shadow-mask tubes with dot screens, the separation between web centers playing a role corresponding to that of the center-to-center aperture separation a. Moiré effects are absent only if the slit apertures extend continuously from the top to the bottom of the mask.

5.3.2 Electron Beam Landing-Pattern Distortions

Effect of Screen Curvature

If both mask and screen are curved in axially symmetric fashion as shown in Fig. 5.12, the tangential magnification with which the mask pattern is projected onto the screen by a source at the center of the deflection plane is still given by

$$\lambda_t = L/p \tag{5.17}$$

The magnification with which a line element normal to the meridional plane in the deflection plane is projected onto the screen through a mask aperture is then

$$m_t = \lambda_t - 1 = q/p \tag{5.18}$$

Here, L, p, and q are all measured along the ray. If the screen is spherical,

with radius of curvature R_s, and the (fixed!) deflection center is at a distance L_0 from the screen, L is given by

$$L = [R_s^2 - (R_s - L_0)^2 \sin^2\theta]^{1/2} - (R_s - L_0)\cos\theta \qquad (5.19)$$

Here θ denotes the deflection angle.

If we further require that the tangential magnification be constant (tangential nesting for a mask with uniform aperture spacing!),

$$\lambda_t = \lambda_0 = L_0/p_0 \qquad (5.20)$$

the coordinates of the mask must be given by

$$r_m = \frac{p_0}{L_0} L \sin\theta, \qquad z_m = -p_0 + \frac{p_0}{L_0} L\cos\theta \qquad (5.21)$$

Eliminating θ from these equations leads to

$$-z_m = \frac{r_m^2}{2p_0}\frac{L_0}{R_s} + \frac{r_m^4}{8p_0^3}\frac{L_0^3}{R_s^3} + \cdots \qquad (5.22)$$

Within the fourth order of approximation Eq. (5.22) is the equation of a sphere of radius of curvature $(p_0/L_0)\,R_s$. This is the prescribed shape of the mask.

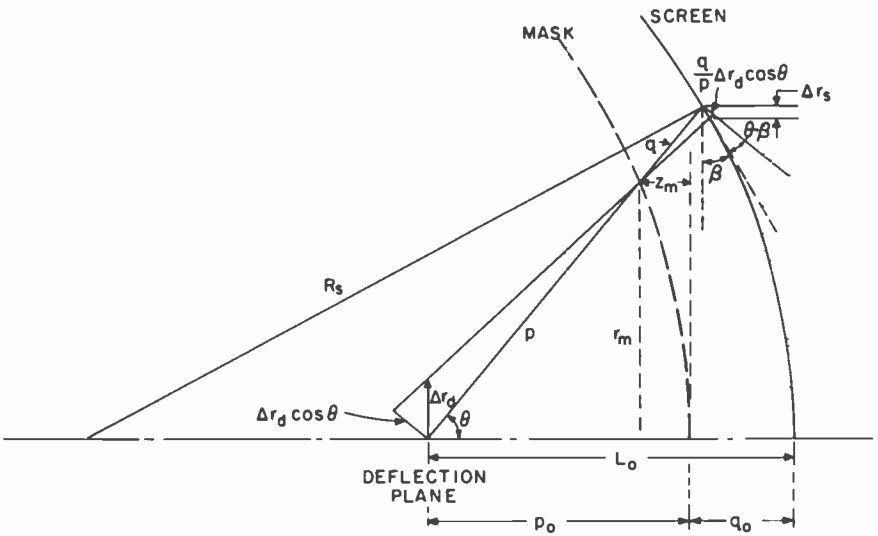

Fig. 5.12. Radial magnification of deflection plane pattern in tube with curved screen. $L = p + q$.

Even though the mask has been shaped to make the tangential magnification λ_t and m_t uniform, this is not true of the radial magnification m_r. The geometry of Fig. 5.12 shows that a radial element Δr_d in the deflection plane is projected into a radial element (projected on a plane normal to the tube axis) Δr_s given by

$$\Delta r_s = \Delta r_d \frac{q}{p} \frac{\cos\theta \cos\beta}{\cos(\theta - \beta)} \tag{5.23}$$

Here β is the inclination of the screen surface to a plane normal to the tube axis at the point of incidence. For uniform tangential magnification we thus find for the radial magnification,

$$m_r = \frac{\Delta r_s}{\Delta r_d} = \frac{\lambda_0 - 1}{1 + \tan\theta \tan\beta} \tag{5.24}$$

For the spherical screen, $\tan\beta$ is given by

$$\tan\beta = \frac{(2R_sL_0 - L_0^2)\sin\theta}{R_s^2\cos\theta + (R_s - L_0)[R_s^2 - (R_s - L_0)^2\sin^2\theta]^{1/2}} \tag{5.25}$$

The dot triads are thus increasingly contracted in a radial direction, from the center of the screen outward. This "crowding" phenomenon is illustrated in Fig. 5.13.

Effect of Deflection-Center Displacement

In the preceding analysis it was assumed that the deflection center remains stationary as the electron beams are deflected. This condition is not fulfilled in actual tubes. Here, the deflection plane moves forward with increasing angle of deflection, so that the separation of the deflection plane and the screen may be written

$$L_0' = L_0 - a_1t^2 - a_2t^4 - \cdots, \qquad t = \tan\theta \tag{5.26}$$

The coefficients $a_1, a_2, \ldots$, depend on the deflection yoke. For a tube with a 500-mm screen diagonal, a_1 may be of the order of 20 mm. In addition, dynamic convergence fields applied to the triple beam some distance ahead of the deflection plane cause the distance of the beam center from the axis in the deflection plane to increase with deflection, in accord with*

$$s = s_0 + b_1t^2 + b_2t^4 + \cdots \tag{5.27}$$

* The simple functional relationships of Eqs. (5.26) and (5.27) assume a symmetrical, anastigmatic yoke.

The value of the coefficients b_1, b_2, . . ., is determined by the distance between the convergence plane and the deflection plane, and by the focusing action of the deflecting field and the increase in deflection-plane-to-screen distance with deflection, which must be compensated by the dynamic-convergence field. The coefficient b_1 is commonly of the order of $s_0/2$.

The requirement of tangential nesting now takes the form

$$m_t = \frac{L}{p} - 1 = \frac{L}{p}\left(1 - \frac{p_0}{L_0}\right)\frac{s_0}{s}, \qquad p = L\left[1 - \left(1 - \frac{p_0}{L_0}\right)\frac{s_0}{s}\right] \tag{5.28}$$

with

$$L = [R_s^2 - (R_s - L_0')^2 \sin^2 \theta]^{1/2} - (R_s - L_s') \cos \theta \tag{5.29}$$

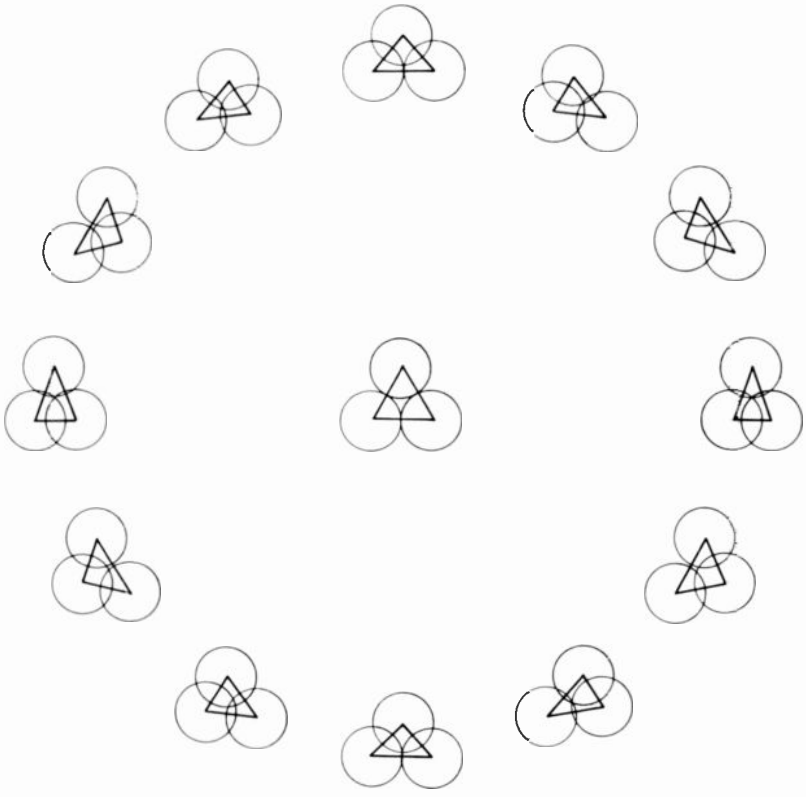

Fig. 5.13. Triad crowding in tube with curved mask and screen.

The relations

$$r_m = p \sin \theta, \qquad z_m = -(L_0' - q_0) + p \cos \theta \tag{5.30}$$

now lead to

$$z_m = -\frac{r_m^2}{2}\left\{\frac{L_0}{p_0 R_s} - 2\left(\frac{a_1}{p_0^2} + \frac{b_1 L_0}{s_0 p_0^2}\right)\left(1 - \frac{p_0}{L_0}\right)\right\} + \cdots \tag{5.31}$$

The variation in the position of the deflection centers thus leads to an increase in the radius of curvature of the mask R_m, given by

$$R_m = \frac{p_0 R_s}{L_0} \Big/ \left[1 - 2\left(\frac{a_1}{p_0} + \frac{b_1 L_0}{s_0 p_0}\right)\frac{R_s}{L_0}\left(1 - \frac{p_0}{L_0}\right)\right] \tag{5.32}$$

Since b_1/s_0 is commonly of the order of 0.5, whereas a_1/p_0 is invariably small compared to unity, the degrouping, or outward movement of the deflection centers with deflection, has the greatest effect on the mask curvature. The crowding effect, or asymmetry of the triads, is similar as in the absence of deflection-center motion, since it is simply the result of radial foreshortening of the deflection plane as seen from the screen and the deviation of the screen inclination from perpendicularity to the axis.

Effect of Ambient Magnetic Fields

The landing points of the electron beams on the screen are also affected by ambient magnetic fields such as the earth's magnetic field, modified by the presence of magnetic materials within and in the neighborhood of the tube. Normally, external or internal magnetic shields and the steel masks greatly reduce the magnetic field intensity within the tube.

In the United States, the earth's magnetic field has a vertical component approximately equal to 0.5 G (0.5×10^{-4} W/m^2), whereas the horizontal component is of the order of 0.2 G. While the effect of the horizontal component depends on the orientation of the TV set, this is not true of the effect of the vertical component. Accordingly, compensation for the effect of the residual vertical component of the earth's magnetic field may fittingly be built into the tube design.

Assume that only a vertical magnetic field component is present and that this is constant throughout the tube volume and given by the induction B. Then the projection of the beam path on a horizontal (or zx) plane is circular, with a radius

$$R' = (1/B)[(mV/2e)(1 - \sin^2 \theta \sin^2 \phi)]^{1/2} \tag{5.33}$$

Here e/m is the specific charge of the electron, V is the anode potential, θ is the deflection angle, and ϕ is the azimuthal angle of the deflected beam

($\phi = 0$ or π for the horizontal plane). If, as shown in Fig. 5.14, the projected beam path between deflection center and mask and that between mask and screen are designated by p' and q', respectively,

$$p' = p(1 - \sin^2\theta \sin^2\phi)^{1/2}, \qquad q' = q(1 - \sin^2\theta \sin^2\phi)^{1/2} \quad (5.34)$$

the action of the field between deflection center and mask effects an angular displacement $\delta\theta'$ in the horizontal projection plane at the mask:

$$\delta\theta' = p'/2R' \quad (5.35)$$

The total displacement in the x direction (the horizontal direction in a plane normal to the tube axis) is hence given by

$$\begin{aligned}\delta x &= \left(q'\,\delta\theta' + \frac{q'^2}{2R'}\right)(1 + \tan^2\beta\cos^2\phi)^{-1/2} \\ &\quad \times \sec[\arccos(1 + \tan^2\theta\cos^2\phi)^{-1/2} - \arccos(1 + \tan^2\beta\cos^2\phi)^{-1/2}] \\ &= \frac{(p' + q')q'}{2R'}\,\frac{(1 + \tan^2\theta\cos^2\phi)^{1/2}}{1 + \tan\theta\tan\beta\cos^2\phi} \end{aligned} \quad (5.36)$$

For a plane screen and mask, with $\beta = 0$, $p = p_0 \sec\theta$, $q = q_0 \sec\theta$, we ob-

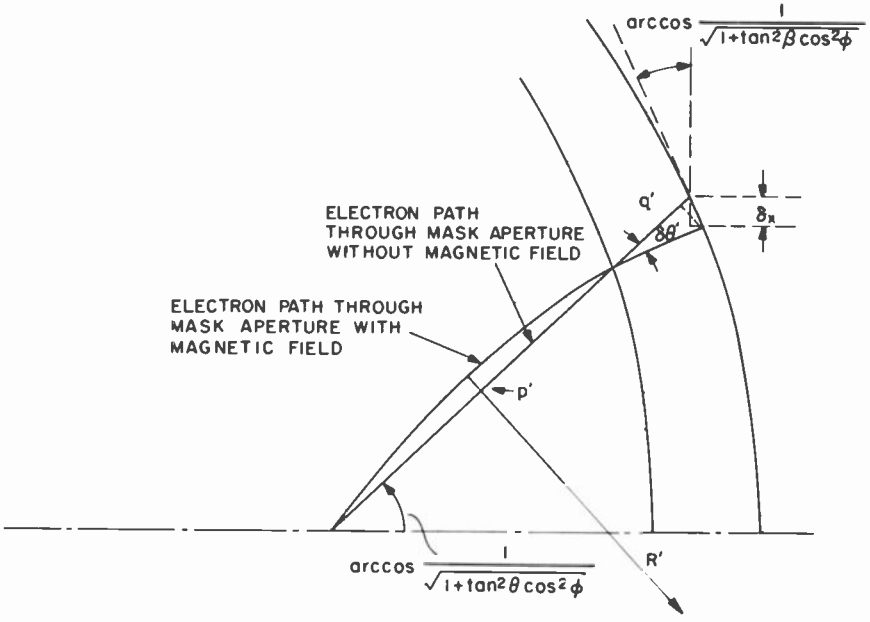

Fig. 5.14. Beam deflection by vertical component of magnetic field.

tain simply

$$\delta x = \frac{(p_0 + q_0) q_0 \sec^3 \theta (1 - \sin^2 \theta \sin^2 \phi)}{2R_0} \tag{5.37}$$

with $R_0 = 33.7\{[V(\text{volt})]^{1/2}/B(\text{gauss})\}$ mm. For example, for a tube with $p_0 + q_0 = 400$ mm, $q_0 = 13.6$ mm, $B = 0.54$ G, $V = 25{,}000$ V, $R_0 = 9867$ mm, we obtain $\delta x = 0.28$ mm for $\theta = 0$. Observed residual displacements in a typical tube using shielding are found to be about 0.05 mm, i.e., less by a factor of the order of 5, indicating the effectiveness of the magnetic shielding. Furthermore, the displacements are not found to increase as $\sec^3 \theta$ for $\phi = 0$, but instead, to decrease slightly with deflection. In practice the increased effectiveness of the shielding toward the periphery or edge of the tube more than compensates the increase with deflection expected for a uniform magnetic field [which is less than given by Eq. (5.37) in view of the curvature of the screen].

In summary, the vertical field component produces a displacement of the landing points of the beam, which is reduced by the shielding of the tube. The shielding, however, also distorts the field so that some nonuniformity in the lateral displacement of the beam landing is produced.

5.3.3 Lighthouse Optics and Limitations for Printing Phosphor Screens

First-Order Printing and Lens Correction for Phosphor-Dot Screens

The screen of the shadow-mask tube, coated with a photosensitized slurry of one of the three phosphors, is printed by exposing the faceplate through the mask to a light source placed at or near the center of deflection of the beam (i.e., the intersection of the axis of the deflected beam with the axis of the undeflected beam, Fig. 5.15). This process is called first-order printing as distinguished from second-order printing which is described in Section 5.3.4. If the deflection center were invariant with deflection, the electron spots on the screen would also be centered on the electron dots; the registration of spots and dots would be perfect. The electron beams and corresponding light beams passing through the center of any one mask aperture would be identical in direction, and the resulting triad of electron spots would be centered on a triad of phosphor dots.

Unfortunately, as we have noted in Section 5.3.2, the deflection centers are not stationary. The properties of the deflecting fields are such as to cause them to move forward, toward the screen, with increasing deflection angle. Dynamic convergence, mentioned in Section 5.1, causes the centers

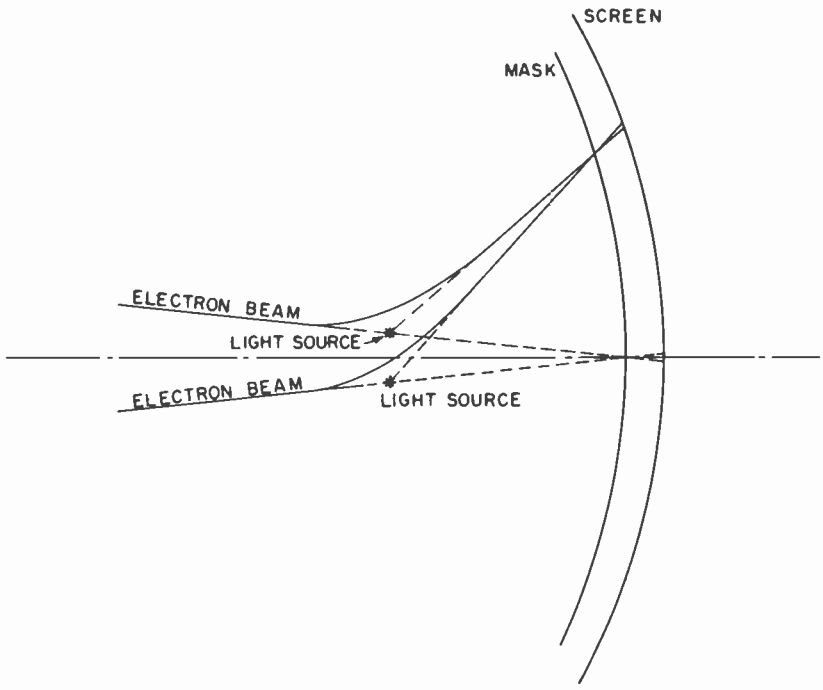

Fig. 5.15. Proper positioning of light source for first-order printing.

to move away from the axis. Finally, residual ambient magnetic fields, after magnetic shielding through which the beams pass, produce a displacement of the deflection centers from their position in the absence of the fields. The effects of these three factors are shown qualitatively in Fig. 5.16.

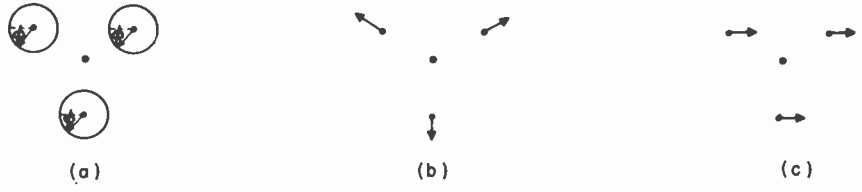

Fig. 5.16. Qualitative effect on apparent position of deflection centers in fixed plane of (a) forward motion of deflection centers with increasing deflection, (b) radial displacement of deflection centers by dynamic convergence fields, and (c) lateral displacement of deflection centers by vertical magnetic field.

Optical correcting elements are generally interposed between the light source and the mask to effect an apparent displacement of the light source corresponding to the displacement of the electron deflection center, or in other words, to cause the directions of the light beams incident on the mask-aperture centers to coincide with the directions of the corresponding electron beams. In this manner, improved registration between electron spots and phosphor dots may be achieved.

We shall now consider the form of the correction lens required. We shall assume that it has a flat back face, a perpendicular distance s_0 from an on-axis printing source (Fig. 5.17). At a point of the lens surface with the coordinates (x, y) we shall assume the lens to have a thickness $D(x, y)$ so that in polar coordinates we can write:

$$x = r\cos\phi, \qquad y = r\sin\phi \tag{5.38}$$

with

$$r = (s_0 + D/N)t, \qquad N = [n^2 + (n^2 - 1)t^2]^{1/2} \tag{5.39}$$

We write t for $\tan\theta_0$, where θ_0 is the angle of inclination of a light ray leaving the source and differs very little from the angle of deflection θ; n is the refractive index of the lens.

We assume the slopes of the lens surface to be very small. For any orientation of the incident light ray (t, ϕ) the lens acts as a combination of an infinitely thin prism with the vertex angle components $(\partial D/\partial x, \partial D/\partial y)$ and a plane parallel slab of glass of thickness D. As such it produces an ap-

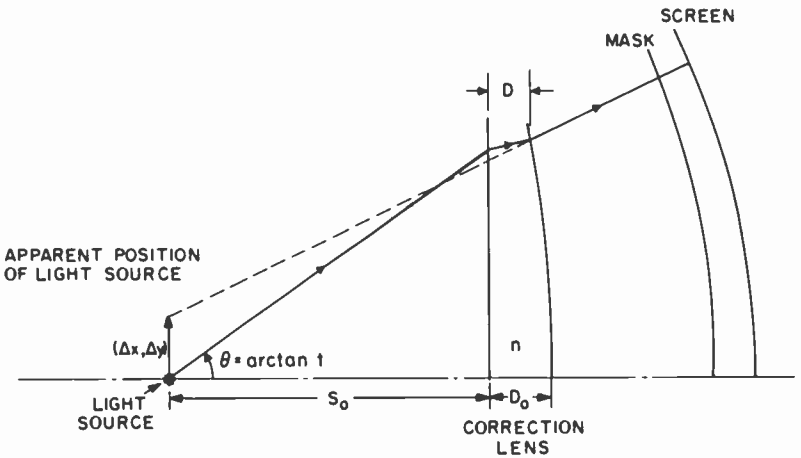

Fig. 5.17. Design of correction lens.

parent shift of the source in the source plane given by

$$\Delta x = -(N-1)\left\{(s_0+D)\left[\frac{\partial D}{\partial x}(1+t^2\cos^2\phi)+\frac{\partial D}{\partial y}t^2\sin\phi\cos\phi\right]+\frac{D}{N}t\cos\phi\right\} \tag{5.40}$$

$$\Delta y = -(N-1)\left\{(s_0+D)\left[\frac{\partial D}{\partial x}t^2\sin\phi\cos\phi+\frac{\partial D}{\partial y}(1+t^2\sin^2\phi)\right]+\frac{D}{N}t\sin\phi\right\}$$

Let the y direction coincide with the direction of displacement of the source from the tube axis, i.e., with the "s direction." Then perfect registration will be realized for

$$\Delta x = -(L_0 - L_0')t\cos\phi, \qquad \Delta y = -(L_0 - L_0')t\sin\phi + (s - s_0) \tag{5.41}$$

Here both $(L_0 - L_0')$ and $(s - s_0)$ are polynomials in t^2, as given by Eqs. (5.26) and (5.27).

If x and y are expressed in terms of t and ϕ, the first Eq. (5.40) becomes

$$\Delta x = -(N-1)\left\{\frac{s_0+D}{s_0+(t/N)(\partial D/\partial t)+n^2D/N^3}\times\left[(1+t^2)\frac{\partial D}{\partial t}\cos\phi-\frac{s_0+(n^2D/N^3)}{s_0+(D/N)}\frac{\partial D}{\partial\phi}\frac{\sin\phi}{t}\right]+\frac{D}{N}t\cos\phi\right\}$$

$$\cong -(N-1)\left\{(1+t^2)\frac{\partial D}{\partial t}\cos\phi-\frac{\partial D}{\partial\phi}\frac{\sin\phi}{t}+\frac{D}{N}t\cos\phi\right\} \tag{5.42}$$

The only approximation involved in Eq. (5.42) is that the separation s_0 is very large compared to the lens thickness D. For Δy we find similarly

$$\Delta y \cong -(N-1)\left\{(1+t^2)\frac{\partial D}{\partial t}\sin\phi+\frac{\partial D}{\partial\phi}\frac{\cos\phi}{t}+\frac{D}{N}t\sin\phi\right\} \tag{5.43}$$

It is convenient to consider separately the lens required to compensate for the forward motion of the deflection plane [Eq. (5.26)] and that needed to correct for degrouping [Eq. (5.27)]. If these lenses are sufficiently weak and thin, their thicknesses may simply be added to form a single lens ac-

complishing both purposes. With

$$D = D_r + D_g \tag{5.44}$$

we demand

$$t(a_0 + a_1t^2 + a_2t^4 + \cdots) = (N - 1)\left\{(1 + t^2)\frac{\partial D_r}{\partial t} + \frac{D_r}{N}t\right\} \tag{5.45}$$

where D_r represents a radially symmetric lens, being a function of t only. The degrouping lens, on the other hand, should satisfy

$$0 = (N - 1)\left\{(1 + t^2)\frac{\partial D_g}{\partial t}\cos\phi - \frac{\partial D_g}{\partial \phi}\frac{\sin\phi}{t} + \frac{D_g}{N}t\cos\phi\right\} \tag{5.46}$$

$$b_1t^2 + b_2t^4 + \cdots$$

$$= -(N - 1)\left\{(1 + t^2)\frac{\partial D_g}{\partial t}\sin\phi + \frac{\partial D_g}{\partial \phi}\frac{\cos\phi}{t} + \frac{D_g}{N}t\sin\phi\right\} \tag{5.47}$$

In Eq. (5.45) we have added a constant term a_0 on the left, to correspond to a fixed displacement of the source plane from the deflection plane for zero deflection. Equation (5.45) is readily solved. In series form we can write

$$\begin{aligned} D_r = D_{r0} &+ \left(-\frac{D_{r0}}{2n} + \frac{a_0}{2(n-1)}\right)t^2 \\ &+ \left(\frac{(3n^2 + n - 1)D_{r0}}{8n^3} - \frac{(3n + 2)a_0}{8n(n-1)} + \frac{a_1}{4(n-1)}\right)t^4 \\ &+ \left(-\frac{(5n^4 + 3n^3 - 3n^2 - n + 1)D_{r0}}{16n^5}\right. \\ &\left. + \frac{(5n^3 + 6n^2 + n - 1)a_0}{16n^3(n-1)} - \frac{(2n + 1)a_1}{8n(n-1)} + \frac{a_2}{6(n-1)}\right)t^6 \\ &+ \cdots \end{aligned} \tag{5.48}$$

If the center thickness D_{r0} of the radial lens approaches zero and the displacement a_0 of the source plane from the deflection plane for zero deflection is also set equal to zero, the radial lens becomes simply a concave fourth-order correction plate with zero central power (Fig. 5.18a). As with Schmidt telescope correction plates, it is preferred to give the lens a small positive refractive power at the center, so as to minimize the maximum slope of the lens surface (*50*). Limiting attention to terms up to the fourth

order in t in Eq. (5.48), this condition is realized for a source displacement

$$a_s = \frac{n-1}{n} D_{r0} - \frac{3}{4} t_m^2 \frac{a_1 - [(n^2-1)/2n^3]D_{r0}}{1 - [3(3n+2)t_m^2/8n]} \tag{5.49}$$

The lens profile becomes

$$D_r = D_{r0} + \left[4\left(1 - \frac{3(3n+2)}{8n} t_m^2\right)\right]^{-1} \times \left(\frac{a_1}{n-1} - \frac{n+1}{2n^3} D_{r0}\right)(-\tfrac{3}{2}t_m^2 t^2 + t^4) \tag{5.50}$$

where

$$D_{r0} \geq \frac{[9a_1/64(n-1)]t_m^4}{1 - [3(3n+2)/8n]t_m^2 + [9(n+1)/128n^3]t_m^4} \tag{5.51}$$

This lens profile is illustrated in Fig. 5.18(b).

Finally, Eq. (5.48) shows that, to the fourth order of approximation, a thick glass plate (*51*) can perform the function of the radial correcting lens

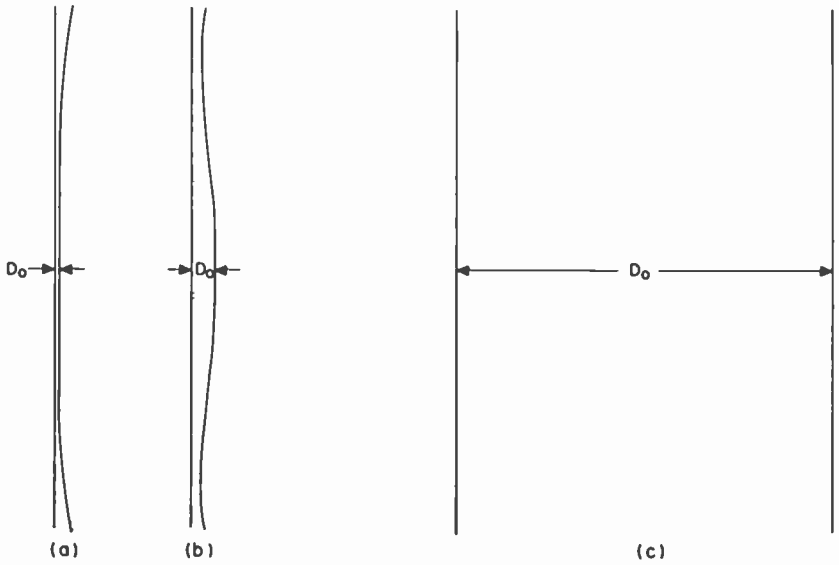

Fig. 5.18. Radial correcting lens: (a) with zero central refractive power, (b) with maximum surface slope minimized, and (c) in the form of a thick plane parallel glass plate.

(Fig. 5.18c). It is only necessary to set the coefficients of t^2 and t^4 equal to zero, leading to

$$a_0 = [(n-1)/n]D_{r0} = [2n^2/(n+1)]a_1,$$
$$D_{r0} = [2n^3/(n^2-1)]a_1 \tag{5.52}$$

In practice, a screen is first printed without a correcting lens. In the finished tube, the radial displacement of the electron spot triads from the corresponding dot triads is then measured. The needed displacement of the source in the source plane may then be computed with the aid of Eq. (5.23):

$$\Delta r_d = \Delta r_s(p/q)(1 + \tan\theta \tan\beta) \tag{5.53}$$

If the screen and mask are spherical, with radii of curvature R_s and R_m, $\tan\beta$ is given by Eq. (5.25), and

$$p = [R_m^2 - (R_m - L_0 + q_0)^2 \sin^2\theta]^{1/2} - (R_m - L_0 + q_0)\cos\theta \tag{5.54}$$

$$q = [R_s^2 - (R_s - L_0)^2 \sin^2\theta]^{1/2} - [R_m^2 - (R_m - L_0 + q_0)^2 \sin^2\theta]^{1/2} + (q_0 + R_m - R_s)\cos\theta \tag{5.55}$$

θ is related to the radial distance from the screen center r_s by

$$\tan\theta = \frac{r_s}{(R_s^2 - r_s^2)^{1/2} - (R_s - L_0)} \tag{5.56}$$

L_0 designates here the distance from the source to the screen, measured along the tube axis.

The quantity Δr_d obtained from Eq. (5.53) is, finally, substituted for the left side of Eq. (5.45), which is integrated numerically for the initial conditions

$$D_r = D_{r0}, \qquad \partial D_r/\partial t = 0 \qquad \text{for} \quad t = 0 \tag{5.57}$$

Greater difficulties are encountered in the solution of the equations for the degrouping lens, Eqs. (5.46) and (5.47). If we define

$$F(t) = -\frac{\Delta y_p}{N-1} = -(b_1 t^2 + b_2 t^4 + \cdots)/(N-1) \tag{5.58}$$

Eqs. (5.46) and (5.47) can be rewritten

$$\frac{\partial D_g}{\partial t}(1 + t^2) + \frac{D_g t}{N} = F(t)\sin\phi \tag{5.59}$$

$$\frac{1}{t}\frac{\partial D_g}{\partial \phi} = F(t)\cos\phi \tag{5.60}$$

We have here written $\Delta y_p(t)$ for the desired degrouping displacement of the source.

Equation (5.60) is solved by

$$D_g = tF(t) \sin \phi + G(t) \tag{5.61}$$

Equation (5.61) substituted into Eq. (5.59) leads to the two equations

$$\frac{1}{F}\frac{dF}{dt} = -\frac{t}{1+t^2}\frac{N+1}{N}, \qquad \frac{1}{G}\frac{dG}{dt} = -\frac{t}{N(1+t^2)} \tag{5.62}$$

This pair of equations has a solution only for $\Delta y_p(t) = \Delta y_0 = \text{const}$, given by

$$D_g = -\frac{t\,\Delta y_0 \sin \phi}{N-1} + D_{g0}\left[\frac{(n-1)(N+1)}{(n+1)(N-1)}\right]^{1/2} \tag{5.63}$$

Thus, the only continuous lens surfaces which produce no lateral displacement of the source ($\Delta x = 0$) produce a fixed source displacement in the s direction. This is, of course, trivial, since a simple source displacement accomplishes the same thing. In fact, one of the earlier approaches for minimizing the degrouping error was to place the source halfway between the position appropriate for the center and that appropriate for the periphery of the screen (*52*). In this manner, the maximum degrouping error was reduced to half the value occurring at the periphery with the source placed so as to achieve perfect registration at the center.

It is not surprising that we cannot design a lens surface which will produce arbitrarily prescribed source displacements $\Delta y_p(t, \phi)$, $\Delta x_p(t, \phi)$: this would mean that we could obtain a continuous lens surface for an arbitrary variation of $\partial D/\partial x$, $\partial D/\partial y$. Actually, if $\partial D/\partial x$ alone is prescribed, along with $D(0, y)$ on some boundary line 0, y, the surface is completely defined; in particular, the y slope at any point is given by

$$\frac{\partial D}{\partial y}(x, y) = \frac{\partial D}{\partial y}(0, y) + \int_0^x \frac{\partial}{\partial y}\left(\frac{\partial D}{\partial x}\right) dx \tag{5.64}$$

Similarly, if we prescribe $\Delta y(t)$, $\Delta x(t)$ is fixed automatically. Thus, for

$$\Delta y(t) = b_1 t^2 \tag{5.65}$$

the solution of Eqs. (5.42) and (5.43) leads to

$$\Delta x(t) = b_1 t^2[\sin(2\phi) + (t^2/3)\sin(4\phi) + \cdots] \tag{5.66}$$

Thus, the error in the source position ranges from 0 along the axes (for $\phi = 0, \pi/2, \pi, 3\pi/2$) to a distance equal to the full prescribed displace-

ments for four intermediate directions ($\phi = \pi/4, 3\pi/4, 5\pi/4, 7\pi/4$). In brief, the error in the source position and the corresponding degrouping error in the spot-dot registration can be distributed in various manners, but cannot be annulled. If the degrouping lens has the symmetry

$$D_g(t, \phi) = D_{gg}(t) \sin \phi \tag{5.67}$$

a lens can be designed which will lead to the same source position error $\Delta\rho(t)$ for all azimuths ϕ and a prescribed deflection t:

$$\Delta y = \Delta y_p - \Delta\rho \cos(2\phi), \qquad \Delta x = \Delta\rho \sin(2\phi) \tag{5.68}$$

Solution of Eqs. (5.42) and (5.43) leads to

$$\Delta\rho = \Delta y_p(t) - \frac{1 + t^2}{t^2} \int_0^t \frac{2t\, \Delta y_p(t)}{(1 + t^2)^2}\, dt \tag{5.69}$$

$$D_{gg}(t) = - \frac{1 + t^2}{t(N - 1)} \int_0^t \frac{2t\, \Delta y_p(t)}{(1 + t^2)^2}\, dt \tag{5.70}$$

For example, for

$$\Delta y_p(t) = b_1 t^2 \tag{5.71}$$

which quite generally represents the degrouping displacement for small deflection angles,

$$\Delta\rho = \tfrac{1}{2} b_1 t^2 \left(1 + \frac{t^2}{3} + \cdots\right) \tag{5.72}$$

$$D_{gg} = - \frac{1}{2(n - 1)} b_1 t^3 \left(1 - \frac{5n + 3}{6n} t^2 + \cdots\right) \tag{5.73}$$

The nature of the residual registration error is illustrated in Fig. 5.19: as the beam, for fixed deflection, rotates about the axis, the effective source position rotates about the desired source position at twice the angular rate. The position error is half the source displacement Δy_p; thus it is half the maximum source displacement at the periphery and zero at the center—a condition much to be preferred over that realizable by a fixed source displacement, which makes the position error half the maximum source displacement at the periphery and at the center.

The degrouping lens represented by Eq. (5.67) can be regarded as a prism whose vertex angle varies quadratically with the deflection t, vanishing on the axis. Its profile in the yz plane resembles a cubic parabola, that in the xz plane is a straight line. The degrouping lens thicknesses given by

Eq. (5.67) for $0 < \phi < \pi$, $t > 0$ are negative; this is permissible, since the degrouping lens thickness is added to a radial lens with finite center thickness. The combination of the two lenses is illustrated in Fig. 5.20.

A partial degrouping correction has also been achieved by tilting and offsetting the radial lens, which has the effect of introducing into the light path a prism varying in power with deflection. However, for large deflection angles such semiempirical procedures are inadequate. The same applies to the theoretical treatment given so far, which has been limited in application to small deflection angles and has assumed, furthermore, yoke properties which are rarely realized. It has served primarily to point out limitations in the degree of correction which can be achieved with continuous-surface correction lenses.

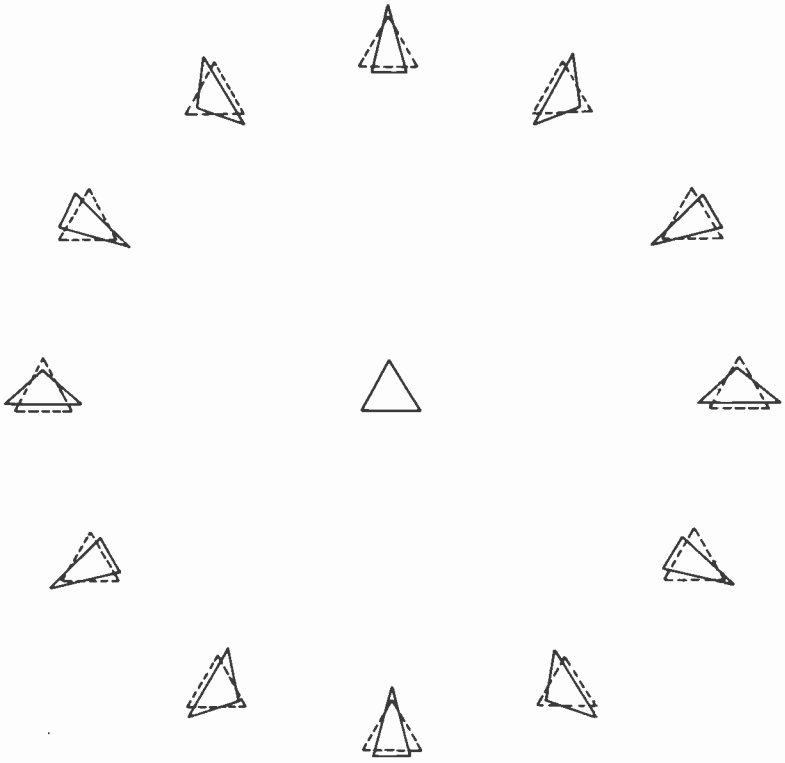

Fig. 5.19. Residual registration error as function of azimuth for degrouping lens given by Eqs. (5.67) and (5.73): dashed lines, trio-center triangle without error; solid lines, trio-center triangle with error.

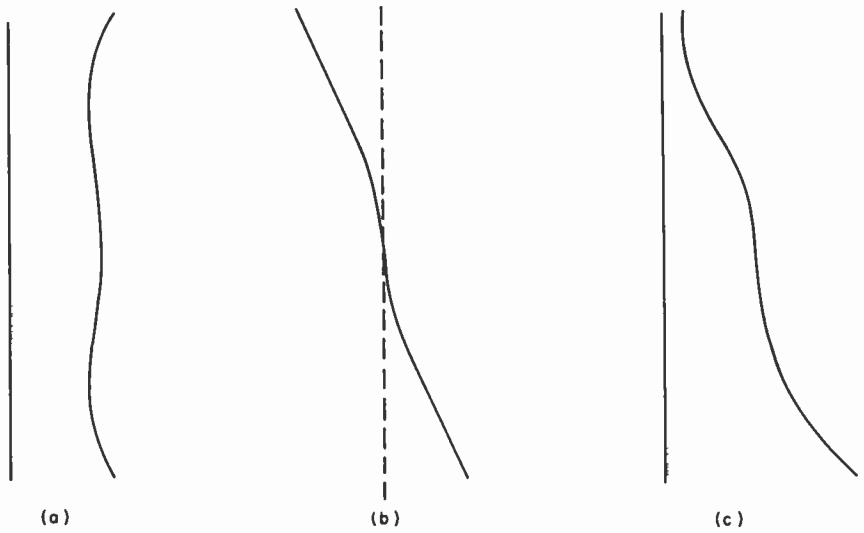

Fig. 5.20. Combination of radial and degrouping lens: (a) radial correcting lens; (b) degrouping component; and (c) final correcting lens (horizontal: vertical scale, 40:1).

A preferred practice (*53*) is to measure spot-dot displacements obtained either without any lens or, better, a correction lens of known surface contour correcting the radial and, eventually, a major portion of the degrouping error. These measurements are then translated into two components of lens-surface slope (for an assumed variation of lens thickness) required to cause the light rays from the source to be incident on the mask aperture centers in the same direction as the electron beam from the corresponding gun. A correcting lens contour of the form

$$D(x, y) = \sum_{j,k} a_{j,k} x^j y^k \tag{5.74}$$

is then obtained, with the coefficients $a_{j,k}$ chosen so as to minimize the mean square error in the surface slope components (and hence in registration) for several hundred reference points, for which registration errors have been measured or interpolated. This rather complex procedure, which requires the use of a large-scale computer, automatically takes care of yoke asymmetries and ambient magnetic fields (assuming that these are the same at the time of measurement and in the final use of the color picture tube). However, the limitation in the degree of correction of the degrouping correction error achievable with a continuous lens surface still applies. The

maximum residual registration error may be of the order of 1/3 of the maximum uncorrected degrouping error.

It should be noted that no improvement in the attainable degree of correction is to be anticipated from the use of a sequence of continuous lenses since the contribution of each of them is subject to the same limitations.

Lens Correction for First-Order Printing of Line Screens

In contrast to the dot screen discussed in the preceding section, a continuous-surface lens can be designed to completely eliminate printing errors in a phosphor line screen. In this case, a displacement of apparent source points parallel to the phosphor lines does not affect registration between the electron lines and the phosphor lines. A longitudinally extended source can advantageously be used for printing the screen. For an anastigmatic yoke the degrouping correcting lens (with zero center thickness) satisfying Eq. (5.43) can be described by

$$D_g(t, \phi) = c_1(t) \sin \phi + c_3(t) \sin(3\phi) + c_5(t) \sin(5\phi) + \cdots \quad (5.75)$$

For the specific degrouping characteristic given by Eq. (5.65) and a displacement along the phosphor lines (in the x direction) given by Eq. (5.66) the degrouping lens component is

$$D_g(t, \phi) = -\frac{(1 + t^2)^{1/2}}{2(N - 1)} b_1 t^3 \left[\left(1 - \frac{t^2}{3} + \cdots\right) \sin \phi + \left(\frac{1}{3} - \cdots\right) \sin(3\phi) + \left(\frac{t^2}{15} - \cdots\right) \sin(5\phi) + \cdots \right] \quad (5.76)$$

Here terms of the seventh and higher orders in t have been omitted.

The lens here described effects a source displacement in a direction normal to the phosphor lines exactly equal to the displacement of the electron source with deflection. The fact that, in the direction of the phosphor lines, it produces a small source displacement [given by Eq. (5.66)], which does not correspond to the electron source displacement, produces no printing error, if the printed phosphor lines are continuous. While the example here presented is specialized and the theoretical treatment given is limited in validity, the conclusion is generally valid: for the first-order printing of line screens, it is possible to design continuous degrouping lenses which eliminate the degrouping printing error if the phosphor lines are continuous. This follows from the fact that only one component of the source displacement, namely that producing a displacement perpendicular to the phosphor lines, must be the same for the light source and the electron source. Accordingly, only one component of the surface slope of the degrouping lens is prescribed over its entire area.

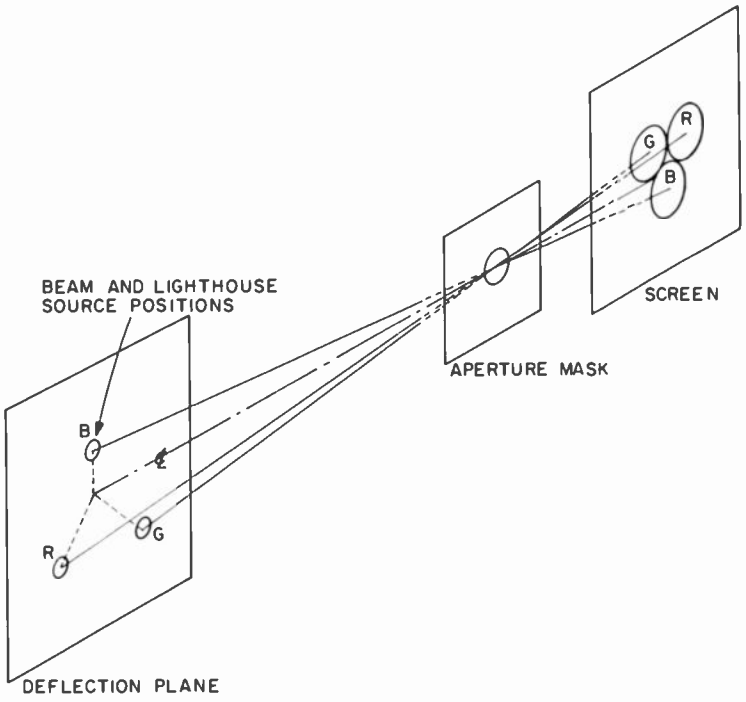

Fig. 5.21. Pictorial representation of first-order lighthouse printing.

Second-Order Printing and Lens Correction for Phosphor-Dot Screens

A different approach to the solution of the register problem due to degrouping is by the use of second-order printing. In the previous section, first-order printing was described. First-order printing may be defined as a printing technique wherein the light source is at, or approximately at, the position in the deflection plane in which the electron beam will appear in the finalized tube, as shown in Fig. 5.21. Second-order printing, however, differs in that the light source used for printing is not in the same location as the electron beam in the final tube, but rather is displaced a distance $3s$. As shown in Figs. 5.22 and 5.23, the displacement is such that a given phosphor dot is printed by exposing the light through the adjacent aperture in the shadow mask to that which will be used by the electron beam.

With second-order printing, as compared with first-order printing, separations of beam centers from the axis in the deflection plane are doubled and the red, green, and blue beam cross sections are rotated through 180°

about the axis. As a result, any triad of adjoining dots is produced by light beams passing through three different mask apertures surrounding the mask aperture utilized for forming the dot triad in first-order printing. This is shown more clearly in Fig. 5.23 where shading marks out the dots printed through the three apertures utilized for the central triad considered.

In Fig. 5.24 it can be shown that in second-order printing three light beams forming a triad will converge, whereas the three electron beams forming the corresponding dot triad diverge. Thus, the adjustment of q may be utilized to obtain a match in the relative size of the beam triad compared to the dot triad. This adjustment, therefore, is in effect a compensation for degrouping. Its limitation is that the degrouping for all three colors must be

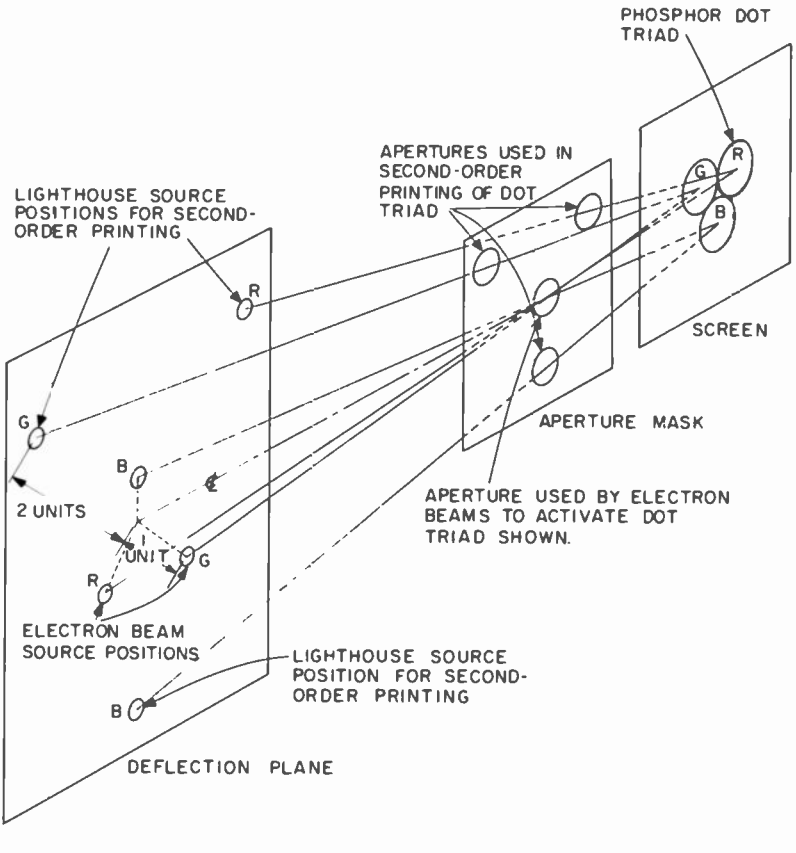

Fig. 5.22. Pictorial representation of second-order lighthouse printing.

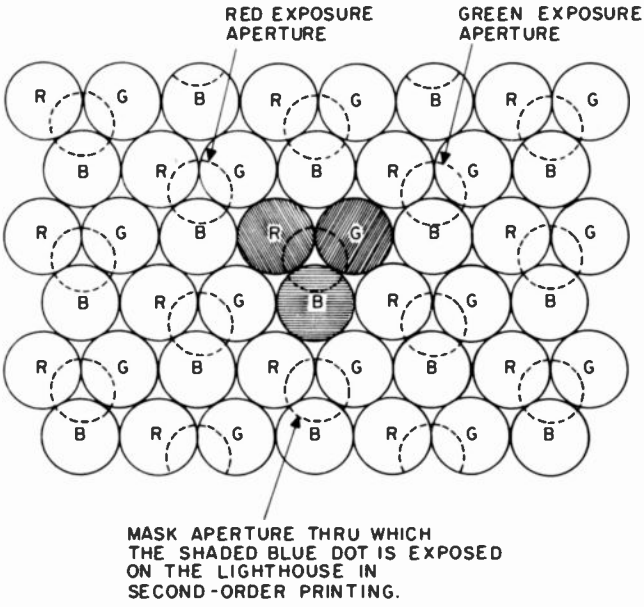

Fig. 5.23. Relation between mask apertures and dots printed through them in second-order printing.

equal in order to have complete compensation. In practice, due to yoke design considerations and foreshortening of dot triads, this is not always possible; however, it is possible to take the bulk of degrouping correction compensation in this manner.

In general, dynamic convergence produces a larger s value; that is, individual beams move away from the axis as the beams are deflected toward the edge of the screen. Therefore, in general, the electron beam triad is too large at the edge of the screen compared to the phosphor dots, hence the term "degrouping." If q is reduced near the edge of the screen, the electron beam triad becomes smaller, and conversely, the phosphor dot triad becomes larger. By selection of the proper value of q the average size of the beam triad and the dot triad may be made to coincide.

The q adjustment, which allows degrouping correction, has a drawback from a practical standpoint. Any variation of the q distance from optimum in tube manufacture will produce a register error. In first-order printing, a change in q will make both the electron beam and phosphor dot triad expand or contract but will not change the relative register between the two.

Hence, q variations with first-order printing will affect overall tube tolerance but will not affect register per se. It is, therefore, a choice between the improvement in the register obtainable with a continuous surface lens and the criticality of maintaining the q adjustment which establishes a relative merit of the two printing systems.

Pursuing further the correction of residual registration errors in second-order printing, it can be shown quite simply that a correction lens can be designed which, in principle, will make these errors vanish provided the deflection yoke has axial symmetry and is anastigmatic.

For an anastigmatic yoke the required degrouping component of the correction lens has the form of Eq. (5.67). Furthermore, if the aperture center pattern of the mask projected on a plane normal to the tube axis is a regular hexagonal pattern with aperture-center separation a, the separa-

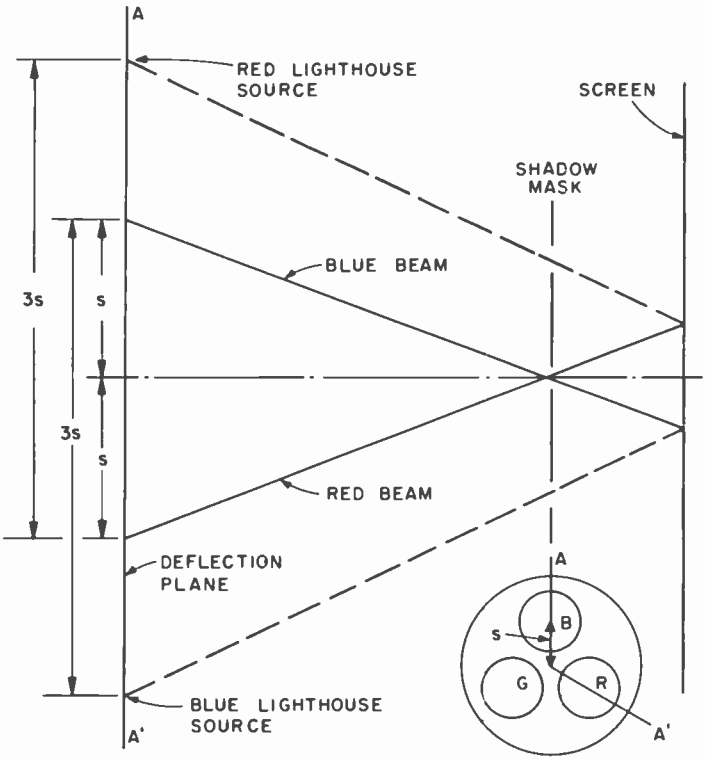

Fig. 5.24. Second-order printing geometry.

tion of the blue electron center from the blue light source center in the deflection plane (made coincident for the two by the radial lens component) is given by

$$\Delta y = a\left(\frac{\cos^2\phi}{m_t} + \frac{\sin^2\phi}{m_r}\right) - (s + 2s_0 - a)$$

$$= \frac{a}{2}\left(\frac{1}{m_t} + \frac{1}{m_r}\right) - (s + 2s_0 - a) + \frac{a}{2}\left(\frac{1}{m_t} - \frac{1}{m_r}\right)\cos(2\phi) \quad (5.77)$$

$$\Delta x = -\frac{a}{2}\left(\frac{1}{m_t} - \frac{1}{m_r}\right)\sin(2\phi) \quad (5.78)$$

Substitution of Eq. (5.67) in Eqs. (5.42) and (5.43) leads to

$$\Delta y = -\frac{N-1}{2}\left\{(1+t^2)\frac{\partial D_{gg}}{\partial t} + \frac{D_{gg}}{t} + \frac{D_{gg}t}{N}\right.$$

$$\left. -\left((1+t^2)\frac{\partial D_{gg}}{\partial t} - \frac{D_{gg}}{t} + \frac{D_{gg}t}{N}\right)\cos(2\phi)\right\} \quad (5.79)$$

$$\Delta x = -\frac{N-1}{2}\left((1+t^2)\frac{\partial D_{gg}}{\partial t} - \frac{D_{gg}}{t} + \frac{D_{gg}t}{N}\right)\sin(2\phi) \quad (5.80)$$

In Eqs. (5.77) and (5.78), m_t and m_r are the tangential and radial magnifications with which the deflection plane is projected through a mask aperture onto the screen, s is the distance of the electron deflection center from the axis, and $2s_0$ is the distance of the source from the axis. $m_t = q/p$ is proportional to q, whereas the ratio m_t/m_r is a function of t independent of the value of q. With Eqs. (5.77)–(5.80) we form:

$$\Delta y + \Delta x\cot(2\phi) = \frac{a}{2}\left(\frac{1}{m_t} + \frac{1}{m_r}\right) - (s + 2s_0 - a)$$

$$= -\frac{N-1}{2}\left((1+t^2)\frac{\partial D_{gg}}{\partial t} + \frac{D_{gg}}{t} + \frac{D_{gg}t}{N}\right) \quad (5.81)$$

$$\Delta y - \Delta x\frac{1-\cos(2\phi)}{\sin(2\phi)} = \frac{a}{m_t} - (s + 2s_0 - a) = -(N-1)\frac{D_{gg}}{t} \quad (5.82)$$

Substitution of a/m_t from Eq. (5.82) in Eq. (5.81) leads to the differential

equation in t:

$$\left(1 - \frac{m_t}{m_r}\right)(s + 2s_0 - a) = (N - 1)\left((1 + t^2)\frac{\partial D_{gg}}{\partial t} - \frac{m_t}{m_r}\frac{D_{gg}}{t} + \frac{D_{gg}t}{N}\right) \tag{5.83}$$

This equation can be integrated for the profile $D_{gg}(t)$ without specifying the variation of q. The latter is then established with the aid of Eq. (5.82):

$$q = pm_t = \frac{pa}{s + 2s_0 - a - [(N - 1)/t]D_{gg}} \tag{5.84}$$

Eq. (5.83) shows that the lens strength is proportional to $m_t - m_r$, i.e., to the radial foreshortening, as expected.

The derivation serves to demonstrate how the added degree of freedom resulting from the possibility of adjusting registration by variation of q permits greatly improved and, under specific circumstances, complete correction of registration errors with a continuous-surface correction lens. The compensating drawback, inherent in second-order printing, of great sensitivity of the registration to deviations from the prescribed q value, has already been noted.

In practice the lens design for second-order printing follows the same concepts as previously described where register data is taken and used to calculate the lens with the aid of a computer.

Discontinuous-Surface Lenses

There is still a third alternative to complete correction of degrouping errors that does not employ second-order printing (*54–56*). If first-order geometry is used, as has previously been shown, a continuous surface lens will not offer complete correction. However, within any given spot on the screen, perfect registration can be achieved merely by obtaining the desired thickness and slope of the lens to provide the proper dot placement. If such a procedure is followed for many small zones, each covering a small portion of the face of the tube, a close approximation to perfect register can be obtained. If this is done by dividing the lens into several hundred zones, the deviations in register between adjacent zones can be made rather small so that discontinuities from the edge of one zone to the beginning of another are relatively small. If, in addition, this lens is caused to vibrate or move during the exposure time so as to blend the adjacent zones together, the effect of the discontinuities can be minimized. Fabrication problems for lenses of this type are more complex than those of the continuous surface lens and, coupled with the need to move the lens during exposure, constitute the primary disadvantage of the system.

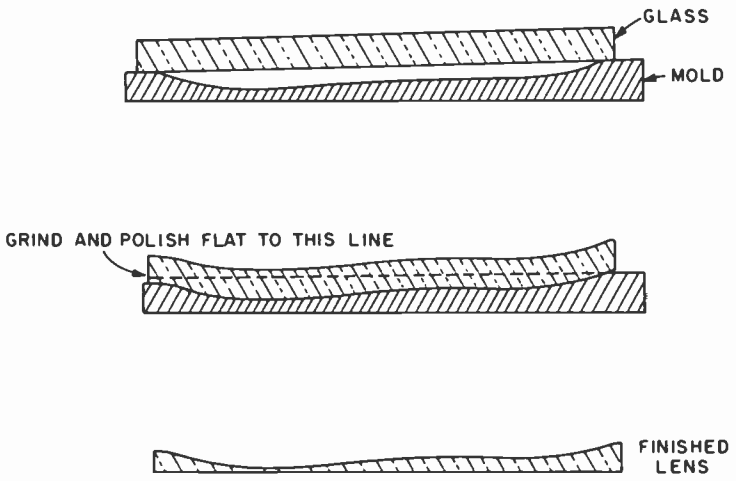

Fig. 5.25. Manufacture of correcting lens by sagging glass plate onto mold.

Fabrication of Continuous-Surface Lenses

Since the optimum continuous lighthouse correction lens seldom has a circular symmetry, its fabrication presents a unique problem. In general, two methods of fabrication have been employed. The first is a sagging technique and the second is a direct grinding technique. In the sagging technique, a ceramic or metal mold is very accurately cut by use of numerically controlled milling machines to the desired contour calculated for the lens. A plane, parallel, flat piece of optical glass is placed upon the mold and the temperature raised until the softening point of the glass is reached. The glass then sags or slumps into the mold, matching the contour of the mold. The upper surface of the glass, which is away from the mold, maintains its good optical finish and is used as the final contoured surface in the lens. The bottom surface of the glass, which was in contact with the mold, is ground in a subsequent operation to a flat surface. This fabrication system is illustrated in Fig. 5.25.

Direct grinding techniques have been employed wherein specialized high-precision numerically controlled grinding machines can generate the desired aspheric surface directly. With controlled polishing the surface may be brought to the proper optical finish. In either case, great skill is required to obtain a quantity of lenses within the tolerances required. In general, slope errors of the lens surface should be less than 1 mrad to meet the required commercial needs.

5.3.4 Phosphors

A phosphor suitable for shadow mask color use consists of a crystalline solid containing a small quantity of activator to produce and control the color of light emitted when the phosphor is struck by high-velocity electrons. Those of interest are limited to inorganic compounds since they must withstand heating to temperatures in excess of 400°C for an hour or more in an oxygen-containing atmosphere. In use, they must neither lose efficiency under prolonged bombardment nor evolve gas or other decomposition products that might adversely affect electron emission from the electron gun.

By today's standards, pictures on the first shadow-mask color tubes were dim; the red was particularly inefficient and required a didymium-glass filter to achieve the correct hue. Since then, the development of phosphors with improved chromaticity and greater luminance efficiency has been an important factor in improving color tube performance. At least 18 phosphors have been developed and successfully used in color tubes. A chronological listing by Hardy (*22*) has been updated to 1973 in Table II (*57*). The intense phosphor development activity, to which Table II attests, has resulted in an increase in basic phosphor screen efficiency from 15 up to

TABLE II

Phosphors (with Activator) Classified According to Color of Emission and Listed in Chronological Order of Commercial Use

Red:	1.	Cadmium borate : manganese
	2.	Zinc orthophosphate : manganese
	3.	Zinc selenide : copper
	4.	Zinc cadmium selenide : copper
	5.	Zinc cadmium sulfide : silver
	6.	Yttrium orthovanadate : europium
	7.	Yttrium orthovanadate : bismuth : europium
	8.	Yttrium oxysulfide : europium
	9.	Yttrium oxide : europium (limited use)
	10.	Gadolinium oxide : europium (limited use)
Green:	1.	Zinc orthosilicate : manganese (low conc.)
	2.	Zinc orthosilicate : manganese (high conc.)
	3.	Zinc aluminate : manganese
	4.	Zinc cadmium sulfide : silver
	5.	Zinc cadmium sulfide : copper : aluminum
Blue:	1.	Calcium magnesium silicate : titanium
	2.	Zinc sulfide : silver
	3.	Zinc sulfide : magnesium

35 lm/watt during the period 1951–1973. In this same period the shadow-mask tube device efficiency for producing white light, including device design improvements, has increased from 0.6 to 8 lm/watt (*57*). One such improvement of major proportions is the matrix screen described later in Section 5.5. Others relate to various design and manufacturing improvements that permit satisfactory tube operation with reduced screen tolerances so the mask transmission may be increased.

The colors produced by phosphors in use in 1973 are described in Fig. 2.2 by plotting the x and y coordinates of the phosphors on the CIE color diagram (*32*). As mentioned in Chapter 2 and shown on the diagram, white for color television receivers is currently adjusted to be near the center point of the diagram. If a straight line is drawn from the white point through any one of the three phosphor points (shown as crosses in the figure) and extended to the spectrum locus, the point of intersection on the locus is the dominant wavelength produced by that phosphor with that white setting. The ratio of the phosphor-point and dominant-wavelength-point distances from the white point gives the percent saturation of the phosphor. Similarly, straight lines drawn from the white point in any direction will define a dominant wavelength and a maximum attainable saturation for that hue determined by the intersection of these lines with the triangle joining the three phosphor points.

A significant new direction in phosphors for color television was taken in 1964 (*21*) by the replacement of red-emitting sulfide with the red-emitting, rare-earth yttrium vanadate : europium. All previous phosphors of all three colors have had broad emission bands with a half-value width greater than 40 nm. Rare-earth emitters are characterized by narrow-line emission from 0.1 to 0.5 nm wide. For equal energy output, and equal subjective color, narrow emission lines have a distinct advantage over broad bands for red because broad-band emitters in the red waste much of their emission at longer wavelengths where the eye is relatively insensitive (*58*). Figure 5.26 compares the spectral distribution curve of red-emitting zinc cadmium sulfide phosphor and red-emitting yttrium vanadate : europium phosphor. The same factors concerning line width obtain at the blue end of the spectrum, but line width is not of great importance in the green because the eye sensitivity here is high and has a wide distribution.

Improved red rare-earth phosphors have been developed since the introduction of yttrium orthovanadate : europium (*59–63*). In late 1973 the efficiency of the green-emitting phosphor was most in need of improvement to achieve approximate unity current ratios of the three beams to make white. Unity current ratio is desirable for two reasons. First, it would then be easier to match drive characteristics of the three guns to obtain a non-

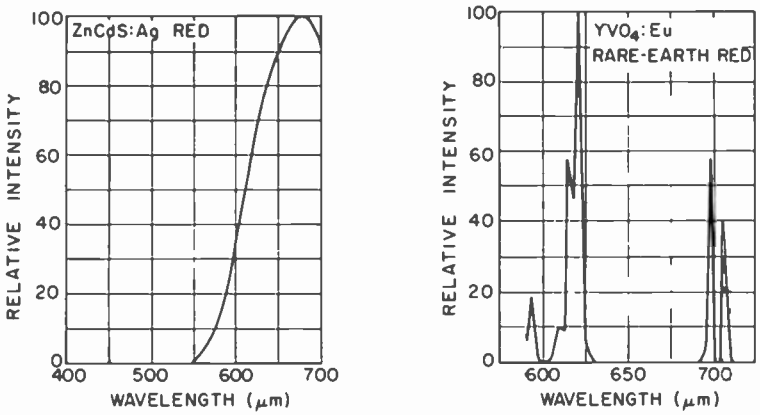

Fig. 5.26. Comparison of the emission spectrum from a broadband and a narrow line-emitting red phosphor.

varying white color temperature as a function of beam current or brightness. Second, brightness would be enhanced since each gun could then be used up to its capability of supplying current limited only by "spot blooming" instead of the limitation being set by the gun that is used for the weak phosphor. That is, if an increase in green-emitting phosphor efficiency can be obtained to bring the current ratios to unity (the red and blue efficiencies assumed to be the same), then the white light brightness would be increased by the same factor as the increase in the green-emitting phosphor efficiency.

5.3.5 Phosphor Application

The procedures employed for making a phosphor-dot screen by photodeposition will now be described (*6*, *7*, *13*, *64*). Recent innovations going beyond these procedures to form black-matrix screens are deferred to Section 5.5. The first step is to coat the inner screen-substrate surface of the glass faceplate panel with a mixture of one of the primary color phosphors, an organic binder such as polyvinyl alcohol diluted with water, and a photoresist sensitizing agent that is usually ammonium dichromate. A machine is used to spin the panel face up, but tilted, while the mixture is introduced near the center and spreads to the edge. The machine then tilts the panel to a nearly vertical position, still spinning, to remove excess material. As the phosphor layer on the panel dries it becomes light sensitive and must be handled in a yellow safelight environment.

The mask associated with the panel is then inserted and the assembly placed face down on the lighthouse. Usually one lighthouse is adjusted to print one phosphor color, which means that the light source position is not changed after being placed at the desired color center as referenced to the panel. A second and a third lighthouse are used for the next two colors.

After exposing for several minutes, the mask is removed and the panel placed on an automatic developing machine. Here it is transported through a number of positions where a stream of water washes away unexposed phosphor and the exposed phosphor remains as a dot pattern. The delicate pattern is dried and is then ready for application of the second, and then the third, color dot pattern by repeating the operations for the first layer, using the lighthouse source at the proper location for each color.

An alternative to the above procedure is to coat the panel surface with photosensitized polyvinyl alcohol and, while it is still wet, dust it with dry phosphor powder to embed the phosphor into the layer. Exposure and development as before then produces the desired dot pattern (*65*).

Up to this point a number of problems may occur. There may be missing phosphor dots or incomplete removal of unexposed phosphor, which contaminates subsequent dots with extraneous color. Blocking of apertures in the mask by dirt is an ever-present problem that contributes to missing dots. The eye is very sensitive to irregularities in the dot patterns so that an unusually high degree of perfection is required. Literally, one missing dot in a million can be annoying if it is near the center of the picture. Such problems are solved by meticulous attention to detail in the production process.

The panel, with its array of three phosphor dot patterns, is next "filmed" with a thin plastic layer preparatory to aluminizing. One method is to wet the screen and then slurry an organic film-forming material, such as methacrylate, on the surface to bridge the openings between phosphor grains when the screen is dry. The plastic film then serves as a smooth substrate for an aluminum film that is evaporated on the organic film to form a continuous, light-reflecting layer. A well-made aluminum film can nearly double the tube brightness by reflecting back through the face of the tube light that would otherwise be lost.

The screen is then baked in air prior to tube exhaust to decompose or burn out the plastic film and all other organic matter left in during the screen-making process. The organic material is decomposed by an air bake to prevent copious release of gaseous products from the material when the tube is exhausted and baked out during processing.

A final process coming into use (1973) consists of applying a blackening layer on the gun side of the aluminum film to improve the screen's heat

absorption characteristic with only a negligible loss in light output. Such a layer improves the screen as a heat sink to help absorb heat radiated from the mask and prevent color distortion that results if the mask expands and moves out of position. Large color tubes with deflection angles greater than 90° are particularly sensitive to mask movement and benefit from the black layer.

5.3.6 Electron Guns

The high-performance objective of shadow-mask color tube guns and the restraints due to other factors have made the design of these guns a major challenge. As previously mentioned, because of the low shadow-mask transmission, only a small part of the electron beam energy is useful in producing light on the screen. This factor is somewhat compensated for by the use of three guns, whose beams must be carefully converged to achieve a useful picture at high brightness. For best resolution, anode voltages on the order of 20–30 kV, or higher, are commonly employed in shadow-mask tubes. Total average anode current of about 1 mA is common. Peak currents may be several times higher.

Physical space limitation, caused by the need to place three guns in a common neck, is a restraint on the diameter of the lenses that can be used and limits the electron optical performance of the gun. Use of a larger neck (larger gun-lens diameter) would help gun performance but would reduce deflection yoke sensitivity and make it much more difficult to properly dynamically converge the three beams. This gun-yoke performance tradeoff has resulted in a situation where for increasing deflection angles the size of the neck, and therefore the corresponding size of the electron gun, has been kept inversely proportional to the deflection angle. For example, the 70° types commonly use a 51-mm diam neck, while the 90° types use a 36-mm neck, and many of the 110° types have 29-mm necks. As a result of a reduction in neck diameter with increase in deflection angle, there has been no great increase in deflection power with increase in deflection angle. The basic diameter of each of the electron guns is 12 mm for 70°, 9 mm for 90°, and 7 mm for 110°. These basic gun diameters have been obtained when the three guns are arranged in a delta fashion that allows a maximum size of electron gun per given neck size.

Figure 5.27 shows photographs of several electron guns commonly used in 70°, 90°, and 110° deflection shadow-mask tubes. The mechanical and electron-optical basic geometry is similar in each. In every case the electron guns are tilted toward the common tube axis at about a 1° angle. A precise angle is selected so that the beams will converge at the center of the screen. Generally the elements of the gun, including the cathode, control grid

Fig. 5.27. Photograph of electron guns commonly used in 70°, 90°, and 110° shadow-mask color tubes.

(grid No. 1), grid No. 2 (G2), G3, and G4 or G5 are held by three glass multiform beads. For assembly, internal mandrels are used to hold the parts. They fit snuggly in the diameter of the grids and associated apertures and are mounted at the required convergence angle. Metal beading straps attached to the various gun elements are imbedded in glass beads that have been softened by heat. Straps from adjacent guns are attached to a common bead. In this manner, the six ends of the beading straps are imbedded in the three glass beads to provide a ruggedized triple gun assembly.

At the anode end of the gun an internal pole piece assembly is mounted. The assembly consists of three pairs of high permeability nickel–iron pole pieces with each electron beam passing between one pair of poles. The pole pieces extend to the glass neck and flare apart so that magnetic drivers can be coupled to them through the neck wall as shown in Fig. 5.28. The con-

figuration of the pole pieces is such that the magnetic flux lines are in a direction to deflect the electron beams radially. The purpose of the pole pieces is twofold: (1) to apply individual fields for convergence to each of the guns, and (2) to minimize curvature of the field by concentrating the magnetic flux lines, and hence, prevent electron beam distortion due to these fields. To minimize interaction between the three pole pieces, a Y-shaped shield of similar nickel-iron alloy is frequently placed between the pairs of pole pieces.

By use of a suitable external driver, a static magnetic field may be applied to correct center convergence to compensate for minor manufacturing variations in the convergence angle of the guns. In addition, a dynamic magnetic field is applied for edge or dynamic convergence.

To obtain complete static convergence of the three beams, a fourth degree of freedom is required. For this purpose an additional magnetic field is usually applied to the blue gun to move the beam in a direction at right angles to the movement provided by the dynamic convergence pole pieces. In some guns the field is produced by external means without use of internal magnetic structures.

Snubbers, for electrical connection of the upper elements of the gun to the neck coating and for mechanical centering of the top of the gun structure, are mounted on the mechanical assembly which houses the internal pole pieces. In addition, a ring-type getter may be mounted on this structure concentric with the mount, or more commonly, an "antenna" getter is

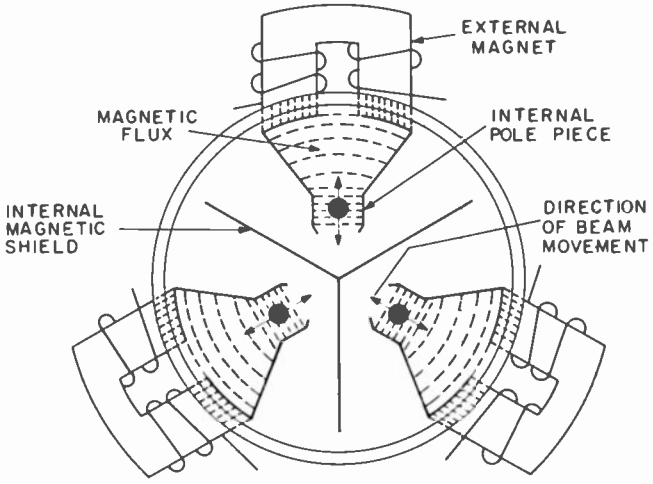

Fig. 5.28. Schematic of radial-converging pole pieces.

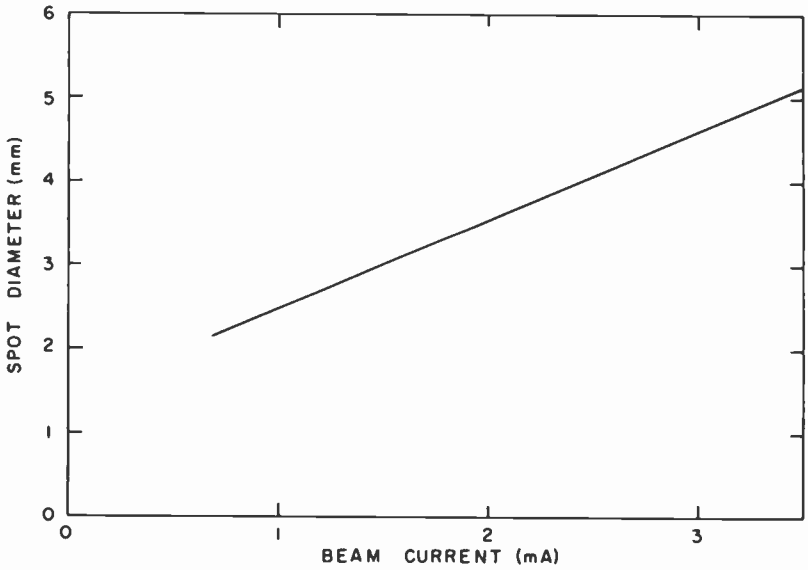

Fig. 5.29. 25V, 90° tube pulsed-spot average diameter vs beam current. Anode voltage 25 kV; focus adjusted at 1 mA; cutoff = −125 V.

slipped further up into the funnel portion of the tube by means of a long spring which fits snugly against the inner edge of the neck assembly.

Gun Performance

Turning now to performance characteristics of the electron guns in color tubes, spot size vs. current for a typical 25V, 90° tube is shown in Fig. 5.29. Spot profiles for several values of current are shown in Fig. 5.30. It is, of course, desirable that the spot size remain as small as possible with increasing current or the "blooming" in the highlights be a minimum.

In addition to a small beam spot size at the screen it is also important that the beam size in the deflection plane be kept to a minimum. There are two reasons: first, a large beam size in the deflection yoke may cause deflection defocusing, so that the spot size at the edge of the screen will be distorted and enlarged compared to that in the center; and second, the electron optics of mask shadowing at the screen makes a small beam size desirable. The following equation shows that the allowable transmission T of the shadow mask, for a given tolerance K at the screen, is a function of the ratio of the two variables s and m, s being the spacing of the electron beam from the central axis of the tube and m the size of the electron beam

in the deflection plane. The mask transmission T is given by

$$T = (\pi/18\sqrt{3})[\sqrt{3} - (m/s) - (K\sqrt{3}/R)]^2 \qquad (5.85)$$

where R is the diameter of tangent phosphor dots and the tolerance K is expressed as the difference in diameters between tangent phosphor dots and the diameter of that portion of the dot excited by the electron beam.

As was noted earlier, for deflection power reasons the neck size (therefore the gun size) and the s value have progressively decreased as the deflection angle has increased in the tube. In order to maintain high transmission of the shadow mask and suitable tolerances it has been necessary to try to maintain the value of m/s by reducing m as much as possible through electron optical design of the gun.

The majority of the guns used in shadow-mask tubes are of the bipotential type; that is, a main focus lens is formed between grid No. 3 (G3) and grid No. 4 (G4). G4 runs at the anode potential, typically 25 kV, while G3 runs at a voltage of about 18% of the anode voltage or about 4.5 kV with respect to cathode voltage. The G1 and G2 voltages are used to adjust the beam current and cutoff. Typically, G2 will be set at a value between 300 and 600 volts such that the cutoff voltage of G1 will have a value of 100 to 150 volts, negative with respect to the cathode. Under these conditions, the adjustment of G1 voltage, or cathode voltage with respect to G1, can produce a beam current up to 3–4 mA depending on the video drive applied.

Another type of gun, used primarily for the smaller screen sizes, employs einzel or unipotential lenses. In a gun employing an einzel lens, G3 is

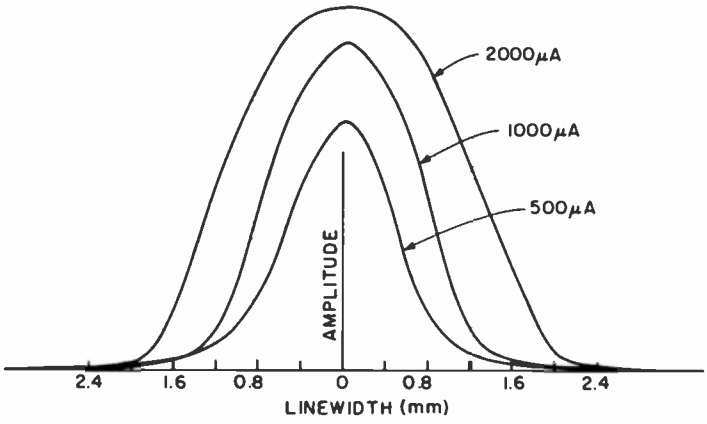

Fig. 5.30. Beam spot profile, 25V, 90° tube, anode voltage 25 kV.

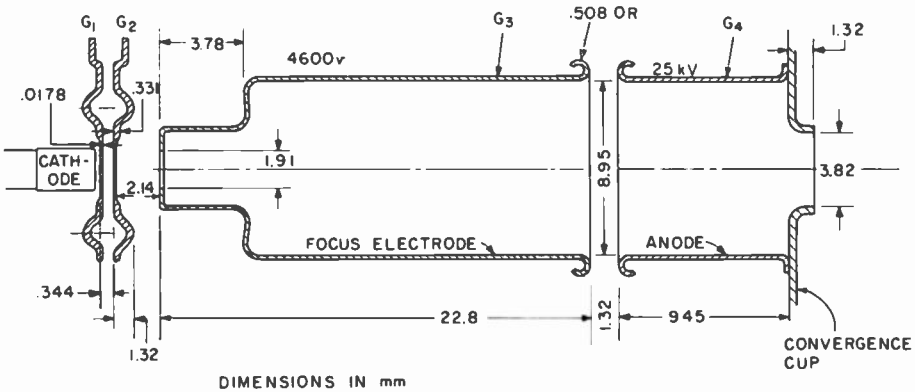

Fig. 5.31. Cross section of typical 25V, 90° gun. The apertures in G1 and G2 are 0.74 mm in diameter, and the cathode-G1 spacing when the cathode is hot is 0.11 mm.

electrically connected to G5 and run at anode potential. G4, between these two elements, is run at ground (cathode) potential or very close to it. The focus of the einzel or saddle lens is slightly less sharp than that of bipotential lenses. However, the einzel lens has the advantage that it does not require a second high voltage for the focus element since its potential is at ground, or within the voltage range available from the receiver. The high-voltage stability, or stability against arcing between electrodes, is somewhat less satisfactory in the einzel gun than in the bipotential gun because of the higher voltage gradient between elements of the gun.

The cathode in a typical gun is formed of a thin nickel cup enveloping the heater, with the end of the cup coated with emissive material. The cathode is operated at a temperature of about 1060°K and is normally insulated either by means of a ceramic disc mounted within the G1 cup or by a separate support element which is brought out directly to the beads, the beads providing insulation from the other elements. G1, having an aperture size varying from 0.6 to 0.9 mm, is shaped either as a cup or as a flat disc. G2, typically, has an aperture equal to or slightly larger than the aperture in G1 and is also either a flat disc or a small cup. G3 has an opening at the end toward the cathode which ranges from 1.5 to 5 mm in size; the main lens at the other end of the tubing is the full diameter of the tubing. G4, the other half of the lens, is normally of similar size and the gap between G3 and G4, typically, is 1–1.25 mm with carefully smoothed and rounded edges to prevent localized high-voltage gradients. Figure 5.31 shows a cross section with the dimensions of a single gun taken from a typical 25V, 90° tube.

Some shadow-mask tubes employ in-line guns wherein the three electron beams are generated in the horizontal plane, side by side. One in-line gun employs the individual delta guns in a line rather than a delta cluster. A gun of this type is shown at the right in Fig. 5.32. In another in-line gun structure, a single large main-focus lens is used for all three electron beams (*24*). In the center photograph of Fig. 5.32 such a structure is shown. In this system the three guns are tilted so the beams leaving the cathode-G1-G2 region cross in the center of the main-focus lens. Then, after being focused by this lens, the outer beams diverge from the center beam and are later bent back by an electrostatic convergence assembly so that they meet at the screen. In this type of structure, in addition to the voltages required for the formation of the electron beam in the individual guns, an additional high-

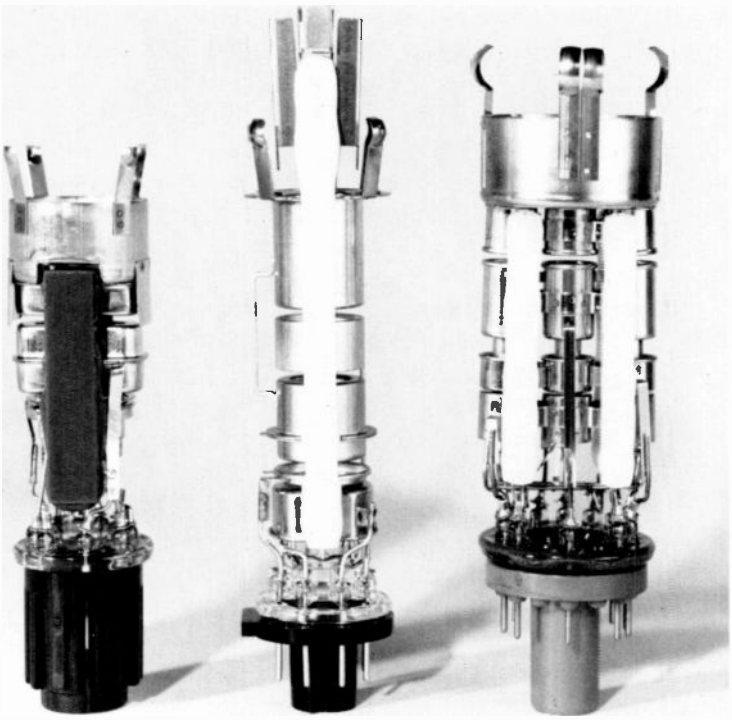

Fig. 5.32. The in-line gun on the left employs unitized construction (RCA precision in-line). The gun in the center has a single main-focus lens for the three beams (Sony in-line gun). On the right is an in-line gun with individual-barrel construction (General Electric).

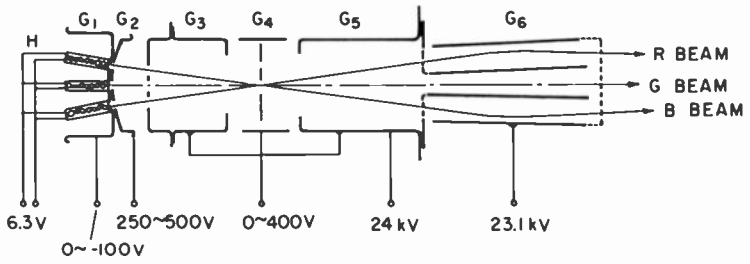

Fig. 5.33. Line drawing of in-line gun with single main-focus lens (Sony).

voltage connection is required for the convergence assembly. Details of this in-line gun structure are shown in Fig. 5.33. A shorter version of this gun has been developed for tubes with deflection angles greater than 90°. The shorter gun-to-screen distance resulting from wider deflection angles, coupled with the large-diameter focus lens, favors formation of a small spot, particularly in the central part of the screen (*66*).

A third type of in-line gun structure, shown at the left in Fig. 5.32, is one in which the guns are combined into one mechanical assembly and the separation of the beams is by means of individual apertures within the common gun electrodes. This is shown in Fig. 5.34. Since the cathodes are the only elements of the gun that are electrically separated between guns, the three color signals must be applied to the three separate cathodes. G1 and G2 have common plates with triple apertures, giving very good alignment between the gun elements. G3 and G4 are similarly constructed. The unique self-converging yoke used with this gun makes provision for dynamic converging elements unnecessary, as described in Section 5.6.1 on in-line deflection systems.

5.3.7 Shadow Masks

The shadow mask is one part of a color tube that has no counterpart in a black-and-white picture tube. The apertures are made by etching thin flat mask metal from both sides at the same time. Technological development of the mask has been a major undertaking that has involved fabricating dot-pattern artwork with unusual dimensional tolerance requirements which are needed to produce very close geometric control of the mask itself. At first the hexagonal-array dot patterns were generated by manipulation of very accurate line rulings; but later, patterns were made by skillfully using very accurate computer-controlled plotting equipment.

Coils of low-carbon steel strip, 0.15-mm thick and left hard-as-rolled, are coated on both sides with glue photoresist. Still in coil form, the metal is

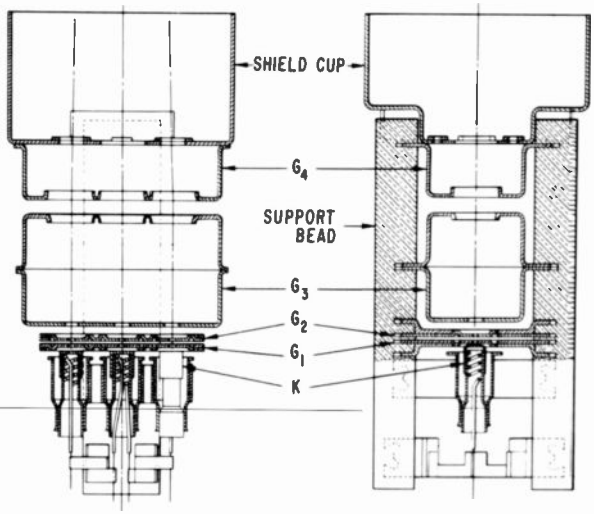

Fig. 5.34. Line drawing of in-line gun with unitized construction (RCA).

exposed to light on both sides using registered patterns of opaque dots and clear border area to produce a resist pattern with holes in the resist where the apertures are to be etched. The dot openings in one pattern are much smaller than the corresponding dots in the pattern on the reverse side. The coil of metal is now etched from both sides at the same time with a forceful spray of hot ferric chloride until apertures of a precise size are produced in the metal.

Figure 5.35 shows the cross section of an aperture produced with the resist still in place. The combination of a larger opening in the resist on one side and a higher etchant spray pressure produces a defining knife-edge aperture located near the other face of the metal containing the small resist openings. In the picture tube, this knife-edge side is placed toward the gun so that a minimum number of scattered electrons, produced by beam elec-

Fig. 5.35. Aperture etched in shadow-mask with photoresist still in place. The surface of the mask with the small opening faces the gun.

trons striking the sidewalls of the apertures, can reach the screen to degrade color saturation and picture contrast.

After etching and resist removal, the masks are torn out of the coil at a half-etched-through boundary line and then annealed. After annealing, the masks are roller-leveled or flexed to break up large crystal structures and then formed to an approximately spherical contour, including a turned edge or skirt to facilitate welding the mask to a frame. Great care must be taken in forming because uniform stretch of the metal is very desirable to prevent aperture pattern distortion. Also, it is necessary that the prescribed contour be accurately produced since the mask-screen spacing, which is critical, is directly affected.

In a final process the mask is treated to obtain a black iron-oxide coating that forms a chemically stable surface with good thermal emissivity. Emissivity is important because heat generated in the mask by the electron beam must be largely dissipated by radiation. If the mask temperature rises excessively, thermal expansion of the mask will cause color impurity (*18*).

5.3.8 Mask Support

In the process of fabricating the phosphor screen of the color picture tube, the mask must be removed from the panel assembly several times during the scanning process. Typically, replaceability errors of greater than 5–10 μm cannot be tolerated for an assembly design to be practical. In addition to the replaceability requirement, the mask-panel system must go through thermal cycles up to 400°–450°C for frit seal and exhaust bake and then return to the original position relative to the screen on the faceplate that it had during the screening operations.

To meet these requirements, the mask is normally mounted on a rigid metal frame and the skirt of the shadow mask is welded to the sidewall of the frame at numerous points around the periphery. The cross-section thickness of the frames used for mounting typical shadow masks range from 1 to 3 mm. In general, they have an L section; in some cases this L is modified by reenforcing gussets or other features. These frames may be fabricated either by a forming operation or by a wrap-and-weld operation. The forming operation allows complete freedom to use a frame with variable cross section of the frame; however, it has the economic disadvantage of wasting material. A wrapped-weld frame is normally made from metal with a constant cross section which is formed into the rectangular shape and the ends of the frame butt-welded. The combination of the shadow mask welded to the frame usually provides a rigidity to the assembly that is substantially greater than that of either frame or mask individually.

The mounting of the mask frame into the panel is achieved by means of tapered-metal studs, which are secured to the glass sidewall of the panel,

and leaf springs welded to the mask frame, each of which has a hole that engages a tapered stud. Such a system of leaf springs and studs as shown in Fig. 5.36 has been used almost universally in all color picture tubes, starting with the 70° round types and then extending into all of the 90° and 110° rectangular types. The metal stud, which is heat-sealed to the side of the glass bulb, is about 6 mm in diameter and employs a tapered end with a 12° angle. The leaf spring is normally made of steel and has either a round

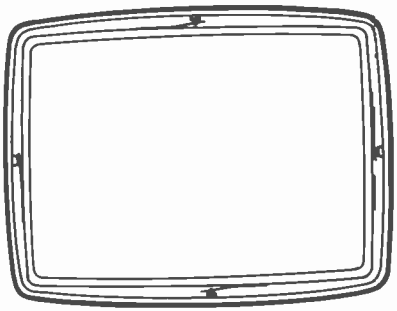

FOUR-STUD ARRANGEMENT

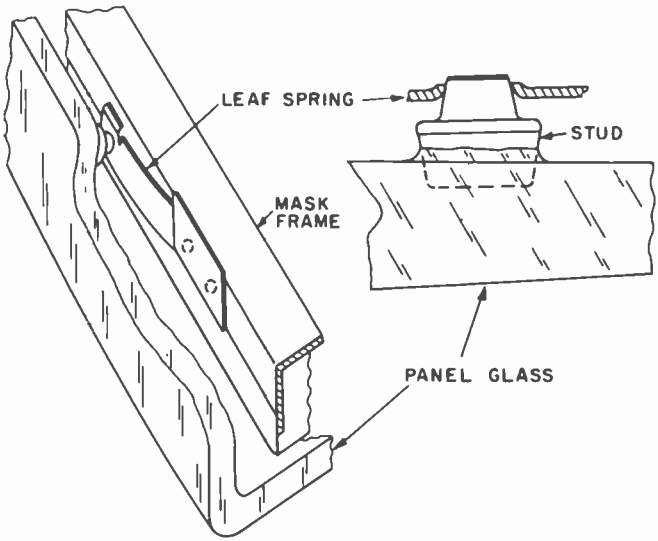

Fig. 5.36. Four-stud leaf-spring arrangement used to hold mask-frame assembly in the bulb panel. Typical studs are shown with a leaf spring design that does not have temperature compensation.

or a slightly triangulated hole in the end to engage the tapered portion of the stud. This triangulation of the hole, or various versions of tapering of the hole, is made so the contact area on the taper is stabilized at the minimum number of points. Flexing of the springs allows for differential thermal expansion during the heat cycles required for tube processing. The panel glass has an expansion coefficient of 99×10^{-7} per °C while that of the frame is typically 130×10^{-7} per °C. Therefore, even with slow thermal cycles a mismatch in size of glass and metal parts of 0.75 mm occurs at peak temperature.

In round tubes, three studs placed approximately 120° apart are used for the support mechanism. This in essence gives a three-point support system which is unique and self-setting; but, upon closer examination, one finds each of the three points has multiple points of contact onto the stud, so that the problem becomes slightly more complex than would seem initially. With the introduction of rectangular bulbs, the same stud system was employed, with some manufacturers continuing to use three studs, and others using a four-stud system. With the three-stud rectangular bulb, the symmetry of the round tube does not exist in that the angular separation of the three studs is no longer 120°. In this case, one stud is normally placed at the top or 12 o'clock position of the panel and two additional studs are placed on either side, somewhat below the center line of the panel. In this system, the same unique three-point system is maintained and therefore the placement of the mask within the panel is relatively simple. In the larger sizes particularly, a disadvantage is the considerable overhang of the frame from its support system and therefore a heavier, more rigid, frame is needed to prevent motion. A further disadvantage is that the center line of the system of the three studs no longer coincides with the geometric center of the mask.

In a four-stud system, the studs are usually located on the major and minor axis of the rectangular bulb; that is, at 12 and 6 o'clock, and 3 and 9 o'clock. With this system, a somewhat lighter frame can be used and the symmetry of the support system is maintained in that expansion of the parts takes place around the center of the system. The disadvantage is that seating of the fourth spring on its stud in the four-stud spring system is no longer automatic. The fourth spring position is uniquely determined when the first three are engaged, so great care must be taken in placing the springs if all four are to give proper support.

Control of Mask-to-Screen Spacing

The spacing, q, between the shadow mask and the faceplate on which the screen is printed, must be controlled very precisely. The typical value of q

is between 8 and 15 mm, depending on the tube size and geometry. Deviations from the design value must be held to within 0.4–0.5 mm. In order to achieve this accuracy the contour of the faceplate must be controlled, as discussed in Section 5.3.9, and the forming of the metal shadow mask must be held to very tight tolerances.

To obtain the proper spacing, various systems of q-setting have been used with a three-stud support system. The studs are normally located accurately in the envelope in relation to the face contour and then placement of the springs on the mask frame assembly can be done in a jig which holds the mask against a contoured metal gauge. The relationship of the springs is established by placing the holes on dummy studs located in the same spatial relationship to the gauged contour of the mask. In this manner, the springs may be welded and when the assembly is placed within the glass panel the q will be held to required tolerances.

A second system which gives somewhat tighter tolerances is to individually set q within the panel where it will be used. In this system a spacer, placed on the glass faceplate surface, is precisely of the thickness required for the q-spacing in the finished assembly. The mask is then placed into the panel and rests on the q-spacer. Thus, with the unique spatial requirements established for that particular panel, the springs are then welded to the frame, or to a second member or clip in order to prevent the welding guns from getting too close to the glass side wall of the panel. This system is also useful for the four-stud approach because then the springs are placed uniquely in relation to the four-studs and the tailored relationship is maintained.

A somewhat different system of q-setting can be employed by delaying the welding of the mask to the frame until the final step. In this system the springs are welded to the frame in a jig and the q-spacer placed in the glass panel. The frame is then placed into the assembly, with the springs engaging the studs. The final operation is to weld the skirt of the mask to the frame, q being set by the q-spacer.

Electron Shield

In a typical mask-frame assembly, see Fig. 5.36, there is a 6–8 mm space between the edge of the frame and the inner side wall of the glass panel. In tube operation, if nothing further is done, the overscanned electron beam could enter into this space between the frame and the side wall and ricochet or bounce onto the faceplate. These electrons do not pass through the mask and therefore flood the entire screen in an uncontrolled manner, generating light of incorrect color and high intensity around the periphery of the screen. To prevent this, a thin metal electron shield is spot-welded to the

frame at final assembly to close the gap between the mask frame and panel. In addition to the flat electron shield, some manufacturers have employed a formed aluminum shield which is tucked down between the frame and the sidewall to form a somewhat tighter seal for complete elimination of electron strays on the screen. An added advantage of this shield is its greater degree of flexibility when the assembly goes through heat cycles. The contact of the shield to the glass is weak enough that it does not cause a distortion or a misplacement of the mask assembly in relation to the panel.

The inner sidewall of the mask or frame can also provide an area on which overscanned electrons may be reflected back through the shadow mask onto the screen. These electrons would be generated from a point other than their color center and would scatter over all three phosphor colors of the screen. To minimize electron reflection, the L section of the frame is designed to mask the majority of these electrons.

Temperature Compensating Mask Mounting

As we previously mentioned, the expansion of the mask frame assembly due to electron bombardment of the mask during tube operation will adversely affect screen register. Figure 5.37 shows how misregister is caused by thermal expansion of the mask. For any radius r_p, the outward radial misregister M_r (for concentric mask and screen) can be predicted by the following equation:

$$M_r = \left(1 + \frac{q}{p}\right) \Delta R \left(\frac{\cos \beta_e \sin \theta - \sin(\theta - \beta)}{\cos(\theta - \beta)}\right)$$

where p is the mask-to-deflection plane spacing along the beam path; q is the mask-to-screen spacing along the beam path; β is the screen inclination angle; β_e is the screen inclination angle for a beam path intercepting the formed mask edge; θ is the beam deflection angle; and ΔR is the thermally induced change in the mask radius of curvature corresponding to: R_m, the mask radius of curvature; α, the coefficient of thermal expansion; and ΔT, the change in mask temperature.

The center-to-edge distribution of the outward aperture shift produced by the expanding dome can be compensated for all radii by a uniform movement of the mask parallel to the tube axis, as illustrated in Fig. 5.38. The axial motion of the assembly Δq is a function of the thermally induced change in the mask radius of curvature (obtained from Fig. 5.37) and other parameters based on the particular tube geometry, and not on the beam deflection angles.

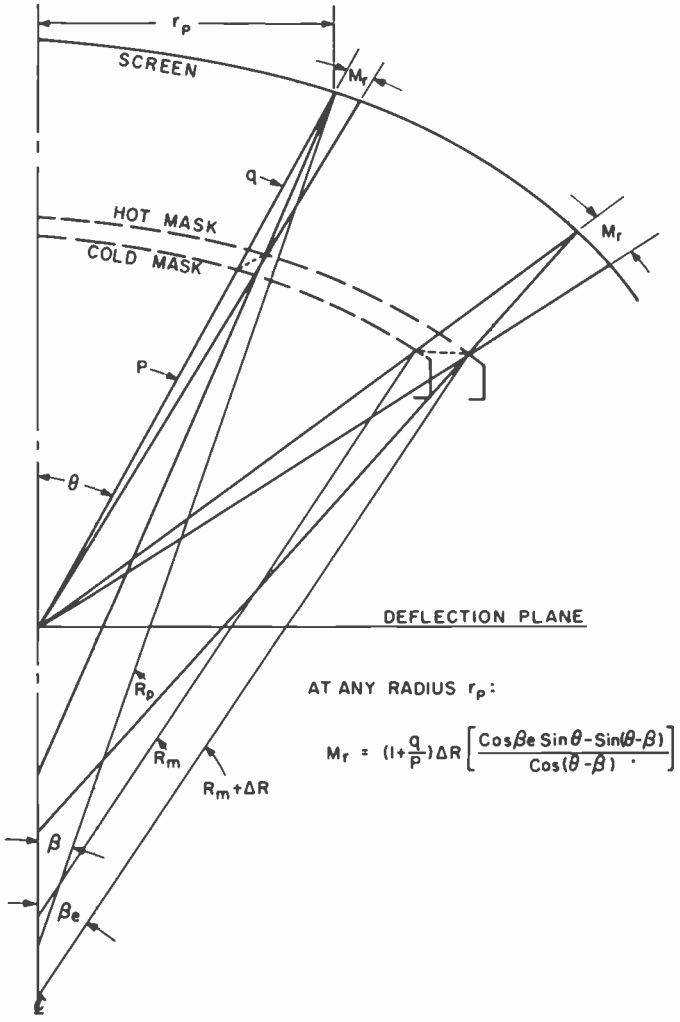

Fig. 5.37. Diagram showing thermally induced radial misregister.

This movement of the mask assembly toward the screen as it heats up may be obtained by use of bimetal elements. They may be mounted between the frame and the leaf spring or they may be the spring itself. A commonly used bimetal element is shown in Fig. 5.39. In the example shown the bimetal element employs a tapered loop that amplifies the

movement. The arrow shows the direction the assembly moves as the bimetal elements heat.

An example of typical misregister produced with and without this type of compensation is shown in Fig. 5.40. Some type of bimetal compensation is used in the majority of color picture tubes.

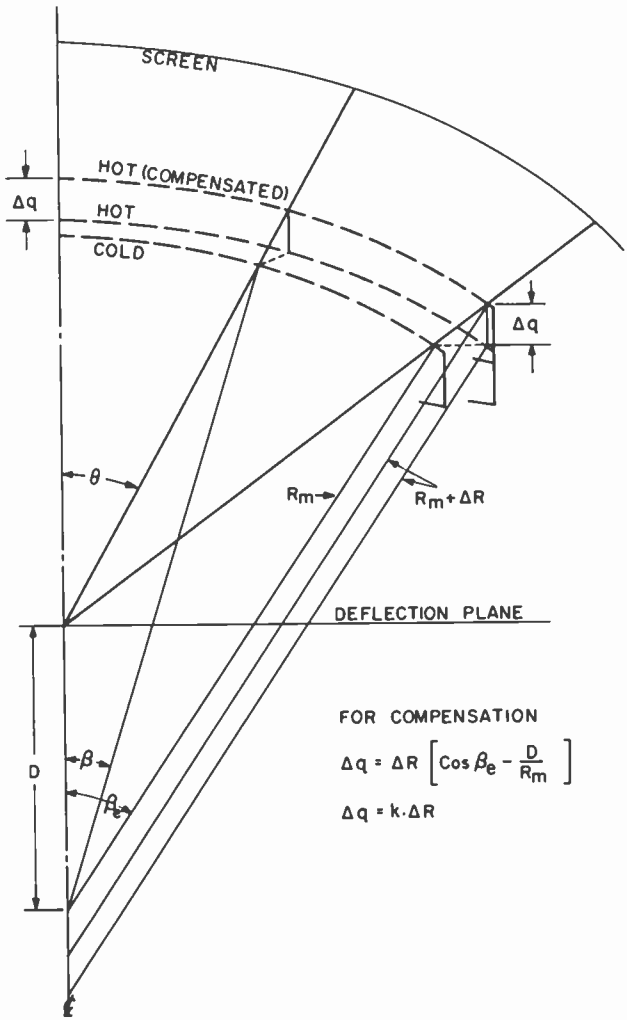

Fig. 5.38. Diagram showing that thermally induced radial misregister can be substantially compensated for by a uniform axial movement of the mask assembly toward the screen.

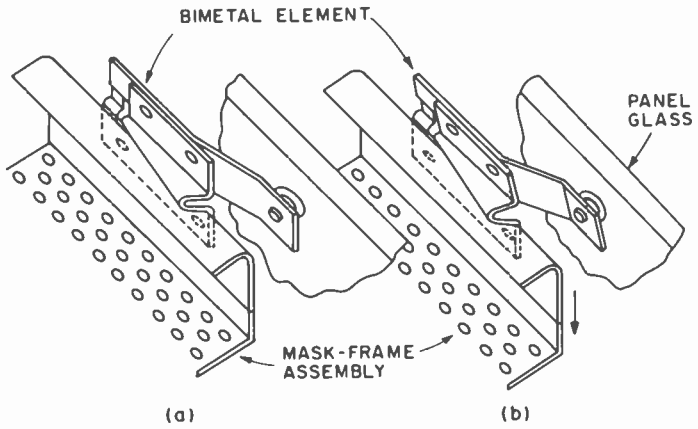

Fig. 5.39. Bimetal element providing axial movement of the mask-frame assembly to compensate for misregister caused by electron-beam heating of the mask, (a) unheated and (b) heated with arrow showing direction of motion.

5.3.9 Color Tube Bulbs

An extensive amount of bulb design work and development of manufacturing processes has been necessary to satisfy color bulb requirements while at the same time keeping the cost of the bulb at a reasonable level. As an indication of the importance of bulb cost, more than half the value of a color tube lies in the bulb itself. Specific information about requirements of the color bulb and a discussion of other features of the bulb will now be given, including a list of commercial color tube dimensions and weights by type as of 1973 which will be found in Table III.

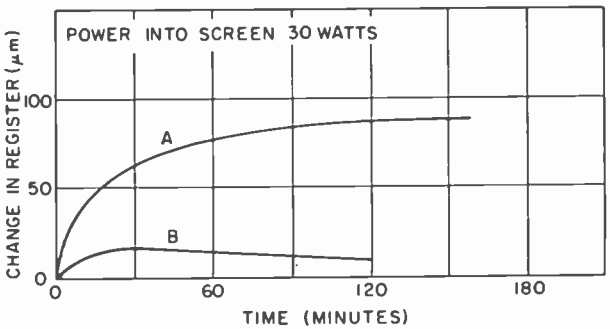

Fig. 5.40. Average thermally induced misregister at the screen corners for a 25 V rectangular picture tube. Curve A is for no compensation; curve B, with compensation.

TABLE III

COMMERCIAL COLOR PICTURE TUBE DIMENSIONS AND WEIGHTS (MAJOR TUBE TYPES AS OF 1973)

Type (Screen diag. to closest in.)	Screen dimensions				Outside tube dimensions				Weight (kg)
	Diag. (mm)	Horiz. (mm)	Vert. (mm)	Area (cm^2)	Diag. (mm)	Horiz. (mm)	Vert. (mm)	Length (mm)	
Types manufactured in the United States									
90° Deflection, delta gun, 36-mm neck diam.									
25V	626.3	527.7	395.8	2032	666.7	571.8	442.5	549.4	20.4
23V	584.1	504.8	395.6	1903	624.0	546.1	438.5	530.9	17.9
21V	530.1	445.5	336.7	1458	564.2	484.3	379.8	483.5	14.2
20V	513.9	443.1	346.5	1465	551.7	482.0	367.0	488.0	13.8
19V	480.0	404.4	303.3	1194	513.5	440.5	341.8	463.5	11.4
18V	459.1	395.9	309.5	1161	493.3	431.2	347.1	458.6	10.7
17V	432.3	364.2	273.2	968	471.0	405.7	315.8	434.9	10.2
16V	411.3	354.4	276.9	935	441.7	385.8	309.6	426.7	8.3
14V	344.4	296.0	232.1	658	374.5	327.7	263.9	386.1	5.4
110° Deflection, delta gun, 29-mm neck diam.									
25V	626.3	527.7	395.8	2032	666.7	571.8	442.5	432.0	19.6
19V	480.0	404.4	303.3	1194	513.5	440.5	341.8	368.1	10.9
90° Deflection, in-line gun, 29-mm neck diam.									
19V	480.0	404.4	303.3	1194	513.5	440.5	341.8	417.0	11.4
17V	432.3	364.2	273.2	968	471.0	405.7	315.8	388.4	10.2
15V	382.3	322.1	241.6	755	417.2	359.0	280.2	360.6	7.1
13V	334.8	282.0	211.5	581	367.1	316.0	247.5	332.1	5.4

Types manufactured in Europe and not previously listed

110° Deflection, delta gun, 36-mm neck diam.									
24V	617.8	518.0	390.0	1966	657.6	556.4	435.3	431.6	20.0
21V	533.0	447.0	337.0	1466	574.0	495.0	391.0	—	—

Types manufactured in Japan and not previously listed

90° Deflection, delta gun, 36-mm neck diam.									
13V	335.4	280.8	210.6	581.2	372.9	317.9	248.9	366.5	6.0
12V	295.2	254.5	199.0	473.0	367.1	300.2	246.5	352.3	4.8
11V	284.0	245.0	191.0	455	314.0	279.0	226.0	355.0	3.6
90° Deflection, in-line gun, 29-mm neck diam.									
12V	302.0	245.0	192.0	463.7	377.0	294.0	246.0	366.3	4.7
9V	228.6	192.6	144.5	268.9	266.1	230.0	179.1	287.0	—
110° Deflection, in-line gun, 36-mm neck diam.									
19V	480.0	404.4	303.3	1190	513.6	440.5	341.8	368.5	11
110° Deflection, delta gun, 29-mm neck diam.									
17V	432.2	364.2	273.2	968	468.8	402.9	312.3	337.0	—
114° Deflection, in-line gun, 29-mm neck diam.									
17V	438.4	357.0	272.5	934.2	479.0	400.0	325.0	337.2	11.2

Color tube bulbs are characterized by several factors:

(1) They are made of harder or higher softening-point glass than for black-and-white bulbs to minimize deformation during thermal processing. The panel glass typically has a strain point of 462°C, annealing point of 503°C, and a softening point of 688°C.

(2) Constituents such as strontium, lead, and barium are used in making the glass panel for absorption of practically all x rays which otherwise would be transmitted through the face of the tube. At the same time, the composition must also be selected to minimize browning effects in the glass caused by these x rays or by the electron beam.

(3) Three alignment pads or reference points are molded on the panel and on the funnel to align the two during the seal, and prior to sealing, as reference points in printing the phosphor screen in the desired location. The reference points are also used to align the gun in the neck for gun-seal which takes place after the panel-funnel seal.

(4) Three or four metal studs are placed on the panel wall to hold the mask-frame assembly.

(5) The inner contour of the faceplate is normally held to a tolerance of 0.43 mm from its prescribed position. This contour is normally measured either from the metal studs or from several selected points on the face contour itself. The achievement of this tolerance has been a major factor in the development of successful color tubes. Considering that this tight tolerance is maintained over an area of about 2000 cm^2, it is an achievement not obtained elsewhere in the glass industry in mass-produced commercial products.

(6) In addition to the tight tolerance on the faceplate, the neck assembly must be aligned so that it is perpendicular to and coaxial with the face. Special jigging is used to obtain perpendicularity of the neck to the seal edge of the funnel during its fabrication. In a further step, the sealed-on neck is held in a jig for precise positioning of its center line. The three pads located near the seal edge are ground to be a precise distance from this center line. By this procedure eccentricity of the neck in relation to the true center of the bulb system is held to less than 0.25 mm. This procedure is necessary so that the deflection center of the electron beams in the final tube will lie at points very close to the light source used in the lighthouse when the phosphor screen is printed; however, minor compensations for lack of coincidence can be achieved by means of the magnetic purity device on the neck of the tube. This device deflects the beams a small amount so as to aim them at the prescribed deflection centers and therefore produce corresponding pure colors on the tube face.

(7) The periphery of the seal edge of the panel and the funnel must be closely controlled so that maximum engagement of the two parts is achieved during the frit-sealing operation. Numerous points around the edge are carefully controlled so that the entire bulb assembly will have an engagement of sufficient width to insure a satisfactory seal. Typically this value is 10 mm or greater.

The thickness of face glass and funnel glass used in the bulb design must provide stability of the glass parts and also sufficient pressure strength for the bulb. Upon evacuation of the picture tube, air pressure exerts a force exceeding two tons on the face of the 25V tube. By proper design, stresses are kept at such low level that the possibility of breakage of the glass is negligible. Typically, a glass bulb used for a color picture tube will withstand 3 atm of pressure before breaking. This, in essence, gives a safety factor of three to the tube.

Stringent safety requirements have been set up by various agencies to guarantee that no harm can come to the user of a tube from inadvertent striking of the glass bulb. Since the face is naturally exposed in the final television receiver, this is most important. Test criteria of pendulum implosion test procedures have been prescribed so that even a blow with a golf club, for example, would cause, at worst, only a crack and devacuation of a tube and not a violent implosion with the throwing of glass particles away from the picture tube.

Supplemental protection is added to the bulb to ensure that such a violent implosion could not occur. One approach to achieve this is the addition of a laminated curved glass section onto the faceplate of the tube, sealed with a thermoplastic resin. A second approach is the use of a metal band tensioned around the sidewall of the panel to provide a compressive force which in turn redistributes the stresses of the face so that in case of a mechanical failure no glass is thrown and the bulb typically will crack and go to air quietly rather than have any violent implosion. In one metal-band system, pieces of metal 0.5 mm thick are formed to the general contour of the faceplate sidewall and extend just around the edge to provide a lip at the external edges of the face of the tube. The pieces are normally secured to the glass sidewall by a resin glue and then held in place by a tensioned band. This band is normally pulled taut with a force of the order of 600 kg, and then secured to itself either by means of a metal crimp or by welding. A combination of this tension band and the glued metal pieces provides complete protection of the finished tube. Various modifications of this system have been used which include a one-piece metal shell about the faceplate end of the tube which is subsequently filled with a resin to completely fill

the area between the glass and the metal part. Another system uses a one-piece metal assembly which may be made of several welded sections and is slightly smaller in size than that of the glass panel. In this case, the metal assembly is heated to 300° or 400°C to expand it and while still hot slipped over the glass panel. As the metal cools it contracts around the panel and puts the glass under compression which provides a system similar to that of the tensioned metal strap previously described.

Various types of mounting lugs or ears are frequently attached to the metal pieces employed in the implosion prevention system to facilitate the mounting of the picture tube in the receiver cabinet.

It has long been the practice to add neutral absorbants in the panel glass to improve picture contrast by suppressing halation in the faceplate and ambient light reflection from the screen. Panel faceplates with as little as 42% transmission have been used for color tubes, but the use of the light-absorbing matrix permits much higher transmission, as will be described in Section 5.5.

Even with highly absorbing glass, front-surface reflectivity from the faceplate glass still exists and may deteriorate the video image as seen by the viewer. For example, the convex curvature of the outer tube face tends to accentuate the formation of reflected lamp images and the like that are superimposed on the picture. Remedies have been developed consisting of a coating or surface finish that smears the reflected image but has little effect on resolution of the video image.

5.3.10 Magnetic Shielding of Shadow-Mask Color Tubes

Magnetic shielding must be provided for shadow-mask color tubes to reduce the influence of magnetic fields on electron trajectories as the tube is scanned. In particular, the angle of incidence of the beam at every point on the mask must not change significantly from the design value, or the beam will move away from its intended landing position on the screen. The magnetic-field sensitivity extends to very small changes in the ambient field relative to the color tube such as those produced by rotation of the TV receiver in the earth's field.

Shield designs using soft magnetic materials have been developed for placing the shield either inside the tube or just outside the tube. Also, the low-carbon-steel shadow-mask is an important part of the shield system. Such materials, to be effective, must be thoroughly demagnetized (degaussed) in position. The degaussing may be done by subjecting the shield to the field from a coil energized by alternating current of progressively reduced amplitude from the power line. This procedure effectively reorients magnetic domains in the shield and tends to leave it magnetized so as to

nullify the field within the shield. The degaussing coil may be built into the receiver and the alternating current automatically reduced from a high value to zero every time the receiver is turned on. This insures against deterioration of color purity and white uniformity caused by changing magnetic field environments.

A better understanding of the effect of a magnetic field is attained by separating it into three orthogonal components. Since the vertical component of the earth's field remains relatively constant when the tube is used in the northern hemisphere, compensation for this component is most easily achieved. This may be done by taking into consideration the magnetic displacement of the beams in the lighthouse lens design. The z component, or the field component parallel to the tube's axis, causes the largest uncorrectable beam displacement and, with shielding, typically produces misregister in the order of 15–25 μm.

Effective shielding of a color tube depends not only on the magnetic properties of the shield and its geometry but also on its placement with respect to the beam path in the color tube. A knowledge of the sensitivity of the beam to magnetic fields as a function of distance along the path is helpful in determining the extent of the shield needed and where best to place the shield. Detailed analysis shows that maximum sensitivity of spot position results from fields at the shadow mask, decreasing linearly toward zero at both the deflection center and at the phosphor screen. Expressions have been given in Section 5.3.2 for the total spot displacement, when a tube is transferred from a field-free environment into a uniform magnetic field.

The coercive force of the magnetic shield should be as low as possible. For cold-rolled steel, this may be obtained by use of low-carbon material and suitable firing to further decarburize the material. In addition to the shield itself, the shadow mask makes a significant contribution to the total shielding of the tube. Cold-rolled steel 0.15 mm thick is commonly used for the mask material. The use of low-carbon materials or decarburization enhances the effectiveness of the shielding.

The shield may be either inside the tube envelope or placed on the outside. The usual practice in the United States is to use an external shield. In Europe, it is customary to use a push-through type of mounting of the picture tube in the receiver wherein the face and a portion of the sidewall of the tube is exposed in the front of the receiver. With this configuration an external magnetic shield which does not extend to the front of the picture tube is used. The shorter length of the shield reduces its effectiveness. In Europe therefore, particularly in the case of 110° tubes, it is the practice to place the magnetic shield inside the tube. This shield is usually made of

0.1–0.15-mm thick cold-rolled steel and is welded to the mask support frame assembly during the tube fabrication. It must be designed to fit the bulb envelope and be as close to the bulb wall as possible so that it will not provide a surface from which overscan electrons will be scattered back onto the screen.

Because of lower coupling to the external degaussing coil, an internal magnetic shield usually requires a higher amount of degaussing current than an external shield. Degaussing is normally expressed in terms of ampere turns, and typically for 110° internal shields, would be in the order of 1500 A turns. An external shield can be degaussed with half this value.

5.4 110° Systems

The obvious advantage of 110° systems over 90° systems is the shorter overall tube length obtained and, therefore, the improved compactness and cabinet styling that is possible in the receiver. For a 25V (626 mm) tube, this saving in overall length is about 100 mm. A second advantage of the 110° system is a shorter throw distance for the electron beam which results in a smaller focused-spot size. In most other aspects, the design of 110° systems becomes more complicated because of the following factors:

(1) Higher deflection power is required if other parameters of the system are kept constant.

(2) Electron-optical distortion of the beam triads and distortion due to obliquity factors in screen geometry become greater with an increase in deflection.

(3) An increased amplitude of dynamic convergence is needed, so the problems of achieving satisfactory convergence become more difficult.

(4) Electron beam deflection defocusing becomes greater.

One approach to mitigate the disadvantages of the 110° system has been to reduce the neck diameter so the deflection power and the dynamic convergence requirements do not greatly increase over the 90° system.

The first commercial 110° color system employed an 18V (457-mm) screen size (*67*). It utilized a 29-mm diam neck which reduced the deflection power and convergence requirements compared to that required in a 36-mm neck 90° system. The yoke and scaled-down version of the gun were very similar to that commonly employed in 90° systems. Even with the smaller gun size (see Fig. 5.27), good resolution was obtained because of the shorter throw distance. The shorter throw distance also aided in convergence.

In larger-size tubes, for example the 25V (626 mm), two different systems have been commercially employed. One system utilizes a 29-mm neck and the second a 36-mm neck. The gun employed with the 36-mm neck is similar to that used in the 90° system; the misconvergence and triad distortion were minimized by the use of a special circuit to provide a "current-difference waveform" to the two halves of the horizontal yoke windings.

The yoke itself was designed to give no astigmatism along the vertical and horizontal axes of the screen which means the equilateral shape of the beam triad will be maintained on axis. The size of the triad may be changed but not the shape when dynamic convergence is applied. With such a yoke, convergence at the corners of the raster cannot be obtained by the simple sum of horizontal and vertical dynamic convergence. To obtain corner convergence, the two halves of the horizontal windings are modulated with an equal, but opposite, current waveform at horizontal rate. The amplitude of this waveform is proportional to the product of the instantaneous values of the horizontal and vertical deflection. This modulation corrects corner astigmatism and produces corner convergence.

Another system, utilizing the smaller 29-mm neck, makes use of a precision toroidal yoke wherein control of the winding distribution can be precisely held by placement of the individual wires in accurate mechanical plastic combs at either end of the yoke. A typical yoke of this type, called *precision static toroid yoke* (*19*), is shown in Fig. 5.41. It has been possible with such a yoke to obtain triad distortions that are comparable to that commonly found in 90° yokes, and to obtain adequate convergence with a

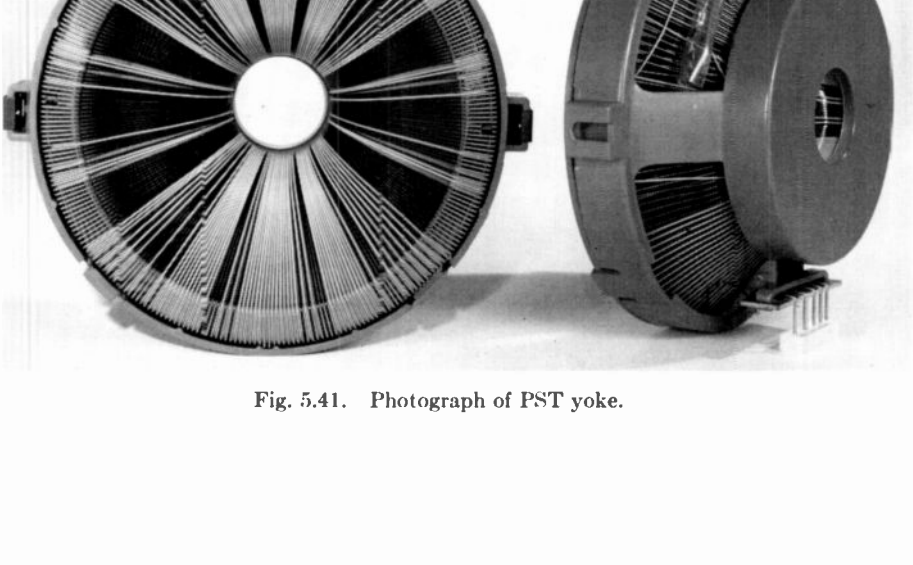

Fig. 5.41. Photograph of PST yoke.

Fig. 5.42. PST winding distribution.

90° dynamic convergence system. This desirable yoke performance is in part due to the longer effective magnetic field of the toroidal yoke. The deflection field originates as the leakage flux from the two opposing sections of each of the vertical and horizontal deflection windings. The mechanical features of the toroidal yoke allow any desired intermixing of vertical or horizontal windings around the circular ferrite core. Figure 5.42 shows a typical winding distribution for a 110° toroidal yoke. Using the freedom to select winding distribution, an optimum design can be achieved for best convergence and for minimum triad distortion. Control of these characteristics is achieved by the accurate and repeatable mechanical placement of the windings.

The problems of obtaining and maintaining good register between phosphor dots and the electron beam spots increase with the higher deflection angle. Of special importance are problems of mechanical stability that will affect the spacing between the shadow mask and faceplate. After the screen is printed on the lighthouse, as described in Section 5.3.5, a change in spacing between the screen and shadow mask will affect register in proportion to the tangent of the half-deflection angle. For example, a change in this spacing by 0.1 mm near the diagonal corner of the screen will affect register on a 90° tube by 0.1 mm and on a 110° tube by 0.143 mm. This increase can be compensated for in the design of the lighthouse lens providing

the increase remains fixed at the new value. Any variation in this value from tube to tube must be accepted as a tolerance. The principal factors causing change in screen-to-mask spacing are the movements of the mask and the glass panel through thermal tube processing cycles. These movements tend to be random in nature except for the tendency of glass to compact or increase in density with thermal cycling and for the face panel to flatten when vacuum-loaded. Typically, a 25V (626-mm) panel will flatten about 0.15 mm under vacuum exhaust.

Other mechanical factors that have a greater effect on 110° than on 90° tubes include the thermal expansion of the mask. While the average steady-state expansion can be corrected completely by the bimetal mask mounting system described in Section 5.3.8, a transient expansion of the mask will cause a reduction in the mask-to-faceplate spacing when it is due to uneven heating or the heating of the mask before the frame temperature has risen. These transient temperature changes will cause more change in register with 110° deflection than with 90° deflection as previously discussed. One method of reducing the transient mask expansion problem has been to put a black, or high thermal-emissivity coating, on the back of the aluminized screen. This coating allows the panel to absorb radiant heat from the mask rather than reflect it as would be the case with a shiny aluminum coating.

The application of an implosion protection system to the panel may also affect register. Since most of these systems, as discussed in Section 5.3.9, place the skirt of the panel in compression, there is a tendency to make the faceplate bulge out slightly. Again, if the distortion is consistent from tube to tube, this effect may be compensated for in the design of the lighthouse optics.

5.5 Matrix-Screen Color Tube Systems

The matrix-screen concept for shadow-mask color picture tubes makes it possible to design the tube for greater brightness and/or greater contrast than is possible in a nonmatrix design (*68*). To understand the basis for the improvements, it may be instructive to review the major factors affecting brightness and contrast. Brightness is primarily determined by the anode voltage, anode current, screen efficiency, and transmission of the faceplate through which light from the phosphor must pass in getting to the viewer. An unwanted factor is ambient light reflected from the screen to the viewer. Its major effect is to degrade picture contrast by limiting the blackness of the black that can be obtained on the screen or to limit the black level in the picture. To counteract this effect, it has been customary

in black-and-white picture tubes, and for many years prior to the advent of matrix screens in color tubes, to use light-absorbing or "gray-glass" faceplates. The advantage of using a gray-glass faceplate is that part of the ambient room illumination which is reflected from the screen and gets to the viewer must pass through the gray glass twice. It is therefore attenuated twice while light originating from the phosphor that gets to the viewer is attentuated only once. The contrast ratio or brightness ratio of the high light to the black level in the picture is thus increased, but at the expense of picture brightness. Generally, the brightness loss is 50–60% in nonmatrix color tubes.

The basis for improvement of the nonmatrix design by incorporation of a matrix is the reduction of screen reflectivity for ambient illumination and at the same time removal of much of the attenuation used in the gray-glass faceplate. By so doing, the black-level degradation which results from ambient light falling on the screen is kept at a low level because the screen is less reflective while the picture is brighter because the picture light is attenuated less in the faceplate.

A reduction in screen reflectivity is possible because the area of the screen hit by the electron beam as the beam comes through the shadow mask is only 50–75% of the total screen area. The unbombarded area serves as tolerance for landing of the beam on the phosphor dot or line. Much of this area can be made nonreflective or converted to a black matrix surrounding the phosphor elements without reducing the light generated in the phosphor.

There are two approaches to designing a matrix for the shadow-mask tube, the difference in the two depending on how the tolerance for beam landing on the phosphor dots is handled. In the first approach, here designated positive-tolerance matrix, the matrix openings or phosphor dot diameters as defined by the matrix openings, are larger than the electron spots. It has an advantage in simplicity of manufacture, but its performance is limited in that only a relatively small black matrix area can be added before the tube screen tolerance is reduced beyond an acceptable level, although screen tolerance requirements may be reduced by improved manufacturing techniques and controls or the acceptance of less rigid performance requirements for color field purity and uniformity of the white field. In the second approach, here designated negative-tolerance matrix, the matrix openings are smaller than the electron spots. In this design it is desirable to both enlarge the mask apertures to achieve larger electron spots and reduce the matrix openings. The inverted phosphor dot-electron spot size relation is responsible for the negative-tolerance designation. Figure 5.43 shows typical nonmatrix and matrix designs to illustrate the geometric relationships that have been described. For simplicity, the screen and electron spot

systems are assumed to be perfectly nested and the electron spots have sharply defined edges without umbra-penumbra gradations that exist in practice.

The simplified Fig. 5.43 also can be used to describe the concept of screen

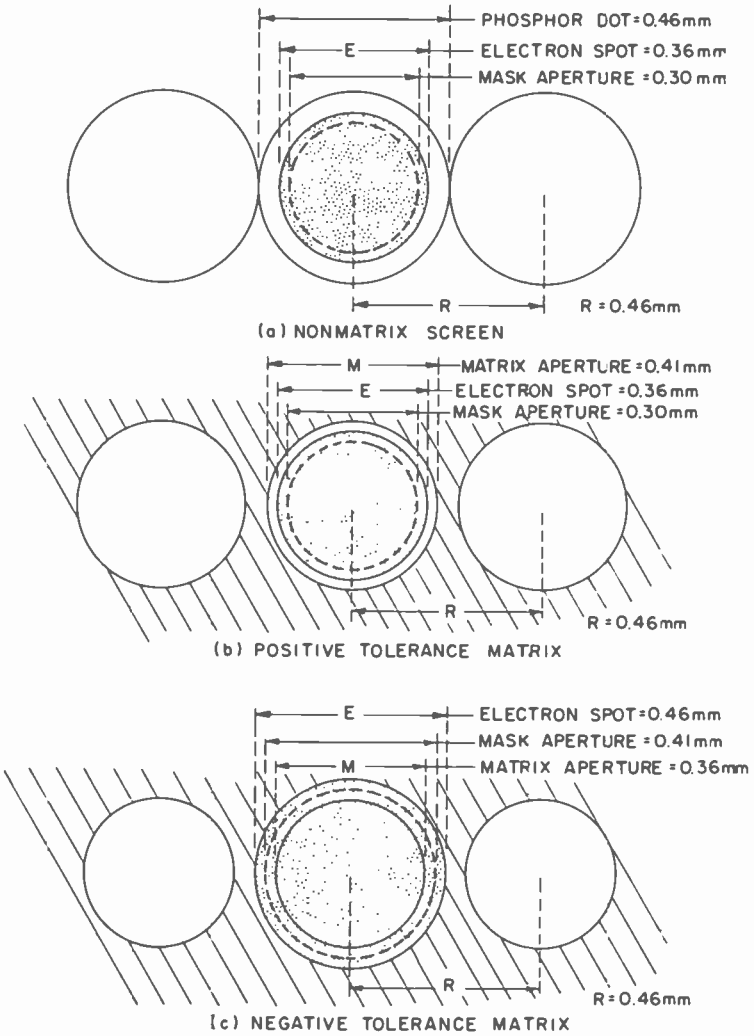

Fig. 5.43. Illustration of (a) nonmatrix, (b) positive-matrix, and (c) negative-matrix designs. The illuminated phosphor-dot areas are the same in each case. R is the distance between phosphor dots.

tolerance for each type of screen. In the nonmatrix case (Fig. 5.43a), the electron spot is smaller than the phosphor dot and will produce the same amount of light as long as it lands within the phosphor dot. The tolerance for the spot beginning to leave the dot, or leaving tolerance, is defined as the total maximum distance the electron spot can move without altering the amount of light emitted from its phosphor dot. For the nonmatrix case the leaving tolerance is then just the difference in diameter of the phosphor dot and electron spot or 0.1 mm as shown in Fig. 5.43a. For the positive matrix, where the phosphor dot diameter is the matrix aperture diameter, the leaving tolerance is 0.05 mm as in Fig. 5.43b. The same definition also applies for determining leaving tolerance in the negative tolerance case, but in this instance the electron spot is larger than the matrix aperture. The sample negative tolerance screen of Fig. 5.43c has a leaving tolerance of 0.1 mm.

If in each of the three screen types the leaving tolerance is exceeded in an operating tube for some reason, the actual hue change produced will depend on whether adjacent phosphor areas are now illuminated by the beam spots that have moved. A second kind of tolerance has been specified to cover this contingency. It is called clipping tolerance. Clipping tolerance is the total distance the electron spot can move before it reaches an adjacent area of visible phosphor. Clipping tolerance is then

$$T_C = 2R - M - E$$

where R is the spacing between matrix apertures (phosphor dots in nonmatrix screen), M is the matrix aperture diameter (phosphor dot diameter in nonmatrix screen), and E is the electron spot diameter. By inspection of Fig. 5.43, the clipping tolerances are:

0.1 mm	nonmatrix
0.15 mm	positive tolerance
0.1 mm	negative tolerance

In the above examples, it is assumed that the beam spots and phosphor dots are in perfect register.

Each of the systems are dependent on leaving and clipping tolerances in ways that play a distinctive role in tube operation. For example, in the nonmatrix screen where leaving and clipping tolerances are equal for tangent phosphor dots, white uniformity is seldom a problem if the screen has good color-field purity. That is, color-field purity requires only that the electron spots fall entirely within the phosphor dots or that leaving tolerance is not exceeded. White uniformity requires in addition that the relative current to the dots of each triad be equal over the screen. Since in the absence of a

matrix in a nonmatrix tube the current for all three beam spots in a given triad is limited by the same aperture, this requirement is met automatically.

In the positive tolerance screen the same situation holds as for the nonmatrix screen, although leaving and clipping tolerance are no longer equal except in the limit when the matrix apertures are tangent. If the matrix openings are smaller than required for tangency, then it is possible for an electron spot to begin leaving an opening without striking an adjacent phosphor dot. If this happens color purity will not be affected as such, but a reduction in light generated in the dot will take place. Should this happen in one phosphor dot of the triad, then white uniformity is degraded. Color purity is therefore easier to maintain than white uniformity.

The negative tolerance situation is much different. Because the electron beam spots completely cover the matrix openings, white uniformity depends on having throughout the screen the same relative transmission of the openings in each matrix triad. In effect there is a potential for building into the screen a nonuniformity in white that cannot be corrected by operating controls in the receiver. More will be said about this in the next section under Matrix Screen Construction. With regard to leaving and clipping tolerances in the negative-tolerance system, it is possible to favor either one over the other by the choice of mask and matrix openings.

In general the discussion has assumed well-nested, equilateral phosphor-dot triads and beam-spot triads. Distortions in the beam-spot triads which may occur particularly near the edge of the picture area, will require that somewhat smaller phosphor dots be used to prevent dot overlap. The situation is further aggravated when phosphor dots cannot be printed in precisely the desired place because of lighthouse lens limitations. As in the nonmatrix system, matrix screen tubes make use of masks with aperture sizes graded to smaller diameter at the edge than in the center to obtain increased tolerance at the edge

The negative-tolerance matrix tube using a faceplate transmission of about 85% had evolved by 1973 as an attractive system. A transmission of 85% is the highest value it is practical to get without objectionable tint and therefore represents a design for maximum light output. Other details of the design such as the choice of mask transmission and the percentage of the screen surface covered by the black matrix are related to trading brightness for screen tolerances which affect color purity and white uniformity. An adequate discussion of these choices, dictated largely by manufacturing considerations, is beyond the scope of this volume, but an illustration of the magnitude of performance changes that can be achieved with a matrix design over a nonmatrix design is given in Fig. 5.44. Typical matrix and nonmatrix tubes are here assumed to be operating under significant

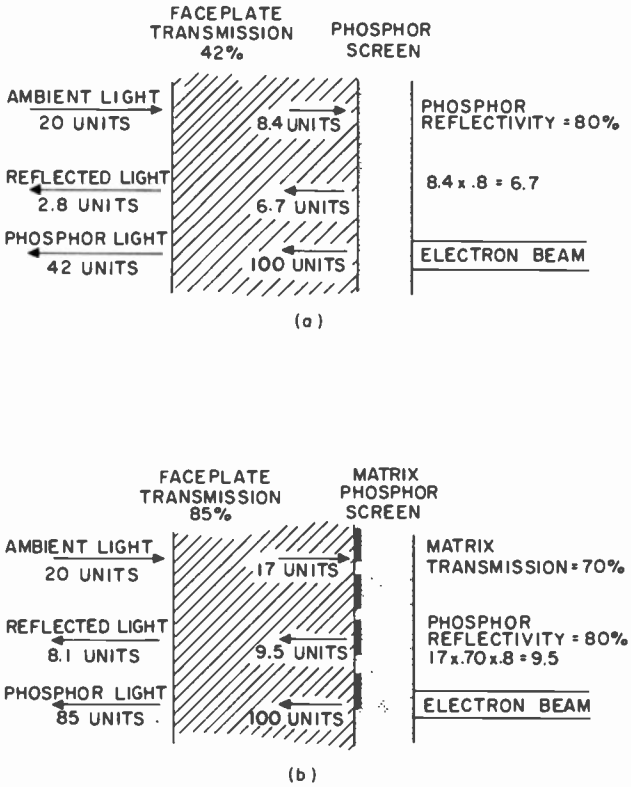

Fig. 5.44. Relative matrix screen brightness gain over nonmatrix screen when the same area of phosphor is exposed to the electron beam in the two systems. (a) Nonmatrix screen: brightness, 42 + 2.8 = 44.8 units; contrast, 44.8/2.8 = 16; black level, 2.8 units. (b) Matrix screen: brightness, 85 + 8.1 = 93.1 units; contrast, 93.1/8.1 = 11.5; black level, 8.1 units. The brightness gain is 93.1/44.8 = 2.1. Both the contrast and black level are less favorable.

ambient light. The relative brightness, contrast, and black level are obtained under the reasonable assumption that the matrix tube phosphor dot as defined by the matrix opening is the same area as the electron spot on the phosphor dot in the nonmatrix tube. That is, assume the same amount of light is generated by the electron beam in the two systems.

Several observations relating to nonmatrix, positive matrix, and negative matrix color tube systems are as follows:

1. In a positive-tolerance matrix tube and in a nonmatrix tube, the largest mask aperture permitted by tolerance considerations is desirable.

In the case of the matrix tube, this corresponds to a large matrix opening and a small amount of black.

2. In a negative-tolerance tube, both brightness and contrast increase as the matrix openings increase, but black level degrades. Thus, the largest matrix opening permitted by tolerance considerations is desirable for best brightness-contrast performance. This corresponds to the least amount of black material.

3. In positive-tolerance tubes, the clipping tolerance is greater than or equal to the leaving tolerance while in negative-tolerance tubes, the clipping tolerance may be either larger or smaller than the leaving tolerance.

4. For the same leaving and clipping tolerance, the mask transmission* of positive-tolerance designs is equal to the effective matrix transmission of negative-tolerance designs. Thus, for the same glass transmission, there is little difference in brightness between the two types. There is, however, a significant contrast advantage in the negative-tolerance type which can be traded for a brightness advantage by increasing the glass transmission.

5. In negative-tolerance tubes, localized variations in the ratios of the red-, green-, and blue-matrix openings will cause a change of white balance. Thus, control of the relative matrix openings is an important factor in the production of a negative-tolerance tube.

Matrix Screen Construction

The processes used in making color screens for shadow-mask tubes have already been described in Section 5.3.5. Matrix screen construction differs primarily by the need to add procedures for printing the matrix.

As indicated in the earlier discussion, the basic screen printing technique is exposure of a light-sensitive colloid, usually PVA, which may contain phosphor as a pigment. The exposed area becomes insoluble and remains after development. On the other hand, matrix printing requires a process that has the reverse polarity because the matrix openings should be clear with the surrounding area black. Several processes have been developed that can produce this result. However, the most common one (*69*) is a reverse printing process that uses PVA photosensitive material which hardens on exposure to ultraviolet light. In this process, clear unpigmented PVA is exposed in the lighthouse from all three color-center positions. After development, the surface contains a system of clear dots in the positions later to be openings in the matrix. Next, a water suspension of graphite is slurried on the surface and dried. An aqueous solution of H_2O_2 is then used to develop the matrix. The H_2O_2 disintegrates the PVA dots and dislodges the

* In the limit of zero electron beam diameter in the deflection plane, or the absence of a penumbra.

overlying black layer while leaving undisturbed the graphite that is in direct contact with the glass. After the matrix is formed, phosphor dots are printed by the processes described for nonmatrix tubes.

Printing negative-tolerance matrix screens poses a problem not encountered in nonmatrix and positive-tolerance matrix screens, because the mask apertures in negative-tolerance tubes are larger than the matrix openings desired. In using the matrix reverse printing process, it is therefore necessary to print PVA dots that are smaller than the mask apertures. Three possibilities exist. First, the mask apertures may initially be made small for printing purposes, and then after the matrix and screen are printed, the mask is postetched to enlarge the apertures to the size required in the operating tube (*70*, *71*). Second, the resist coating containing small openings that is applied to the mask when etching the mask apertures may be left on after the etching is completed and serve as a printing mask for the large apertures (*72*), or the mask apertures may be initially large and then temporarily restricted in size by a coating applied to the mask. The coating is removed after the printing operations are completed. Third, an appropriately chosen printing light-source size aided by light diffraction at the apertures may be used with precise exposure control to "print down" and obtain dots smaller than the mask apertures.

The first method is the basis of a commercial process. In the second method, where the etch resist is left on, heat treatment of masks after etching is not possible. Hence the mask must be etched after forming the mask to a spherical curvature, which severely limits the method. Coating methods are the subject of many patents which describe techniques such as plating, spraying, cataphoretic deposition, etc., but none has been used commercially. The third method, print down, plays a part in printing even nonmatrix phosphor screens; properly used, it becomes very important as the basis for an attractive matrix printing process that does not require alteration of the mask for printing the matrix and screen. That is, the size of the printing light source and diffraction of light at the aperture edge influence the light distribution in the dot projected on the screen in the printing process. The intensity profile of this distribution relative to the mask aperture dimension can, under certain conditions, become favorable for printing PVA dots smaller than the apertures. For example, if the light intensity distribution at the screen plane from an aperture falls off with sufficient gradient at the desired dot diameter, then dots of this diameter may be printed by precise control of exposure. Fortunately, clear or unpigmented PVA photoresist may be used so that light scattering is a minimum during exposure. The basic simplicity of printdown makes it important to review the optical principles involved so that full advantage may be taken of this method of matrix printing.

Assume a monochromatic point light source of wavelength λ is produced, for example, by focusing a laser beam with a microscope objective of large numerical aperture. If this source is placed at the deflection center, a distance p from the mask aperture of diameter B, the intensity distribution $I(r)$ on the screen, a distance q from the mask, is given by

$$\frac{I(r)}{I_0} = F(\rho, y) \qquad \text{with} \qquad \rho = \frac{2rp}{B(p+q)}, \quad y = \frac{\pi(p+q)B^2}{2pq\lambda} \tag{5.86}$$

Here I_0 is the intensity in the absence of diffraction within the geometrically projected light spot of radius $B(p+q)/(2p)$ and F is a universal function of the relative radial distance ρ and the parameter y. Figure 5.45 shows the function $F(\rho, 25)$, the parameter $y = 25$ corresponding, for example, to

$$B = 0.3 \text{ mm}, \qquad q = 15 \text{ mm}, \qquad p = 245.9 \text{ mm}, \qquad \lambda = 4 \times 10^{-4} \text{ mm}$$

These geometric parameters might be realized in a large-screen, large deflection-angle tube with a matrix screen. Since $25 \cong 8\pi$ and, quite generally,

$$I(0)/I_0 = 4 \sin^2(y/4) \tag{5.87}$$

the intensity is seen to drop to zero at the center of the light spot. On the other hand, for $y = 10\pi = 31.42$, realized by reducing, in the preceding example, the wavelength to 3.18×10^{-4} mm or q to 11.79 mm we would obtain the dotted curve for the distribution near the spot center, with $I(0)/I_0 = 4$.

The distribution near the center of the light spot is thus highly wavelength-and-q-dependent. At the geometric shadow edge it is much less so. For $B/2 \gg (\lambda q)^{1/2}$, we must expect behavior similar to that at the shadow edge of a straight edge, i.e., $I/I_0 \cong 0.25$ at the shadow edge ascending to a maximum of the order of $I/I_0 = 1.37$ a distance approximately equal to $(\lambda q)^{1/2}$ from the edge toward the center of the light spot and decreasing monotonically from the edge into the shadow region. For a point source with a wide spectral distribution we might thus expect the distribution in the interior of the spot to be smoothed out, retaining the reduction of the intensity at the geometric edge to 1/4 the mean intensity in the spot and an intensity variation characteristic of a median wavelength near the geometric edge. If, in addition, the light source is relatively large, i.e., has a diameter of the order of $(p/q)B$, the distribution is both broadened and changed from a flat-topped to a more nearly conical shape.

The sources most commonly used for printing shadow-mask screens utilize high pressure mercury arcs, with spectral distributions similar to that shown in Fig. 5.46 (*73*). The spectral response of the photoresist is such that only the narrow spectral distributions centered about 365 nm and

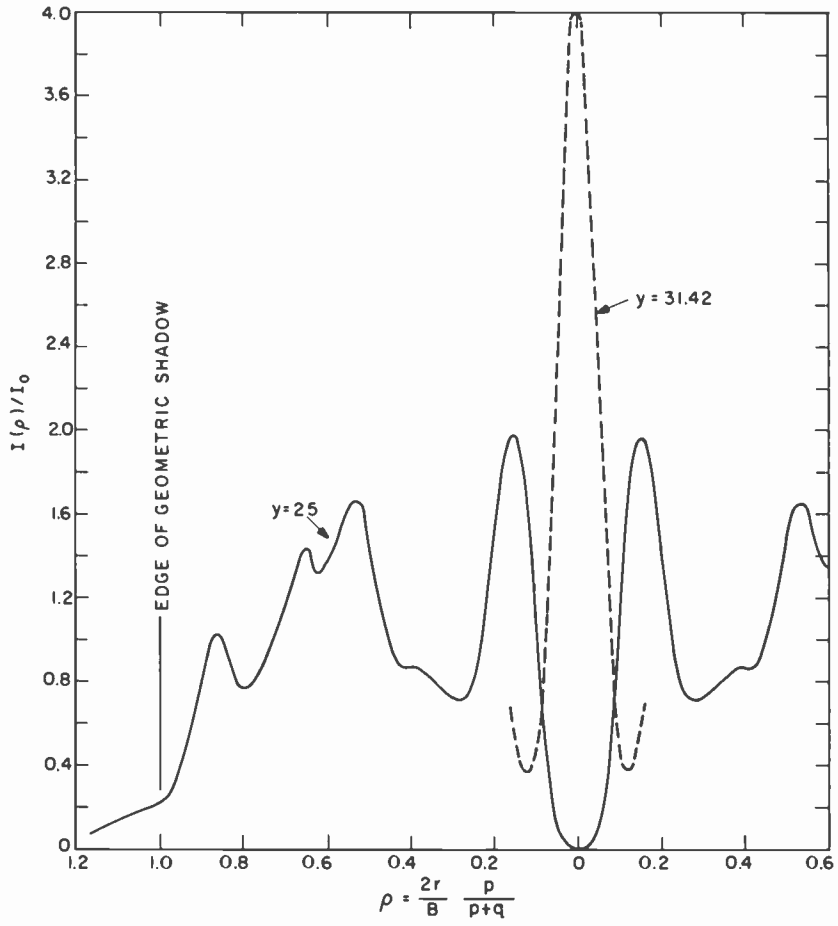

Fig. 5.45. Intensity distribution in light spot projected on screen by monochromatic point source at deflection center through mask aperture.

400 nm are effective (Fig. 5.47) (*74*). It is thus not surprising that the intensity distribution at the screen plane of light that has passed through an aperture in the mask should exhibit a very striking intensity variation when produced by a source with diameter much less than $(p/q)B$ and measured with a sensor with the spectral response of the photoresist. The result of such a measurement is shown in Fig. 5.48.* As the source diameter

* Measured by P. Kuznetsoff and J. Mirsch at the David Sarnoff Research Center, Princeton, New Jersey.

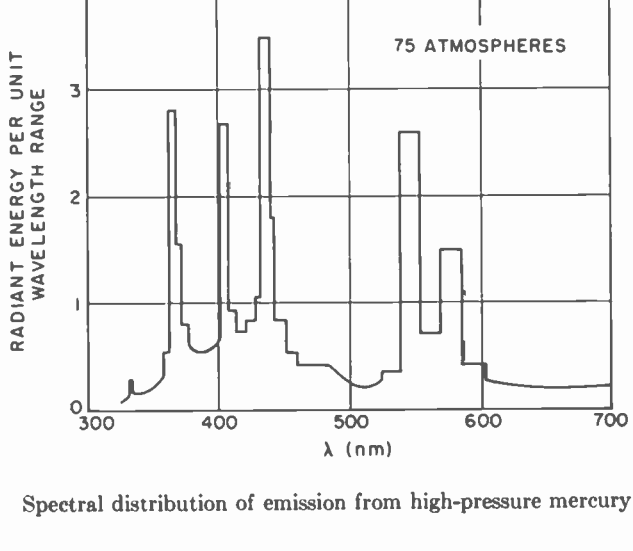

Fig. 5.46. Spectral distribution of emission from high-pressure mercury arc (*73*).

D_o is increased to the point that

$$[q/(p + q)]D_o = 0.38B \tag{5.88}$$

the effective distribution is found to assume a conical shape, leaving only a slight dip at the center (Fig. 5.49).*

As previously indicated, the intensity distribution in the light spot is of particular importance in matrix printing. The accuracy with which the

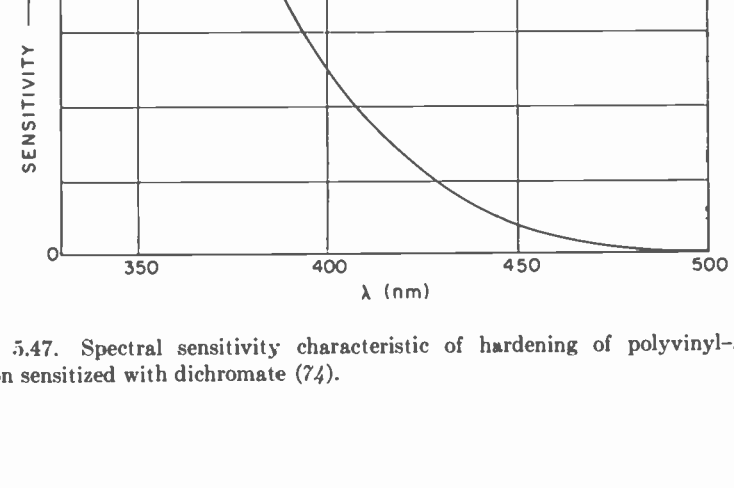

Fig. 5.47. Spectral sensitivity characteristic of hardening of polyvinyl-alcohol solution sensitized with dichromate (*74*).

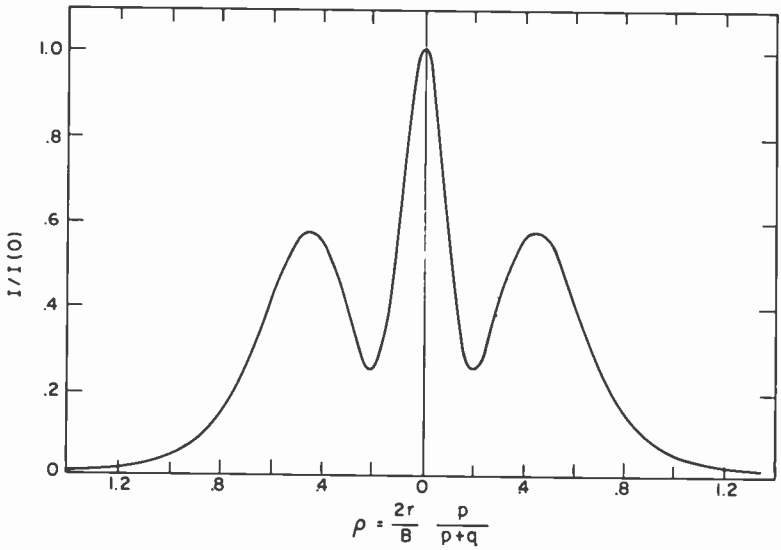

Fig. 5.48. Effective intensity distribution in spot projected by 0.38 mm source.

printed dot area can be realized is proportional to the quantity

$$\frac{\text{fractional error in exposure } E}{\text{fractional error in dot area } \pi D^2/4} = \frac{D}{2E}\frac{dE}{dD} = \frac{r}{2I}\left(-\frac{dI}{dr}\right) \qquad (5.89)$$

This quantity obviously has a large value if the critical exposure which marks the boundary of the developed dot corresponds to a large value of the diameter $D = 2r$ and a small value of I, close to the edge of the intensity distribution, where the slope $-dI/dr$ is still large.

In summary, dots larger than mask apertures are readily printed, but in printing a negative-tolerance matrix by the reverse-printing process described above, the PVA dot size should be smaller than the mask aperture size. We can obtain the smaller dot size by employing a printing light source that gives a more or less conical light intensity distribution back of each aperture at the screen plane and reducing the exposure to such an extent that the critical exposure occurs at the much smaller dot diameter desired, and at a correspondingly much greater value of $I(r)/I_0$. The relative printing accuracy given by Eq. (5.89) is now much smaller or, in other words, the required uniformity in exposure and photoresist sensitivity much greater.

5.6 In-Line Gun Systems

The advantage of an in-line configuration of guns in a shadow-mask display is the potential for simplified convergence. With spots from coplanar beams initially converged at the center, and the beams well aligned with the yoke, all that should be required to maintain convergence during scan is to move the outside beam spots along the line of centers to the center spot. Moreover, the basic delta-gun shadow-mask tube can be designed to use an in-line gun with essentially no geometric modification of the shadow mask or phosphor dot screen pattern. As shown in Fig. 5.50, when the in-line gun array is horizontal, the phosphor dot triads become three dots in a horizontal line, and the triads nest together to form the same overall phosphor dot pattern as in the delta system. An individual mask aperture is aligned with the center phosphor dot of the line triad in contrast to the delta-gun system where the aperture is aligned with the center of the triangle of phosphor dots forming the triad.

However, distortion of the electron-spot triads, as described in Section 5.3.2 and illustrated in Fig. 5.13 for the delta system, is also present in the in-line system because of the spherical shape of the mask and screen. The distortion is a foreshortening of the triads in the radial direction; and, in the case of line triads, results in an effective rotation or tilt of the line

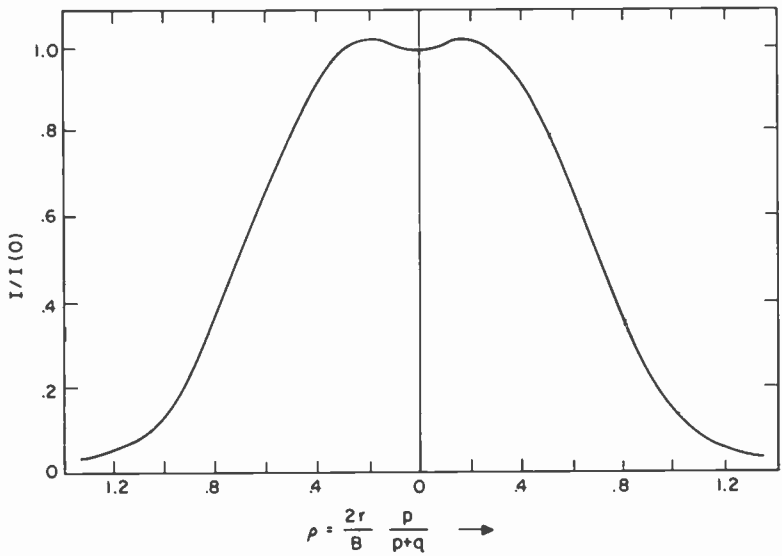

Fig. 5.49. Effective intensity distribution in spot projected by 2.0 mm source.

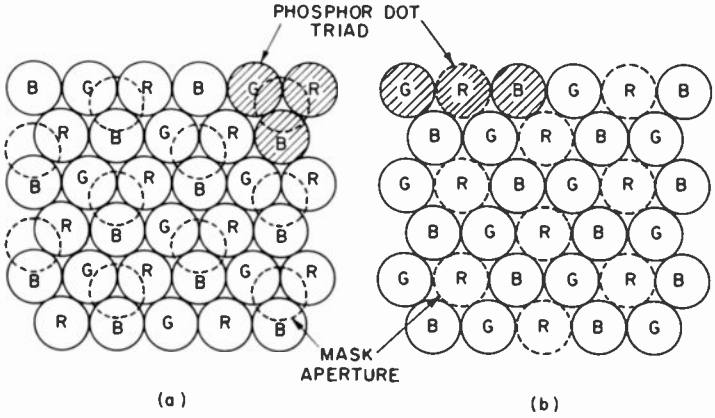

Fig. 5.50. Nesting of (a) delta gun-mask and (b) in-line gun-mask phosphor-dot triads, and the geometric arrangement of the triads with respect to mask apertures.

triads in the corners shown in Fig. 5.51. The geometric or obliquity distortion causes sufficient tilt to seriously reduce color purity tolerance, unless corrective measures are taken. One such measure is to distort the mask aperture array (*75*) so that rows of apertures tend to follow the direction of triad tilt. Another is to design astigmatism into the yoke to produce a triad tilt in the opposite direction to nullify the obliquity tilt, but this method would require corner convergence waveforms.

An entirely different approach that largely avoids this screen tolerance problem, while retaining simplified convergence, is to change the round mask apertures into vertical slits and use a phosphor screen in the form of continuous vertical stripes. Tilt of the electron spot-line triads can then be tolerated without causing color impurity if proper nesting of the electron spots on the screen surface is obtained by the appropriate choice of mask-to-screen distance. Screen printing is made easier because a lighthouse lens can now be designed to print phosphor lines in exact horizontal register with the electron-beam pattern, as discussed in Section 5.3.3. However, in practical development of simplified convergence for in-line systems employing round apertures as well as slit apertures in the mask, there are a number of important considerations which will now be discussed.

5.6.1 Deflection and Convergence of In-Line Gun Color Tubes

In discussing the convergence errors that take place during magnetic deflection, it is convenient to consider deflection defocusing of a hypothetical, large composite beam of circular cross section that, when undeflected, is focused to a point at the center of the screen. Three of its rays

represent the central ray of each of three individual beams. In the delta configurations, these rays lie on the surface of the large composite beams, separated by 120°; in the in-line configuration, they are the two external rays on the horizontal diameter and the central ray.

The ideal deflection yoke for in-line systems would cause no defocusing of the principal rays of the composite beam in its horizontal dimension as the composite beam is deflected. It would, however, cause deflection defocusing in the vertical dimension, to the point where the composite beam becomes distorted with deflection into a vertical line; but the rays of the composite beam, representing the central rays of the in-line beams, would still be converged as illustrated in Fig. 5.52. Such a yoke is designated a vertical line-focus yoke and ideally would exhibit vertical line focus at all points on the screen.

The design of a practical vertical line-focus yoke has to be carefully tailored to achieve a prescribed magnitude of astigmatism along the horizontal and vertical axes (slight over or under convergence), no anisotropic astigmatism (spot rotation in the corners), and no coma (raster-size mismatch on axes). Such a vertical line-focus yoke would deflect three horizontal in-line beams to all points of the screen with minimum misconvergence, provided the beams are initially converged at the center of the screen and properly aligned with the yoke. In the delta-gun system, no similar drastic simplification is possible. This is due to the fact that yoke design can eliminate deflection defocusing in only one dimension (horizontal

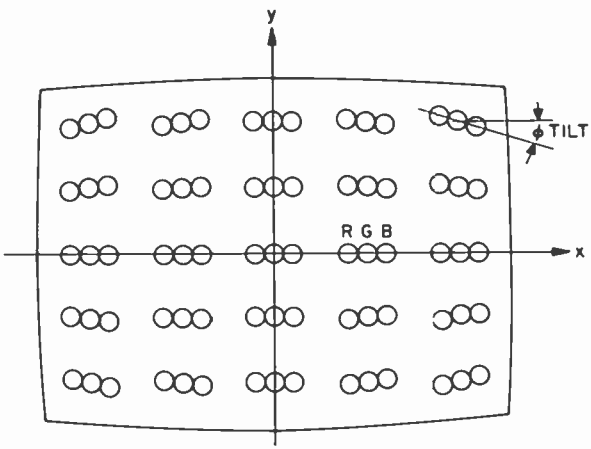

Fig. 5.51. Distortion of electron-spot triads at the screen when using an in-line gun and a spherical mask and faceplate.

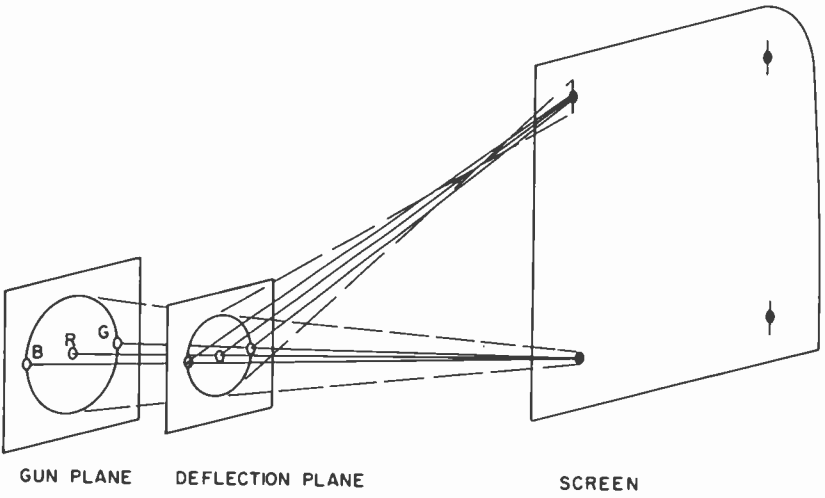

Fig. 5.52. Convergence characteristic of a line-focus deflection yoke.

or vertical) of the composite beam, but not in both. In the delta configuration, the three beams effectively span both dimensions of the composite beam. Yoke design can eliminate either misconvergence between horizontal lines with a horizontal line-focus yoke or misconvergence between vertical lines with a vertical line focus yoke, but not both together.

Display systems using horizontal in-line configuration of the three beams in shadow-mask (or grill mask) tubes have achieved simplified convergence in comparison with the delta-gun system. Two distinct 90° systems have been realized. In one case (*76*), the yoke exhibits essentially vertical line focus along the axes of the screen, but has horizontal and vertical coma. Line focus along the axes eliminates misconvergence between the two offset beams; coma causes a mismatch in the size of the rasters scanned by these two offset beams relative to the central-beam raster. In a commercial realization of this design (*23*), the raster-size mismatch is corrected by simple dynamic convergence waveforms (sawtooth at the horizontal and vertical scanning frequencies) applied to a simplified convergence assembly. The latter consists of four convergence exciters that act on the offset beams through two sets of internal pole pieces in the picture tube neck to produce horizontal and vertical convergence motions.

In another case (*77*), the yoke exhibits essentially vertical line focus along the vertical axis of the screen, but insufficient negative astigmatism (noticeable overconvergence) with substantial coma along the horizontal

axis. Here two magnetic exciters, driven by horizontal-frequency sawtooth and parabola currents that are controlled by one adjustment, act on the offset beams without internal pole pieces to produce the horizontal convergence motions required along the horizontal axis. In addition, two beam-alignment coils generating axial fields are driven by preset horizontal- and vertical-frequency sawtooth to provide vertical convergence motions of the offset beams along both axes of the screen for alignment correction.

A 114° version of this system was announced in 1973 (*66*). Here the yoke is free of coma and almost anastigmatic along both axes of the screen (substantial overconvergence along the axes). This system also uses two magnetic exciters, driven by horizontal- and vertical-frequency parabola and sawtooth currents that are controlled by two adjustments to produce the required horizontal convergence motions of the offset beams along both axes of the screen. In addition, two axial-field generating beam-alignment coils are driven by horizontal-frequency parabola and vertical-frequency sawtooth to provide vertical convergence motions of the offset beams for correction of beam/yoke-field misalignments.

The potential for simplification of convergence inherent in the in-line gun system has been fully realized in the *precision in-line* system (*25*). This system consists of (1) a shadow-mask picture tube including a unitized close-spaced horizontal in-line gun, (2) a toroid deflection yoke that exhibits effectively vertical line focus over the whole screen, (3) a means for centering the yoke on the picture tube to properly align the three beams in the yoke, and (4) an external static multipole low-permeability center convergence device. The absence of internal magnetic structures (except for small raster-size matching elements) permits achievement of optimum convergence by positioning the yoke in relation to the picture tube neck. The result is an inherently self-converging in-line shadow-mask display system that achieves convergence without the use of any dynamic convergence means (circuits, exciters, pole pieces).

5.6.2 In-Line Mask Construction Features

Two forms of masks have been developed especially for in-line gun tubes. In one, the mask consists of vertical strips formed by etching slit openings from top to bottom in a thin piece of metal (*24*). Higher transmission can be used with this type of aperture mask than a round-hole mask (approximately 19% vs. 16%), but the absence of cross ties restricts it to a flat or cylindrical shape and requires that it be mounted under tension on a relatively massive frame. In the cylindrical case, one or more fine wires under moderate tension may be placed on the convex surface of the mask to suppress vibration of the strips. Because of its shape, the aperture grill is used

with a cylindrically curved faceplate in contrast to the usual spherical curvature of a dot-type shadow-mask tube face.

The second type of mask, also made by etching thin metal, has vertical slits (*25*) separated by narrow horizontal webs, as shown in Fig. 3.1, that make it strong enough to be formed into a spherical shape; it provides the same transmission as the round-hole aperture mask. It is resistant to damage from mechanical and thermal loads because of its cross webs and can be used with the conventional spherical faceplate.

CHAPTER 6

Focus-Mask Tubes

6.1 Principle of the Focus Mask

The most obvious shortcoming of the shadow-mask tube is the absorption of about $\frac{5}{6}$ of the beam power by the mask; even with shadow-mask tubes having matrix screens, the fraction of beam electrons which do not excite the phosphors is of this order, the increased mask transmission being offset by the fraction of the beam electrons which impinge on black portions of the screen. Conceptually, the simplest remedy for this shortcoming of the shadow-mask tube is to increase the size of the mask apertures and to create an electron lens at each aperture which images the electron beam cross sections in the deflection plane on the phosphor screen (Fig. 6.1). Then, if the imaging process were perfect, the electron spots on the screen would be no larger than those which would be formed by infinitesimal pinholes or slits, located at the center of each aperture.

Electron lenses of sufficient perfection are readily realized. Davisson and Calbick showed in 1931 (*78*) that a round aperture in an electrode at potential V_m (measured with respect to cathode potential as zero) separating regions of uniform field E_1 and E_2 constitutes an axially symmetric lens of focal length

$$f = 4V_m/(E_1 - E_2) \tag{6.1}$$

and that a slit aperture in a similar electrode constitutes a cylindrical lens of focal length

$$f = 2V_m/(E_1 - E_2) \tag{6.2}$$

Assume now that the apertured mask electrode is a distance q from the screen at potential V_s and that the space between the electron gun and the

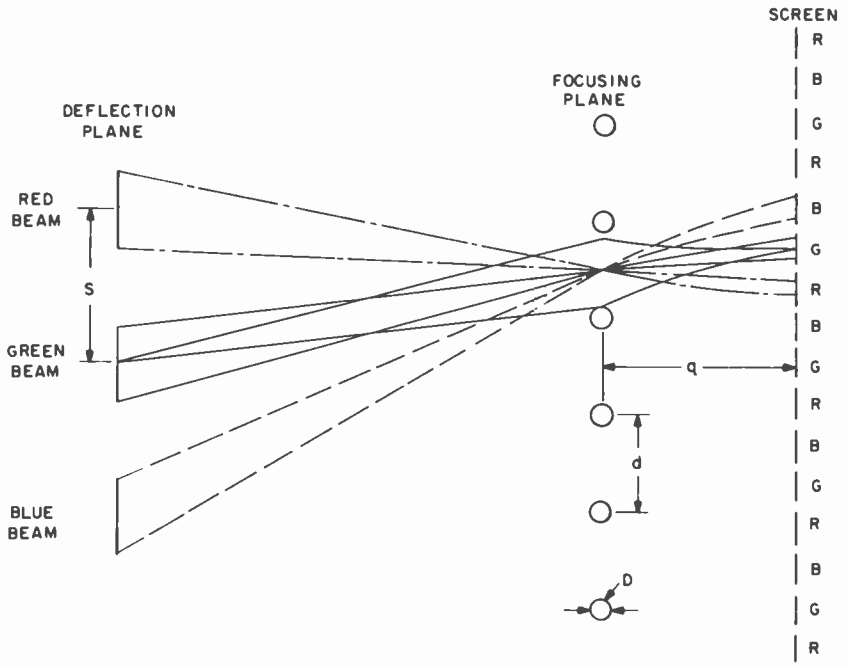

Fig. 6.1. Principle of the focus mask.

mask is field-free. Then

$$E_1 = 0, \qquad E_2 = (V_m - V_s)/q \tag{6.3}$$

In the transit from the mask to the parallel screen the transverse component of the electron velocity v_n (radial in the case of the round aperture and normal to the centerline of the slit in the case of the slit aperture), remains unaltered. For an electron beam normal to the mask plane, an electron path incident at a distance h from the lens center will reunite at the screen with a path through the lens center if

$$v_n t = -\frac{h}{f}\left(\frac{2eV_m}{m}\right)^{1/2} \frac{2q}{(2eV_m/m)^{1/2} + (2eV_s/m)^{1/2}} = -h \tag{6.4}$$

or

$$(2q/f)[1 + (V_s/V_m)^{1/2}]^{-1} = 1 \tag{6.5}$$

Here t is the transit time of the electron between mask and screen. Substitution of f from Eqs. (6.1) and (6.2) with Eq. (6.3) in Eq. (6.5) leads to

the condition for sharp focus for the mask with round apertures:

$$V_s/V_m = 9 \tag{6.6}$$

and for the mask with slit apertures:

$$V_s/V_m = 4 \tag{6.7}$$

If we take into consideration the fact that we image a source in the deflection plane, a finite distance p from the mask, onto the screen, we must replace $1/f$ in Eq. (6.5) by $(1/f - 1/p)$ and find, for the mask with the round apertures,

$$V_s/V_m \cong 9[1 + (2q/3p)] \cong 9(1 + \tfrac{4}{3}M)$$
$$M \cong (2q/p)[(V_s/V_m)^{1/2} + 1]^{-1} \cong q/2p \tag{6.8}$$

and for the slit mask,

$$V_s/V_m \cong 4[1 + (2q/3p)] \cong 4(1 + M), \qquad M \cong 2q/3p \tag{6.9}$$

M is here the (absolute value of the) magnification with which the individual lenslet projects the source onto the screen. Since this magnification is of the order of $\frac{1}{20}$, the correction of Eqs. (6.6) and (6.7) is minor.

Equations (6.6) and (6.7) tell us that if we just maintain the proper voltage ratio between mask and screen, the beam cross section in the deflection plane will be sharply imaged on the screen, irrespective of the mask-to-screen separation q. Moreover, a careful examination indicates that the focusing properties of the mask apertures remain essentially unaltered when the isolated aperture is replaced by an array of similar apertures formed by electrode elements which are narrow compared with the aperture diameter. In particular, a slit mask may be formed by a sequence of parallel wires with diameters $\frac{1}{10}$ of their center-to-center spacing; such a slit mask, in this instance with 90% transmission, is called a focus grill.

6.2 Three-Beam Focus-Grill Tube

The focus-mask principle, in the form of the focus-grill tube, was proposed in a patent awarded to Werner Flechsig (*79*) in 1941. A one-gun version, in which color selection is achieved by local deflection of the beam by electric fields between grill wires in a manner described by A. C. Schroeder (*80*), has become widely known as the "Lawrence tube," after the physicist E. O. Lawrence, who developed it in cooperation with Chromatic Television Laboratories, Inc. (*81*). One-gun focus-grill tubes, under

the trade names "Chromatron" and "Colornetron" have been produced commercially in Japan in limited numbers, by Sony Corporation and Kobe Kogyo Corporation, respectively. Their special features will be indicated in a later paragraph.

Three-gun focus-grill tubes have not attained large-scale commercial production. Their properties, and the special problems involved in their manufacture have, however, been investigated in considerable detail in industrial laboratories.

Focus-grill tubes quite generally employ line screens and in-line guns. With in-line guns, unlike delta guns, the lines traced by the two outer guns are symmetric with respect to the line traced by the central gun, so that nesting can be achieved simply by an appropriate variation of the mask-to-screen distance q over the screen surface. If, as usual, the phosphor line pattern is vertical, the variation of the horizontal component of the earth's magnetic field with change in orientation of the set has, furthermore, no effect on color purity—an advantage of line screens already noted in the discussion of shadow-mask tubes.

Early focus-grill tubes, like early shadow-mask tubes, were constructed with plane grills and plane screens, mounted within an evacuated envelope (*10*). The screens were generally printed by silk-screen techniques from masters prepared by electron exposure. The red, green, and blue phosphor line patterns were printed in succession, shifting the master by a phosphor line width between printings.

Later focus-grill tubes were prepared with the screen deposited directly on a curved faceplate (*11*, *82*). Under these circumstances a lighthouse technique becomes appropriate (*83*). Again, an optical master has to be prepared for the screen exposure since the gaps between wires are much too wide to permit shadow projection.*

The light source may be placed at a distance yielding the same average grill pattern magnification on the screen as that effected by the electron beams and a correcting lens employed to assure that the printing light beams (projected on a plane normal to the grill wires) are incident on the screen at an angle equal to the mean inclination of the corresponding electron paths between grill and screen. Under these circumstances variations in the q value for different screens prepared with the same lighthouse (including correction lens) do not lead to registration errors (Fig. 6.2). As has already been noted, continuous-surface correction lenses for first-order printing can yield full correction of registration errors in line-screen

* It is interesting to note that Flechsig, in his original patent application, suggested thickening the grill wires with gelatin to permit screen deposition by a projection technique, the gelatin being washed off after screen preparation.

tubes since displacements along the phosphor lines do not affect the printed pattern.

The performance of focus-grill tubes has been studied most fully for tubes with plane grills and screen (*10, 84, 85*) and cylindrical grills and screens (*11, 86*). While screens and grills in commercial designs can be expected to deviate from these simple shapes, the results obtained for them give useful design guidance.

Consider a plane grill at voltage V_m, equal to the gun anode voltage and spaced a distance q from a plane screen at voltage V_s. For a parallel electron beam incident at the (deflection) angle θ in the azimuthal plane ϕ ($\phi = 0$ corresponding to the meridional plane perpendicular to the grill wires), the

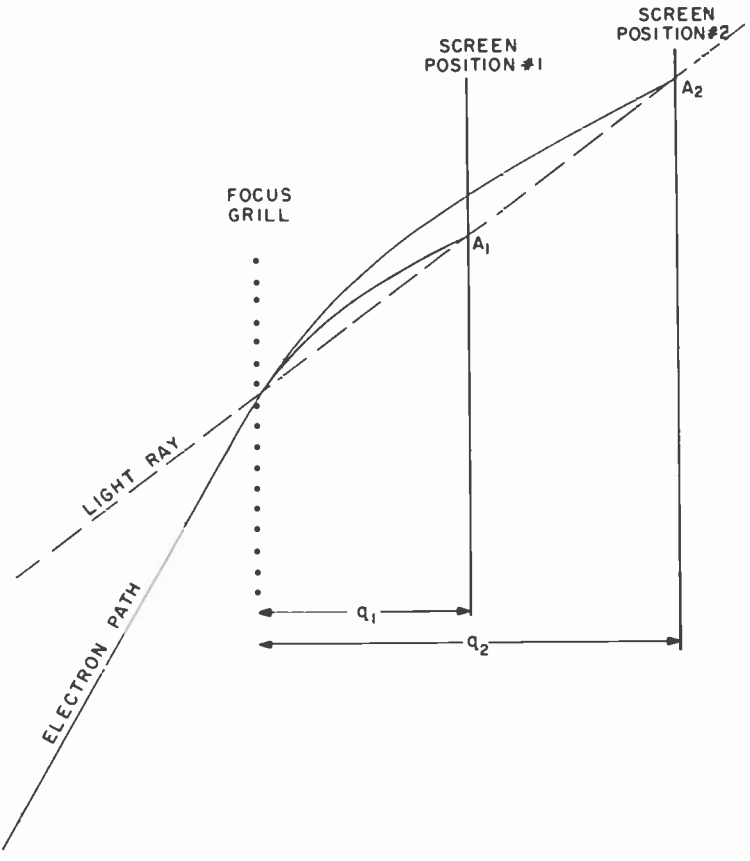

Fig. 6.2 Preservation of registration between electron spots (or lines) and optically recorded phosphor dots (or lines) with variations in q.

change in the transverse velocity component effected by the electrostatic field for a ray incident a distance h from the center line of the aperture between wires is given by (*85*)

$$\Delta v_x = -\frac{h}{2q}\left(\frac{V_s}{V_m} - 1\right)\left(\frac{2eV_m}{m}\right)^{1/2} \frac{\cos\theta}{1 - \sin^2\theta \sin^2\phi} \tag{6.10}$$

Again we compute the transverse displacement of the ray considered from one passing through the center of the slit, $\Delta(v_x t)$, from

$$v_x = \left(\frac{2eV_m}{m}\right)^{1/2} \sin\theta\cos\phi, \qquad t = \frac{2q}{(2eV_m/m)^{1/2}(X+1)\cos\theta} \tag{6.11}$$

$$\Delta t = -\frac{h(X-1)\sin\theta\cos\phi}{(2eV_m/m)^{1/2}X(1 - \sin^2\theta\sin^2\phi)}$$

with

$$X = \{(V_s/V_m) + [(V_s/V_m) - 1]\tan^2\theta\}^{1/2} \tag{6.12}$$

We find

$$\Delta(v_x t) = -\frac{h(X-1)}{1 - \sin\theta^2\sin^2\phi}\left(\cos^2\theta + \frac{1}{X}\sin^2\theta\cos^2\phi\right) \tag{6.13}$$

The condition for sharp focus is that this quantity be equal to $-h$. It is fulfilled for

$$X = 1 + (1 + \tan^2\theta\cos^2\phi)^{1/2} \tag{6.14}$$

$$V_s/V_m = 2 - \sin^2\theta\sin^2\phi + 2\cos\theta(1 - \sin^2\theta\sin^2\phi)^{1/2} \tag{6.15}$$

For large deflection angles, this represents a large range of voltage ratios required for sharp grill focus. For example, for a 110° tube with 4 : 3 aspect ratio, we find that the required voltage ratio at the top and bottom of the vertical axis is 2.74, at the left and right end of the horizontal axis, 3.32, and in the corners, 2.76, as compared with 4 in the center. If the voltage ratio is chosen to be 3.226, the lenslets will be equally "underfocused" at the center of the screen and "overfocused" at the center of the upper and lower edge, the width of the trace for an infinitely narrow source giving rise to a line width which is 0.204 times the clear space between wires at either point. Color purity throughout the field can thus be realized only if the beam diameters in the deflection plane are at most equal to

$$\frac{0.333 - 0.204(d - D)/d}{0.333}\, s = 0.45s \tag{6.16}$$

The ratio of the wire diameter D to the center-to-center wire spacing d is

here assumed to be 0.1; s denotes the center-to-center beam spacing in the deflection plane. The impossibility of realizing sharp grill focus throughout the field thus reduces the permissible beam width in the deflection plane by a factor greater than 2.

The simple focus-grill tube has other limitations. If the gun anode and the grill are maintained at the same voltage V_m, the beam current, for equal spot size, is reduced by a factor V_m/V_s. For small screen sizes the corresponding loss in brightness (by a factor of $\frac{1}{3}$ or $\frac{1}{4}$) can be tolerated and may, in fact, be outbalanced by the advantage of reduced deflection power (in the same ratio V_m/V_s). For larger screen sizes the loss in brightness can be reduced (but not eliminated) by operating the gun anode at screen potential and terminating the cone electrode in a manner which minimizes the phosphor line pattern distortion on the screen. The loss in brightness (for equal spot size) is not eliminated completely since, for example, for a uniform retarding field, the presence of the retarding field increases the spot diameter in the ratio $2/[1 + (V_m/V_s)^{1/2}] \cong \frac{4}{5}$.

Another shortcoming of the focus-grill tube is contrast reduction by secondary and scattered electrons (Fig. 6.3). Secondary electrons emitted by the wire edges are drawn straight toward the phosphor screen and produce a faint ghost image of slightly reduced size. In addition, secondary electrons emitted from the side of the wires facing the electron gun may be drawn back toward the screen by the penetrating electrostatic field and spread over a wider area, reducing both the contrast and the color saturation; these electrons can be prevented from reaching the screen by applying a positive bias to the cone electrode with respect to the grill. Finally, electrons scattered by the phosphor screen with energies comparable to the energy of incidence are returned to the screen by the retarding field be-

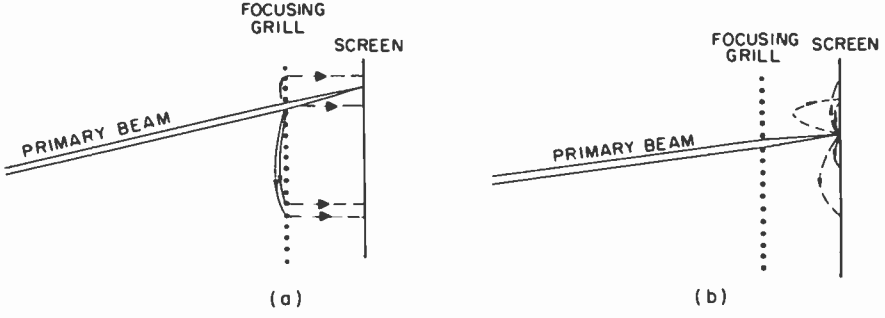

Fig. 6.3. Effect of (a) secondary electrons and (b) backscattered electrons in focus-grill tube.

tween grill and screen, producing a halo which, again, reduces both contrast and saturation. For a voltage ratio $V_s/V_m = 4$, the maximum radius of the halo is $(\frac{8}{3})q$, where q is the grill-to-screen distance. According to measurements by Gentner (*87*), the angular distribution of the back scattering of 25 kV electrons from an aluminum target has a rather sharp maximum for a glancing angle of 15°, with a mean energy equal to 0.45 times the primary energy. Measurements by Palluel (*88*) and others equate the percentage of backscattering from targets of atomic number less than 30 to the effective atomic number; thus, for aluminum, approximately 13% of incident 25 kV electrons are backscattered. Taking a number of factors into account, the contribution of backscattering to screen brightness in a focus-grill tube may be as large as 6% (*12*).

Both secondary electrons from the grill and the backscattered electrons strike the screen with energies smaller than those of the primary beam electrons. Hence, their contrast-diminishing and color-desaturating effect can be reduced by increasing the thickness of the aluminum film overlying the phosphor or, better, by supplementing it with a film of still lower atomic number. However, this cannot be accomplished without a loss of screen brightness.

6.3 Double-Grill Tubes

The indicated limitations of focus-grill tubes can be eliminated or greatly reduced by the addition of a second, or auxiliary, grill which may be placed either on the gun side or on the screen side of the focusing grill (*12*, *89*). The orientation of the auxiliary-grill wires is perpendicular to the focus-grill wires and the spacing q' between grills is made small compared to the separation q of the screen and the grill nearest to it. The three grill-screen assemblies systems I–III illustrated in Fig. 6.4 have the common property that the region between the gun and the nearest grill is field-free (making the electron paths straight lines in this region), and that only one tube voltage (the focus-grill voltage V_m) is required in addition to the maximum tube voltage V. In systems I and II, the screen voltage is V_m, the lower of the two voltages, whereas in system III it is V, the maximum tube voltage. On the other hand, the gun anode voltage is V in system I and V_m in systems II and III. For small values of the ratio q'/q, the deviation of the voltage ratio V/V_m from 1 (for sharp focus at the screen center) also is small, as illustrated in Table IV, so that the screen brightness per unit screen current, the spot diameter, and the deflection power all differ relatively little from

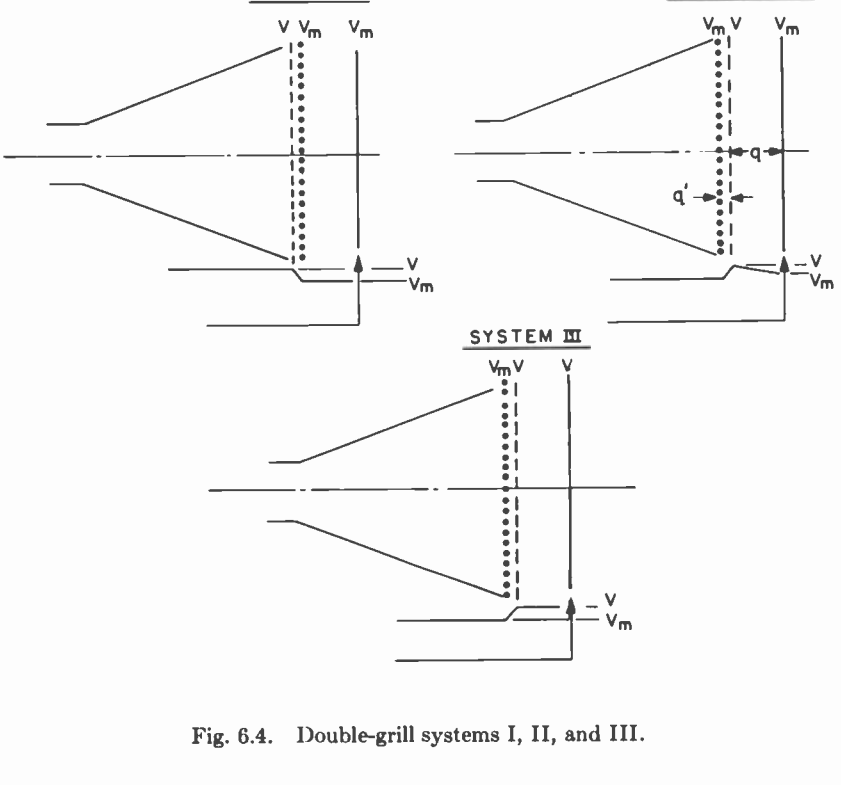

Fig. 6.4. Double-grill systems I, II, and III.

TABLE IV

VOLTAGE RATIOS V/V_m FOR DOUBLE-GRILL SYSTEMS[a]

	System I	System II	System III
$\frac{q'}{q}$	$\frac{q+2q'}{q}$	$\left(\frac{q+2q'}{q+q'}\right)^2$	$\left(\frac{(q^2+2qq'+4q'^2)^{1/2}+2q'}{q+2q'}\right)^2$
$\frac{1}{4}$	1.5	1.44	1.48
$\frac{1}{8}$	1.25	1.23	1.25

[a] q denotes separation of screen and nearest grill; q' denotes separation of auxiliary grill and focus grill.

the values for a shadow-mask tube with equal maximum voltage (screen voltage) V.

The beam electrons experience a converging cylindrical lens action at the focusing grill, a diverging cylindrical lens action at the auxiliary grill (Fig. 6.5). The diverging cylindrical lens action spreads the beam at the screen by an amount at most equal to the clear spacing between auxiliary-grill wires. If the spacing of the auxiliary-grill wires is small enough (smaller than that of the focus-grill wires!), the effect of this beam spreading on the resolution is minor. Since the spread is in the direction of the phosphor lines it has, in the first approximation, no effect on color purity.

With double-grill tubes, sharp grill focus can be realized over the entire screen area by appropriately shaping the screen surface. For flat grills the required screen surface is found to be slightly concave toward the gun. For a 627-mm (screen diagonal) 90° tube with $q = 25.4$ mm, the central radius of curvature of the screen becomes about 2500 mm. The possibility of mounting the grills on slightly curved grill supports affords the degree of freedom required for achieving both uniform nesting along the two principal axes and uniform grill focus over the entire screen.

Since the gun anode voltage in double-grill tubes is either equal to the

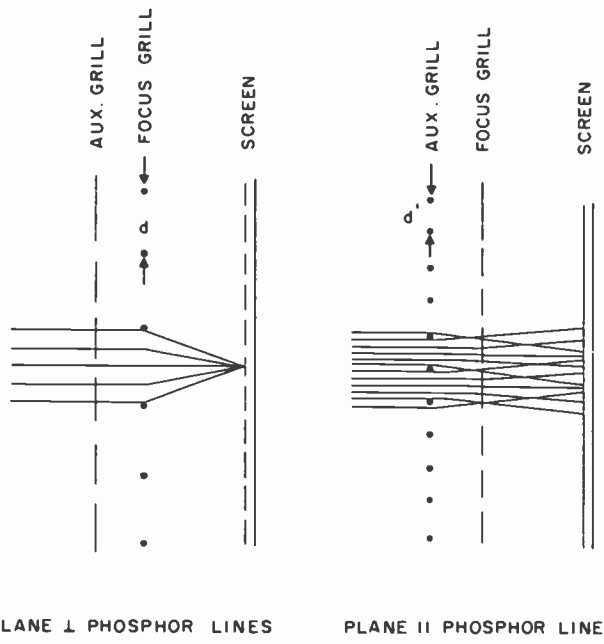

Fig. 6.5. Lens action at mutually perpendicular wire grills (system I).

maximum tube voltage (in system I) or only slightly smaller (in systems II and III), the beam currents achievable in shadow-mask and double-grill tubes with similar gun structures should be comparable.

Finally, in systems I and II neither secondary electrons from the grills nor electrons backscattered by the screen contribute to the screen brightness. Hence, there is no resultant contrast loss and color desaturation. In system III, which has the advantage of operating with a screen voltage equal to the maximum tube voltage, the fraction of the backscattered electrons which return to the screen is smaller than for the single-grill tube and this source of contrast reduction and color desaturation is correspondingly less serious.

Double-grill tubes thus offer the possibility of achieving screen brightnesses greater than those obtained with shadow-mask tubes of comparable dimensions without a loss in contrast. This property has been demonstrated empirically. At the same time, they introduce difficult new construction problems. In tubes built at the RCA Laboratories, 0.076-mm wires of Nichrome V were stretched under about 500 g tension per wire on threaded steel frames, to which they were either clamped or plated. With a spacing of 3.2 mm between grills, arcing could be avoided between grills as long as their potential difference did not exceed 5 kV. Grill-wire vibration (at a resonant frequency of about 600 Hz) could be suppressed by placing a 0.03-μF condenser between the grills. The optical transparency of each grill was of the order of 0.9, leading to an overall grill transmission of about 0.8; 610-mm 65° rectangular double-grill tubes of the system III type have been constructed in this manner.

6.4 Three-Beam Focus-Mask Tubes

The focus-mask principle has also been applied to tubes with masks containing hexagonal arrays of round apertures. Such masks have the obvious advantage that they can be given a spherical shape which is mechanically stable and self-supporting. On the other hand, larger potential differences must be applied between the mask and screen (or the focus mask and adjoining auxiliary mask), as compared with focus-grill tubes, to achieve a given increase in permissible mask transmission. Thus, for a tube with the focus mask and gun anode at the common potential V_m and the screen at the potential V_s, the spot diameter projected by an incident parallel electron beam is reduced, as compared with shadow-mask operation ($V_m \rightarrow V_s$), by a factor $\frac{1}{2}[3 - (V_s/V_m)^{1/2}]$. To achieve equal projected spot size, the apertures can thus be increased in diameter by the inverse factor, leading to an increase in mask transmission

$$T/T_{SM} = 4/[3 - (V_s/V_m)^{1/2}]^2 \tag{6.17}$$

Since, for equal beam diameter, the current delivered by the gun can be expected to be proportional to the anode voltage, the screen is increased in brightness (as compared with shadow-mask operation) by a factor

$$\frac{I}{I_{SM}} = \frac{T}{T_{SM}} \frac{V_m}{V_s} = \left\{ \frac{T_{SM}}{T} \left[3 - 2 \left(\frac{T_{SM}}{T} \right)^{1/2} \right]^2 \right\}^{-1} \tag{6.18}$$

For a focus-grill tube the corresponding relation is

$$\frac{I}{I_{SM}} = \left\{ \frac{T_{SM}}{T} \left(2 - \frac{T_{SM}}{T} \right)^2 \right\}^{-1} \tag{6.19}$$

The intensity gain and voltage ratio are plotted as functions of the transmission ratio T/T_{SM} for both types of tubes in Fig. 6.6. It is seen that with focus-mask tubes with round apertures, no gain in brightness is achieved until the transmission ratio of the mask is greater than 4, corresponding to voltage ratios V_s/V_m which also exceed 4. For grill tubes, intensity gains are realized when both ratios exceed 2.6.

The achievement of substantial intensity gains in round-aperture focus-mask tubes thus requires either the use of a high-transmission auxiliary mask or operation of the gun with the anode at screen voltage and a suitably shaped electrostatic retarding field between gun and mask. Both approaches have been employed. Rauland (*90*) has constructed 480- and 610-mm tubes with a total deflection angle of 62° with an auxiliary mesh and flat mask and internal screen. CBS-Hytron (*91*) built tubes with a spherical aperture mask made of glass, preceded by a decelerating lens, with the screen deposited on the faceplate. Screen diameters were 480 and 560 mm, with overall deflection angles of 62° and 72°, respectively. In both cases the decelerating region (between gun or auxiliary mesh and mask) and the accelerating region (between mask and screen) were so dimensioned that the electron spots formed a pattern obtained by straight-line projection from the deflection center. This permitted the use of photographic techniques for the preparation of the dot screens.

In the Rauland tubes, the auxiliary mesh, focus mask, and screen were maintained at 10.5, 4.7, and 20 kV, respectively, and spaced approximately 10 mm apart; the auxiliary-mesh and focus-mask transmissions were 80 and 50%. As compared with a shadow-mask tube with 12% mask transmission, this should yield an increase in screen brightness by a factor of 1.8. It should be noted that, here, unlike the double-grill tube, the auxiliary mesh spreads the spot in such a fashion as to reduce the tolerances for color purity. In addition, backscattered electrons reduce contrast and desaturate the color.

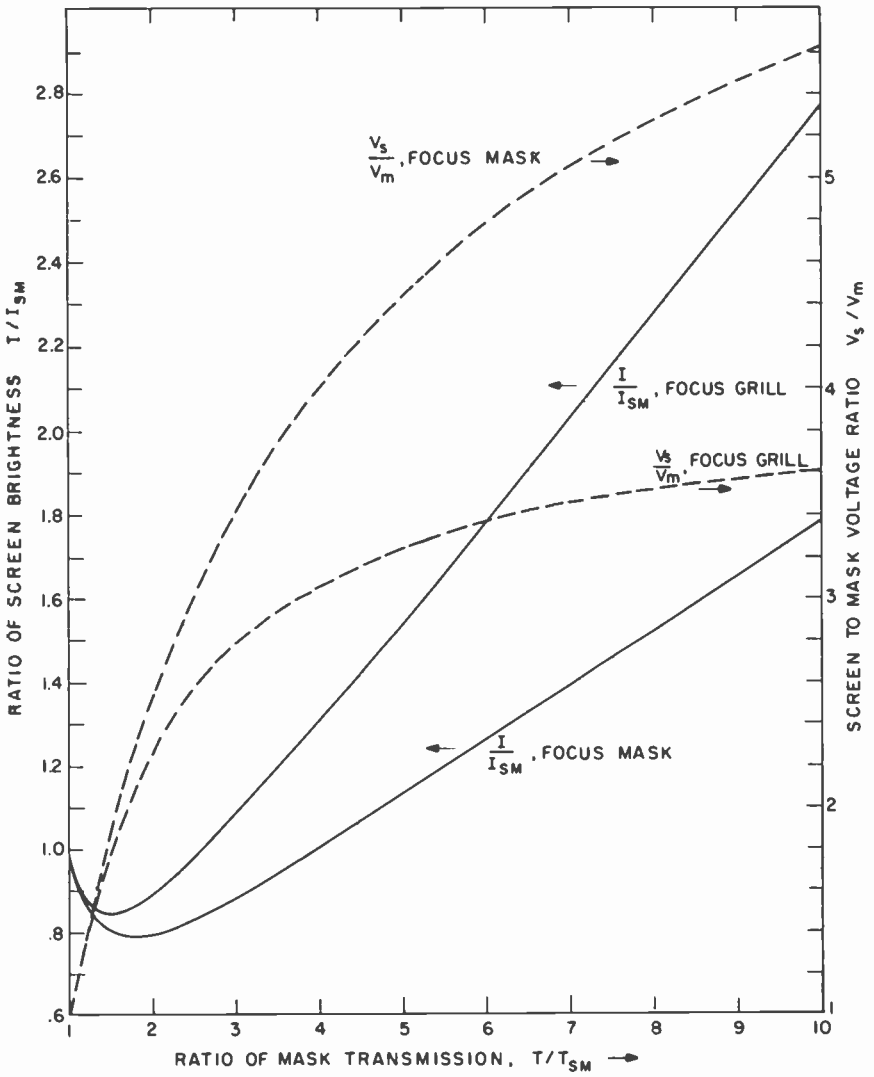

Fig. 6.6. Ratio of screen intensities of focus-mask or grill tubes to screen intensity of shadow-mask tube and corresponding tube voltage ratios as function of mask (or grill) transmission ratios. The gun anode voltage is assumed to equal the mask or grill voltage V_m. The screen voltage V_s, the screen size, the deflection angle, and the gun design are assumed to be the same.

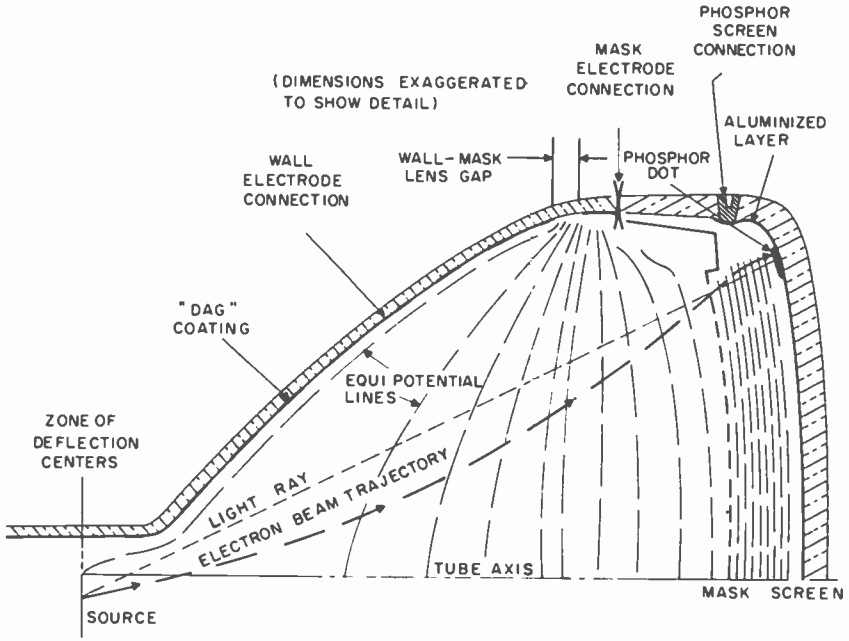

Fig. 6.7. Schematic representation of field distribution and structure of "unipotential mask-focusing Colortron" (CBS-Hytron).

In the CBS-Hytron tube the mask transmission was increased to 30%. With the aluminum thickness increased to reduce the effect of the back-scattered electrons, the residual brightness gain (over a shadow-mask tube with mask transmission 0.12) was found to be 2. The impact of secondary electrons from the mask was minimized by tapering the apertures in the relatively thick (1.3 mm) mask, reducing the diameter to a minimum on the gun side. The structure and the field distribution of the tube are indicated in Fig. 6.7.

6.5 Single-Beam Focus-Grill Tubes

Structurally, single-beam focus-grill tubes differ from three-beam focus-grill tubes in just three respects:

(1) The gun generates a single beam.

(2) Alternate wires of the focus grill are connected to two different electrodes; these are commonly joined by an internal resonating coil.

(3) The color sequence of the phosphor lines is, for example,

RGRBRGRB, with the green and blue phosphor stripes centered behind alternating grill wires, rather than RGBRGB, with the wire positions corresponding to the boundaries between successive triads.

The color selection voltage W is applied between the two sets of grill wires. For a flat grill and screen, and with the grill at the same potential as the gun anode, we can deduce the relationship between beam displacement Δx normal to the grill wires and the voltage W, for any direction of incidence (θ, ϕ) of the electron beam, in the manner used for deriving the condition for sharp focus. If E_x is the transverse field component resulting from the application of the potential difference W between the wires, the resulting change Δv_x in the x component of the velocity is given by

$$\Delta v_x = -(e/m) \int E_x \, dt$$

$$= -(e/mv)[(1 + \tan^2\theta \cos^2\phi)^{1/2}(1 - \sin^2\theta \sin^2\phi)^{1/2}]^{-1} \int E_n \, ds \tag{6.20}$$

Here E_n is the field component normal to the path projected on a plane normal to the grill wires and the integral over s is an integral over this projected path. The second root is the cosine of the projection angle, the first root is the secant of the angle between the projected path and the tube axis. v is the total velocity $(2eV_m/m)^{1/2}$. Application of Gauss' theorem to a slab of unit height bounded by planes parallel to the wires and passing through paths traversing the centers of adjoining spaces between wires in identical directions leads to (Fig. 6.8):

$$\int E_n \, ds = \frac{Q}{2\epsilon} = \frac{CW}{2\epsilon} \qquad \text{with} \quad C = -\frac{\pi\epsilon}{\ln(\pi D/4d)} \tag{6.21}$$

Here Q is the charge and C the capacitance per unit length of wire. ϵ is the dielectric constant (of vacuum), D the grill-wire diameter, and d the grill-wire center-to-center spacing. For the displacement Δx at the screen we find

$$\Delta x = \Delta(v_x t) = (\Delta v_x)\frac{2q}{v}\frac{\sec^3\theta}{X+1}\left(\cos^2\theta + \frac{\sin^2\theta\cos^2\phi}{X}\right)$$

$$= \frac{W}{V_a - V_m}\frac{\pi q}{2\ln(\pi D/4d)}\frac{X-1}{1-\sin^2\theta\sin^2\phi}\left(\cos^2\theta + \frac{\sin^2\theta\cos^2\phi}{X}\right) \tag{6.22}$$

Here X is defined by Eq. (6.12). Comparison of Eq. (6.22) and Eq. (6.13)

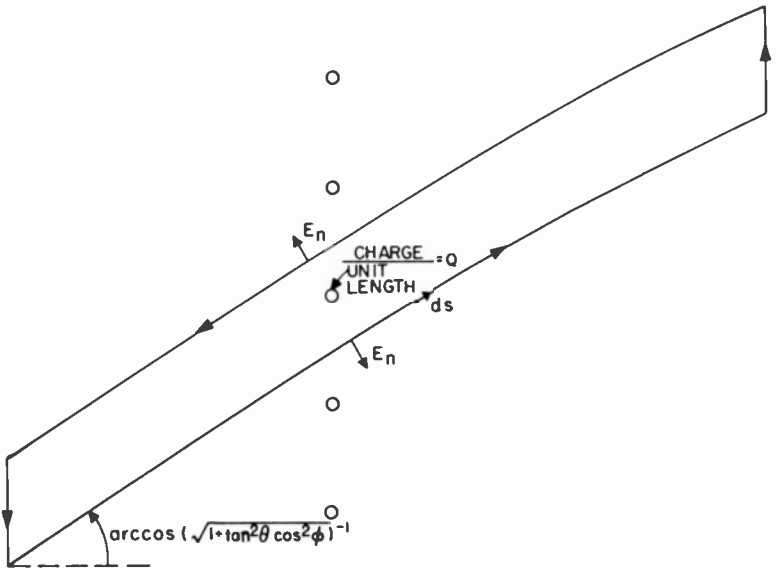

Fig. 6.8. Application of Gauss' theorem to the determination of the grill deflection field integral.

shows that the variation of grill deflection sensitivity ($\Delta x/W$) with the beam deflection is proportional to the variation in the focusing displacement.

On the axis the deflection voltage W leading to a displacement from the center of one phosphor stripe to the center of the adjoining phosphor stripe,

$$\Delta x = \left(1 + \frac{2q}{3p}\right)\frac{d}{2} \tag{6.23}$$

is given by

$$W = \frac{d}{\pi q}\ln\left(\frac{\pi D}{4d}\right)\left(1 + \frac{2q}{3p}\right)\left[\left(\frac{V_s}{V_m}\right)^{1/2} + 1\right]V_m \tag{6.24}$$

Consider as an example a 280-mm 90° one-gun "Chromatron" (*92*) with a grill of 3.3 wires/mm (700 wires altogether) with a wire diameter $D = 0.05$ mm. With $d = 0.30$ mm, $q = 14$ mm, $p = 140$ mm, $V_m = 4700$ V, $V_s = 18{,}800$ V we find

$$W = 209 \text{ V}$$

A sinusoidal voltage variation with this amplitude (or an rms amplitude of 148 V) will lead to a spot displacement (from the center of the red

phosphor line) given by

$$x = (d/2)\sin(\omega t) \tag{6.25}$$

The displacement given by Eq. (6.25) corresponds to equal dwell-times of the electron spot center on the three phosphor lines. If the phosphors are balanced (i.e., equal excitation of the red, green, and blue phosphors produces white light), this means that the tube screen will appear white when no chrominance signal with the color subcarrier frequency $\omega/(2\pi)$ as a fundamental component is applied to the tube gun.

For a 700-wire grill, with a wire length of 178 mm, the capacitance becomes, according to Eq. (6.21),

$$C = \frac{(3.14)350(0.178)8.84 \times 10^{-12}}{2.033} F = 850 \text{ pF}$$

The maximum energy stored in the grill capacitance is thus $CW^2/2 = 18.6\ \mu J$, and the circulating power at a color frequency of 3.58 MHz,

$$(2\pi)3.58 \times 10^6(850 \times 10^{-12})(148)^2 = 418 \text{ W}$$

More generally, the capacitance is roughly proportional to the product of the number of grill wires and the picture height, whereas the deflection voltage (for equal grill-deflection angle or equal d/q) is simply proportional to the grill voltage V_m. Thus, for a 560-mm 90° focus-grill tube with 1000 wires and a mask voltage of 7 kV (*82*), the circulating power would be increased to over 1800 W, corresponding to an rms current of over 8 A. To reduce the high-frequency current in the grill leads, as well as radiation from the grill electrodes, toroidal coils resonating with the grill capacitance at 3.58 MHz are connected across the grill terminals within the tube envelope. The total resonant inductance $1/(\omega^2 C)$ would be 2.3 and 0.8 μH, respectively, for the 280-mm and 560-mm tubes here considered. For the larger tube the high-frequency input power required to maintain the oscillation was found to be 30 W.

In the last-mentioned 560-mm 90° Chromatron (*82*), the gun anode was operated at the screen voltage of 25 kV, to provide relatively large beam current for a prescribed spot size. The field distribution was thus qualitatively similar to that shown for the focus-mask tube in Fig. 6.7, with a "hat electrode" at the junction between funnel coating and grill support shaped so as to minimize screen pattern distortion near the periphery. The grill wires were sealed with frit to the cylindrical grill support frame and the faceplate given a toroidal shape (with larger radius in the vertical plane) so as to lead to uniform grill-deflection sensitivity. Electron printing served to assure registry for the electrons incident on the phosphor screen.

As the electron beam is deflected back and forth across the phosphor lines of a triad, proper color reproduction is obtained by gating the beam on by a signal proportional to the red, green, and blue color signals while it sweeps across the red, green, and blue phosphors, respectively (*93*). In practice, this may be achieved by synchronizing the local oscillator providing the grill deflection signal with the transmitted burst signal and deriving appropriate dc, fundamental, and harmonic terms from the transmitted chrominance and luminance signals. Gating signals for the three colors, with a duty cycle of $\frac{1}{3}$, are approximated by terms up to the fourth harmonic of the color subcarrier if the following signal is applied to the gun (*93*):

$$\begin{aligned} E = {} & \tfrac{1}{3}(E_r' + E_g' + E_b') + (\sqrt{3}/\pi)(E_g' - E_b')\sin(\omega t) \\ & + (\sqrt{3}/\pi)[E_r' - \tfrac{1}{2}(E_g' + E_b')]\cos(2\omega t) \\ & + (\sqrt{3}/2\pi)[E_r' - \tfrac{1}{2}(E_g' + E_b')]\cos(4\omega t) \end{aligned} \tag{6.26}$$

Here E_r', E_g', E_b' are the transmitted gamma-corrected red, green, and blue signals and $\omega/(2\pi)$ is the color subcarrier frequency. It can readily be verified that for $\omega t = 0$ and π, when the electron beam is centered on the red phosphor line, E is given approximately by E_r', whereas for $\omega t = \pm\pi/2$, when the beam is centered on the green or blue line, E is given by E_g' and E_b', respectively. A reduced conversion efficiency of the red-emitting phosphor can be compensated for by increasing the fractional dwell-time on the red phosphor by slightly reducing the beam oscillation amplitude. Under the same circumstances, the light contributed by backscattered and secondary electrons gives the picture a blue-green cast, which can be rendered neutral by the use of a pink filter.

It should also be noted that, with a 30% duty cycle for each color, the color will be substantially desaturated by beam overlap on the adjoining phosphor stripe unless, either the electron spot width or the phosphor line width is made very narrow compared to $\frac{1}{2}[1 + (2q/3p)]d$, or half the projected wire spacing; in the second case the phosphor lines would be bordered by guard bands of a black inactive material. Either approach diminishes the realizable light output to substantially less than $\frac{1}{3}$ of the light output of a monochrome tube of equal size and screen voltage and equal phosphor conversion efficiency. The grill absorption and the increased aluminum film thickness required to lessen the contrast loss arising from backscattered and secondary electrons further reduce the ratio of the light output of the one-gun focus-grill tube and a monochrome tube. In a comparison of the brightness of a three-gun and one-gun focus-grill tube, the brightness loss resulting from the short duty cycle of the one-gun tube may

be offset in part by the larger beam diameter achievable with equal neck size (and deflection power).

The "Colornetron" of the Kobe-Kogyo Corporation (*94*) represents an interesting deviation in design and operation from the usual one-gun focus-grill tube. Color switching takes place at a line-sequential rate, so that vertical resolution is well below 200 television lines. This automatically limits the design to small displays, the commercially offered tube having a screen diameter of 190 mm. Line-sequential operation has the compensating advantages of low switching power, nearly 33% duty cycle without resulting loss in color purity, and no difficulties from high-frequency radiation. The other unique feature of the tube is the presence of an auxiliary grill at 6 kV preceding the switching grill at 4.5 kV and the screen at 14 kV. The auxiliary grill is aligned with the switching grill and has the primary purpose of permitting the printing of the phosphor line pattern on the screen by optical projection onto a curved screen plate subsequently inserted in the tube envelope (Fig. 6.9).

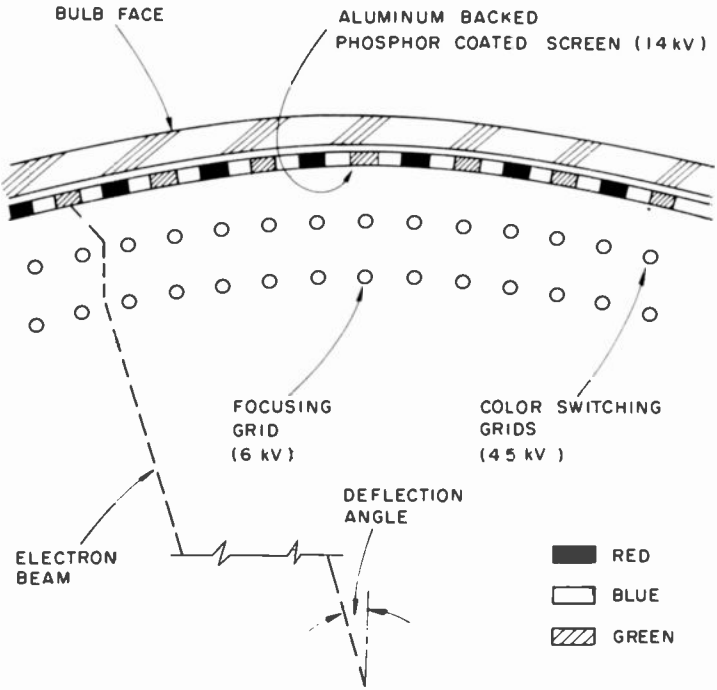

Fig. 6.9. Schematic representation of "Colornetron" focus-grill tube with aligned grills.

6.6 Mechanical Problems

Grills do not have the inherent mechanical stability of formed curved shadow masks. The grill wires are commonly mounted under tension on frames, to which they are sealed by plating or by frit (*12*, *82*). They have also been transferred from a mandrel to glass ledges integral with the screen panel of the tube, sealing being effected with an air-drying cement (*11*). The weaving of fine glass threads across the grill has been found effective in damping microphonic vibrations of the wires.

6.7 Summary

Replacement of the shadow mask by a focus mask or grill with higher transmission offers the possibility of achieving higher screen brightness at prescribed maximum tube voltage. This gain is reduced by contrast loss resulting from secondary and backscattered electrons. The maximum gain in brightness, without contrast loss, can, in principle, be obtained with three-beam double-grill tubes. Their production would, however, demand the solution of problems not encountered in shadow-mask tubes. One-gun focus-grill tubes with color switching at the grill have found limited application, combining relatively high screen brightness with low deflection power and absence of convergence problems.

CHAPTER 7

Beam-Index Tubes

7.1 Principles

Conceptually, the simplest color television system with electron beam scanning is realized by assuming perfect synchronization between the beam exploring the camera tube target overlaid by a three-color filter mosaic and a beam exciting a "white" phosphor overlaid with a geometrically similar color filter mosaic in the receiver. Such a system was proposed by Zworykin (*95*) as early as 1925. Much later Bond *et al.* (*96*) constructed tubes in which proper color reproduction depended on great precision of deflection in one direction (i.e., the vertical) only. The screens of these tubes had horizontal phosphor line triads. Secondary-emitting index markers at the beginning of each line provided correction signals for the vertical deflection which centered the beam on the triad. In addition, a staircase signal at color subcarrier frequency was applied to the vertical deflection to cause the beam to come to rest successively on the red, green, and blue phosphor lines of the triad at the appropriate phase of the color signal. An essentially similar system (without the staircase deflection voltage) was shown to be applicable to a tube with a vertical line screen and precision horizontal deflection.

These systems, too, proved impractical in view of the precision demanded of their deflection systems and the required freedom from disturbing fields. It was soon recognized that in a practical color tube without any masking system, indications of the instantaneous location of the beam relative to the phosphor triad centers would have to be provided over the entire screen area. The problem is solved most readily for a vertical phosphor line screen, on which "beam-index stripes" are provided which are related in some regular manner to the phosphor line triads. The beam-index stripes,

when struck by the scanning beam, must generate a "beam-index signal" indicating the beam location. They may do so, in principle, by acting as beam current collectors, secondary emitters, or emitters of some kind of, preferably, invisible radiation. The preferred types of index stripes incorporated in operating color tubes have been secondary-emitting (magnesium oxide) stripes and UV-emitting phosphor stripes, both deposited on the gun side of the aluminum blanket covering the phosphor screen (Fig. 7.1). The secondary electrons are collected by a positively biased funnel coating of the tube, insulated from the screen. A multiplier phototube mounted behind a window in the funnel coating generates the index signal derived from the emission of the UV-phosphor stripes. A UV filter in front of the multiplier photocathode eliminates ambient light from the radiation otherwise incident on the photocathodes.

In principle, beam-index tubes, like other color viewing tubes, can be either three-beam or single-beam tubes. In three-beam tubes it would be essential that the spots formed by the three beams would precisely maintain their relative separation (in a direction normal to the phosphor lines) with deflection. With large deflection angles this requirement becomes very difficult to fulfill. It is thus not surprising that all operating beam-index tubes described so far have had a single beam modulated by the picture signal.

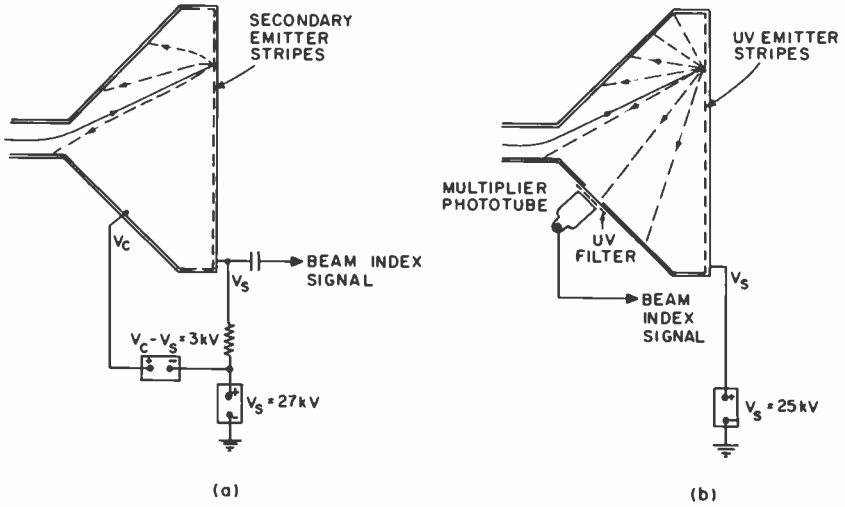

Fig. 7.1. Beam-index signal generation with (a) secondary-emissive and (b) UV-phosphor index stripes.

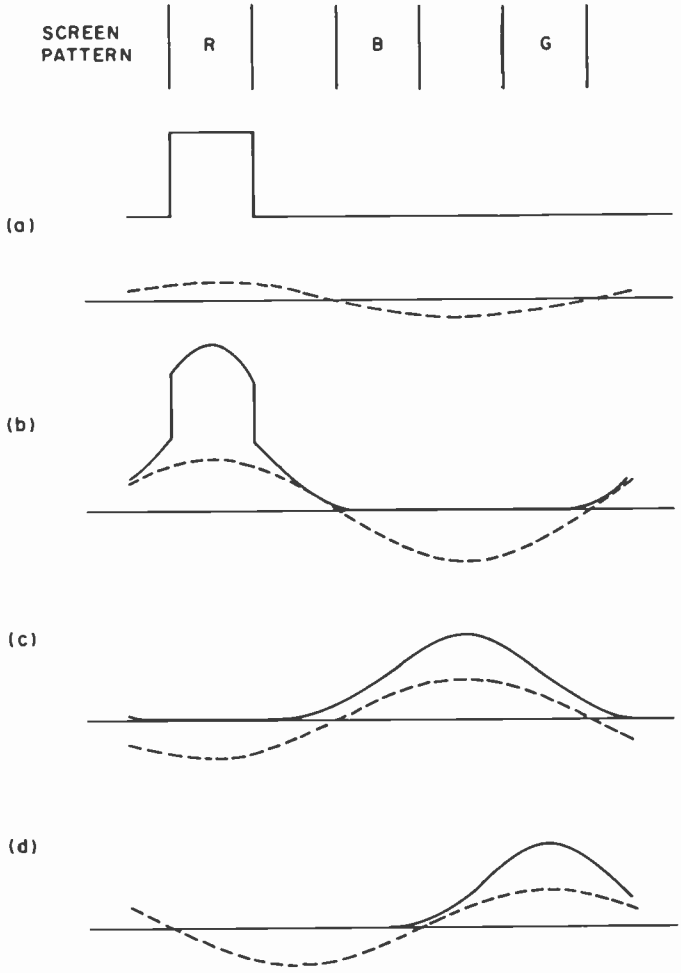

Fig. 7.2. Phase of beam index signal as function of color phase for secondary-emissive index stripe coincident with red phosphor stripe: (a) white field, (b) saturated red field, (c) saturated cyan field, and (d) saturated green field.

The utilization of the index signal also presents alternatives. Thus, a signal proportional to a phase difference between the phase of the transmitted color burst and the simultaneous location of the beam relative to the nearest triad center on the screen may be used as a supplementary horizontal deflection signal, to "correct" the beam location. As an alternative, the same phase difference may be applied to the chrominance signal

applied to the gun grid, so as to bring it in phase with the beam position. The last alternative has been chosen in all the more recently described beam-index systems. It has the advantage of being a simple open-loop system, in which errors need result only from variations in the time taken by the signal to return to the grid, measured in triad periods traversed by the beam. The system which corrects the beam position by supplementary deflection is a closed-loop system, in which, depending on loop gain, the adjustment process may stretch over a number of loop delay times even for uniform horizontal deflection and triad spacing.

The last paragraph assumes that the phase of the beam-index signal is actually uniquely related to the position of the index stripes. This is not generally true. In particular, with the simplest beam-index systems, the phase of the beam-index signal depends on the chrominance signal as well as the index stripe location. Consider, for example, a secondary-emissive beam-index stripe located back of every red phosphor stripe, the screen-current/beam-current ratio of the index stripe being twice that of the aluminum film on which it is deposited, and assume further that the beam-index signal is provided by the fundamental frequency component of the screen current resulting from the presence of indexing stripes. As shown in Fig. 7.2, the phase of the beam-index signal corresponds exactly to the location of the index stripe, in back of the red phosphor stripe, both for a white field (constant beam current) and a saturated red field. On the other hand, for a blue-green field, with the chrominance signal 180° out of phase with the actual index stripe location, the phase of the beam-index signal would be shifted to coincidence with the phase of the chrominance signal. Thus, the beam-index signal could not discriminate between saturated red and its complementary color, and would be totally useless for assuring proper color reproduction.

Various methods have been adopted to minimize the influence of the phase and amplitude of the chrominance signal on the beam-index signal, a phenomenon leading to a hue oscillation commonly designated as "color pulling." In all of them this is accomplished by some form of "frequency separation," i.e., employing a beam-index signal which differs in frequency from the color change frequency. Examples will be described in Section 7.2.

7.2 Index Systems

Two basically different types of beam-index systems have been investigated in detail. One of them, which was the subject of intensive engineering effort by the Philco Corporation in the 1950's and was desig-

nated by this organization as the "Apple" system (*9, 97*), utilized secondary-emissive index stripes. The other, which has been described in more recent publications from the Philips Research Laboratory (*98, 99*) in Holland, and the Sylvania-Thorn Colour Television Laboratories (*100*) in England, uses UV-emissive phosphor index stripes. While this distinction, by itself, may seem rather trivial, the different characteristics of the index stripe media have led to major differences in the design and operation of the two systems.

7.2.1 The "Apple" System

The "Apple" system solves the color pulling problem in radical manner by employing a separate, low-current, high-frequency modulated pilot beam to generate the beam-index signal. The pilot beam spot is deflected along with the video-signal modulated writing beam spot across the screen, a vertical separation of about 2.5 mm being maintained between spot centers. Since the maximum pilot beam current is 50 μA, whereas the high-light writing beam current is 1.5 mA, a maximum contrast ratio of 60 can be realized.

The screen structure of an earlier version of the Apple tube (*101*) is indicated in Fig. 7.3. The index stripes, behind the red phosphor stripes,

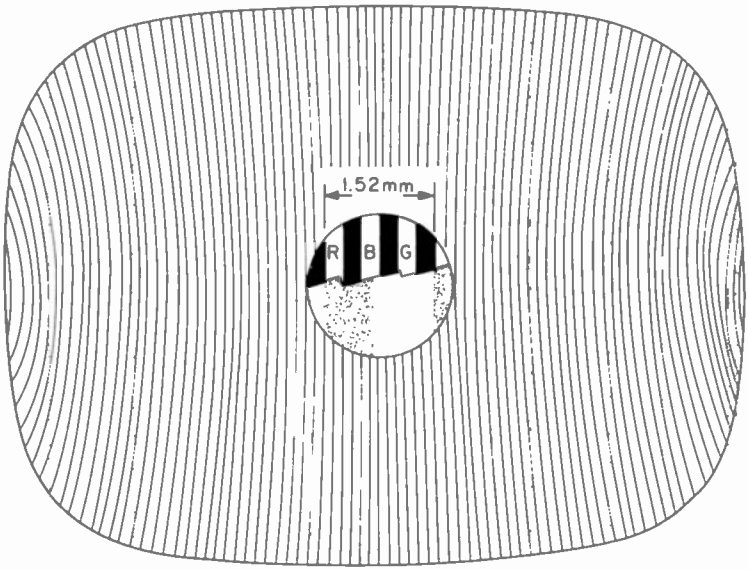

Fig. 7.3. Screen structure of Apple tube.

occupy about 40% of a color period and impose a modulation of about 50% (at color change frequency) on the electron current leaving the screen. This applies, of course, both to the current generated by the main writing beam, and that generated by the pilot beam, modulated at 41.7 MHz. However, the beam-index signal amplifier, with a passband of 2 MHz, selects out frequency components centered about 48.1 MHz, the sum frequency of the pilot beam modulation frequency and the color change frequency of 6.4 MHz (corresponding to about 350 phosphor line triads on the screen). At this frequency (which falls halfway between the seventh and eighth harmonic of the color change frequency), the contribution of the main writing beam and the resulting possibility of color pulling is negligible.

The utilization of the beam-index signal is shown in Fig. 7.4 (*9*, *97*, *102*). The color subcarrier reference signal, derived from the transmitted color burst, and the chrominance signal itself are mixed with the output of a local 38.1-MHz oscillator to deliver sum frequency terms of the form

$$\cos(\omega_p t - \phi_r), \qquad A_s \cos(\omega_p t - \phi_c), \quad \omega_p/(2\pi) = 41.7 \text{ MHz} \qquad (7.1)$$

Here ϕ_r and ϕ_c are the reference phase and the color phase, respectively, and ω_p represents the pilot beam frequency. The first term provides the pilot beam modulation signal. The modulated beam impinging on the index

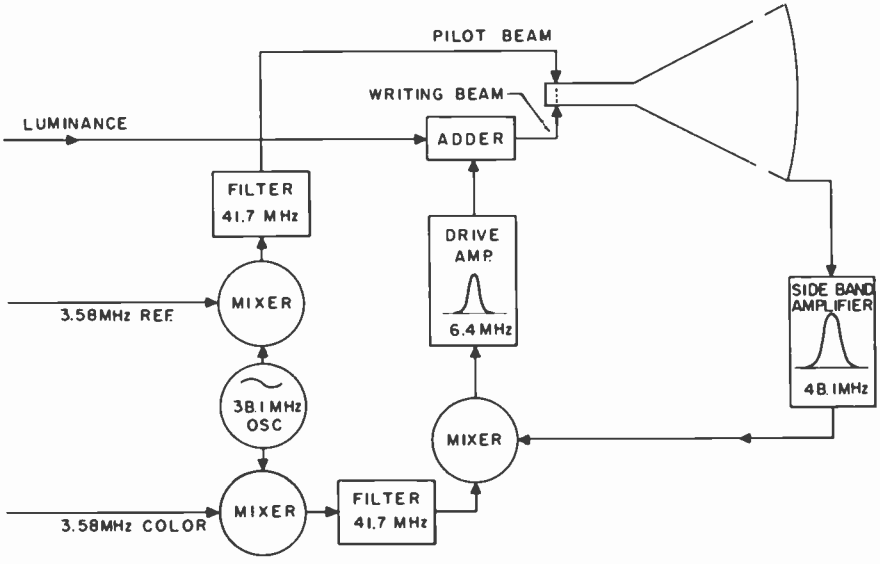

Fig. 7.4. Block diagram of Apple system.

stripe array leads to a sum-frequency term in the collected screen current,

$$\cos(\omega_p t - \phi_r)[1 + k\cos(\omega_c t - \phi_i)] \rightarrow \cos[(\omega_p + \omega_c)t - \phi_r - \phi_i]$$

$$\omega_c/(2\pi) = 6.4\ \text{MHz} \tag{7.2}$$

This sum frequency term is amplified by a sideband amplifier and mixed with the color signal represented by the second term in Eq. (7.1) to yield a difference term of the form

$$A_s \cos(\omega_c t + \phi_c - \phi_r - \phi_i) \tag{7.3}$$

This, duly amplified, constitutes the chrominance signal, which, added to the luminance signal, becomes the control signal for the writing beam of the gun. The reference phase ϕ_r is manually adjusted to account for the position of the index stripes with respect to the phosphor line triads and phase delays in the signal return loop (which have been left out of the expressions). For example, if the index stripes coincide with the red phosphor lines and the color phase for red is 0, we must set $\phi_r = 0$. A red color signal then reaches its maximum value at $\omega_c t = \phi_i$, i.e., when the beam sweeps across the center of the red phosphor line (and the index stripe). For a symmetrical color signal, the color phase for green will be $\phi_c = 2\pi/3$. For a signal with this phase, the beam current becomes a maximum for $\omega_c t = \phi_i - 2\pi/3$, i.e., as the beam sweeps across the center of the green phosphor stripe, a third of a color period beyond the center of the red stripe, etc.

It has already been noted that color signals can be accurately synchronized with the sweep across the phosphor line triads only if, over the entire screen, the number of color periods traversed by the beam in the signal-loop transit time is constant. Since the scanning speed increases from the center to the periphery, this necessitates some pincushion distortion of the phosphor line pattern. In addition to this, the deflection process results in some rotation of the line joining the writing spot and pilot spot centers and a corresponding horizontal displacement of the second spot with respect to the first. This effect is compensated by using a pattern for the index stripes which differs from that of the phosphor lines and provides a horizontal displacement varying in similar manner over the face of the tube.

In forming the screens, the screen surface is coated with photoresist and master patterns corresponding to a particular phosphor line sequence (or sequence of guard bands separating the phosphor lines) are imaged by a lens placed at the deflection plane onto the photoresist with UV illumination (Fig. 7.5). The exposed photoresist is coated with a phosphor slurry, dried, and developed by washing off the unhardened portions. The index stripes

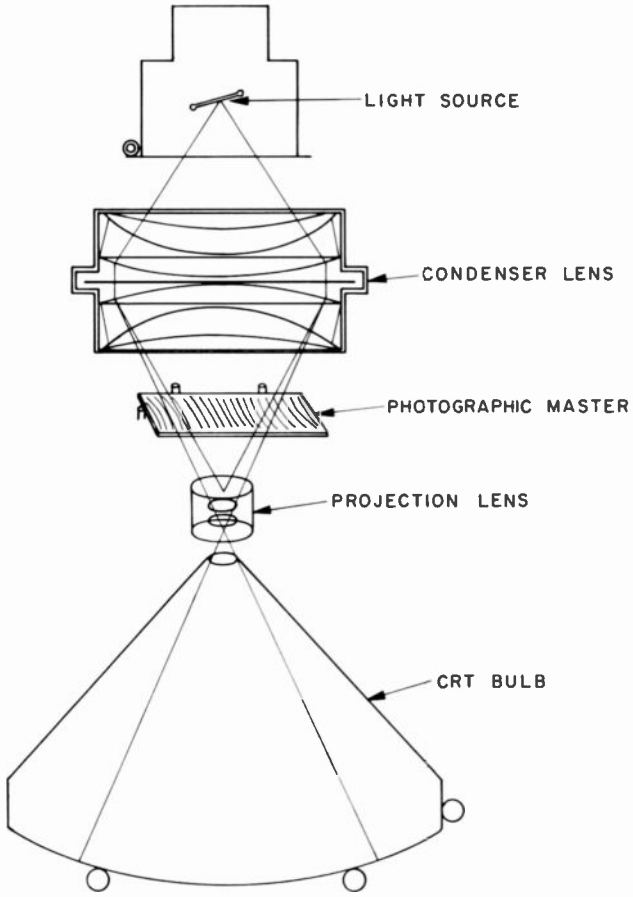

Fig. 7.5. Photographic recording of patterns of phosphor stripes, guard bands, and index stripes on screen of Apple tube.

of magnesium oxide are deposited in similar manner on the aluminum blanket deposited over the screen, temporarily stiffened by a lacquer coating.

Black guard bands equal in width to the phosphor coating are inserted between the phosphor stripes to permit the use of larger spot sizes, leading to greater screen brightness and better contrast for a prescribed attainable color saturation, as has been noted in Section 4.3.

The gun in the Apple tube presents special problems (*101*). It must deliver two closely spaced beams of which one, the writing beam, should

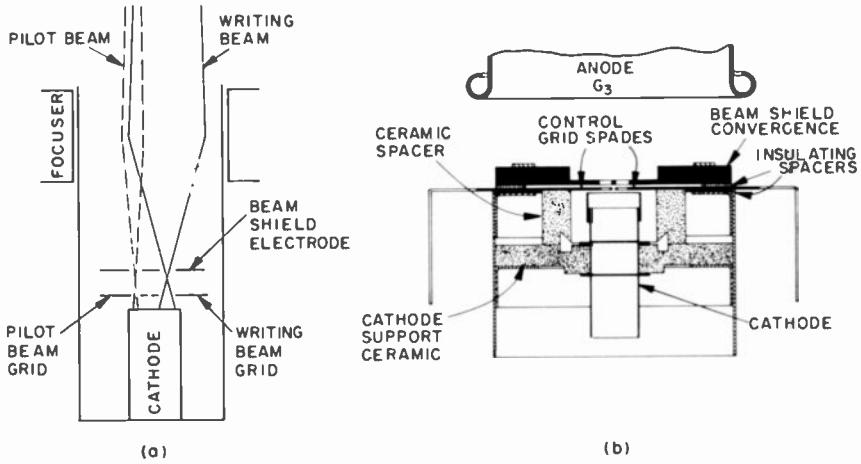

Fig. 7.6. Electron gun in Apple tube: (a) principle of operation and (b) structural detail.

provide a 1.5-mA current in a spot 0.75 mm in diameter, 355 mm from the deflection plane at a 30-kV gun anode and a 27-kV screen voltage. The two beams are separately modulated and care must be taken to prevent cross-talk between them.

Figure 7.6 shows the gun design which accomplishes this. Two closely spaced grids, with grid apertures of 0.50 and 0.35 mm, thinned to 0.01–0.02 mm, are mounted 0.05 mm apart in front of the cathode, with a center-to-center separation of the two apertures of only 0.74 mm. Cross talk is prevented by mounting a beam shield electrode, with apertures for the two beams, just beyond the grids. It is held at the mean space potential in its absence, i.e., about 600 V, so as to minimize lens fields at the apertures. The common cylindrical anode produces a weak converging field, which causes the beams to cross at the center of deflection, so that they are subject to identical deflecting fields. The final lens is a magnetic lens, partly to minimize spherical aberration (as a result of its larger clear diameter), partly to permit final alignment outside of the tube.

For the early version of the "Apple" tube here considered, a highlight screen brightness of the order of 140 cd/m^2 was indicated in a 535-mm 74° tube with a screen voltage of 27 kV (*101*).

7.2.2 Beam-Index Tube with UV-Phosphor Index Stripes

The replacement of the secondary-emissive index stripes by UV-phosphor index stripes both requires and permits changes in the mode of operation of

the index system. The persistence of the emission of available UV phosphors is too long to allow the use of high-frequency modulation of the exciting beam at frequencies of the order of 40 MHz (much greater than the color change frequency), so as to make possible frequency separation in the same manner as in the Apple system. The practical frequency limit of the UV phosphor commonly employed (the P16 phosphor or calcium–magnesium silicate activated with cerium) is about 15 MHz (*100*).

On the other hand, the UV phosphor has the advantage that the index signal current drops to zero when the spot leaves the index stripe, whereas with the secondary-emissive stripe it is reduced by only about half its maximum value because the screen between index stripes also has a secondary emission ratio substantially greater than 1. Furthermore, the index signal current is simply proportional to the beam current incident on the index stripe, a condition not fulfilled with secondary-emission index stripes, presumably owing to space charge effects. A consequence of these properties is that the writing beam itself may be used to generate the index signal, making a pilot beam superfluous. In fact, if both the index stripe (one per triad) and the scanning spot were infinitely narrow, there would be no color pulling.

In practice, of course, the scanning spot must be at least comparable to a phosphor line in width to yield acceptable screen brightness and the index stripe, similarly, must have an appreciable width to yield an index signal which is not masked by noise. With the phosphor lines separated by guard bands of equal width, it is convenient to let the index stripes coincide with individual guard bands, so that their presence does not attentuate the emission from phosphor stripes located behind them. An index frequency equal to the color change frequency will then lead to very serious color pulling. Color pulling can be greatly reduced by choosing a rational number m/n different from 1 for the ratio of the index frequency and the color change frequency—the ratio must be rational since a signal of color change frequency must be derived from the beam-index signal.

In view of the fact that the color period is made up of three equally spaced phosphor lines, the choice $m = 3$ permits placing the index stripes in the guard bands; for $n = 1$, all of the bands will be so occupied; for $n = 2$, every second band; and for $n = 4$, every fourth band. The first choice has the drawback that it requires an excessively narrow spot to deliver an adequate beam-index signal which, furthermore, is appreciably attenuated by the persistence of the UV phosphor. The last choice, $n = 4$, on the other hand, leads to a beam-index frequency sufficiently low that the video content of the picture may influence the phase information delivered by the beam-index signal. Thus, a beam-index frequency $\frac{3}{2}$ times the color change frequency has, in general, been preferred.

With the beam-index signal frequency m/n times the color change frequency and $n \neq m > 1$, color phase errors (for constant scanning speed, measured in terms of color periods per unit time) result only from gun nonlinearity. The beam-index current can be written in the form

$$c[V_m + V_c \cos(\omega_c t - \phi_c)]^\gamma \{B_0 + \sum_k B_k \cos[k(m/n)(\omega_c t - \phi_i)]\} \quad (7.4)$$

Here the first factor represents the beam current, proportional to the γ power of the grid signal with color phase ϕ_c. The second expresses, in the form of a Fourier series, the signal current as a function of displacement with respect to the index stripe for constant beam current and spot diameter (spot size variation as result of modulation is here neglected!). The index signal amplifier selects the fundamental component of frequency $(m/n)(\omega_c/2\pi)$. For $\gamma = 1$ this has an amplitude equal to cV_mB_1 and is independent of the color phase ϕ_c. For actual values of γ (e.g., $\gamma = 2.6$), however, a third-harmonic term from the first factor combines with first- and third-harmonic terms of the Fourier series to deliver additional terms, dependent on ϕ_c, to the fundamental index-signal term, leading to a small phase error.

Figure 7.7 indicates how the color signal may be generated. The fundamental component of the beam-index signal delivered by the signal amplifier

$$\cos(\tfrac{3}{2}\omega_c t - \tfrac{3}{2}\phi_i) \quad (7.5)$$

is frequency-divided by 3 and mixed with the reference signal derived from the color burst, $\cos(\omega t - \phi_r)$, $\omega/2\pi = 3.58$ MHz. The resultant difference term can be written

$$\cos[(\omega - \tfrac{1}{2}\omega_c)t - \phi_r + \tfrac{1}{2}\phi_i] \quad (7.6)$$

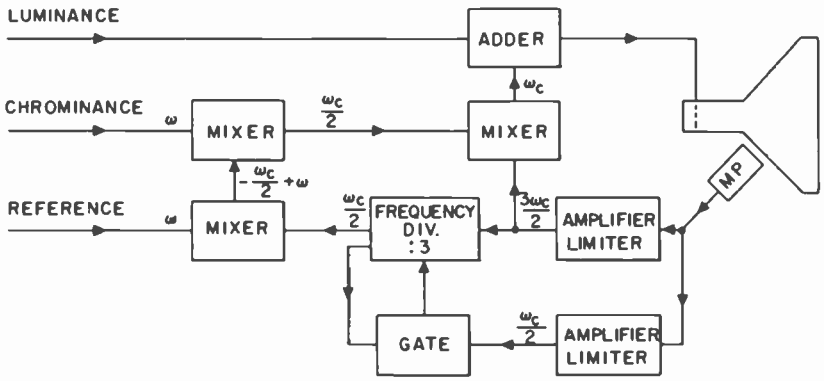

Fig. 7.7. Signal generation in photoelectric beam index system with $m/n = 3/2$.

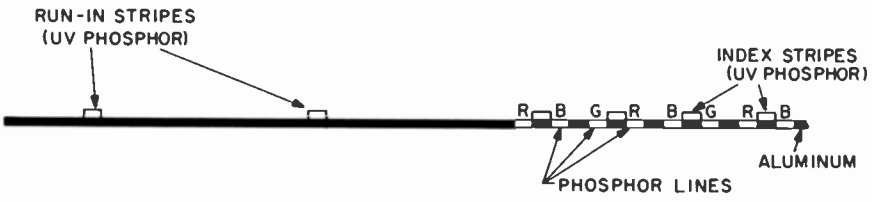

Fig. 7.8. Index stripe pattern with "run-in stripes" for beam index system with $m/n = 3/2$.

This, in turn, is mixed with the chrominance signal, $A_s \cos(\omega t - \phi_c)$, to yield a difference term

$$A_s \cos[(\tfrac{1}{2}\omega_c)t - \phi_c + \phi_r - \tfrac{1}{2}\phi_i] \tag{7.7}$$

Mixing this with the output of the index signal amplifier yields the chrominance component of the signal applied to the gun grid,

$$A_s \cos(\omega_c t + \phi_c - \phi_r - \phi_i) \tag{7.8}$$

ϕ_r is here a constant, permanently adjusted to take account of the position of the index stripes relative to the triads and the phase delay in the signal loop. With Eq. (7.8) the color signal is appropriately related to the index stripe position.

The process of frequency division by a factor m involves essentially the triggering of an oscillator with the (low) output frequency by the peaks of the input signal; it thus leads to a phase uncertainty by multiples of $2\pi/m$. In the beam-index tube this phase uncertainty is removed by providing a sequence of "run-in index stripes" separated by two color periods at the start of the scanning lines (Fig. 7.8). These select, in effect, the appropriate one of the three possible output waves of the frequency divider, by means of the circuit indicated at the bottom of Fig. 7.7. A black-level limiter for the grid signal makes certain that the index signal, and with it the proper phase selection at the divider, is maintained throughout the scanning line. Since a variation in the beam-index signal over a range 500 : 1 is permissible, the background intensity imposed by such black-level limiting does not lead to a serious reduction in picture contrast.

The multiplier phototube, generally of the head-on type, is mounted on the tube funnel in a position minimizing the variation in UV flux reaching the photocathode with position of the scanning spot. A gain of 5000 was found sufficient to override noise injected in the following amplifier circuits. However, a higher multiplication ratio may be advantageous to permit effective current limitation by the multiplier phototube.

Optical magnification of a master can be utilized for laying down the screen and index stripes in a manner similar to that described for the Apple system. The problem is simplified insofar as the UV-phosphor pattern becomes similar to that of the phosphor lines and guard bands.

The electron gun is simpler for the tube with UV-emissive index stripes than for the Apple tube in view of the absence of the pilot beam. The basic requirements, and design possibilities, for the writing beam gun are the same. As noted in Chapter 4, a gain in current by a factor of 3–4 may be realized by making the electron spot distribution elliptical, with a 3 : 1 ratio for the vertical and horizontal axes. Reports from Philips (*40*) cite spot widths between 0.3 and 0.4 mm and spot heights of the order of 2.5 mm. These apply to beam currents as high as 1.5 mA at a tube voltage of 25 kV; the width corresponds to $\frac{1}{4}$ to $\frac{1}{3}$ a triad width, with individual phosphor lines and guard bands 0.2 mm wide. The grid aperture, and at times the first-anode aperture, deviate from axial symmetry. Magnetic focus was replaced by electrostatic focus in later tube models (*99*). Since, with elongated spots, it is essential that the spot rotation match the inclination of the phosphor lines in the corners, and spot focus is modified by deflection, yoke design and gun design were carefully coordinated to achieve maximum brightness and adequate color purity over the entire screen area. A minimum current of 2.5 μA was found sufficient to maintain the proper phase of the chrominance signal derived from the multiplier phototube current.

7.3 Common Requirements of Beam-Index Systems

The appropriate grid signal for a dot-sequential display such as that of the beam-index tube may be written:

$$E = E_m' + \tfrac{2}{3}\{E_r' \cos(\omega_c t) + E_g' \cos[\omega_c t + \tfrac{1}{3}(2\pi)] + E_b' \cos[\omega_c t + \tfrac{1}{3}(4\pi)]\} \tag{7.9}$$

$$E = E_m' + E_c' \cos(\omega_c t + \phi_c) \tag{7.10}$$

with

$$E_m' = \tfrac{1}{3}\{E_r' + E_g' + E_b'\} \tag{7.11}$$

$$E_c' = \tfrac{2}{3}(E_r'^2 + E_g'^2 + E_b'^2 - E_r'E_g' - E_g'E_b' - E_b'E_r')^{1/2} \tag{7.12}$$

$$\phi_c = \arctan[(3)^{1/2}(E_b' - E_g')/(2E_r' - E_g' - E_b')]$$

Ways of deriving the symmetrical signal given by Eqs. (7.9) and (7.10) from the transmitted NTSC signal are indicated by Loughlin (*103*). For a

white field ($E_r' = E_g' = E_b'$), E_c' vanishes, whereas for a saturated primary color it becomes equal to $2E_m'$. As Chatten and Gardner (*104*) indicate, in practice the factor $\frac{2}{3}$ in Eq. (7.12) is replaced by an arbitrary factor k_2, adjusted by the chroma control, while the constant term E_m' is replaced by $E_m' - k_1E_c'$. The subtracted term, obtained by rectifying the chrominance signal, reduces the duty cycle of the beam current for saturated colors—for $k_1 = 1/(3k_2)$ from $\frac{2}{3}$ to $\frac{1}{2}$—and thus improves the saturation of the reproduced colors. The effective duty cycle is further narrowed by the nonlinear variation of beam current with drive (typically related by a power law, $I \propto V_g^{\gamma}$ with, e.g., $\gamma = 2.6$), while it is broadened by the finite spot size. These effects are indicated qualitatively in Fig. 7.9. Chatten and

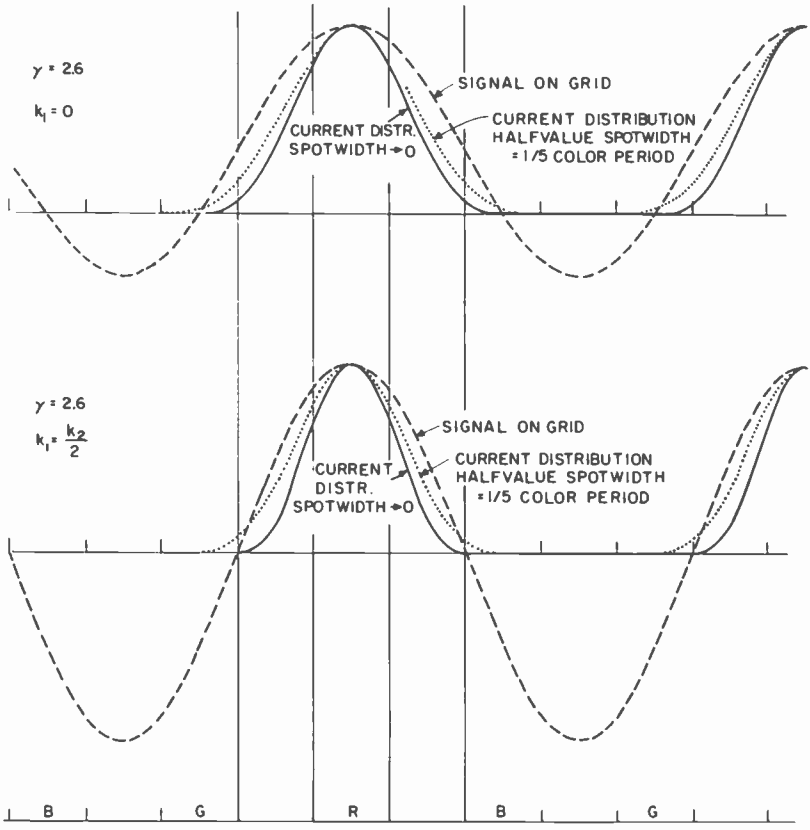

Fig. 7.9. Effect of γ and spot width on reproduction of saturated primary color with a sinusoidal color signal.

Gardner (*104*) found that, for a saturated primary signal, it should have been possible to obtain 93% saturation for the reproduced color with the spot size realized in the Apple tube. A rapid increase in spot size for beam currents in excess of 1 mA placed a practical limit on the screen brightness which could be achieved.

In beam-index tubes the conversion efficiencies of the three phosphors must be matched so that a beam sweeping at uniform velocity across the line structure generates white light. With symmetrical phosphor line structures, this is accomplished by diluting the two more efficient phosphors to the level of the least efficient phosphor (in terms of the individual excitation required to produce white light in combination). With earlier phosphor combinations, this resulted in a great loss in overall conversion efficiency, since the red phosphor required approximately twice the excitation needed by the green and blue phosphors. Thus, in Apple tubes, 50% gain in screen brightness was realized by doubling the width of the red phosphor line in comparison with the two other phosphor lines, resulting in the line pattern indicated in Fig. 7.10. With the introduction of rare-earth red phosphors, the advantage to be gained from asymmetrical line patterns became insignificant and more recent beam-index tubes employ phosphor lines and guard bands of identical width (*105*). It remains a characteristic of one-gun tubes, as compared with three-beam tubes, that the screen color for a monochrome signal is fixed by the ratio of phosphor areas and cannot be adjusted by adjusting the bias and gain of three individual signal circuits.

Since the phase shift impressed by the beam-index signal loop delay must be a constant in beam-index tubes, the scanning velocity, measured in color periods per second, should also be constant. In the Apple tube the circuit delay was found to be 0.9 μsec (*102*). For 400 color periods per line (including the portion corresponding to horizontal return time) and a line

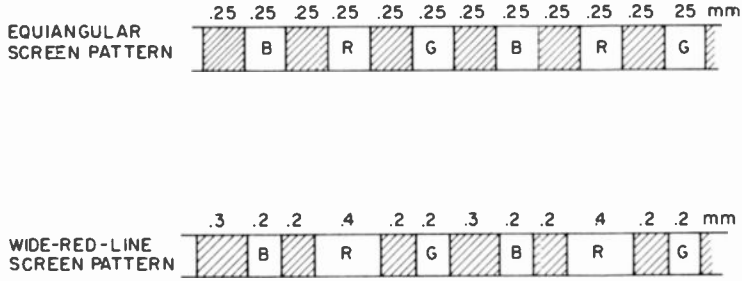

Fig. 7.10. Comparison of wide-red-line screen pattern with equiangular screen pattern for Apple tube.

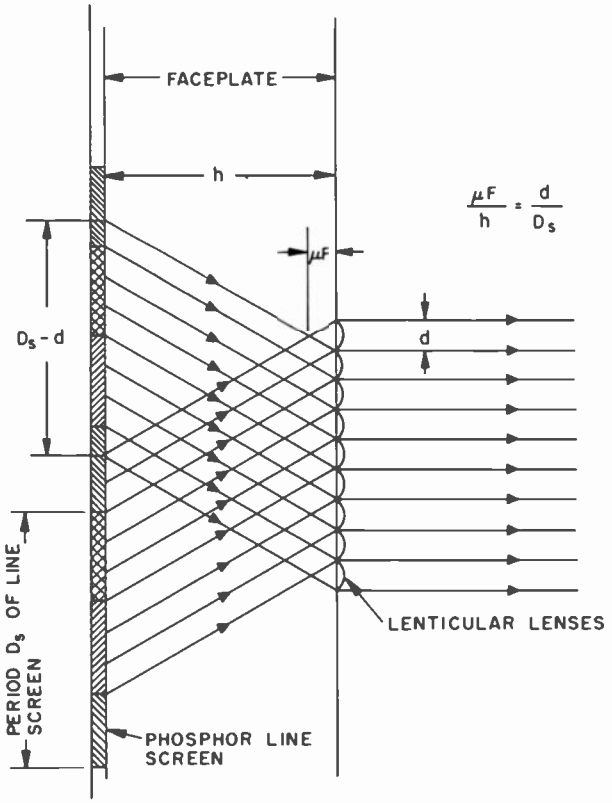

Fig. 7.11. Lenticular filter for suppressing structure of period D_s. Filter causes variation $\cos[(2\pi x/D_s) - \phi]$ to appear as variation $\cos\{2\pi[1 - (d/D_s)](x/d) + \phi\}$.

frequency of 15,750 sec^{-1}, the permissible deviation Δv of the velocity from the prescribed value v is given, for a maximum phase error of 10°, by

$$[(\Delta v)0.9 \times 10^{-6}(400)15{,}750]/v = 10°/360° \quad \text{or} \quad \Delta v/v = 0.005 \tag{7.13}$$

The variation in beam velocity and the phosphor-line pattern scale variation should thus be held within 0.5% of the prescribed values. In systems in which the index stripe frequency is a nonintegral multiple of the color change frequency, this requirement can be relaxed by balancing the delays in different arms of the feedback loop (*100*).

In beam-index tubes, the prominence of the line structure can prove objectionable even when the limitation in the recognition of picture detail

which it imposes is tolerable. This is, of course, a property common to all line-screen tubes. It is perhaps of greatest importance in beam-index tubes because of the great cost in terms of picture brightness of any reduction in the color period.

A simple way of reducing the prominence of the line structure with minor adverse effects on other aspects of picture quality consists in placing a molded lenticular filter, with cylindrical lenticules parallel to the phosphor lines, on the faceplate surface (*106*) (Fig. 7.11). The width d of the individual lenticule is made very small compared to the period D_s of the screen structure. If F is the focal length of the individual lenticule in air, h the thickness of the faceplate, and μ its refractive index, the ratio of the width of the lenticule to its focal length is chosen to be

$$d/F = D_s/(h/\mu) \tag{7.14}$$

The modulation transfer function of such a filter for a space frequency (normal to the lenticules) f is

$$\text{MTF} = (f_0/\pi f)\sin(\pi f/f_0), \qquad f_0 = 1/D_s \tag{7.15}$$

Since this vanishes for f_0 and all of its harmonics, the structure becomes invisible and periodic variations of higher space frequency are strongly attenuated. This applies for viewing the screen in a normal direction. When the screen is viewed at an angle, the cutoff frequency occurs at smaller values, corresponding to larger space periods, and the line structure becomes again visible at reduced intensity.

7.4 Summary

Beam-index tubes offer a way of simplifying color tube design at the expense of increased complexity of the auxiliary circuitry. The principal simplifications are the use of a one-piece bulb and the absence of a color-selecting mask or grill. On the other hand, screen preparation is rendered more complex by the addition of an index stripe system. In addition, the currently favored photoelectric system requires a multiplier phototube. While only a single gun is required (again, for the photoelectric beam-index system), the small and sharp spot needed to provide adequate color purity demands great care in the design of the gun and great precision in its fabrication. The potential of the beam-index tube for brightness is comparable to that of the shadow-mask tube, while in color saturation and screen structure it is likely to be somewhat inferior (*98*). Picture sharpness, in the reproduction of both color and monochrome pictures, is necessarily good. Along with other one-gun color tubes, the beam-index tube has the

drawback that it is impossible to adjust the white balance of the finished tube.

Only two types of beam-index tubes, using secondary emission or UV emission to generate the beam-index signal, have been considered in detail in this treatment. Both have demonstrated acceptable performance. It should be stressed, however, that there are many other possible realizations of the beam-index principle, which have been subjected to more or less intensive examination (*106a*).

CHAPTER 8

Penetration Tubes

8.1 Principles

Penetration tubes are color viewing tubes which avoid both the color-selecting mask or grill and the geometrically patterned screen. Instead, the macroscopically uniform screen is made voltage-sensitive, in the sense that the spectral composition of the emitted light changes with the accelerating voltage of the incident beam. This type of screen may be very useful in certain applications, especially where screen structures could present a major problem.

In general, penetration screens have two inherent properties that require special consideration.

(1) The color gamut of the screen and its conversion efficiency are a function of the screen design but inherently cannot equal that obtainable from the basic phosphors used.

(2) The landing position of the beam (or beams) on the screen will change with a color change unless compensation in some form is employed to prevent it. The compensating methods to be employed, as the accelerating voltage is varied to change color, may include high voltage modulation of the screen, deflection sensitivity modulation in analog or digital fashion, and partial beam shielding from the deflection field in multibeam tubes, with use of dynamic correction to obtain register of the color images in much the same manner as for shadow-mask tubes.

8.2 Layer Phosphors

The desired voltage sensitivity of the screens is achieved by arranging the red, green, and blue phosphors in layers, separated in general by layers

of inert or nonluminous materials. Such layered phosphors can be made macroscopically by a uniform layer of one color phosphor on the screen, covered by an inert layer and then a phosphor of a second color, etc. Such phosphor and barrier layers can be deposited in succession as uniform films by evaporation (*107*, *108*) or by surface reaction (*109*) onto the faceplate. Techniques have also been developed for depositing on the faceplate phosphor and barrier layers of uniform thickness from suspensions of very fine particles, less than 0.1 μm in diameter (*110*). Alternatively, the very fine particles can be deposited on small core particles, wherein the surface of each small core particle is constituted of three layers having different color properties separated by inert barriers. These three-color surface layers may be formed either on small glass beads or on relatively large core particles of one of the three phosphors (*110*, *111*) which act as cores. In either case, the screen emits any of the three primary colors depending on the electron velocity and the penetration depth that ensues.

Both the yellow ZnS(Mn) phosphor films, formed by Studer *et al.* (*109*) by passing Zn vapor over a heated glass substrate in an H_2S atmosphere, and a great variety of phosphor films [$CaWO_4$(W): blue, ZnS(Mn): yellow, Zn_2SiO_4(Mn): green, $MgSiO_3$(Mn) or $Zn_3(PO_4)_2$: red], formed by Feldman (*107*) by evaporation and subsequent heat treatment, exhibited conversion efficiencies of the same order as powder screens. With the evaporated films, heat treatment must be carried to the point of clouding the initially fully transparent films to prevent trapping of radiation within the high-refractive-index medium of the phosphor.

Feldman (*107*) also showed that, with a 0.3-μm layer of $CaWO_4$(W) deposited on top of a 2-μm layer of ZnS(Mn), a shift from substantially saturated blue cathodoluminescence to yellow cathodoluminescence could be obtained by changing the accelerating voltage of the incident beam from 8 to 16 kV. Comparable results were obtained by Koller and Coghill (*108*). More recently, Sylvania has marketed cathode-ray tubes for two-color displays with a screen consisting of a red europium phosphor and a green phosphor separated by a barrier layer, with operating voltages of 6 and 12 kV for the two colors (*112*).

Methods of building up phosphor and barrier layers from suspensions of fine particles have been described by Kell (*110*). In one of these the support surface (e.g., the faceplate) is first coated with a particle-adsorbing substance, such as a 0.1% gelatin solution, and is then thoroughly washed until gelatin is absent from the rinse water, but a thin layer remains on the support surface. A phosphor dispersion (with a concentration of 10–30 mg/cm^3) is then poured on the surface, causing the particles to adhere to the gelatin-coated substrate in a monoparticle layer. The dispersion is poured off and the surface thoroughly washed with water. If this wash is

followed by an acetic acid wash having a pH of 4, the density of the phosphor monolayer may be increased by again applying a phosphor dispersion followed by a wash. The deposition of additional phosphor monolayers may be effected by repeating the sequence of gelatin coating, washing, phosphor deposition, excess phosphor removal, and a final wash. After one phosphor has been laid down to a desired thickness, the same procedure is followed for the remaining barrier layers [using, for example, ludox (silica) or vermiculite (mica) particles] and phosphors.

Precisely the same procedure can be followed in the preparation of multiple-coated particles: The core particles (which may be particles of the phosphor to be excited at the highest operating voltage) are simply coated with gelatin in an aqueous solution, removed from the latter and washed, and then immersed and agitated in a suspension of the fine (barrier-layer

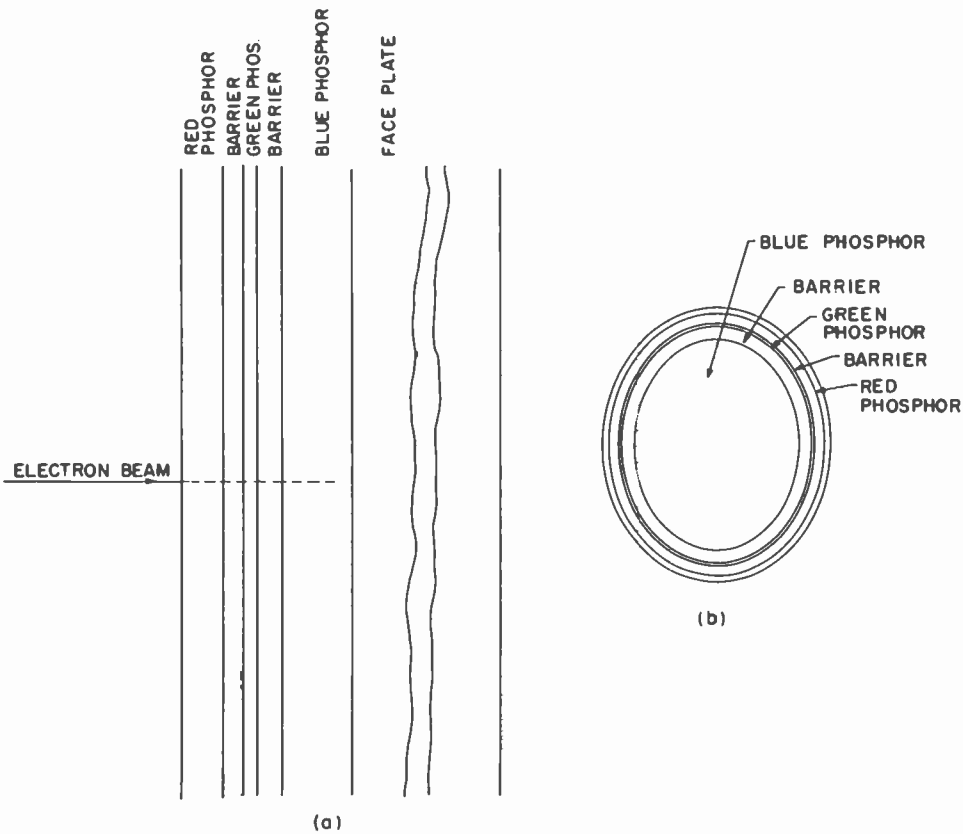

Fig. 8.1. Layered phosphor on (a) a flat substrate and (b) a core particle (schematic).

or phosphor) particles to be deposited on the core-particle surface. These processes can be repeated just as for the faceplate layer screen until the complete layer structure has been built up on the core particle. As a final step, a gelatin coating may be applied to the particle and hardened with acid hardener to provide a protective coating.

When the core particles consist of particles of the phosphor to be excited at the highest velocity, Messineo and Thompson (*113*) have produced an integral barrier or nonluminescent layer in the surface of the individual grains by diffusing an emission-killing material into the surface to the desired depth. Prener and Kingsley (*114*) have used homogeneous precipitation of nonluminescent ZnS or CdS to deposit the barrier layer.

The procedure as outlined for multiple-coated phosphors permits the formation of phosphor and barrier layers which are quite uniform in thickness and free from gaps. Unless this condition is satisfied, it is impossible to obtain high-saturation primary colors, since all three phosphors will be excited to some extent even at the lowest operating voltage. Figure 8.1 shows schematically layered phosphor structures on a flat surface and on a core particle. RCA has made available commercially a red-white tube using phosphor of this latter type where the layers are on individual phosphor grains.

The principles which must guide the selection of the layer thicknesses and design methods for multilayer screens for color viewing tubes are described in detail by Pritchard (*111*).

Electrons, in passing through matter, lose energy to the electrons of the medium by inelastic collisions. This energy loss, for electrons in the range of 10–20 kV, with which we are here concerned, is given fairly accurately by the Thomson–Whiddington law (*115*):

$$1 - (V^2/V_0^2) = \rho x/p(V_0) \tag{8.1}$$

Here eV_0 is the initial kinetic energy of the electrons and eV is their kinetic energy after having penetrated to a depth of x cm in the medium of density ρ g/cm³. The mass thickness $p(V_0)$ is the "penetration" of electrons of energy eV_0 into the medium. To a first approximation the penetration, measured in g/cm², is independent of the composition of the medium and a function only of the accelerating voltage V_0. Measurements of Terrill (*116*) on aluminum films led to the relation*

$$p(V_0) = bV_0^n \tag{8.2}$$

* A somewhat better approximation to the range data is given by $p = 4.45 \times 10^{-11} V_0^{1.7}$. Also, as W. H. Fonger has pointed out in a private communication, the Gentner curve in Fig. 8.2 necessarily underestimates the energy absorption just below the surface. For a fuller discussion, see Birkhoff (*117*).

with $n = 2$, $b = 2.3 \times 10^{-12}$ g/(cm^2 · V^2). The Thomson–Whiddington law does not represent the energy loss of an electron beam penetrating into a medium, since in addition to the decrease in the mean energy of the electrons with distance from the surface of entry, there is also a decrease in the number of electrons in the beam. Lenard (*118*) has given the following absorption law for the variation of the beam current:

$$i(x + dx)/i(x) = e^{-\alpha dx}, \qquad \alpha = b'\rho/V^2 \tag{8.3}$$

Unlike the constant b in Eq. (8.2), we must expect b' to increase with the effective atomic number of the absorbing medium since the "absorption" depends on nuclear scattering. It must be stressed, furthermore, that Lenard's law applies only after the electron beam has reached an equilibrium state of angular diffusion and hence cannot apply for small values of x, close to the surface of entry. If the last circumstance is disregarded, a combination of Eqs. (8.1)–(8.3) leads to the following law for the ratio of the beam energy $W(x)$ dissipated beyond the depth x to the initial beam energy W_0:

$$\frac{W(x)}{W_0} = \frac{V}{V_0}\exp\left(-\int_0^x \alpha\, dx\right) = \left(1 - \frac{\rho x}{p}\right)^{1/2} \exp\left(-bb'\int_0^x \frac{\rho\, dx}{p[1 - (\rho x/p)]}\right)$$

$$= \left(1 - \frac{\rho x}{p}\right)^{1/2+bb'} \tag{8.4}$$

Terrill's (*116*) data for aluminum films yielded $b' = 8 \cdot 10^{11}$ V^2 cm^2/g, so that the exponent in the power law of Eq. (8.4) becomes about 2.4.

Equation (8.4) has been cited by Koller and Alden (*119*) and was found by Koller to give a reasonably good representation of the variation of light emission of a thin evaporated phosphor film with accelerating voltage. However, Eq. (8.4) gives a monotonic decrease of energy dissipation within the medium as a function of depth x, and this is in disagreement with more detailed investigations of the energy dissipation. A particularly careful study of the energy dissipation of 25.6 kV electrons in aluminum, taking proper account of backscattering, has been carried out by Gentner (*120*). The variation of energy dissipation as function of fraction of penetration depth found by Gentner is shown in Fig. 8.2. We shall assume, with Pritchard (*111*), that the distribution shown in Fig. 8.2 applies irrespective of the accelerating voltage V_0 [just as for the relation in Eq. (8.4)] and equally for the different layers of which the composite phosphor screen may consist. The fraction of the energy, $F(\rho x)/p$, absorbed within a mass-thickness depth ρx, is then given by the universal curve shown in Fig. 8.3, obtained by integration of the function shown in Fig. 8.2. We shall further-

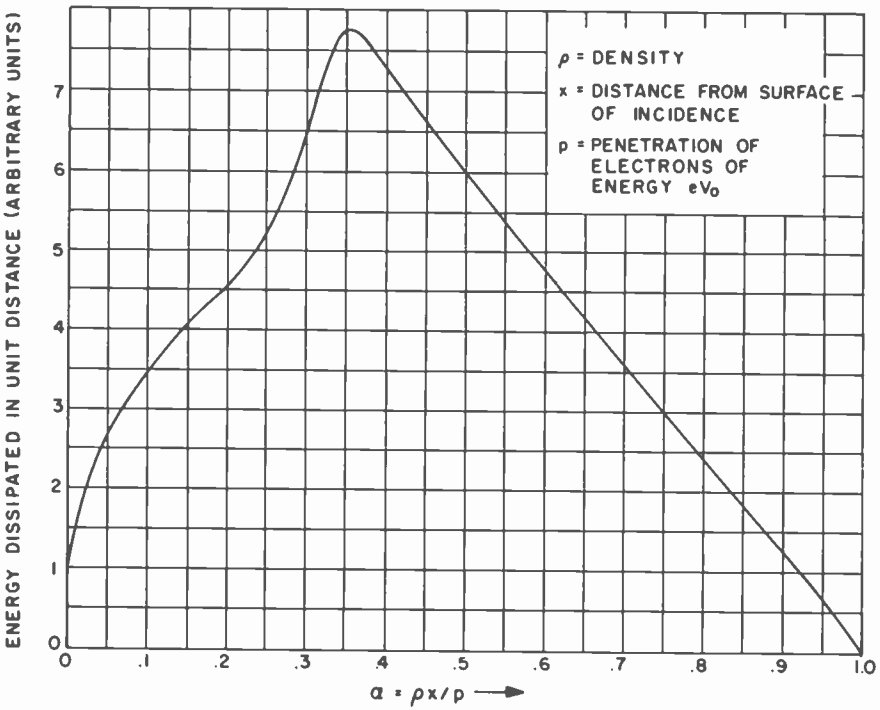

Fig. 8.2. Distribution of energy dissipation of 25.6 kV electrons in aluminum according to Gentner (*87*).

more assume that the light emission of any one phosphor is proportional to the beam energy absorbed by it.

Other observations support the general character of the energy absorption curves in Fig. 8.2 and 8.3. In particular, Ehrenberg and Franks (*121*) have observed the distribution of the luminescent glow produced by an electron probe 0.75 μm in diameter incident on transparent phosphor crystals through a polished lateral face. As expected, the maximum of the energy dissipation was found to be displaced toward the surface with increasing mean atomic number of the medium. A curve for the energy dissipation in ZnS derived from their data was found to be sufficiently close to that shown in Fig. 8.2 to lead to only minor changes in the expected performance of layered phosphors.

The screen must be designed so that, for a prescribed condition of operation, it produces a prescribed white (e.g., C-illuminant white, with color coordinates $x_w = 0.310$, $y_w = 0.316$) and, for a prescribed voltage

range, an acceptable color gamut; within limits, the color gamut can be increased at the expense of screen efficiency by increasing the thickness of the barrier layers. The realization of a good red and a good rendition of flesh colors, which are primarily mixtures of red and green with white, prescribes the order in which the phosphors should be laid down; the red phosphor should be closest to the gun since, for sufficiently low voltages,

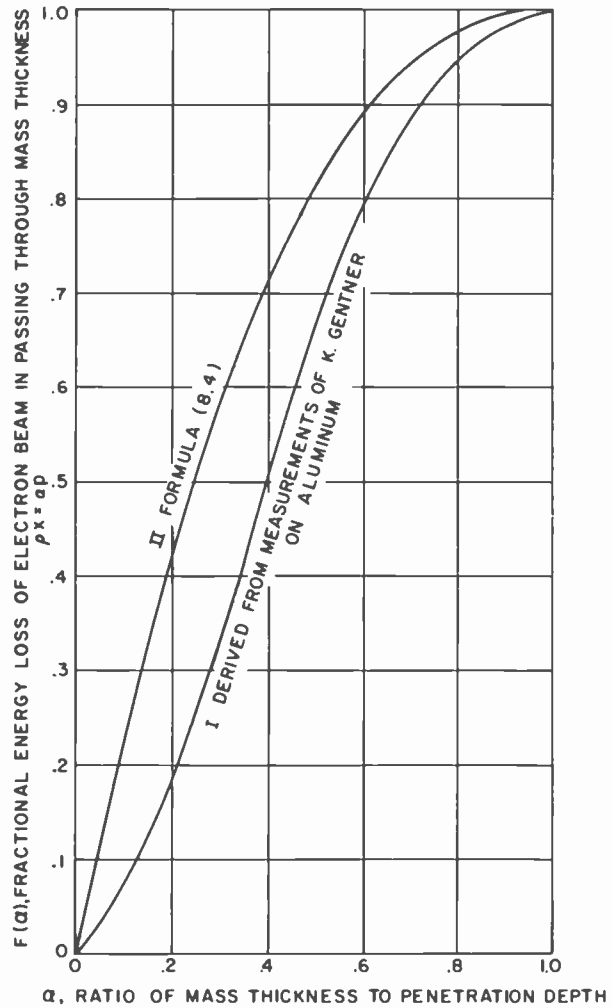

Fig. 8.3. Fraction of total energy absorbed within a layer containing a fraction α of the penetration mass thickness.

red can be reproduced without admixture of green and blue. The good reproduction of flesh colors suggest placing the green phosphor next and the blue phosphor farthest from the gun, directly on the faceplate. Finally, the use of green and blue phosphors which have much higher conversion efficiences than the red phosphor is advantageous for minimizing the voltage range required for a prescribed color gamut, since they reduce the extent to which the penetration range must project into the green and blue phosphor to generate an adequate contribution of green and blue light.

If the total energies E_r, E_g, E_b dissipated in the three phosphors with conversion efficiencies C_r, C_g, C_b are known, the color coordinates x, y of the light output can be determined from (*122*)

$$x = \frac{C_rE_r(x_r/y_r) + C_gE_g(x_g/y_g) + C_bE_b(x_b/y_b)}{(C_rE_r/y_r) + (C_gE_g/y_g) + (C_bE_b/y_b)}$$

$$y = \frac{C_rE_r + C_gE_g + C_bE_b}{(C_rE_r/y_r) + (C_gE_g/y_g) + (C_bE_b/y_b)} \tag{8.5}$$

Here (x_r, y_r), (x_g, y_g), and (x_b, y_b) are the color coordinates of the three phosphors. Furthermore, if in Eq. (8.5) we substitute for x, y the color coordinates for white (e.g., $x_w = 0.310$, $y_w = 0.316$ for C-illuminant white), Eq. (8.5) can be solved for the relative magnitude of the excitations E_r^w, E_g^w, E_b^w of the three phosphors required to produce white light:

$$\begin{aligned} C_rE_r^w : C_gE_g^w : C_bE_b^w = {} & y_r[(x_g - x_w)(y_b - y_w) - (x_b - x_w)(y_g - y_w)] \\ & : y_g[(x_b - x_w)(y_r - y_w) - (x_r - x_w)(y_b - y_w)] \\ & : y_b[(x_r - x_w)(y_g - y_w) - (x_g - x_w)(y_r - y_w)] \end{aligned} \tag{8.6}$$

For the P22 phosphor group with

$$\begin{aligned} x_r &= 0.678, \qquad y_r = 0.322 \\ x_g &= 0.204, \qquad y_g = 0.732 \\ x_b &= 0.146, \qquad y_b = 0.088 \end{aligned} \tag{8.7}$$

this leads to the ratio

$$C_rE_r^w : C_gE_g^w : C_bE_b^w = 0.29 : 0.58 : 0.13 \tag{8.8}$$

For a particular phosphor combination found suitable for screen preparation, i.e., red (Mg, Cd, Zn) SiO_3(Mn), green Zn_2SiO_4(Mn), and blue ZnS(Ag), the conversion efficiencies had the ratio

$$C_r : C_g : C_b = 1 : 11.7 : 13.2 \tag{8.9}$$

Thus, to produce white, the relative energy absorptions in the three phosphor layers become

$$E_r^w : E_g^w : E_b^w = 0.830 : 0.142 : 0.028 \tag{8.10}$$

Assume that, for white excitation, 40% of the beam energy shall be absorbed in the separator layers; since the rendition of a good red is regarded as most important, let a major portion of this (25%) be dissipated in the first separation layer (between the red and green phosphors) and the remainder (15%) in the second separation layer. We then have the requirement for the fractional energy absorptions in the several layers (normalized to total unity):

$$E_r^w = 0.498, \quad E_{s1}^w = 0.25, \quad E_g^w = 0.085, \quad E_{s2}^w = 0.15, \quad E_b^w = 0.017 \tag{8.11}$$

If the operating conditions (i.e., beam voltages and currents) are prescribed, the fractional energy dissipations in the several layers, given by Eq. (8.11), suffice to determine the mass thicknesses of these same layers. Let the total mass thickness of the layer phosphor up to the far end of the nth layer (measured from the gun side) be given in terms of the penetration depth for the median voltage V_0 by $\alpha_n p(V_0)$. Then, for a one-gun tube with constant beam current for white and a screen potential variation as function of the phase angle $\theta = \omega_c t$ (with reference phase derived from the transmitted color burst) given by $V(\theta)$, α_1, α_2, α_3, α_4 are determined by the four equations:

$$E_r^w = \frac{1}{2\pi}\int_{-\pi}^{\pi} \frac{V(\theta)}{V_0} F\left(\alpha_1 \frac{V_0^2}{V(\theta)^2}\right) d\theta \tag{8.12a}$$

$$E_{s1}^w = \frac{1}{2\pi}\int_{-\pi}^{\pi} \frac{V(\theta)}{V_0} \left\{F\left(\alpha_2 \frac{V_0^2}{V(\theta)^2}\right) - F\left(\alpha_1 \frac{V_0^2}{V(\theta)^2}\right)\right\} d\theta \tag{8.12b}$$

$$E_g^w = \frac{1}{2\pi}\int_{-\pi}^{\pi} \frac{V(\theta)}{V_0} \left\{F\left(\alpha_3 \frac{V_0^2}{V(\theta)^2}\right) - F\left(\alpha_2 \frac{V_0^2}{V(\theta)^2}\right)\right\} d\theta \tag{8.12c}$$

$$E_{s2}^w = \frac{1}{2\pi}\int_{-\pi}^{\pi} \frac{V(\theta)}{V_0} \left\{F\left(\alpha_4 \frac{V_0^2}{V(\theta)^2}\right) - F\left(\alpha_3 \frac{V_0^2}{V(\theta)^2}\right)\right\} d\theta \tag{8.12d}$$

For α_5 we have simply the requirement

$$\alpha_5 > V_{max}^2/V_0^2 \tag{8.12e}$$

This means that the blue phosphor layer, of mass thickness

$$\rho_b d_b = (\alpha_5 - \alpha_4) p(V_0) \tag{8.13}$$

TABLE V

LAYER PROPERTIES OF PENETRATION SCREEN IN FIG. 8.4

Layer	Mass thickness (mg/cm^2)	Density (g/cm^3)	Thickness (μm)
Blue phosphor	>0.25	4.1	>0.62
Separator *s*2	0.256	1.64	1.56
Green phosphor	0.066	3.9	0.17
Separator *s*1	0.113	1.64	0.69
Red phosphor	0.24	3.83	0.61

is thick enough that, even for the highest accelerating voltage, the beam does not penetrate through it into the faceplate. Utilizing the functional variation $F(\alpha)$ given for example by Fig. 8.3, the value of α_1 which satisfies Eq. (8.12a) is found by trial and error. Having found α_1, α_2 can be determined from Eq. (8.12b) in similar manner, etc. Assuming a simple sinu-

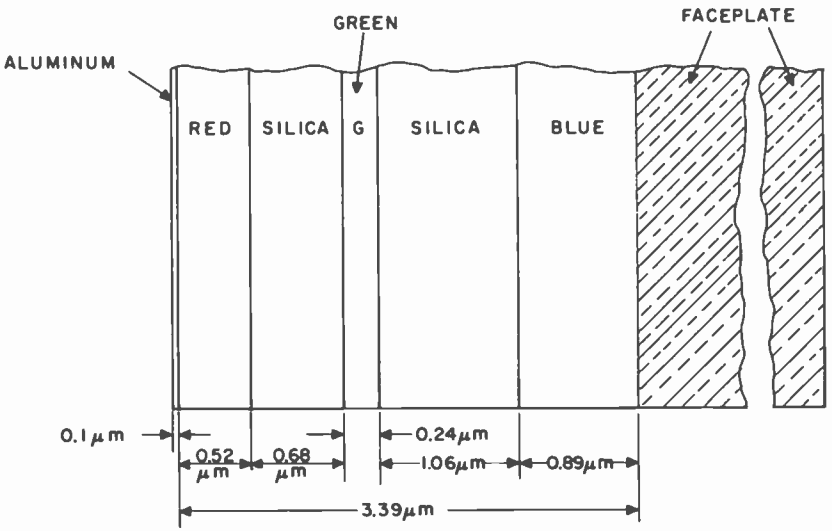

Fig. 8.4. Structure of layered phosphor screen producing white light for constant beam current and sinusoidally modulated screen voltage: $V = V_0(1 + 0.2 \sin \theta)$, $V_0 = 16$ kV.

soidal variation for V,

$$V = V_0(1 + 0.2 \sin \theta), \qquad V_0 = 16 \text{ kV} \tag{8.14}$$

Pritchard's (*111*) findings for the mass thicknesses of the several layers (and corresponding thicknesses for the indicated densities of compact layers of the materials) are given in Table V.

The effect of the thin aluminum layer over the red phosphor has here been neglected. Figure 8.4 shows the structure of the layered phosphor screen. Figure 8.5 indicates the absorbed energy and the light output of the phosphors as function of depth of penetration for three different voltages; the light output curves are obtained by multiplying the energy absorption curves by a factor proportional to the product of the operating voltage and the conversion efficiency. Figure 8.6 shows the variation of light output (in units producing white for equal contributions of red, green, and blue) of the three phosphors as function of voltage. We see immediately that, for the range of 12.8–19.2 kV here considered, an excellent red can be obtained, but that both green and blue are strongly diluted.

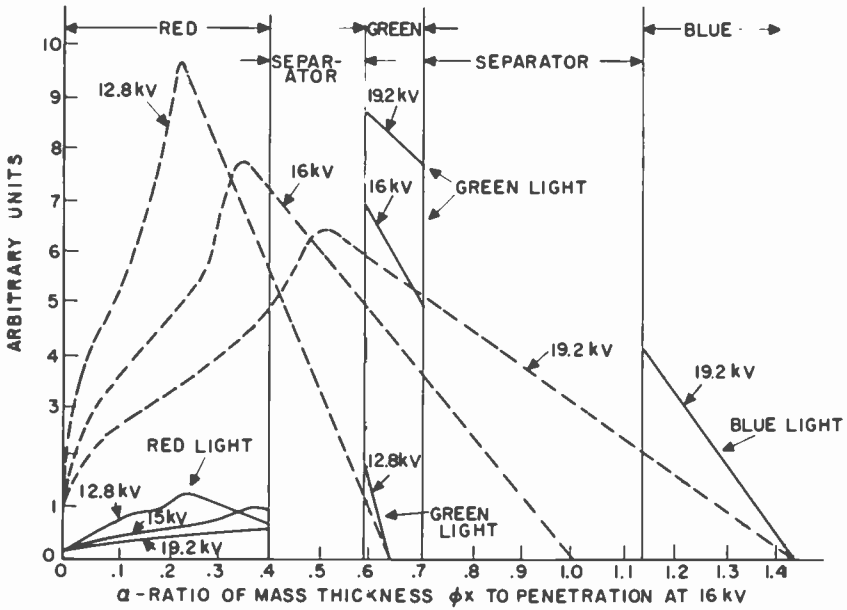

Fig. 8.5. Energy absorption and light output of phosphors as function of depth at three different operating voltages (screen of Fig. 8.4); dashed line, energy absorbed per unit mass thickness; solid line, light emitted per unit mass thickness.

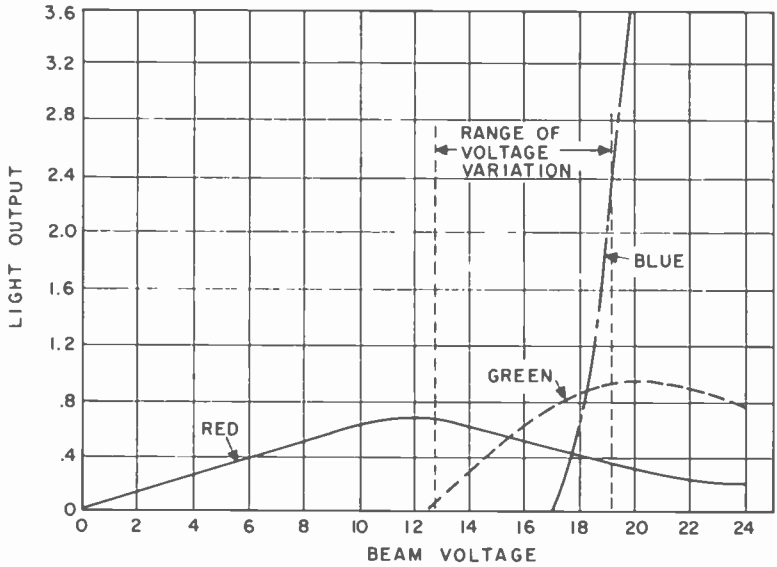

Fig. 8.6. Variation of light output (in units producing white for equal contributions of red, green, and blue) of three phosphors in screen of Fig. 8.4 as function of voltage.

The values $VC_rE_r/0.29$, $VC_gE_g/0.58$, and $VC_bE_b/0.13$ plotted in Fig. 8.6 are obtained from the relations

$$E_r = F\left(\alpha_1 \frac{V_0^2}{V^2}\right), \quad E_g = F\left(\alpha_3 \frac{V_0^2}{V^2}\right) - F\left(\alpha_2 \frac{V_0^2}{V^2}\right), \quad E_b = 1 - F\left(\alpha_4 \frac{V_0^2}{V^2}\right) \tag{8.15}$$

If these quantities E_r, E_g, and E_b are substituted in the expressions (8.5) for the color coordinates, we obtain the sequence of points on the chromaticity diagram shown in Fig. 8.7. The curve defined by these points, together with the straight line joining the 12.8 and 19.2 kV points, encloses the entire gamut of colors which can be reproduced by the screen for the indicated voltage range.

Actually, the gamut shown in Fig. 8.7 for the screen here considered could only be approached with a three-beam tube. With the three beams having accelerating voltages of 12.8, 16.8, and 19.2 kV, the color gamut would be defined by the triangle with vertices at the 12.8-, 16.8-, and 19.2-kV points, which differs very little from the total gamut of which the

screen is capable. For a one-gun tube E_r, E_g, and E_b would be given by

$$E_r = \int_{-\pi}^{\pi} i(\theta)\, V(\theta) F\left(\alpha_1 \frac{V_0^2}{V(\theta)^2}\right) d\theta \Big/ \int_{-\pi}^{\pi} i(\theta)\, V(\theta)\, d\theta \tag{8.16a}$$

$$E_g = \int_{-\pi}^{\pi} i(\theta)\, V(\theta) \left\{F\left(\alpha_3 \frac{V_0^2}{V(\theta)^2}\right) - F\left(\alpha_2 \frac{V_0^2}{V(\theta)^2}\right)\right\} d\theta \Big/ \int_{-\pi}^{\pi} i(\theta)\, V(\theta)\, d\theta \tag{8.16b}$$

$$E_b = \int_{-\pi}^{\pi} i(\theta)\, V(\theta) \left\{1 - F\left(\alpha_4 \frac{V_0^2}{V(\theta)^2}\right)\right\} d\theta \Big/ \int_{-\pi}^{\pi} i(\theta)\, V(\theta)\, d\theta \tag{8.16c}$$

Here $i(\theta)$ is the beam current as function of color phase. The color gamut approaches that of the three-beam tube only for very narrow sampling, i.e., if the current is pulsed on briefly at the phase angles corresponding to $V(\theta) = 12.8$, 16.8, and 19.2 kV.

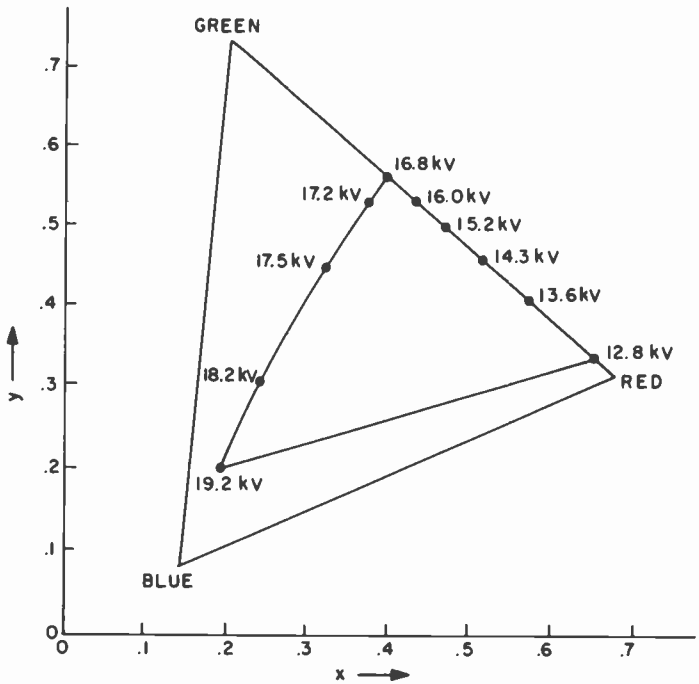

Fig. 8.7. Color gamut of screen shown in Fig. 8.4.

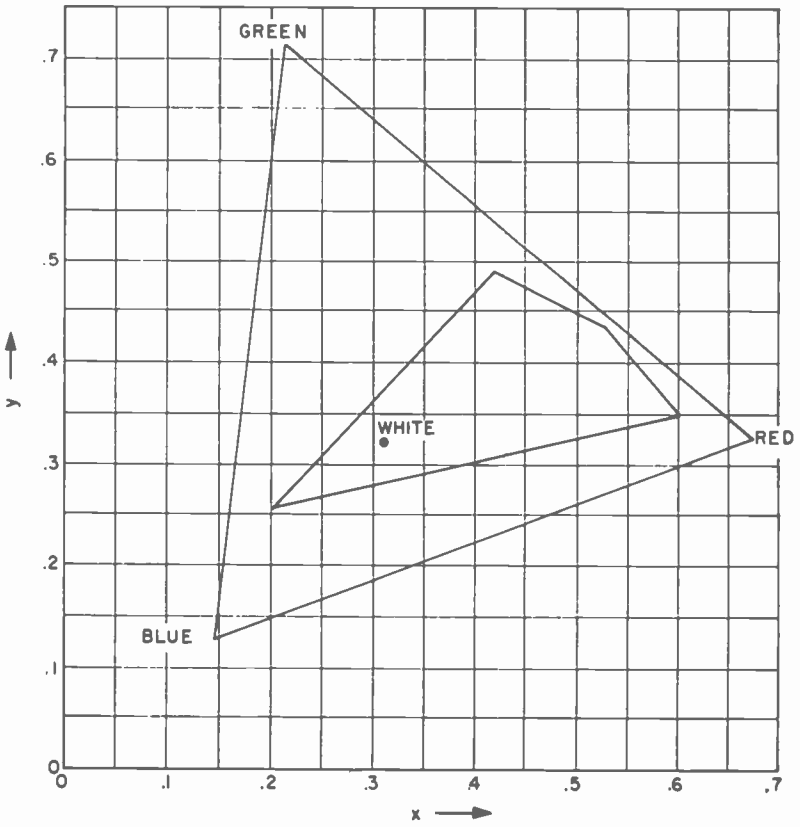

Fig. 8.8. Color gamut of screen designed for one-gun operation.

The color gamut realizable with a one-gun tube with a reasonable duty cycle is shown in Fig. 8.8. In the computation for this screen it was assumed by Pritchard (*111*) that the screen potential was given by

$$V(\theta) = V_0\{1 - 0.2[\sin\theta - \tfrac{1}{2}\sin(2\theta)]\}, \qquad V_0 = 16\ \text{kV} \quad (8.17)$$

and that gating pulses with a duty cycle of 61% were applied to the gun at $\theta = (2\pi/3)n$, where n is any integer. The addition of the second harmonic term in Eq. (8.17) increases the voltage modulation factor to 0.26, corresponding to a voltage swing from 11.8 to 20.2 and causes the voltage wave to have a flat shoulder at the three primary-color sampling points. Even so, the color gamut shown in Fig. 8.8 is considerably smaller than that obtained for three-beam operation with the screen shown in Fig. 8.7.

For a three-beam tube with operating voltages V_r, V_g, V_b, the colors reproduced for beam currents i_r, i_g, i_b can be obtained by means of Eq. (8.5) from

$$E_r = \sum_{k=r,g,b} i_k V_k F\left(\alpha_1 \frac{V_0^2}{V_k^2}\right) \Big/ \sum_{k=r,g,b} i_k V_k \tag{8.18a}$$

$$E_g = \sum_{k=r,g,b} i_k V_k \left[F\left(\alpha_3 \frac{V_0^2}{V_k^2}\right) - F\left(\alpha_2 \frac{V_0^2}{V_k^2}\right)\right] \Big/ \sum_{k=r,g,b} i_k V_k \tag{8.18b}$$

$$E_b = \sum_{k=r,g,b} i_k V_k \left[1 - F\left(\alpha_4 \frac{V_0^2}{V_k^2}\right)\right] \Big/ \sum_{k=r,g,b} i_k V_k \tag{8.18c}$$

If the relative magnitudes of the gun currents i_r^w, i_g^w, i_b^w required for a white-light output are prescribed and the fractional beam energy E_{s1}^w and E_{s2}^w dissipated in the barrier layers in similarly specified, the α_n of relative mass thicknesses of the layer extending from the gunside to the nth interface are determined by trial and error from

$$E_r^w = \sum_{k=r,g,b} i_k^w V_k F\left(\alpha_1 \frac{V_0^2}{V_k^2}\right) \Big/ \sum_{k=r,g,b} i_k^w V_k \tag{8.19a}$$

$$E_{s1}^w = \sum_{k=r,g,b} i_k^w V_k \left[F\left(\alpha_2 \frac{V_0^2}{V_k^2}\right) - F\left(\alpha_1 \frac{V_0^2}{V_k^2}\right)\right] \Big/ \sum_{k=r,g,b} i_k^w V_k \tag{8.19b}$$

$$E_g^w = \sum_{k=r,g,b} i_k^w V_k \left[F\left(\alpha_3 \frac{V_0^2}{V_k^2}\right) - F\left(\alpha_2 \frac{V_0^2}{V_k^2}\right)\right] \Big/ \sum_{k=r,g,b} i_k^w V_k \tag{8.19c}$$

$$E_{s2}^w = \sum_{k=r,g,b} i_k^w V_k \left[F\left(\alpha_4 \frac{V_0^2}{V_k^2}\right) - F\left(\alpha_3 \frac{V_0^2}{V_k^2}\right)\right] \Big/ \sum_{k=r,g,b} i_k^w V_k \tag{8.19d}$$

It is possible to express the energy dissipation in thin spherical phosphor and barrier layers deposited on a spherical core by a generalized function in much the same manner as for flat layers. The principal change is a displacement of the maximum of the curve toward a smaller fraction α of the penetration depth and a corresponding reduction in the color gamut for a given voltage range. Figure 8.9 shows an example of the color gamut realizable with a particular particle coating pattern as computed by Pritchard. The rounded peak arises from a more gradual contribution of blue light, corresponding to a more nearly asymptotic approach of the dissipation curve to the axis at the end of the range.

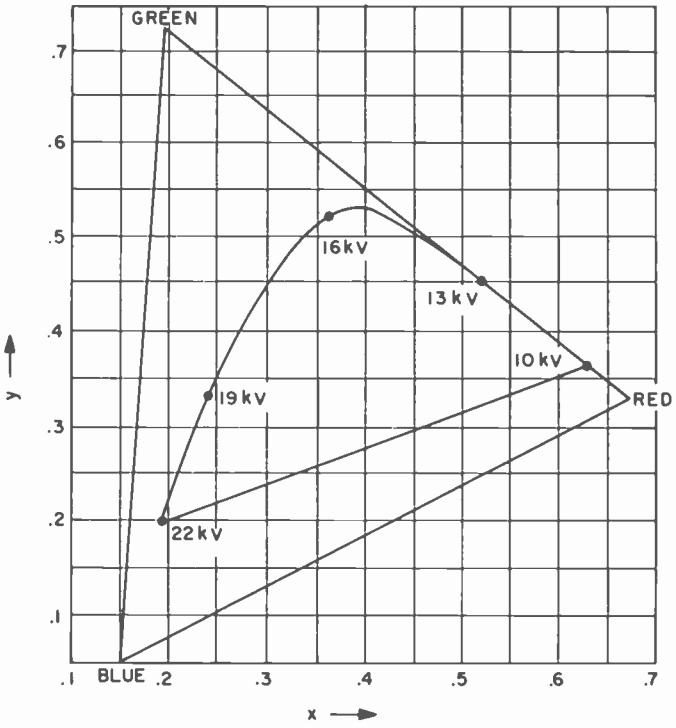

Fig. 8.9. Color gamut for coated particle screen.

8.3 Methods of Operation

As has been noted repeatedly, the layered phosphor screen can be excited either by a single electron beam, generating light of different colors in temporal succession; or it can be excited by three beams, with fixed velocities of impact on the screen, reconstructing the red, green, and blue components of the picture, respectively.

A general block diagram for the operation of the one-gun penetration tube is shown in Fig. 8.10. A fine-mesh electrode maintained at the mean potential V_0 of the screen shields the funnel and deflection region of the tube from the varying potential of the screen. A potential difference between the mesh and funnel coating produces an accelerating converging electron lens with focal point at the deflection center which results in approximately perpendicular incidence of the deflected beams on the screen with screen potential (*123*, *124*). The screen modulation, at the color sub-

carrier frequency $\omega/(2\pi)$, is synchronized with the color burst so that the proper phase relationship is maintained between the screen potential and the chrominance signal applied to the tube control grid.

The form of the chrominance signal to be applied to the grid depends on the character of the screen modulation. Assume that the screen is modulated by a simple sinusoidal waveform,

$$V = V_0 - V_m \sin(\omega t) \tag{8.20}$$

Then the appropriate signal to be applied to the grid corresponds to a reversing color sequence BGRRGBBGRRGB as described by Loughlin (*103*). If narrow gating pulses are applied at $\omega t = n(\pi/3)$ ($n = 1, 2, 3, 4, 5, 6, \ldots$), the correct color signals E_b', E_g', E_r' are successively applied to the grid for a signal

$$E = \tfrac{1}{3}\{(E_r' + E_g' + E_b') + \sqrt{3}(E_r' - E_b') \sin(\omega t) + (2E_g' - E_r' - E_b') \cos(2\omega t)\} \tag{8.21}$$

The manner in which such a signal may be derived from the transmitted NTSC color signal has been indicated by Loughlin. Without narrow sampling the coefficients of the fundamental and second harmonic terms are slightly modified and the saturation of the reproduced colors is diminished. A waveform which includes fourth-harmonic terms and effects sampling at the appropriate color phases has been given in Eq. (6.26).

It has already been noted that greater constancy of the beam voltage during sampling periods (and, hence, an improved color gamut) is realized by the addition of a second-harmonic term to the screen voltage modulation,

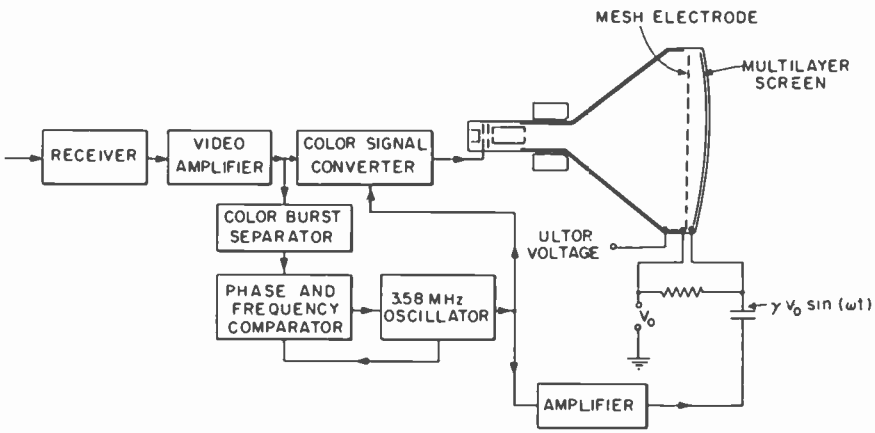

Fig. 8.10. Block diagram for one-gun penetration-tube receiver.

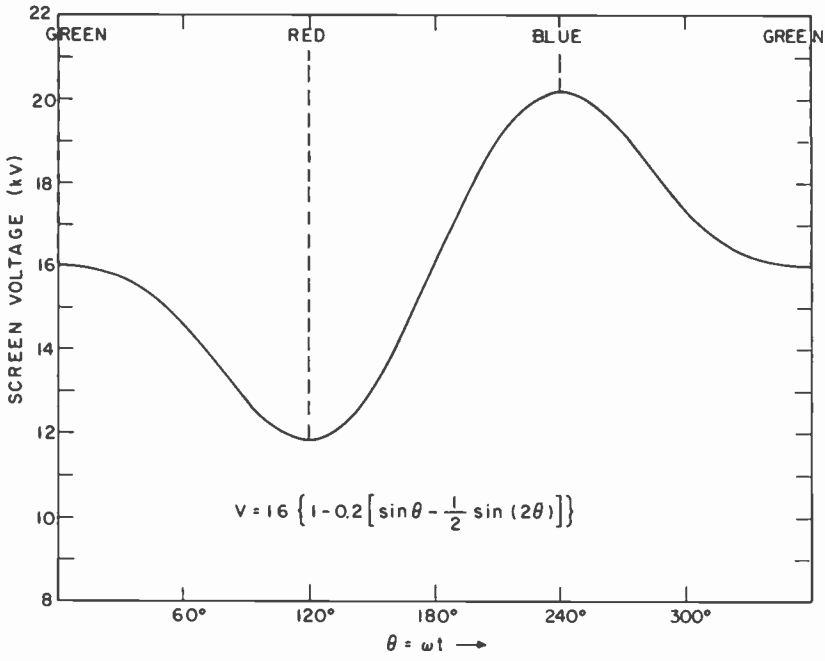

Fig. 8.11. Screen modulation waveform including second-harmonic term, for continuous color sequence operation.

as indicated in Eq. (8.17). The screen voltage modulation for this waveform is shown in Fig. 8.11. According to Pritchard (*111*), the desired screen-oscillation wave form is obtained across two resonant circuits in series, tuned to the fundamental and second harmonic of the color subcarrier and excited by a class-C oscillator phase-controlled by the transmitted color burst. The relative amplitude of the two time-varying terms is adjusted by adjusting the L/C ratios of the two circuits and the phase of the second harmonic by the fine tuning of the second-harmonic resonant circuit.

With the screen voltage given by Eq. (8.17), the appropriate grid signal corresponds to the continuous color sequence GRBGRB and is given by the symmetrical form

$$E = \tfrac{1}{3}\{E_r' + E_g' + E_b' + 2E_g' \cos(\omega t) + 2E_r' \cos[\omega t - (2\pi/3)] + 2E_b' \cos[\omega t - (4\pi/3)]\} \tag{8.22}$$

As noted before, the flattened potential variation in the neighborhood of the red, green, and blue color phases ($\omega t = 0,\ 2\pi/3,\ 4\pi/3$) permits the

realization of a color gamut close to that of which the screen is capable with duty cycles of the order of 60° for each color phase, sufficient to yield acceptable screen brightness.

One of the obvious drawbacks of the one-gun tube is the very large circulating power required to swing the screen, at color subcarrier frequency ω, between the potentials required for minimum and maximum penetration. For a 535-mm diag. screen, with a 4 : 3 aspect ratio, spaced 10 mm from a mesh electrode at fixed potential, the capacitance is 121 pF. For the indicated geometry, this would be the minimum capacitance of the resonant circuit maintaining the voltage oscillation. For a total voltage swing of $2V_m$, the circulating power becomes (for a simple sinusoidal voltage variation) $\omega CV_m^2/2$. With $V_m = 5$ kV and $\omega/(2\pi) = 3.58$ MHz, this becomes 34 kW. The generation of circulating powers of this order of magnitude, even with high-Q circuits, and the suppression of radiation from the circuits presents an obvious problem.

Three-beam penetration tube designs have been described by Messineo and Gross (*125*). Three-beam operation has the advantage of permitting the realization of very nearly the total color gamut of which the screen is capable at the design voltage range and of permitting adjustment of white balance after completion of the tube by adjusting the dc bias on the three-tube grids. The color gamut is given by the interior of a triangle inscribed in the color gamut curve of the screen, as shown for example in Fig. 8.7, with the vertex determined by the operating voltage selected for the green gun.

The structure of the triple gun required for the penetration tube is shown schematically in Fig. 8.12 (*125*). Cathode, grid, screen grid, and focusing electrode for each component gun are brought out independently to the base, while the group of the three final anode cylinders are connected in common to the funnel and screen coating of the tube. For the two guns corresponding to the two lower beam voltages (i.e., the red and the green gun), the anode cylinders are continued in the form of magnetic shielding tubes into the deflection field region, so as to make the deflection field integral along the electron paths for the three beams approximately proportional to the square root of their accelerating potentials. The materials for the shielding tubes must be such that the shielding is equally effective at the horizontal and vertical deflection frequencies, e.g., 60 and 15,750 Hz, respectively. Ferrites employed for deflection yokes, as well as certain special magnetic alloys formed into concentric shielding tubes, satisfy this requirement.

The deflection compensation effected by the two shielding tubes is not exact. Hence, the convergence cage, which imparts to each of the beams an

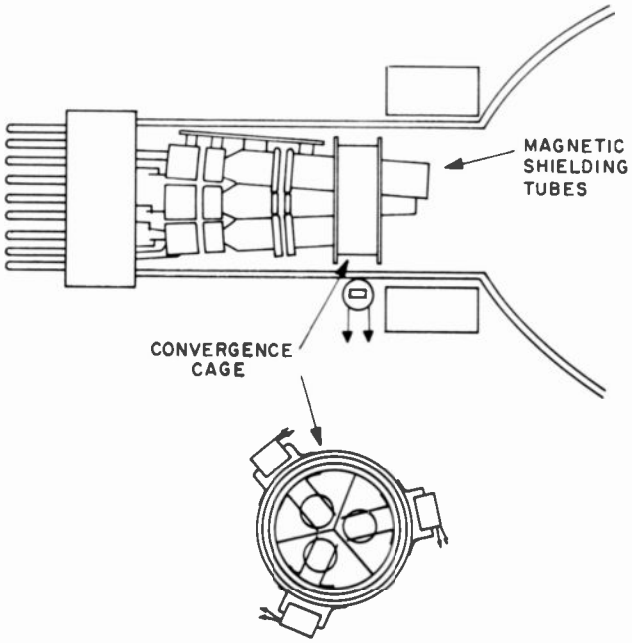

Fig. 8.12. Gun structure for three-beam penetration tube.

individually controlled radial angular displacement varying with deflection, plays an essential role. The waveforms which excite the three external electromagnets are derived from the deflection voltages.

The application of the video signals to the three-beam penetration tube differs from that to a three-beam shadow mask tube only in the addition

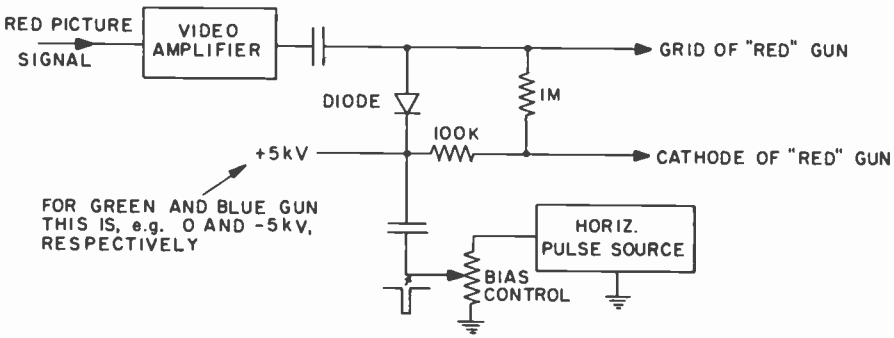

Fig. 8.13. Dc insertion in three-beam penetration tube.

of dc potentials differing by several thousand volts to the cathode. Under the circumstances the dc bias of the individual grids is derived by the rectification of horizontal pulses, capacitively coupled into the grid circuit and rectified there (Fig. 8.13) (*111*).

8.4 Summary

Penetration screens can be formed by the deposition of a sequence of flat layers by evaporation or surface reaction, by the successive laying down of fine-particle screens of different composition, or by the deposition, in a single step, of multiply coated particles on the faceplate. In all cases, the interposition of barrier layers of inactive material between the phosphor layers is essential for the attainment of an acceptable color gamut with a range of beam voltages not exceeding a ratio of 2 : 1. The presence of the barrier layers, as well as the special conditions of preparation of the screen, leads to a reduced overall conversion efficiency of the screen which tends to offset the gain realized by the absence of any form of mask between gun and screen. Furthermore, the color gamut, even when adapted to the special needs of entertainment television by the proper choice of the order of deposition of the phosphors (BGR, from the faceplate toward the gun), is still perceptibly less than for the shadow-mask and other color viewing tubes. One-gun operation requires voltage modulation of the screen which, if done at element rate, would result in circulating powers of the order of tens of kilowatts with attendant radiation-screening problems. With three-beam operation, the gun structure is rendered more complex by the necessity of magnetic screening for two of the guns; in addition, greater demands are placed on magnetic convergence correction than in other tubes.

As of 1973, one-gun penetration tubes are used in limited quantities for commercial applications, but penetration tubes are not used for consumer-type TV displays.

CHAPTER 9

Miscellaneous Color Systems

9.1 Coverage

In this chapter we consider various color television display systems which deviate materially from the conventional color viewing tube. The number of such systems is very large. We limit our consideration to those which have been subjected to extensive tests or have found at least limited application.

9.2 Flat Color Television Tubes

The primary incentive for flat television displays is to provide large-area displays of small bulk, appropriate for the living room. The same characteristics (large ratio of area to thickness) have made such displays valuable for supplying visual information to pilots, in the confined space of an airplane cockpit.

A tube particularly adapted for the second purpose is the Aiken tube (*126*, *127*), the structure of which is indicated schematically in Fig. 9.1. The electron beam is injected parallel to the screen and passes through a sequence of U-shaped horizontal deflection electrodes. These are modulated by the deflection sawtooth in such fashion that the beam encounters a transition field from anode voltage to cathode voltage at a point progressively more remote from the point of injection. Near the point of transition the beam is deflected by the transition field toward a slotted base electrode at the fixed anode potential of, for example, 1000 V, and passes through it and pairs of parallel accelerating electrodes, one on each side, into the region between the screen and a set of some eight transparent vertical

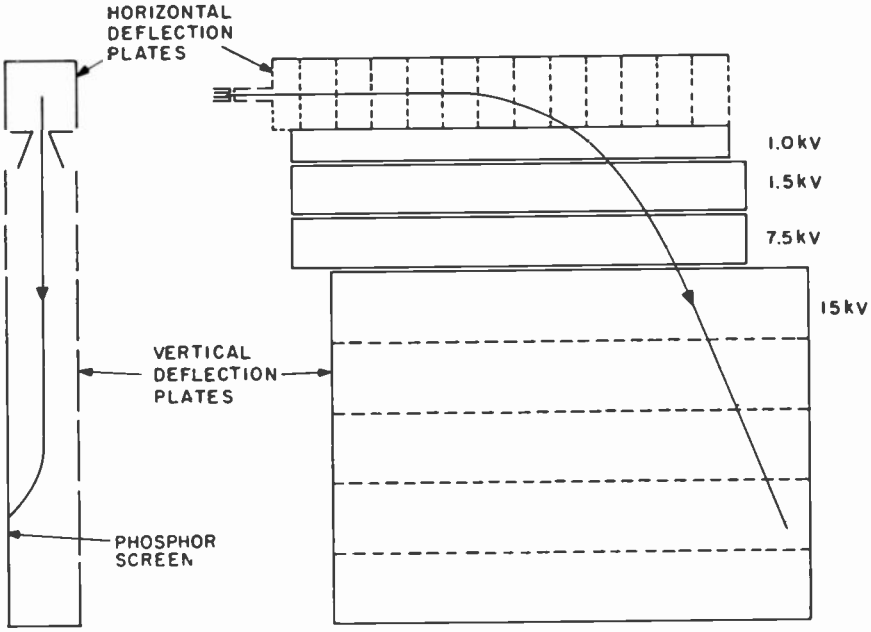

Fig. 9.1. Structure of the Aiken flat television tube (schematic).

deflection electrode strips. While the screen is maintained at a fixed voltage of 12.5–15 kV, the voltage of the vertical deflection electrodes is controlled by the vertical sawtooth in such a fashion that, again, the beam encounters a transition from screen voltage to cathode voltage at a point progressively more remote from the point of entry and is here bent toward the screen, forming the luminous scanning spot. Deflection focusing at the two points of deflection and the cylindrical lens action at the slot and between the accelerating electrodes cooperate to produce simultaneous focusing in the horizontal and vertical directions. A slight modulation of the horizontal deflection by the vertical deflection sawtooth leads to a square scanning pattern.

The phosphor screen may be transparent if desired, using an evaporation process to deposit it onto a glass substrate. For two-color operation, the gun and deflection structure may be duplicated on the two sides of the screen support, which is then coated on each side by a different color phosphor. Three-color operation can be realized by making one of the screens a line screen and placing a focus grill similar to that employed in the Lawrence tube in front of it.

The cost of the high-voltage modulation of the vertical deflection plates is one of the factors that makes such tubes noncompetitive in the entertainment field. If transparent phosphors are used, there is a sacrifice in efficiency over the more customary particulate kind, a disadvantage. Monochrome Aiken tubes with screen dimensions of 30 × 30 cm have been built and have given satisfactory performance for special applications.

Another flat tube which, from the very beginning, has been planned as a color viewing tube, is the Gabor tube, shown in Fig. 9.2 (*128*). While this extraordinarily complex device has never been completely assembled, all of the constituent parts have been examined analytically and tested experimentally. Here an in-line electron gun back of a wall with a magnetic shield generates three beams subjected to a common horizontal electrostatic deflection through a moderate angle. At the bottom of the wall the beams encounter an electrostatic reversing lens, which causes them to enter the space in front of the wall from below, greatly increasing their horizontal displacement at the same time. A stationary magnetic field gives them a vertical direction as they enter the region between the screen and an array of some 100 floating electrode strips mounted on an insulating base. These fulfill the function of the vertical deflection electrodes in the Aiken tube; however, their voltage is not modulated by an external circuit. Instead, the beam itself charges them negative during horizontal fly-back time, causing a gradual downward motion of the point of impingement of the beam on the screen during a field period. During vertical return, the same beam, at the opposite side of the screen, recharges the strips by secondary emission to anode potential, so that the next field is begun again at the top of the screen area.

The screen itself is a horizontal line color screen, with a line mask spaced about 0.5 mm from it. The large difference in the angle of incidence of the three beams, spaced apart in a direction normal to the screen (with an assumed dimension of 18 × 24 cm) leads to a mask-screen spacing which is of the same order as the width of a line trio.

9.3 Banana Color Television System

The Banana color television system was developed by Mullard Research Laboratories in England (*129–134*) with a view to minimizing the cost of the color cathode-ray tube, making the balance of the purchase price of the receiver available for auxiliary equipment. The essential components of the system are shown in section in Fig. 9.3.

The tube itself, which gives the system its name, is a long cylinder 100 mm in diameter, with a narrow neck to accommodate the electron

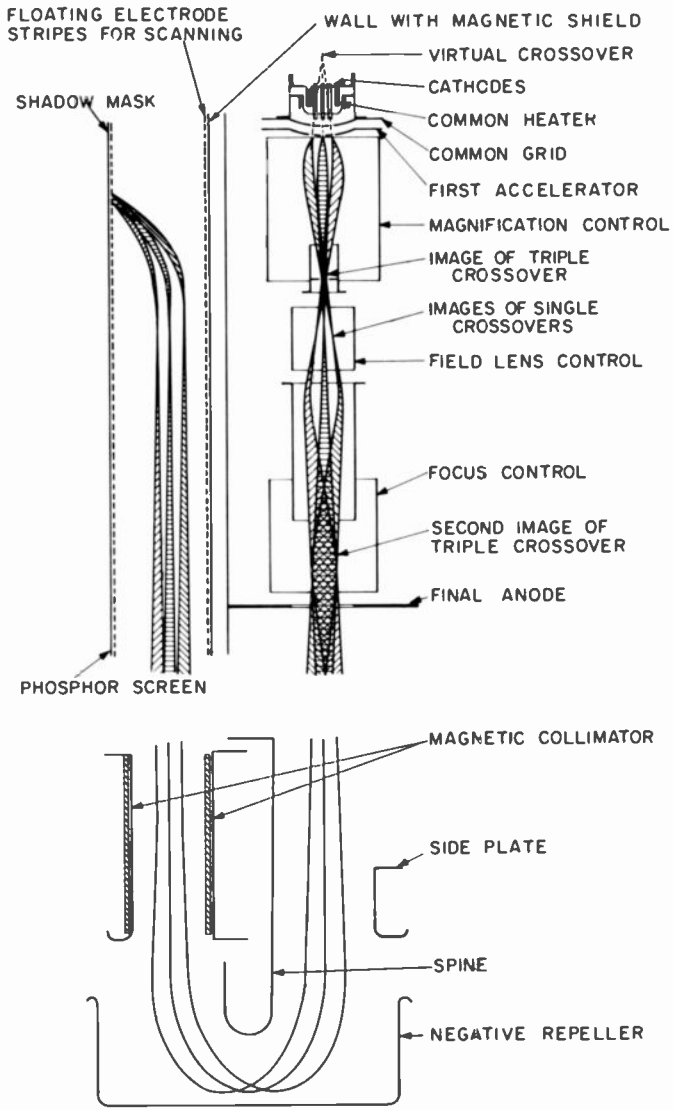

Fig. 9.2. Cross section of the Gabor flat color television tube (schematic). The three beams are electrostatically deflected through a small angle as a group in a direction normal to the diagram by a pair of deflection plates, not shown, which are located just below the final anode.

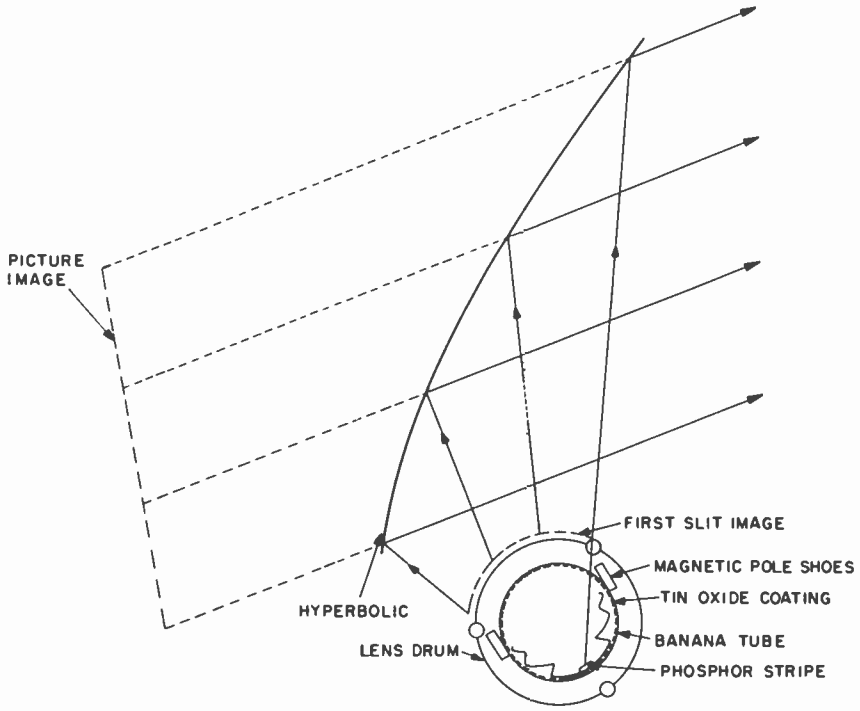

Fig. 9.3. Banana display system optics.

gun and magnetic deflection and focusing systems at one end. It contains a parallel red, green, and blue phosphor stripe, each 2 mm wide with a 1-mm separation, deposited on a metal substrate. These are scanned along the stripes by the electron beam at a line frequency of 10 kHz, the spot being at the same time displaced transversely across the line triad at the color subcarrier frequency of 2.67 MHz, corresponding to the early British 405-line standards, for which the system was designed. The length of the phosphor stripes is made equal to the width of the picture to be displayed, which was 400 mm. As shown in Fig. 9.4, the angle of incidence of the beam on the phosphor is reduced by subjecting the deflected beam to a stationary transverse magnetic field, increasing toward the end of the tube, which bends the beam toward the screen; as a result the ratio of the major to the minor axis of the spot ellipse does not exceed 2:1 even at the point farthest from the gun. Without this artifice the incidence of the beam on the screen at maximum deflection would be very nearly grazing and the spot correspondingly elongated.

Vertical picture scanning is achieved mechanically. An open-ended cylindrical drum mounted on rollers, about 150 mm in diameter and 560 mm long, surrounds the cathode-ray tube. The matte-black drum has three rod-shaped cylindrical lenses, 13 mm in diameter, mounted on its periphery, which are used in succession as the drum rotates. In combination with a stationary hyperbolic mirror, these lenses project a virtual image of the scanned phosphor lines into the picture image plane. The image position is defined by the apparent point of divergence of rays of a single object point intercepted by the pupils of the two eyes of the viewer. Since the pencil defined by these two rays is normal to the plane of the drawing in Fig. 9.3, a direction for which both the cylindrical lenses and the hyperbolic mirror have zero refractive power, the image lies behind the mirror simply by the optical distance between the phosphor stripes and the point of incidence on the mirror. The drum is rotated at 1/3 field frequency, or 1000 rpm. The distance of the mirror from the drum is made such as to realize the desired 4:3 aspect ratio; its hyberbolic shape leads to uniform displacement of the line image with the rotation of the drum.

In the plane of the drawing in Fig. 9.3, the cylindrical lenses image the phosphor strip triad into a very narrow "first slit image" close to the lens, which in turn is imaged into a slightly wider "second slit image" by the stationary mirror. The viewing rays all pass through this slit image. Since it is displaced from the picture image plane, a displacement of the viewing direction in the plane of the drawing leads to a vertical shift in the apparent image, which is unobjectionable. The aperture angle of the cylinder lenses (i.e., the diameter-to-focal length ratio), reduced by the mirror magnification of about 2, defines, furthermore, the vertical viewing angle of the system; in the horizontal direction, the viewing angle is extended to 50° by making the hyperbolic mirror 710 mm in width, i.e., nearly twice as wide as the image itself.

The reduction ratio of the width of the phosphor triad image formed by the cylindrical lenses and the hyperbolic mirror is $M = 0.2$. Thus, the apparent triad width is about 1.4 mm or 1.5 scanning-line width. The

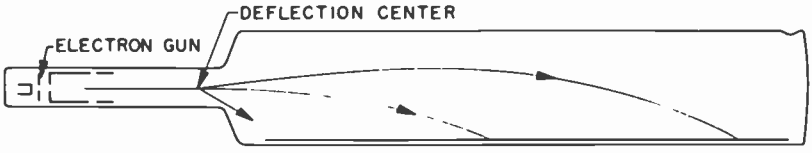

Fig. 9.4. Beam paths in the Banana tube.

corresponding vertical displacement of the three, red, green, and blue component images relative to each other, by a fraction of a line width, leads to no appreciable deterioration in image definition.

The apparent picture brightness is also proportional to the reduction ratio M. Since, apart from optical absorption and reflection losses, the brightness of the phosphor line image is equal to that of the object, the amount of light intercepted by the eyes of the viewer is simply proportional to the image width, or to M. If T is the optical transmission factor of the system, C, the mean conversion efficiency (measured, for example, in lm/W) of the phosphor screen, I, the average beam current, V, the accelerating voltage, and A, the image area, the image brightness can be written

$$B = (TCIVM)/A \tag{9.1}$$

Here the transmission factor can be held close to 0.9. Spot sizes from 0.5 mm × 0.5 mm at the tube end closest to the gun to 1.0 mm × 0.6 mm at the far end of the phosphor stripes could be realized for $I = 400$ μA and V = 25 kV, yielding satisfactory color purity with a total duty cycle of about 85%. Picture brightnesses up to 100 cd/m² were reported for an image area of 0.12 m². With 16% blanking time, Eq. (9.1) would imply a mean phosphor conversion efficiency of 25 lm/W.

In the Banana tube, the average loading of the phosphor is comparable to that in a projection tube (0.5 W/cm²), although the maximum instantaneous power density is very much less. The metallic substrate with corrugated blackened radiating fins prevents excessive temperature rise and consequent reduction in phosphor efficiency. Sulfide phosphors with persistence less than 0.1 msec are employed to prevent vertical streaking.

Since both the drum and the screen support are blackened, the picture contrast is singularly insensitive to ambient illumination; at any one time, only 1.5 scanning lines of the image area act as effective scatterers of ambient light. However, although the Banana color television system is outstanding in this respect and appears to give acceptable results in picture brightness and definition, the mechanical scanning would seem to constitute a material drawback from the point of view of noise and maintenance. Furthermore, the fact that the picture is at some distance behind the viewing mirror demands, as already noted, that the apparatus be much wider than the picture itself. This would make it scarcely competitive with present compact wide-angle shadow-mask tube receivers.

9.4 Projection Systems

Color television projection systems can operate with three cathode-ray tubes or with a single cathode-ray tube; they may, furthermore, serve

two different functions; the projection of large pictures, suitable for viewing by audiences in theaters or lecture halls, or of pictures suitable for individual viewing, in the home or on color monitors in broadcast studios.

The simplest color projection systems employ three monochrome kinescopes, each mounted in its individual Schmidt projection system, as shown in Fig. 9.6a. The Schmidt projector, consisting of a spherical mirror with an aspheric correction plate near its center of curvature, is universally preferred to projection lenses in view of its very large optical efficiency (F-numbers of the order of 0.7), optical simplicity, and compactness. If the image distance is relatively small, as it is in projection systems for individual viewing, the light from the three Schmidt projectors is superposed by a pair of crossed dichroic mirrors (Fig. 9.5) with the properties that one of them transmits blue and green light and reflects red light, whereas the other transmits red and green light and reflects blue light. The compactness is here maximized and the size of the dichroic mirrors minimized by the employment of folded Schmidt systems (Fig.

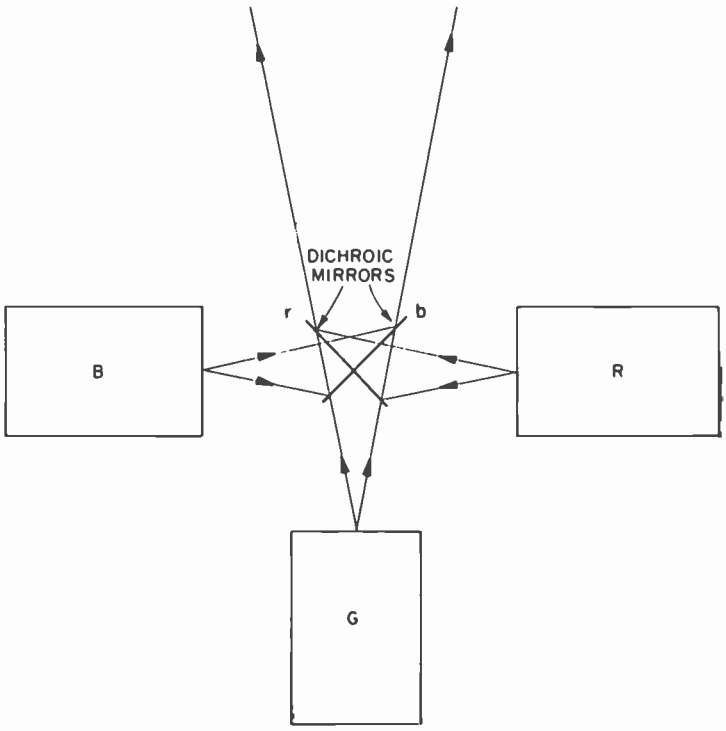

Fig. 9.5. Image superposition with crossed dichroic mirrors.

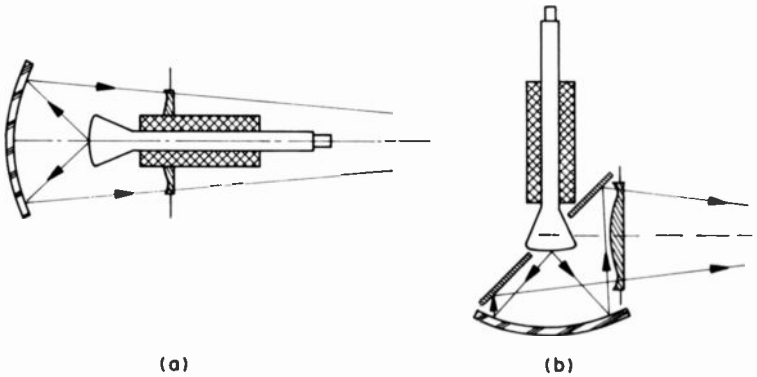

Fig. 9.6. (a) In-line and (b) folded Schmidt projection systems.

9.6b), in which a 45° mirror causes the imaging beam to emerge at right angles to the tube axis. With the dichroic mirrors the optical registration of the three component images is perfect and there are no registration errors, provided that the three optical systems, kinescopes, and scanning patterns are identical.

If the image distance is very large, as is commonly the case in theater projection, the dichroic mirrors become superfluous. The three Schmidt projectors are placed simply side-by-side, the in-line form (Fig. 9.6a) being preferred because of its greater symmetry. The keystone error resulting from the slight tilt of the two lateral systems (Fig. 9.7) required to achieve image superposition can be adequately compensated by a slight modification of the scanning waveforms.

Poorter and de Vrijer (*135*) have studied systems of both types. Pictures 3 m × 2.25 m in size with a maximum luminance of 20 cd/m² were obtained with three 130 mm kinescopes operating at 50 kV in in-line Schmidt projectors; folded Schmidts with crossed dichroics yielded half the screen brightness and lower definition with otherwise similar dimensions. In both cases the directional gain of the screen was 2.8. Smaller pictures (46 cm × 35 cm) with a maximum luminance of 200 cd/m² were obtained with folded Schmidts and dichroics using kinescopes with 60-mm diam screens operating at 25 kV and viewing screens with a directional gain of 7.

Color television pictures of considerably larger size than 3 m × 2.25 m have been projected with Schmidt systems. Thus Evans and Little (*136*) describe a projector with three in-line Schmidts forming images 6 m × 4.5 m in size on an embossed aluminum screen, with a luminance of 18 cd/m². Here the projection kinescopes had 180-mm diam screens and were operated

at 80 kV; the Schmidt mirrors were 660 mm in diameter. Normally, however, Schmidt color television projectors are used only for medium-sized screens (e.g., 1.5- to 3-m diagonal) and employ projection kinescopes of small dimensions (60 mm) and moderate operating voltage (~25 kV) (*137*).

Color television projection systems have also been proposed in which the cathode-ray tubes, instead of supplying the screen illumination, act as light valves, controlling light derived from an external source. The only successful systems of this kind incorporate the Eidophor principle, pioneered by F. Fischer in Zurich (*138*). The Eidophor is also the prototype

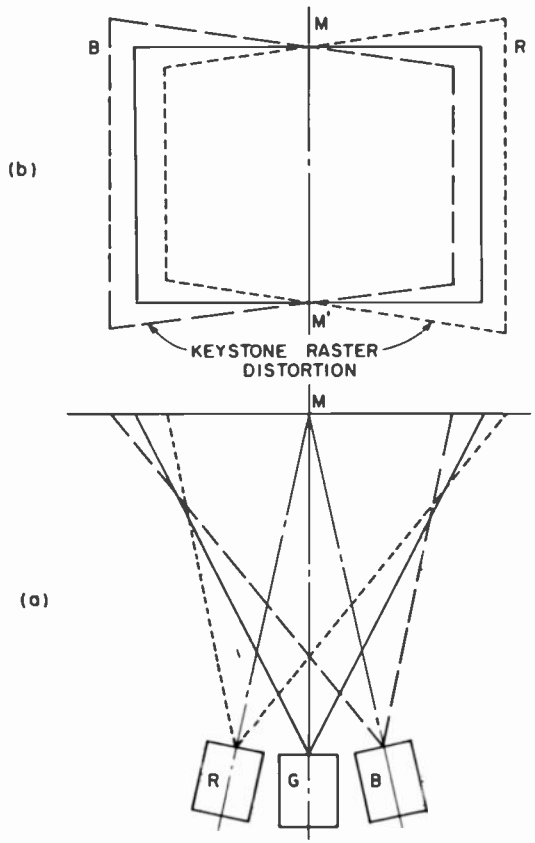

Fig. 9.7. Origin of keystone error in the superposition of images from three projectors placed side by side.

of the ingenious oil-film color projection systems described more recently by W. E. Good (*139*) and his associates at the General Electric Company. In the Eidophor a low-vapor-pressure oil film on the target surface of a cathode-ray tube is inserted in a schlieren optics system which transmits light from a powerful external light source (mercury or xenon arc) to the screen only when high-frequency velocity modulation of the scanning beam imparts a grating-like modulation to the oil surface. For color projection, three Eidophors may be used, the light from the source being first split into its red, green, and blue components by a dichroic mirror system (*140*); the images formed by the three Eidophors are recombined at the screen. Figure 9.8 shows schematically one branch of the system. The incident light is reflected completely by a set of mirror stripes onto the oil film deposited on a concave mirror surface. In the absence of film modulation the light reflected by the concave mirror is fully intercepted by the mirror stripes. With modulation, light is diffracted so as to pass

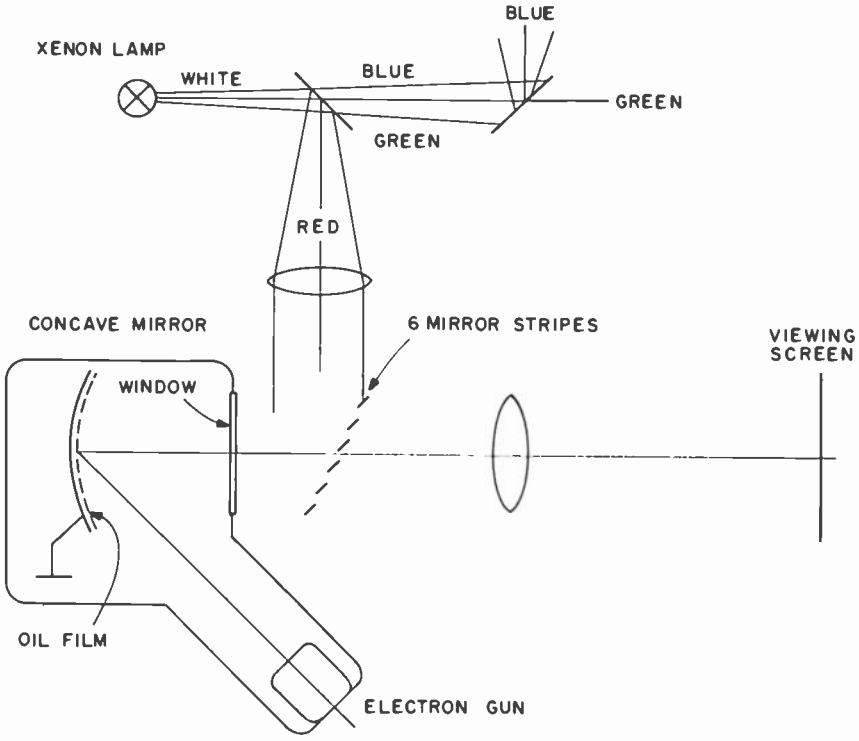

Fig. 9.8. Eidophor system for color projection.

through the interstices between the mirror stripes and, thus, contributes to the image formed on the screen.

Good and his co-workers (*141–143*) have introduced an important modification of the Eidophor principle, based on earlier work by Glenn (*144*), making it possible to use a single tube with white-light illumination for the projection of color television images. The basic idea is to utilize the modulation of the oil film in a direction transverse to the scanning lines to control the green content of the picture and modulation at two different frequencies along the scanning lines to control the red and blue components of the picture, the schlieren optics system being designed so as to select out radiation of the appropriate wavelength range from the light diffracted by the grating patterns on the oil film. This system has been shown capable of projecting color pictures with a brightness of 35 cd/m² on a 3-m wide screen with a directional gain of 2.5, a contrast range of 50:1, acceptable color rendition, and a picture resolution up to 400 TV lines. The light source employed to achieve this is a 650-W xenon arc. The light-valve modulation is controlled by an electron beam with 5-μA beam current and 8 kV anode voltage.

A number of the optical and electron-optical design features of the system are evident from Fig. 9.9. The light flux for illuminating the light valve is supplied by a sealed-beam xenon arc lamp L with an elliptical cold-coating reflector, which images the small arc source at the center of the scanning raster (Fig. 9.10). A filter disk, with a central magenta

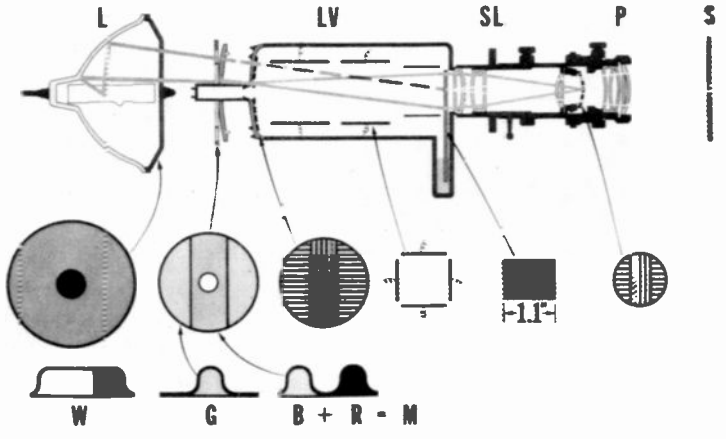

Fig. 9.9. Schematic diagram of single-gun color TV light valve (*142*). L-Xenon arc lamp with elliptical reflector; LV-light valve; SL-schlieren lens; P-projection lens; S-screen.

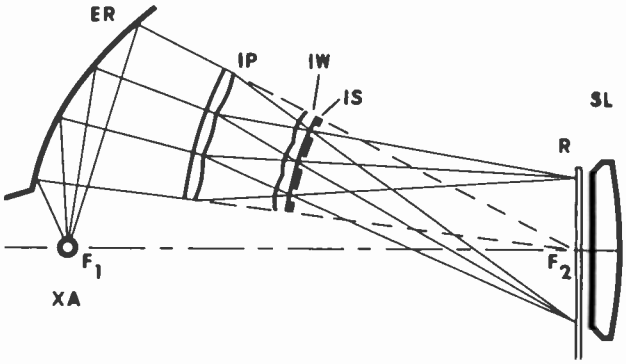

Fig. 9.10. Schematic diagram of optical system for illuminating raster plane of single-gun color TV light valve (*142*). XA-Xenon arc; ER-Elliptical reflector; F_1 and F_2-Foci of elliptical reflector; IP-Lenticular plate imaging arc source into slots of input bar patterns; IW-Lenticular plate imaging individual lenticules of IP onto raster frame; IS-Input bar pattern; R-Raster frame; SL-schlieren lens.

band and outer green bands is mounted on the electron-gun neck of the light valve and divides the light flux into magenta and green portions. This is followed by a second disk with some 600 rectangular lenticules which concentrate the light falling on them on the clear slots of the input bar system, deposited on the window of the light-valve tube LV. A second lenticular plate, located just to the left of the input bar system, images the individual lenticules of the first lenticular plate on the 28-mm wide raster surface. Thus, while the first lenticular plate increases the light transmission of the input bar system by a factor of about 4, the second assures great uniformity of the illumination of the raster surface with the magenta and green components of the white light.

The input bar disk is imaged by a schlieren lens SL located just beyond the light-valve raster frame onto an output bar disk with complementary bars and slots, so that no light is transmitted when the oil film is smooth. Furthermore, since the bars in the portion of the bar pattern illuminated by green light are horizontal and those illuminated by magenta (red plus blue) light are vertical, modulation of the oil film in the vertical direction results in the transmission of green light, whereas modulation of the film in a horizontal direction results in the transmission of red or blue light. The projection lens P, finally, images the raster frame on the viewing screen S, utilizing the light transmitted by the output bar system.

The scanning beam in the light valve is electrostatically focused and deflected by a sequence of large-aperture electrodes. Since the scanning spot so obtained has about 1/2000 the width of the raster, it can generate grating patterns with a sufficient number of periods per picture element to achieve adequate color resolution for red and blue. The green resolution is not limited horizontally by the schlieren system.

In the absence of a green signal voltage, the scanning beam is vertically defocused so as to produce a smooth field. A VHF voltage with a signal amplitude of 1 V applied to the vertical deflection plates is sufficient to produce maximum green intensity at a picture element. Signal amplitudes of the same amplitude at 16 MHz and 12 MHz applied to the horizontal deflection plates produce maximum red and blue intensities, respectively. To transmit only red light, the grating pattern (corresponding to 16 MHz) is matched to the bar spacing in the output bar pattern so that the different orders of blue radiation at, e.g., 450 nm from any one slot of the input bar pattern, are centered on successive adjoining bars of the output bar pattern; for the transmission of blue light at 450 nm, the different orders of red radiation at 600 nm are then blocked by the same bars when a 12-MHz deflection voltage is applied to the horizontal plates. The low signal amplitudes required for light modulation follow from the fact that the groove depth of the diffraction gratings need be only a fraction of a wavelength of light to produce maximum intensity at the screen.

The electrical and mechanical properties of the film are made such that the relaxation time of the thickness modulation approximately equals a field period; this provides the best compromise between maximum light transmission and minimum picture lag. The output bar pattern then has a maximum transmission approximately equal to 65% for each color. Glenn (*145*) has discussed in some detail the factors governing the relaxation properties of the oil film, as well as the design of the electron gun and alternative choices for the schlieren optics. In the commercial system the synthetic oil film is continuously renewed by rotating the disk supporting the film at a speed of three revolutions per hour, with the lower part of the disk dipping into an oil sump. The drive for the disk is magnetically coupled to a small motor through the glass wall of the light-valve chamber. With a small electronic vacuum pump mounted on the latter, a lifetime in excess of 1000 hr has been realized. The overall optical efficiency of the system is such that, of the 11,000 lumens emitted by the xenon arc, over 300 lumens may contribute to the picture on the screen.

Finally, it should be mentioned that color television pictures have been projected on viewing screens by the simple expedient of direct imaging of the screen of a conventional color viewing tube. For large magnification

M, the brightness B of the image on the viewing screen can be expressed by the brightness B_0 of the image on the tube screen by

$$B = B_0 TG[1/(M + 1)^2][1/(2\nu)^2] \tag{9.2}$$

Here T is the optical transmission of the system (including the reflection efficiency of the viewing screen), G is the directional gain of the viewing screen, and ν is the F-number of the imaging system. With the exception of G, the four factors on the right of Eq. (9.2) are all less than 1. Furthermore, for infinite G (i.e., an idealized corner-cube screen), for which Eq. (9.2) ceases to be valid, we would find simply $B \to B_0 T$, with the viewing angle limited to

$$[2/(M + 1)] \arcsin (1/2\nu)$$

In practice, the accommodation of a reasonably large audience limits the directional gain to about 7. We then find for a magnification $M = 5$ for an imaging system with the very small F-number 0.75 and an optical transmission of 0.5,

$$B = 0.043\, B_0$$

A material gain in picture size can thus only be realized at the cost of greatly reduced picture brightness. Furthermore, since good definition in conventional color viewing tubes can be obtained only with relatively large viewing screens, the large-aperture optical system required becomes both cumbersome and costly. The direct projection imaging of conventional color viewing tube screens is thus quite limited in its application.

CHAPTER 10

Present Status and Future

Color television picture tubes have been the subject of active research and development since the late 1940's. During this time many reproducer systems have been invented and a few have been intensively investigated in research laboratories. Most, if not all, of the more promising of these have been described earlier in this paper.

Although the shadow-mask system has dominated the field for consumer-type color television displays, there is continuing interest in other systems, mainly because of certain outstanding features the system might have. For example, penetration color kinescopes offer picture reproduction without color-element structure. Beam-index color tubes are characterized by sharp, perfectly registered color pictures since the nature of the tube operation requires a single gun for producing the picture where the gun must deliver a very small electron spot. Focusing tubes are still intriguing because they offer potential large increases in mask transmission with resulting brighter pictures. However, since the early 1960's, most effort has gone into improving shadow-mask tube performance. Many technical details of this work have been discussed in this paper.

Particularly in the United States, great emphasis has been placed on improving picture brightness. Figure 10.1 shows the progress made per unit of beam power through improved phosphors and the use of matrix-screen tubes. Improved electron guns have also contributed to brighter pictures by providing small spots with higher beam current. Operation at voltages up to the limit of practical x-ray protection has been the rule to enhance overall operating performance.

Maximum picture size has remained relatively stable at about 626-mm diag. with a trend to shorter tubes made possible by an increase in deflection angle. Pictures of even larger size and improved performance capability

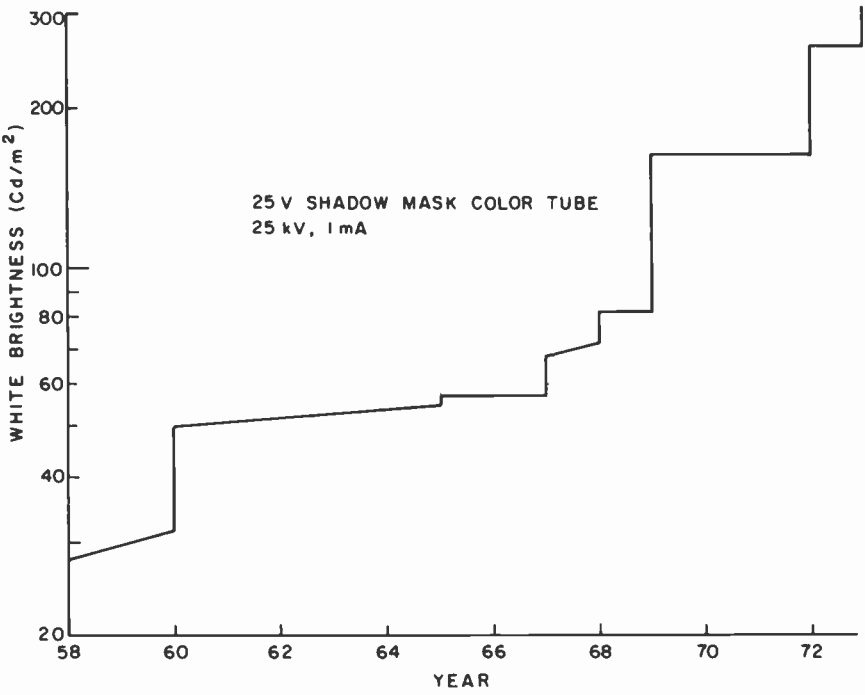

Fig. 10.1. Progress made in improving brightness of shadow-mask color tubes.

may be useful if concepts materialize for an expanded range of services into the home via wideband cable. However, physical and economic limitations are severe for extension of the 626-mm shadow-mask system to significantly larger size. This situation could be avoided if the intensified effort in the early 1970's on thin, flat, commercial matrix displays is successfully extended to displays suitable for color TV picture presentation; but, although great progress has been made through use of solid-state technology, the technical-economic problems yet to be solved for a large, flat, high quality, color TV display are truly enormous.

There is a trend to simplified, small color systems of 480-mm diag. or less, as exemplified by shadow-mask systems employing in-line guns. The in-line geometry has distinct advantages in simplifying convergence or even eliminating dynamic convergence.

Undoubtedly further improvements in color picture tube performance will be made but increasing attention will probably be given to reliability and lowering of costs in order to complement advances made in the receiver system through use of solid-state circuits.

References

1. E. W. Herold, Methods suitable for television color kinescopes. *Proc. IRE* **39**, 1177–1185 (1951); also in *RCA Rev.*, **12**, 445–465 (1951).
2. P. C. Goldmark, J. N. Dyer, E. R. Piore, and J. M. Hollywood, Color television—Part I. *Proc. IRE* **30**: 162–182 (1942); P. C. Goldmark, E. R. Piore, J. M. Hollywood, and T. H. Chambers, Color television—Part II. *Proc. IRE* **31**: 465–478 (1943).
3. T. R. Kennedy, Jr., RCA shows all-electronic tube as key to color television. *The New York Times* **XCIX**, No. 33,667 (1950); see, also, General description of receivers which employ direct-view tri-color kinescopes. *RCA Rev.* **11**: 228–232 (1950).
4. H. B. Law, A three-gun shadow-mask color kinescope. *Proc. IRE 39*, 1186–1194 (1951); also in *RCA Rev., 12*, 466–486 (1951).
5. A. C. Schroeder, Picture reproducing apparatus. U. S. Patent 2,595,548 (1952).
6. N. F. Fyler, W. E. Rowe, and C. W. Cain, The CBS Colortron. *Proc. IRE* **42**, 326–334 (1954).
7. H. B. Law, Photographic methods of making electron-sensitive mosaic screens. U. S. Patent 3,406,068 (1968).
8. New Lawrence tricolor tube shown, *Electronics* **24**, 146 (1951).
9. R. G. Clapp, E. M. Creamer, S. W. Moulton, and M. E. Partin, A new beam-indexing color television display system. *Proc. IRE* **44**, 1108–1114 (1956).
10. R. Dressler, The PDF Chromatron—a single or multi-gun cathode-ray tube. *Proc. IRE* **41**, 851–858 (1953).
11. C. G. Lob, General Electric post-acceleration color tube. *IRE Nat. Conv. Rec.* **4**, Part 3, 114–117 (1956).
12. E. G. Ramberg, H. B. Law, H. S. Allwine, D. C. Darling, C. W. Henderson, and H. Rosenthal, Focusing-grill color kinescopes. *IRE Nat. Conv. Rec.* **4**, Part 3, 128–134 (1956).
13. H. R. Seelen, H. C. Moody, D. D. Van Ormer, and A. M. Morrell, Development of a 21-inch metal envelope color kinescope. *RCA Rev.* **16**, 122–139 (1955).
14. R. B. Janes, L. B. Headrick, and J. Evans, Recent improvements in the 21AXP22 color kinescope. *RCA Rev.* **17**, 143–167 (1956).
15. C. P. Smith, A. M. Morrell, and R. C. Demmy, Design and development of the 21CYP22, 21-inch glass color picture tube. *RCA Rev.* **19**, 334–348 (1958).
16. A. M. Morrell and A. E. Hardy, Development of the RCA 25-inch 90-degree rectangular color picture tube. *IEEE Trans. Broadcast Telev. Receivers* [N.S.] **10**, 15–22 (1964).

17. A. M. Morrell, Development of the RCA family of 90-degree rectangular color picture tubes. *IEEE Trans. Broadcast Telev. Receivers* [N.S.] **11**, 90–95 (1965).

18. R. H. Godfrey, T. M. Shrader, and R. C. Demmy, Development of the permachrome color picture tube. *IEEE Trans. Broadcast Telev. Receivers* [N.S.] **14**, 8–11 (1968).

19. C. W. Thierfelder, RCA large-screen, narrow-neck 110-degree color television system. *IEEE Trans. Broadcast Telev. Receivers* [N.S.] **17**, 141–147 (1971).

20. J. P. Fiore and S. H. Kaplan, The second generation color tube providing more than twice the brightness and improved contrast. *IEEE Trans. Broadcast Telev. Receivers* [N.S.] **15**, 267–275 (1969).

21. A. K. Levine and F. C. Palilla, A new highly-efficient red emitting cathodoluminescent phosphor. *Appl. Phys. Lett.* **5**, 118–120 (1964).

22. A. E. Hardy, The performance of color television picture tube phosphor screens. *IEEE Trans. Broadcast Telev. Receivers* [N.S.] **11**, 33–37 (1965).

23. GE 11-inch color TV: The new look in color receivers. *Electron. World* **75**, No. 3, 39–41 (1966).

24. S. Yoshida and A. Ohkoshi, The Trinitron—a new color tube. *IEEE Trans. Broadcast Telev. Receivers* [N.S.] **14**, 19–27 (1968).

25. R. L. Barbin and R. H. Hughes, A new color picture tube system for portable TV receivers. *IEEE Trans. Broadcast Telev. Receivers* [N.S.] **18**, 193–200 (1972).

26. A. H. Holway and E. G. Boring, Determinants of apparent visual size with distant variant. *Amer. J. Psychol.* **54**, 21–37 (1941).

27. O. H. Schade, A method of measuring the optical sine-wave spatial spectrum of television image display devices. *J. SMPTE (Soc. Motion Pict. Telev. Eng.)* **67**, 561–566 (1958).

28. R. L. Donofrio, Image sharpness of a color picture tube by modulation transfer techniques. *IEEE Trans. Broadcast Telev. Receivers* [N.S.] **18**, 1–6 (1972).

29. R. D. Kell, A. V. Bedford, and G. L. Fredendall, A determination of optimum number of lines in a television system. *RCA Rev.* **5**, 8–30 (1940).

30. G. C. Higgins and F. H. Perrin, The evaluation of optical images. *Photogr. Sci. Eng.* **2**, 66–76 (1958).

31. Unpublished work of P. Warter, formerly at RCA Laboratories. See also E. W. Engstrom, A study of television image characteristics. Part 2. Determination of frame frequency in terms of flicker characteristics. *Proc. IRE* **23**, 295–310 (1935).

32. W. D. Wright, "The Measurement of Colour," 4th ed., Van Nostrand Reinhold, Princeton, New Jersey, 1969.

33. D. B. Langmuir, Limitations of cathode-ray tubes. *Proc. IRE* **25**, 977–991 (1937).

34. M. Ploke, Elementary theory of electron beam formation with triode systems. *Z. Angew. Phys.* **3**, 441–449 (1951); **4**, 1–12 (1952).

35. E. G. Ramberg, Variation of axial aberrations of electron lenses with lens strength. *J. Appl. Phys.* **13**, 582–594 (1942).

36. M. von Ardenne, "Tabellen zur angewandten Physik," Vol. 1, pp. 46–47. VEB Deutscher Verlag Der Wissenschaften, Berlin, 1962.

37. M. Morikawa, Polynomial approximation to focal constants of equidiameter two-cylinder lenses. *J. Appl. Phys.* **34**, 1657–1660 (1963).

38. J. W. Schwartz, Space-charge limitation on the focus of electron beams. *RCA Rev.* **18**, 1–11 (1957).

39. S. Miyaoka, A. Ohkoshi, and S. Yoshida, The Trinitron—a new color TV tube. *IEEE Student J.* **8**, 11–15 (1970).

40. J. Hasker, Astigmatic electron gun for the beam-indexing color television display. *IEEE Trans. Electron Devices* **18**, 703–712 (1971).

41. H. B. Law, Art of making color-kinescopes, etc. U. S. Patent 2,625,734 (1953).

42. N. B. Mears, Method and apparatus for producing perforated metal webs. U. S. Patent 2,762,149 (1956).

43. N. S. Freedman and K. M. McLaughlin, Phosphor-screen application in color kinescopes. *Proc. IRE* **39**, 1230–1236 (1951).

44. M. J. Grimes, A. C. Grimm, and J. F. Wilhelm, Improvements in the RCA three-beam shadow-mask color kinescope. *Proc. IRE* **42**, 315–326 (1954).

45. B. E. Barnes and R. D. Faulkner, Mechanical design of aperture mask tri-color kinescope. *Proc. IRE* **39**, 1241–1245 (1951).

46. R. R. Law, A one-gun shadow-mask color kinescope. *Proc. IRE* **39**, 1186–1194 (1951).

47. E. G. Ramberg, Elimination of moiré effects in tri-color kinescopes. *Proc. IRE* **40**, 916–923 (1952).

48. J. D. Robbins and D. G. Mackey, Moiré pattern in color television. *IEEE Trans. Broadcast Telev. Receivers* [N.S.] **12**, 105–121 (1966).

49. P. G. J. Barten, Cathode ray tube for displaying color pictures. U. S. Patent 3,486,061 (1969).

50. D. W. Epstein, P. Kaus, and D. D. Van Ormer, Improvement in color kinescopes through optical analogy. *RCA Rev.* **16**, 491–497 (1955).

51. S. H. Kaplan, Error correction in mask type colour television tubes. *J. Telev. Soc.* **8**, 470–480 (1958).

52. A. M. Morrell, Color kinescopes, etc. U. S. Patent 2,855,529 (1958).

53. F. Herzfeld and F. van Hekken, Cathode ray tube and method of manufacture. U. S. Patent 3,476,025 (1969).

54. E. G. Ramberg and D. W. Epstein, Optical system for use in making color-phosphor mosaic screens. U. S. Patent 3,385,184 (1968).

55. E. Yamazaki, K. Maruyama, and I. Ogura, Correcting lens. U. S. Patent 3,628,850 (1971).

56. E. Yamazaki, K. Maruyama, and I. Ogura, A segmented lens for improving color television dot patterns. *J. SMPTE (Soc. Motion Pict. Telev. Eng.)* **82**, 149–150 (1973).

57. S. Larach and A. E. Hardy, Cathode-ray-tube phosphors: Principles and applications. *Proc. IEEE* **61**, 915–926 (1973).

58. A. Bril and H. A. Klasens, Phosphors for tricolour television tubes, *Philips Res. Rep.* **10**: 305–318 (1955).

59. G. A. Burdick, R. C. Miller, and B. E. Bartels, The performance of europium-activated phosphors in color picture tubes. *Electrochem. Technol.* **4**, 12-15 (1966).

60. A. K. Levine and F. C. Palilla, YVO_4: Eu, a new highly efficient phosphor for color television. *Electrochem. Technol.* **4**, 16-20 (1966).

61. S. Z. Toma, F. F. Mikus, and J. E. Mathers, Energy transfer and fluorescence processes in Bi^{3+} activated YVO_4. *J. Electrochem. Soc.* **114**, 953–955 (1967).

62. R. K. Datta, Bismuth in yttrium vanadate and yttrium europium vanadate phosphors. *J. Electrochem. Soc.* **114**, 1057–1063 (1967).

63. A. E. Hardy, The Performance characteristics of yttrium oxysulfide—a new red phosphor for color television. *IEEE Trans. Electron Devices* **15**, No. 11, 868-872 (1968).

64. S. Levy and A. K. Levine, The preparation of phosphor screens for color television tubes. *J. Electrochem. Soc.* **101,** 99 (1964).
65. T. V. Rychlewski, Method of forming patterns. U. S. Patent 3,025,161 (1962).
66. S. Yoshida, A. Ohkoshi, and S. Miyaoka, A wide-deflection angle (114°) Trinitron color picture tube. *IEEE Trans. Electron Devices* **19,** No. 4, 231–238 (1973).
67. W. D. Masterton and R. L. Barbin, Development and performance of the RCA 19V and 18V 110° color picture tubes and deflection yoke. *Electronics* **44,** No. 9, 60–64 (1971).
68. J. P. Fiore *et al.*, Cathode-ray tube with color dots spaced by light-absorbing areas. U. S. Patent 3,146,368 (1964).
69. E. E. Mayaud, Method for producing a graphic image. U. S. Patent 3,558,310 (1971).
70. S. H. Kaplan, Control of fluorescent screen dot size for color TV. *J. SMPTE (Soc. Motion Pict. Telev. Eng.)* **65,** 407–410 (1956).
71. S. H. Kaplan, Process of screening a shadow-mask color tube. U. S. Patent 3,666,462 (1972).
72. E. F. deHaan and H. Zimmer, Postfocussing colour tubes. *Acta Electron.* **2,** 189–193 (1957–1958).
73. E. B. Noel and R. E. Farnham, A water-cooled quartz mercury arc. *J. Soc. Motion Picture Eng.* **31,** 221–239 (1938).
74. R. R. Bathelt and G. A. W. Vermeulen, Experimental fluorescent screen in direct-viewing tubes for colour television. *Philips Tech. Rev.*, **23,** 133–141 (1962).
75. Y. Naruse, K. Utsonomiya, and Y. Fuse, An improved shadow-mask design for in-line three beam color picture tubes. *IEEE Trans. Electron Devices* **18,** No. 9, 697–702 (1971).
76. R. B. Ashley, Simplified deflection system for plural in-line beam cathode-ray tube. U. S. Patent 3,430,099 (1969).
77. Color TV KV-1710 (with 17V, 90° Trinitron picture tube). "Sony Service Manual." 1971.
78. C. J. Davisson and C. J. Calbick, Electron lenses. *Phys. Rev.* **38,** 585 (1931); **42,** 580 (1932).
79. W. Flechsig, Cathode-ray tube for the production of multicolored pictures on a luminescent screen. French Patent 866,065 (1941).
80. A. C. Schroeder, Color television tube. U. S. Patent 2,446,791 (1948).
81. Phosphor strip color tube. *Electronics* **24,** 89–91 (1951).
82. B. D. Loughlin, A review of some of the recent developments in color television. *IRE Trans. Broadcast Telev. Receivers* [N.S.] **8,** 55–69 (1962).
83. H. Heil, Correct prints of color tube screen. *IRE Nat. Conv. Rec.* **4,** Part 3, 118–121 (1956).
84. J. M. Lafferty, Beam deflection color picture tubes. *Proc. IRE* **42,** 1478–1495 (1954).
85. C. P. Carpenter, C. W. Helstrom, and A. E. Anderson, An analysis of focusing and deflection in the post-deflection-focus color kinescope. *IRE Trans. Electron Devices* **2,** 1–7 (1955).
86. D. W. Epstein and E. G. Ramberg, Post-accelerated color-kinescopes. U. S. Patent 2,795,720 (1957).
87. K. Gentner, On the energy absorption of fast cathode rays. *Ann. Phys. Leipzig* [5] **31,** 407–424(1938).

88. P. Palluel, Status of our knowledge of the secondary emission of solids. *Ann. Radioelec.* **2**, 199–223 (1947).

89. E. G. Ramberg, Cathode-ray tubes of the lenticular grill variety. U. S. Patent 2,728,024 (1955).

90. M. E. Amdursky, R. G. Pohl, and C. S. Szegho, A new high-efficiency parallax-mask color tube. *Proc. IRE* **43**, 936–943 (1955).

91. N. Fyler, C. Cain, and P. Hambleton, The unipotential mask-focusing Colortron. *IRE Nat. Conv. Rec.* **4**, Part 3, 122–127 (1956).

92. L. Blaser and D. Bray, Chromatron television color processing using semiconductor circuits. *IEEE Trans. Broadcast Telev. Receivers* [N.S.] **11**, 38–49 (1965).

93. J. D. Gow and R. Dorr, Compatible color picture presentation with the single-gun tricolor Chromatron. *Proc. IRE* **42**, 308–314 (1954).

94. Y. Sugihara, H. Ito, and A. Horaguchi, From Japan, a startling new color television set. *Electronics* **38**, 81–85 (1956).

95. V. K. Zworykin, Television system. U. S. Patent 1,691,324 (1928).

96. D. S. Bond, F. H. Nicoll, and D. G. Moore, Development and operation of a line-screen color kinescope. *Proc. IRE* **39**, 1218–1230 (1951).

97. J. S. Bryan, R. G. Clapp, E. M. Creamer, S. W. Moulton, and M. E. Partin, A new color television display—the Apple system. *IRE Nat. Conv. Rec.* **4**, Part 3, 94–100 (1956); *Proc. IRE* **44**, 1108–1114 (1956).

98. E. F. deHaan and K. R. U. Weimer, The beam indexing colour display tube. *R. Telev. Soc. J.* **11**, 278–282 (1967).

99. G. J. Lubben, The index tube. *Onde Elec.* **48**, 918–920 (1968).

100. R. Graham, J. W. H. Justice, and J. K. Oxenham, Progress report on the development of a photo-electric beam-index colour-television tube and system. *Proc. Inst. Elec. Eng., Part B* **108**, 511–523 (1961).

101. G. R. Barnett, F. J. Bingley, S. L. Parsons, G. W. Pratt, and M. Sadowsky, A beam-indexing color picture tube—the Apple tube. *Proc. IRE* **44**, 1115–1119 (1956); *IRE Nat. Conv. Rec.* **4**, Part 3, 101–106 (1956).

102. R. A. Bloomsburgh, W. P. Boothroyd, G. A. Fedde, and R. C. Moore, Current status of Apple receiver circuits and components. *Proc. IRE* **44**, 1120–1124 (1956); *IRE Nat. Conv. Rec.* **4**, Part 3, 107–112 (1956).

103. B. D. Loughlin, Processing of the NTSC color signal for one-gun sequential color displays. *Proc. IRE* **42**, 299–308 (1954).

104. J. B. Chatten and R. A. Gardner, Accuracy of color reproduction in the 'Apple' system. *IRE Nat. Conv. Rec.* **5**, Part 3, 230–237 (1957).

105. P. M. van den Avoort, Signal processing in the index tube. *Onde Elec.* **48**, 921–924 (1968).

106. R. A. Bloomsburgh, A. Hopengarten, R. C. Moore, and H. H. Wilson, Jr., An advanced color television receiver using a beam indexing picture tube. *IRE Nat. Conv. Rec.* **5**, Part 3, 243–246 (1957).

106a. See, for example, R. D. Thompson, U. S. Patents 2,962,546 (1960); 3,443,139 (1969).

107. C. Feldman, Bilayer bichromatic cathode screen. *J. Opt. Soc. Amer.* **47**, 790–794 (1957).

108. L. R. Koller and H. D. Coghill, Electron excitation of bilayer screens. *J. Appl. Phys.* **29**, 1064–1066 (1958).

109. F. J. Studer, D. A. Cusano, and A. H. Young, Transparent luminescent film *J. Opt. Soc. Amer.* **41**, 559 (1951); F. J. Studer and D. A. Cusano, Transparent phosphor coatings. *ibid.* **45**, 493–497 (1955).

110. R. D. Kell, Method of adhering particles to a support surface. U. S. Patent 3,275,466 (1966).

111. D. H. Pritchard, Penetration color screen, color tube, and color television receiver. U. S. Patent 3,204,143 (1965).

112. W. Zwingers, Multicolor cathode ray tubes. *Int. Elektron. Rundschau* **22**, 113 (1968).

113. P. J. Messineo and S. M. Thompson, Luminescent screens utilizing nonluminescent separator layers. U. S. Patent 3,294,569 (1966).

114. J. S. Prener and J. D. Kingsley, Voltage-controlled multicolor CRT phosphors: Preparation and characteristics. *J. Electrochem. Soc.* **119**, 1254–1258 (1972).

115. R. Whiddington, Transmission of cathode rays through matter. *Proc. Roy. Soc., Ser. A* **89**, 554–560 (1914).

116. H. M. Terrill, Absorption of cathode rays in aluminum. *Phys. Rev.* **24**, 616–621 (1964).

117. R. D. Birkhoff, The passage of fast electrons through matter. *In* "Handuch der Physik" (S. Flugge, ed.), Vol. 34, pp. 53–138. Springer Verlag, Berlin and New York, 1958.

118. P. Lenard, "Quantitatives über Kathodenstrahlen," p. 73. Heidelberg, 1918.

119. L. R. Koller and E. D. Alden, Electron penetration and scattering in phosphors. Phys. Rev. **83**, 684–685 (1951).

120. K. Gentner, The energy absorption of fast electrons. *Ann. Phys.* (*Leipzig*) [5] **31**, 407–424 (1938).

121. W. Ehrenberg and J. Franks, The penetration of electrons into luminescent materials. *Proc. Phys. Soc., London, Sect. B* **66**, 1057–1066 (1953).

122. W. T. Wintringham, Color television and colorimetry. *Proc. IRE* **39**, 1135–1172 (1951).

123. J. E. Kuehne and R. G. Neuhauser, An electrostatically focused vidicon. *J. SMPTE* (*Soc. Motion Pict. Telev. Eng.*) **71**, 772–775 (1962).

124. J. H. T. van Roosmalen, Experimental electrostatically focused "plumbicon" tubes. *Philips Tech. Rev.* **28**, 60–66 (1967).

125. P. J. Messineo and J. Gross, Cathode-ray tube. U. S. Patent 3,164,737 (1965).

126. W. R. Aiken, A thin cathode-ray tube. *Proc. IRE* **45**, 1599–1604 (1957).

127. E. G. Ramberg, Electron-optical properties of a flat television picture tube. *Proc. IRE* **48**, 1952–1960 (1960).

128. D. Gabor, P. R. Stuart, and P. G. Kalman, A new cathode-ray tube for monochrome and colour television. *Proc. Inst. Elec. Eng. Part B*, **105**, 581–606 (1958).

129. P. Schagen, The banana-tube display system. A new approach to the display of colour television pictures. *Proc. Inst. Elec. Eng., Part B* **108**, 577–586 (1961).

130. B. A. Eastwell and P. Schagen, Development of the banana tube. *Proc. Inst. Elec. Eng., Part B* **108**, 587–595 (1961).

131. H. Howden, Mechanical and manufacturing aspects of the banana-tube colour-television display system *Proc. Inst. Elec. Eng., Part B* **108**, 596–603 (1961).

132. K. G. Freeman, Circuits for the banana-tube colour-television display system. *Proc. Inst. Elec. Eng., Part B* **108**, 604–612 (1961).

133. R. N. Jackson, Colorimetry of the banana-tube colour-television display system. *Proc. Inst. Elec. Eng., Part B* **108,** 613–623 (1961).
134. K. G. Freeman and B. R. Overton, Appraisal of the banana-tube colour-television display system. *Proc. Inst. Elec. Eng., Part B* **108,** 624–630 (1961).
135. T. Poorter and F. W. de Vrijer, The projection of color-television pictures. *Philips Tech. Rev.* **19,** 338–355 (1958).
136. L. L. Evans and R. V. Little, Large-screen color-television projection. *J. SMPTE* (*Soc. Motion Pict. Telev. Eng.*) **64,** 169–173 (1955).
137. S. L. Bendell and W. J. Neely, Medium-screen color television projection. *J. SMPTE* (*Soc. Motion Pict. Telev. Eng.*) **67,** 166–168 (1958).
138. E. Baumann, The Fischer large-screen projection system. *J. Brit. Inst. Radio Eng.* **12,** 69–78 (1952).
139. W. E. Good, A new approach to color television display and color selection using a sealed light valve. *Proc. Nat. Electron. Conf.* **44,** 771–775 (1968).
140. Color television large-screen projection with the simultaneous Eidophor system. *Intn. Elektron. Rundschau* **21,** 78 (1967).
141. W. E. Good and T. T. True, Single gun color TV projector. *Proc. Electro-Opt. Syst. Des. Conf., 1969,* pp. 74–78 (1969).
142. W. E. Good, T. T. True, R. W. Granville, and H. J. Vanderlaan, System concepts and recent advancements in a light valve color TV projector. *Proc. Int. Symp. Soc. Inform. Display, 1971* pp. 24–25 (1971).
143. T. T. True and W. E. Good, Principles of dynamic color selection in a light valve color-TV projector. *Proc. Int. Symp. Soc. Inform. Display, 1971* p. 26-27 (1971).
144. W. E. Glenn, New color projection system. *J. Opt. Soc. Amer.* **48,** 841–843 (1958).
145. W. E. Glenn, Principles of simultaneous-color projection television using fluid deformation. *J. SMPTE* (*Soc. Motion Pict. Telev. Eng.*) **79,** 788–794 (1970).

Author Index

The complete references appear in a numbered list on pages 211–217.

Subject Index

D

E

F

G

A 4
B 5
C 6
D 7
E 8
F 9
G 0
H 1
I 2
J 3